

Université du Maine  
UFR Sciences

Unité de Chimie Organique Moléculaire et  
Macromoléculaire-UMR CNRS 6011  
LCOM-Chimie des Polymères

THÈSE DE DOCTORAT DE L'UNIVERSITÉ DU MAINE

**Spécialité: Chimie et Physicochimie des Polymères**

Présentée par

**Ekasit ANANCHAROENWONG**

Pour obtenir le grade de

**Docteur de l'Université du Maine**

**Synthesis and characterization of cis-1, 4-polyisoprene-based polyurethane coatings; study of their adhesive properties on metal surface.**

*Soutenue le 21 septembre 2011, devant le jury composé de:*

M. J.-P. Couvercelle	Professeur à l'Université de Bourgogne	<b>Rapporteur</b>
M. R. Muller	Professeur à l'Université de Strasbourg	<b>Rapporteur</b>
M. P. Bertus	Professeur à l'Université du Maine	<b>Examineur</b>
M. J.-F. Pilard	Professeur à l'Université du Maine	<b>Directeur</b>
Mme S. Bistac	Professeur à l'Université de Haute Alsace, Mulhouse	<b>Co-directrice</b>
Mme I. Campistron	Ingénieur CNRS à l'Université du Maine	<b>Co-encadrante</b>

*To my father and my mother*

*To my brothers*

*To my teachers*

## Acknowledgement

Foremost, I would like to express my sincere gratitude to my advisor Prof. Jean-François PILARD for the continuous support of my Ph.D study and research, for his patience, motivation, enthusiasm, and immense knowledge. His guidance helped me in all the time of research and writing of this thesis. I am extremely grateful to Dr. Irène CAMPISTRON for the time spent discussing the results of my experiment, I would like to thank for having confidence in me and for finding the time to read through the manuscript and correct it. Most importantly, I would like to thank her for her encouragement, patience and also much assistance in my personal life for the past 4 years. I would like to thank Dr. Albert LAGUERRE invaluable advice and discussion about the result of experiments. I also thank Dr. Frédéric GOHIER, for his availability, suggestions about organic synthesis and column chromatography, his patient and useful advice.

I am extremely grateful to Professor Sophie BISTAC for her availability, patient, invaluable advice and discussion about the result of experiment and also many help in a personal life, especially when I do my research in Mulhouse. A special thanks goes to Pr. Maurice BROGLY for his help and advice in carrying out in part of ATR-FTIR.

I would like to thank also Pr. Laurent FONTAINE, Dr. Daniel DEROUET, Dr. Véronique Montembault, Dr. Michel THOMAS, Dr. Sagrario PASCUAL, Dr. Jean-Claude SOUTIF, for their kindness advice and availability. I am also grateful to Professor Jean-Claude BROSSE, for his helpful, guidance and support for my study here.

I would like give thanks to Anita LOISEAU, Jean-Luc MONEGER and Aline LAMBERT for their support and help in materials and administration.

Next, I would like to express gratefulness to Pr. René MULLER, Professeur at Université de Strasbourg, Pr. Jean-Pierre COUVERCELLE, Professor at Université de Bourgogne, for acceptance to be member of jury as reporter for my work and participant in my thesis defend.

I would like also give appreciation to Pr. Philippe BERTUS, professor at Université du Maine, for their kindness acceptance to be member of jury in my thesis defend.

Thank you all friends in LCOM laboratory, Faten, Hoa, Sandie, Charles, Dao, Hien, Jean-Marc, Martin and Rachid for their friendship and good atmosphere in laboratory. I would like to give special thanks to Supinya, Chuanpit, Nitinart and Anuwat for their suggestions, comments and valuable contributions throughout the study.

I would like also thank to all Thai students at Le Mans for their help and many parties during I stay here.

Finally, I am truly in debt to my father and my mother for their endless support, understanding, and belief in me.

*This thesis was done at the Laboratoire de Chimie Organique Macromoléculaire (LCOM), UCO2M under financial support of Prince of Songkla University, Thailand, and French government.*

## Adhesion properties of cis-1, 4-polyisoprene-based polyurethane coatings.

**Ekasit ANANCHAROENWONG**

Industrially, metal/polymer adhesion is involved in a wide range of industries such as automotive industry, or aeronautic and electronic applications.

Polyurethanes (PU) are frequently used as structural adhesives, and are based from polyols obtained from petrochemical products (polyester and polyether polyols). However, these products have some disadvantages as they are non-renewable resources, they may cause environmental pollution, and they tend to be exhausted in the near future. Natural rubber (NR) is an interesting choice to use as a starting material in PU synthesis, due to the fact that they are renewable source, abundant polymer and they have interesting mechanical properties and can be chemically modified.

In this work, hydroxytelechelic polyisoprene (HTPI) having a hydroxyl functionality of 2 was successfully performed via controlled epoxidation and cleavage of high molecular weight polyisoprene, following by a selective reduction reaction of the obtained carbonyltelechelicoligoisoprenes. These HTPI with different molecular weights (1000-8000 g mol<sup>-1</sup>) were reproducibly obtained. Chemical modifications on HTPI were performed by various percentage of epoxidation (10-60%, EHTPI). The different microstructures of these oligomers were evidenced by the characterization techniques FT-IR, NMR, SEC. Their thermal properties were also investigated by TGA and DSC.

Surface properties (surface energy, optical microscopy) and adhesion properties (wedge test) of different materials have been characterized.

To resume adherence results, pure HTPI samples (without any epoxy group) present a very high adhesion level. Epoxidation degrees close to 30-40% allow to obtain interesting adhesive performance. Elsewhere, the effect of molecular weight is slight (nevertheless, a higher  $M_n$  of HTPI induces globally a better adherence). The adherence level is similar to those measured for structural adhesive used in car or aeronautic industry. The wedge test is a severe adherence test, and the low crack propagation observed for some formulations underlines promising industrial developments for this new polymers.

**KEYWORDS** : Cis-1,4-polyisoprene, Natural rubber, Polyurethane , Telechelic oligomer, Degradation, thermal properties, adhesion properties, physicochemical properties

# Etude des propriétés d'adhésion de revêtements polyuréthane à base de cis-1,4-polyisoprène

**Ekasit ANANCHAROENWONG**

Industriellement, les problématiques d'adhésion polymère/métal se rencontrent dans de nombreux secteurs tels que l'industrie automobile, ou les applications aéronautiques et électroniques. Les polyuréthanes (PU) sont fréquemment utilisés comme adhésifs structuraux, et sont obtenus à partir de polyols provenant de la pétrochimie (polyester et polyéther polyols). Cependant, ces produits ont des inconvénients notables sur le plan écologique car ils sont produits à partir de ressources non renouvelables, ils peuvent également générer une pollution de l'environnement, et leurs matières premières de départ sont d'une part de plus en plus coûteuses et d'autres part amenées à se raréfier dans les années à venir.

Le caoutchouc naturel (NR) est une alternative intéressante aux polyols de synthèse car il est issu d'une ressource végétale (hévéa), renouvelable et abondante, et également car il présente des propriétés mécaniques intéressantes. De plus, il peut être facilement modifié chimiquement, afin notamment d'apporter des groupements hydroxyle capables de réagir ensuite avec des fonctions isocyanate pour former un polyuréthane.

Dans ce travail, le polyisoprène hydroxytéléchélique (HTPI) ayant une fonctionnalité en hydroxyle de 2 a été synthétisé avec succès par époxydation contrôlée suivie de coupure oxydante de polyisoprène de hautes masses, puis réduction sélective des oligoisoprènes carbonyltéléchéliques obtenus. Ces HTPI de différentes masses molaires ( $1000-8000 \text{ g mol}^{-1}$ ) ont été obtenus de façon reproductible. Des modifications chimiques ont été effectuées par époxydation à différents taux (10-60% EHTPI). Les différentes microstructures de ces oligomères ont été mises en évidence par FT-IR, RMN and SEC. Leurs propriétés thermiques ont été déterminées par ATG et DSC.

Les propriétés de surface (énergie de surface, microscopie optique) et les propriétés d'adhésion (test de clivage) de différents matériaux ont été caractérisées.

Les échantillons à base de HTPI pur (sans époxyde) présentent un niveau d'adhésion élevé. Des taux d'époxydation proches de 30-40% permettent d'obtenir des performances adhésives intéressantes. D'autre part, l'effet de la masse molaire est faible (cependant, une masse molaire plus élevée entraîne globalement une meilleure adhérence). Le niveau d'adhérence observé est similaire à ceux mesurés pour des adhésifs structuraux utilisés dans l'industrie automobile ou aéronautique. Le test de clivage est un test d'adhérence sévère pour un joint adhésif, et les faibles propagations de fissures observées pour certaines formulations permettent d'escompter des développements industriels prometteurs pour ces nouveaux polymères.

**MOTS CLES:** Cis-1,4-polyisoprène, caoutchouc naturel, polyuréthane, oligomères téléchéliques, dégradation, propriétés thermiques, propriétés d'adhésion, propriétés physicochimiques

## List of abbreviations :

<b>NR</b>	Natural rubber
<b>EPI</b>	Epoxidized cis-1,4-polyisoprene
<b>HTPI</b>	Hydroxytelechelic cis-1,4-polyisoprene
<b>CTPI</b>	Carbonyltelechelic cis-1,4-polyisoprene
<b>EHTPI</b>	Epoxidized hydroxytelechelic cis-1,4-polyisoprene
<b>m-CPBA</b>	meta-chloroperbenzoic acid
<b>FTIR</b>	Fourier Transform Infrared Spectroscopy
<b><sup>1</sup>HNMR</b>	Proton-1 Nuclear Magnetic Resonance spectroscopy
<b><sup>13</sup>CNMR</b>	Carbon-13 Nuclear Magnetic Resonance spectroscopy
<b>SEC</b>	Size Exclusion Chromatography
<b>M<sub>w</sub></b>	Weight average molecular weight
<b>M<sub>n</sub></b>	Number average molecular weight
<b>PU</b>	Polyurethane
<b>TDI</b>	Tolylene-2,4-diisocyanate
<b>H<sub>12</sub>MDI</b>	Dicyclohexylmethane diisocyanate
<b>I-IPDI</b>	Isocyanurate of isophone diisocyanate
<b>DBTL</b>	Dibutyltin dilaurate
<b>DSC</b>	Differential scanning calorimetry
<b>TGA</b>	Thermogravimetric analysis
<b>DTG</b>	Derivative thermogravimetry

## Table of Contents

<b>General Introduction</b> .....	1
<b>Chapter1 – Literature Review</b> .....	6
1.1 Introduction.....	7
1.2 Theories of adhesion.....	7
1.2.1 Mechanical interlocking.....	8
1.2.2 Diffusion Theory.....	9
1.2.3 Electronic Theory.....	10
1.2.4 Molecular bonding.....	10
1.2.5 Thermodynamic Theory.....	12
1.3. Surface characterization techniques.....	14
1.3.1 Atomic force microscopy (AFM).....	15
1.3.2 Time-of-flight secondary ion mass spectrometry (ToF-SIMS).....	15
1.3.3. X-ray photoelectron spectroscopy (XPS).....	16
1.3.4. Scanning electron microscopy (SEM).....	17
1.3.5. Optical contact angle analysis.....	18
1.3.6. Attenuated total reflectance infrared spectroscopy (ATR-IR).....	18
1.4. Adhesion measurement.....	19
1.4.1 Peel test.....	20
1.4.2 Lap shear test.....	22
1.4.3 Pull out test.....	23
1.4.4. Torque test.....	26
1.4.5. Scratch test and nanoindentation test.....	26
1.4.6. Pull off test or Stud/butt test.....	29
1.4.7 Wedge test or Cleavage Tests.....	31



1.5 Metal-Polymer adhesion.....	33
1.5.1 Classification of Polymers According to Their Wettabilities.....	33
1.5.2 Metal Adhesion to Low Wettability Polymers.....	34
1.5.3 Metal Adhesion to Medium Wettability Polymers.....	37
1.5.4 Metal Adhesion to High Wettability Polymers.....	38
1.5.5 Metal-Rubber Adhesion.....	41
1.6. Chemical structure of Natural Rubber based adhesives .....	44
1.6.1. Natural Rubber based adhesive blends.....	44
1.6.2. Epoxidized Natural Rubber based adhesive blends.....	45
1.6.3. Graft and block copolymers.....	46
1.7. Conclusion .....	47
References.....	48

**Chapter 2- Synthesis and characterization of telechelic cis -1, 4-polyisoprene**  
.....53

2.1 Introduction.....	54
2.2 Bibliographic part on Telechelic polyisoprene .....	54
2.2.1. Definition.....	54
2.2.2. Obtaining of telechelic polyisoprene by controlled degradation.....	55
2.2.3 Reactivity of telechelic liquid natural rubber.....	68
2.2.4 Modification of functional end –groups of telechelic natural rubber.....	72
2.2.5 Chain extension reaction of telechelic natural rubber.....	74
Conclusion on the bibliographic part.....	74
2.3. Oxidative degradation of cis-1, 4-polyisoprene.....	75
2.3.1. Epoxidation of cis-1,4-polyisoprene.....	75
2.3.2. Cleavage of epoxidized cis-1,4-polyisoprene 2 in organic medium.....	78

2.4. Synthesis and characterization of hydroxytelechelic polyisoprene precursor of polyurethane.....	82
2.5. Modification of hydroxytelechelic cis-1,4-polyisoprene precursor of polyurethanes.....	85
2.5.1. Epoxidation of hydroxytelechelic cis-1,4-polyisoprene 4.....	85
2.6 Conclusion .....	94
References.....	95
<b>Chapter 3 - Synthesis and characterization of polyurethane base on cis-1,4-polyisoprene</b> .....	<b>97</b>
3.1 Introduction.....	98
3.2 Bibliographic part on polyurethane .....	99
3.2.1 History and Development of Polyurethanes.....	99
3.2.2 Raw Materials in polyurethane synthesis.....	101
3.2.2.1 Isocyanates.....	101
3.2.2.2 Polyols.....	103
3.2.2.3 Chain Extenders.....	105
3.2.2.4 Additives.....	106
3.2.3 Method of synthesis of polyurethanes.....	106
3.2.3.1 One step method.....	106
3.2.3.2 Two steps method.....	107
3.2.4 Properties of polyurethanes.....	108
3.2.4.1 Structure Property Relationship.....	109
3.2.4.2 Parameters influencing physical properties.....	110
3.2.4.3 Thermal stability.....	114
3.2.4.4 Surface Properties of Polyurethane.....	116
Conclusion .....	117

3.3. Synthesis of linear and crosslinked polyurethanes .....	117
3.3.1 ATR-FTIR Analysis Results.....	123
3.3.1.1 Effect of varied molecular weights of diol precursor.....	126
3.3.1.2 Effect of varied epoxidized diol precursors.....	129
3.3.1.3 Effect of varied diol precursors in presence of D-glucose.....	132
3.3.1.4 Effect of varied chain-extenders.....	134
3.3.1.5 Effect of mixing HTPI and EH.....	136
3.3.2 Thermal properties of polyurethane.....	137
3.4 Conclusion .....	145
References.....	146
<b>Chapter 4 - Adhesive Properties of Polyurethane Prepared from Hydroxytelechelic Cis-1,4-Polyisoprene .....</b>	<b>148</b>
4.1 Introduction.....	149
4.2 Wettability measurements.....	150
4.3 Wedge test results.....	157
4.4 Conclusion.....	164
References.....	165
<b>General conclusion.....</b>	<b>166</b>
<b>Experimental part.....</b>	<b>169</b>
<b>Appendix.....</b>	<b>186</b>

# ***General Introduction***

Industrially, metallized polymer films are widely used for gas barrier applications, composite and photoconductive materials, for decorative purposes, in the automotive industry, etc. But, as already established, most synthetic polymers used as commercial materials have low surface energy and as a result these materials have a low adhesion to high surface energy metallic coatings [1]. All of the above considerations make the realization and reproducibility of good adhesion of metallic coatings on polymer substrates an important industrial and scientific challenge.

The interaction between a metal and a polymer strongly depends on the type of the metal and on the functional groups present in the polymer. Oxidation of polymer substrate surfaces is one of the techniques most commonly used to promote the adhesion of polymers to metals. The oxidation can be done prior to, or during the interface formation [2, 3-7]. Chemical modification of the interfacial polymer chains with polar groups, like hydroxyl, carbonyl and carboxylic acid moieties is also used. Plasma treatment of the metallic surfaces seems to be favourable to adhesion as well [8, 9].

There are a large number of areas where adhesives are used to join materials. In the automotive industry, examples of the use of adhesive bonding include the manufacture of doors, engines and car bodies. Other industrial examples include bridge construction and electronic component manufacture [10]. Polyurethanes (PU) today account for the largest percentage (by weight or volume) of any plastic materials used in automotive industry and their growth rate is also faster than that of other plastics [11,12]. Nowadays, an estimated 20 kg of various PU are used per automobile, ranging from all foam seat cushions and backs to crash pads, bumpers, fenders, etc [13]. The developments in adhesives technology, particularly the discovery of PU adhesives [14] have lead to the recommendation to use adhesive bonding technology in many industrial applications [15].

A typical urethane adhesive may contain, in addition to urethane linkages, aliphatic and aromatic hydrocarbons, esters, ethers, amides, urea and allophanate groups. An isocyanate group reacts with the hydroxyl groups of a polyol to form the repeating urethane linkage. Isocyanates also react with water to form a urea linkage and carbon dioxide as a by-product (gaz which induces the formation of a foam). Urethane adhesives have some advantages due to the following reasons: (1) they effectively wet the surface of most

substrates, (2) they readily form hydrogen bonds to the substrates, (3) small molecular size allows them to permeate porous substrates, and (4) they can form covalent bonds with substrates that have active hydrogens. One of the primary mechanisms of bonding by urethane adhesive is believed to be through non-reacted isocyanate (-NCO) to the active hydrogen containing surfaces [16] and through polar, (-NH and C=O) groups. These polar groups are capable of forming strong chemical/physical interactions with the polar surfaces (functional group having active hydrogens).

Polyols currently used in the production of urethanes are petrochemical, being generally derived from propylene or ethylene oxides. Polyester polyols and polyether polyols are the most common polyols used in urethane production. There is a very wide variety of polyester and polyether polyols available for use, with particular polyols being used to engineer and produce a particular urethane elastomer or foam having desired particular final toughness, durability, density, flexibility, compression set ratios and modulus, and hardness qualities [17].

Use of petrochemicals such as polyester or polyether polyols is disadvantageous for a variety of reasons. As petrochemicals are ultimately derived from petroleum, they are nonrenewable resources. The production of a polyol requires a great deal of energy, as oil must be drilled extracted from the ground, transported to refineries, refined, and otherwise processed to yield the polyol. These required efforts add to the cost of polyols and to the disadvantageous environmental effects of its production. Also, the price of polyols tends to be somewhat unpredictable and tends to be exhausted in the near future. Also, as the consuming public becomes more aware of environmental issue and exhaustive issue, there are distinct marketing disadvantages to petrochemical based products. Consumer demand for “bio-based” or “green chemistry” products continues to grow. The term “bio-based” or “green chemistry” polyols for the purpose of this application is meant to be broadly interpreted to signify all polyols not derived exclusively from non-renewable resources. As a result, it would be most advantageous to replace polyester or polyether polyols, as used in the production of urethane foams and elastomers, with more versatile, renewable, less costly, and more environmentally friendly components[17].

Researchers have successfully synthesized PU elastomers using vegetable oil-derived polyols and observed improvements in both thermal stability and oxidation resistance [18-20].

Natural rubber (NR) is an abundant renewable source polymer. It is an important industrial material, particularly in the tire industry or in the manufacture of various products including household, engineering, medical and commercial goods. The chemical modification of NR is one of alternative methods to increase its value and to develop versatile applications. Actually, the NR double bonds in the chains are prone to varieties of chemical reactions. An alternative way to transform NR into useful products is by starting with a low molecular weight NR which is widely known as liquid natural rubber.

An Indian scientist group has been interested to the possibility of developing new polymeric materials from hydroxyl terminated liquid natural rubber [21-22], but radical mechanism of the degradation of the NR by H<sub>2</sub>O<sub>2</sub> under UV leads to secondary and not well defined structure of the HTNR. HTNR is the interesting choice of the starting materials in use in the development of block copolymers polyurethanes as soft segment [23-26]. A wide range of physical and morphological properties can be obtained, depending upon the composition and chemical structure of the hard segments in the block copolymer structure to prepare solid polyurethane such as membrane, coating or film applications.

Our groups focused research a original controlled degradation of high molecular weight cis-1,4-polyisoprene[27], obtaining difunctional HTPI for use in PU synthesis [28].

This thesis focus on synthesis of various polyurethanes with different molecular weights and microstructures of hydroxytelechelic polyisoprene, and different types of chain extenders for the study of the adhesion properties on metal surface. FT-IR, <sup>1</sup>H-NMR, <sup>13</sup>C-NMR were employed to investigate the chemical structure. In addition, the modification of oligomer structure by epoxidation was also studied. The molecular weights of telechelic polyisoprenes are defined by SEC, <sup>1</sup>H-NMR. Their thermal and physicomechanical properties were also investigated.

The first chapter is the literature survey of the theories of adhesion, surface characterization, adhesion measurement and metal-polymer adhesion, focusing on the metal-rubber adhesion and the chemical structure of natural rubber-based adhesives.

The second chapter deals with the reaction of controlled cleavage of high molecular weight epoxidized synthetic cis-1,4-polyisoprene or natural rubber using periodic acid in organic medium to obtain carbonyl telechelic cis-1,4-oligoisoprene (CTPI). The chain-end modification of carbonyl groups to hydroxyl groups to obtain hydroxytelechelic cis-1,4-polyisoprene (HTPI) is presented. Moreover, main chain isoprene unit modifications by epoxidation of HTPI for preparing different precursors of polyurethane are described.

The third chapter describes preparations of polyurethanes. Characterization by FT-IR allows an approach of the effect of  $\overline{M}_n$  of the oligoisoprenes precursors, the effect of percentage of epoxide, the effect of chain extender and the effect of mixing precursor with and without epoxide, on the hydrogen bondings appearance. Their thermal and physico-mechanical properties were determined by DSC and ATG.

The fourth chapter implicates the characterization of adhesive properties of polyurethane prepared from hydroxytelechelic cis-1,4-polyisoprene. The study of wettability, the wedge test and the optical microscopy were used for analyzed.

Finally, a general conclusion summarizes the main results and presents some further perspectives.

- 
- [1] B. Rånby, *Int. J. Adhes. Adhes.* **1999**, *19*, 337.
  - [2] J. Cognard, C. R. *Chimie*, **2006**, *9*, 13.
  - [3] J. Y. Song, J. Yu *J. Acta Mater.* **2002**, *58*, 3985.
  - [4] S. S. Pesetskii, B. Jurkowski, A. I. Kuzakov, *Int. J. Adhes. Adhes.* **1998**, *18*, 351.
  - [5] M. Kalnins, J. Malers, *J. Adhes.* **1995**, *50*, 83.
  - [6] S. Siau, A. Vervaet, E. Schacht, S. Degrande, K. Callewaert, A. van Calster, *J. Electrochem.Soc.* **2005**, *152*, D136.
  - [7] J. L. Jordan, P. N. Sandra, J. F. Morar, C. A. Kovac, F. J. Himpsel, R. A. Pollak, *J. Vac. Sci.Technol. A*, **1986**, *4*, 1046.
  - [8] M. Mantel, J. P. Whightman, *Surf. Interface Anal.* **1994**, *21*, 595.
  - [9] J. Ghädhe, *J. Adhes. Sci. Technol.* **1992**, *6*, 569.
  - [10] A.J.Kinloch, *Adhesion and Adhesives Science and Technology*, Chapman and Hall London **1990**, Chapter 1.
  - [11] K. W. Suh, C. P. Park, M. J. Maurer, M. H. Tusim, R. De Genova, R. Broos, D. P. Sophiea. *Adv. Mater.* **2000**, *12(23)*, 1779.
  - [12] J. W. Leenslag., E. Huygens, A. Tan. *Cell. Polym.* **1997**, *16(6)*, 411.
  - [13] E. Van Eetvelde., C. Banner., J. Cenens., S. J. Chin., *Cell. Plast.* **2002**, *38(1)*, 31.



- [14] J. Saunders., K. Frisch, *Polyurethane Chemistry and Technology, Part I*: Interscience, New York, **1963**
- [15] J.M. DeBell., W. C. Goggin., W. E. Gloor. *German Plastic practice*, DeBell and Richardson, Cambridge, Mass. **1946**.
- [16] G. L. Dennis., C. Paul. A. Pizzi., K.L. Mittal.,. *In Hand Book of Adhesive Technology*. New York ed. Marcel Dekker: **1994**, Chapter. 24
- [17] T.M. Kurth., R.A Kurth., R.B. Turner. and L.P. Kreifels, **2006**. US 7084230.
- [18] I. Javni., W. Zhang., and Z.S. Petrovic.,. *J. Appl. Polym. Sci.*, **2003**, 88(13), 2912.
- [19] I. Javni., Z.S. Petrovi., A. Guo., and R. Fuller. *J. Appl. Polym. Sci.*, **2000**, 77(8), 1723.
- [20] K.I. Suresh., and V.S. Kishanprasad.. *Ind. Eng. Chem. Res. Data*, **2005**, 44(13), 4504.
- [21] T. Ravindran., M.R.G. Nayar., and D.J. Francis. *J. Appl. Polym. Sci.*, **1988**, 35(5), 1227.
- [22] T. Ravindran., M.R.G. Nayar., and D.J. Francis.,. *Makromol. Chem., Rapid Commun.*, **1986** 7(3), 159.
- [23] S. Gopakumar., and M.R.G. Nair. *Eur. Polym. J.*, **2005**, 41(9), 2002.
- [24] S. Gopakumar., and M.R.G. Nair. *Polymer*, **2005**, 46(23), 10419.
- [25] C.J. Paul.,M.R.G. Nair.,M., P.Koshy, and B.B.Idage. *J. Appl. Polym. Sci.*, **1999**, 74(3), 706.
- [26] T. Ravindran., M.R.G. Nayar., and D.J. Francis. *J. Appl. Polym. Sci.*, **1991**, 42(2)
- [27] N. Kebir, I. Campistron, A. Laguerre, J.-F. Pilard, C. Bunel, J.-P. Couvercelle, C.Gondard, *Polymer*, **2005**, 46, 6869
- [28] S. Gillier- Ritoit, D. Reyx, I. Campistron, A. Laguerre, R.P. Singh, *J. Appl. Polym. Sci.* **2003**, 27(1), 42.

---

## ***Chapter1 – Literature Review***

## 1.1 Introduction

The process that allows the adhesive to transfer a mechanical stress from the adherend to the adhesive joint is known as the adhesion. In general the adhesive is a polymer-based material, which intimately interacts, either through chemical/physical forces, to the adherend surface to which it is being applied. The physical and chemical interactions result from atomic scale attractions between specific functional groups of the adhesive and the adherend surface. For thermoset adhesives, during the early phase of the curing process the viscous adhesive material will flow to enable contact with the adherend and penetration of the surface asperities. As curing proceeds, the viscous mixture becomes a rigid solid as the compounds react and cohesively link the adhesive, often referred to as crosslinking. This process enables strength to be established between the joined adherends [1].

When it comes to measuring the adhesion, there are more than adhesion tests [2]. The choice of the test depends solely on the material system investigated and the structure of the sample. If one is dealing with sputtered metallic films on ceramic substrates the scratch test [3] is suitable while for metallic films on polymer substrates the peel test [4] is a good choice.

This bibliographic part will present the different the adhesion concepts and tests, and then will focus on metal/polymer adhesion, and natural rubber based adhesives.

## 1.2 Theories of adhesion

Adhesion corresponds to the interatomic and intermolecular interactions at occurring at interface between two surfaces. [5]

It is important to realize that, although some theories of adhesion emphasize mechanical aspects and others put more emphasis on chemical aspects, chemical structure and interactions determine the mechanical properties and the mechanical properties determine the force that is concentrated on individual chemical bonds. Thus, the chemical and mechanical aspects are linked and cannot be treated as completely distinct entities. In addition, some of the theories emphasize macroscopic effects while others are on the molecular level. [6]

Adhesion is acknowledged to be one of the more complex phenomena to describe in simple terms. Adhesion to and by polymers is a particularly subtle part of the subject, and one of increasing applied importance. The subtlety lies in the many characteristic properties of polymer surfaces and interfaces. [7]

In the past thirty years, the level of basic adhesion research has outnumbered the growing use of the technological applications. Despite this, a single unifying theory that adequately describes all adhesion phenomena is yet to be proposed. However, several basic models have been established. The following mechanisms of adhesion are emphasized in the literature.

### **1.2.1 Mechanical interlocking**

This theory essentially proposes that mechanical keying, or interlocking, of the adhesive into the irregularities of the substrate surface is the major source of intrinsic adhesion. [8] Although a number of examples relating joint strength and durability to increased surface roughness exists in the literature, the theory is not universally applicable since good adhesion occurs between smooth surfaces, such as the adhesion that occurs between wet glass microscope slides. Also, it has been observed that increased roughness can result in lower joint strengths. [9] Mechanical interlocking can make a significant contribution towards the joint strength if the adherend surface geometry is specifically fabricated to enhance adhesive penetration. It is still debatable whether the increase in joint strength can be directly related to a mechanical interlocking or to secondary mechanisms such as an increase in specific surface area for chemical bonding or improved kinetics of wetting [9].

Some authors have studied the importance of the surface porosity in the mechanism of adhesion. Packham suggests that the shape of the pore (cylindrical versus ink bottle) is a crucial factor in controlling the pore filling process [10]. Penetration of the adhesive into pores on the surface can contribute significantly towards high joint strengths, since it is believed that the adhesive that penetrates into the pores requires considerable plastic deformation, and thus high fracture energy. Packham and Johnston [11] were able to vary the porosity of a ceramic by varying the firing temperature, and showed that the bonding strength of polyethylene to the fired ceramic was a function of the degree of porosity of the ceramic.

Many researchers have noted the significance of mechanical interlocking in explaining adhesion phenomena but in combination with other forces. Adhesion between surfaces is influenced by the presence of van der Waals forces in addition to mechanical coupling, but it was noted that these forces are not sufficient to create the strong interfacial bonding observed between polymers [12]. Bright *et al.* [13] and Arrowsmith [14] suggested that the number of pores penetrated by the adhesive is linked with adhesion strength. These findings revived the mechanical adhesion theory. Venables [15] work of examining the phosphoric acid anodise (PAA) process indicated a link with surface micro-porosity and bond strength. Evans *et al.* [16] and Wang *et al.* [17] have studied the anodizing process on metal surface where they found that the surface roughness contribute to increase the energy dissipation processes in the zone of interface separation.

### 1.2.2 Diffusion Theory

Wool [18] described the concept of the diffusion theory as the penetration of adhesive into the substrate. The diffusion theory of adhesion proposes that adhesion can be attributed to the interdiffusion of polymer molecules at the interface [19]. Since this requires that the adhesive and substrate are mutually miscible and have significant mobility, the mechanism does not directly apply in the case of metal/polymer adhesion [20]. Allen [19] argues that the penetration of polymers into interstices of a metal surface involves a diffusion mechanism, although he admits that this is an extreme interpretation of the original proposals of Voyutskii [21] who believes that the adhesion between two polymers is a result of interfacial interdiffusion of polymer chains. Critics of the theory believe that if the interdiffusion process is involved, the joint strength should depend on the type of the material, contact time and pressure, temperature, molecular weight, and formation of primary and secondary interfacial forces [22]. The fundamental understanding of the molecular dynamics of entangled polymers has advanced due to the theoretical approach proposed by a number of authors [23-25]. This new approach stems from the idea that polymers cannot pass each other in concentrated solution or melt or solid form. Therefore, a chain with a random coil conformation is trapped in an environment of fixed obstacles has assumed a wormlike motion of confined chains and gave it the name “reptation”. The most important and useful application of reptation concept is the crack healing [26]. The problem of healing is to correlate the macroscopic strength measurements to the microscopic description of motion. The difference between self diffusion

phenomena in the bulk polymer and healing is that the polymer chains in the former case move over distances larger than their gyration radii, whereas in the other case, healing is essentially complete in terms of joint strength.

### 1.2.3 Electronic theory

This theory postulates that adhesion arises from the interaction of point charges, positive and negative, on either side of an interface, where on one side there is a solid, and on the other an electric double layer composed of solvated ions and counter-ions. This model finds much application in colloid science [11].

This theory states that the work of adhesion is due to the formation of an electrical double layer between the adhesive and substrate. According to Deryaguin[27] the high joint strength results from the electrostatic interactions between the adhesive and the adherend. As the distance between the charges increases so does the electrostatic potential. When the bonds break, the discharge energy provides a measure of the interfacial adhesion forces present. Evidence for the theory provided by Deryaguin [27] and Weaver [28] suggested the interfacial charge was an important parameter in determining the adhesive strength. However, work by Skinner *et al.* [23] and Chapman [30] indicated that these forces were small relative to the forces of molecular attraction, i.e. van der Waals interactions.

Although the mechanism is likely to occur in metal / polymer systems, researchers have calculated, from charge densities at surfaces, that the electronic contribution to the thermodynamic work of adhesion (WA) is small compared to the contribution from chemical interactions [20].

### 1.2.4 Molecular bonding

Molecular bonding is the most widely accepted mechanism for explaining adhesion between two surfaces in close contact. It entails intermolecular forces between adhesive and substrate such as dipole-dipole interactions, van der Waals forces and chemical interactions (that is, ionic, covalent and metallic bonding). This mechanism describes the strength of the adhesive joints by interfacial forces and also by the presence of polar groups [31]. Molecular bonding mechanisms require an intimate contact between the two substrates. However,

intimate contact alone is often insufficient for good adhesion at the interface due to the presence of defects, cracks and air bubbles [32]. The molecular bonding mechanism is not yet fully understood and there have been many theories proposed to explain it. Mutsuda and Komada [33] studied poly(oxy- 2,6-dimethyl-1,4-phenylene) (PPE) bonding to rubber and reported that the adhesion mechanism was based on a hydrogen abstraction reaction. This occurs when the separation between two polymer substrates becomes negligible, allowing radicals from one substrate to attack the other causing the formation of more radicals. Recombination of these radicals with the polymer allows chemical bonding between substrates [34]. Further evidence for this hypothesis was seen in the XPS and ToF-SIMS work conducted by other researchers [35, 36]. It was shown that interfacial bonding was the crucial factor in the adhesion strength between silanes and metals [32, 34, 35]. Another theory is discussed in the review article written by Basin [48] which considers adhesion between solid substrates and organic coatings. Basin [36] reported that as the number of chemical bonds increased at the contact zone, adhesion strength passed through a maximum value.

This finding is supported by the study investigating the shear strength of aluminium–polypropylene lap joints by Chen *et al.* [37]. They found that the overriding adhesive mechanism was the chemical interaction between the functional groups at the interface and also concluded that excessive chemical bonding at the adhesive interface could have a negative effect on the interface strength. Adhesion strength has been shown to depend on the thickness of the adhesive layer for composite interfaces. Interfacial bonding strength increases as the thickness of the adhesive layer is reduced as stress is able to dissipate through the interface with greater ease [38]. Polar adhesives have been used previously to change the polarity in rubber systems [38, 39]. It has been shown that there is a parallel relationship between the hydrophilic properties of the surface and its subsequent polarity [38,]. Hutchinson and Iglauer [39] studied tack and peel tests of foam and sealants used in building construction. They found no sign of interdiffusion or electrostatic interaction at the adhesive interface while mechanical interlocking only had a marginal role in the adhesive strength of the system. The primary adhesive mechanism identified was chemical bonding of the substrates at the interface [39].

### 1.2.5 Thermodynamic Theory.

Adhesion by this mechanism is attributed to surface chemical forces, and the chemisorption or physisorption of atomic and molecular species. The attractive forces working across two surfaces include weak dispersion forces and stronger forces due to hydrogen, covalent, and ionic bonding [20].

According to the adsorption theory of adhesion, the interatomic and intermolecular interactions between adhesive and substrate are responsible for adhesive forces. These interactions are classified into primary (chemical bonding) and secondary forces (physical interactions, e.g. hydrogen bonding). The primary bonds are the strongest with energies in the range of 1000-100 kJ/mol as compared with 40-20 kJ/mol of secondary forces. In case of urethane adhesives bonded to active hydrogen containing substrates, a primary bond is believed to exist [40].

Zisman has shown that van der Waals dispersion and polarization forces are more than adequate to account for the observed strengths of adhesive joints [41]. The types of bonds formed between two surfaces depend upon the chemical constitution of the interface. The criterion for chemisorption / physisorption processes to occur across the interface is that the adsorbate wet the substrate. In general, for spontaneous wetting, the surface energy of the solid must be greater than that of the liquid. Then the thermodynamic work of adhesion between the solid and the liquid can be expressed as:  $W_A = \gamma_S + \gamma_L + \gamma_{SL}$  where  $\gamma_S$  is the surface energy of the solid,  $\gamma_L$  is the surface tension of the liquid, and  $\gamma_{SL}$  is the solid / liquid interfacial tension.

Schultz, *et al.*[42] proposed that the surface free energy can be generally expressed by two terms corresponding to dispersion forces and to polar forces:  $\gamma_S = \gamma_S^D + \gamma_S^P$ . Carré and Schultz, [43] using a two liquid contact angle method developed for high-energy solids, determined the surface energetics of aluminum that had received various pretreatments. They concluded that for good “dry” adhesive joint strength, and for good durability in the presence of moisture, the surface should have a high dispersive component of surface energy,  $\gamma_S^D$ , and a low polar component,  $\gamma_S^P$ . The contribution of dispersion and polar components can then be used to predict interactions at the interface. It was hypothesized that the work of adhesion,  $W_A$ , can be correlated to the measured joint strength.



Lee [44] using contact angle measurements, determined the wettability of silica surfaces primed with reactive silanes. The wettability was determined by the conformation of the organic portion, R, of the silane molecule: R - Si(OR')<sub>3</sub>. Lee classified various silanes into three groups based on polarity of the R group. For example, if the R group was vinyl-, the silane treated surface was classified as having low polarity, for amino- groups, the silane treated surface was classified as having medium polarity, and for glycidoxy- groups, the surface was classified as having high polarity.

Baier *et al.* [45] using the concept of critical surface tension,  $\gamma_C$ , have measured  $\gamma_C$  on several structurally homologous series of solids, including unbranched polyethylene, and chlorinated and fluorinated analogues of polyethylene. They correlated these empirical measurements of surface energy “with respect to the most probable exposed atoms.” In the same work, Baier *et al.*, [45] concluded that in order to get good adhesion, the adherend surface should be kept free from low surface tension organic films. They predicted that substituent groups, such as -OH, -SH, -COOH, and -NH<sub>2</sub>, at the outermost surface, would increase the “adhesiveness” of the surface by increasing the surface energy; whereas less polar groups, such as -CH<sub>3</sub> or -CH<sub>2</sub>- would decrease the bondability of the surface.

In another class of interaction, namely acid-base, is in part responsible for the intrinsic adhesion forces at inorganic / polymer interfaces. Fowkes [46] extended this viewpoint to the understanding of adhesion of polymers on inorganic surfaces, by proposing that the thermodynamic work of adhesion could be separated into components of: London dispersion (d) forces, hydrogen-bond (h) forces, acid-base (ab) forces, dipole-dipole (p) interactions, and induced dipole-dipole (i) interactions. Namely:  $W_A = W_A^d + W_A^h + W_A^{ab} + W_A^p + W_A^i$

Later, Fowkes [47] demonstrated that hydrogen bonding is a subset of the acid-base reactions. Using the Drago E and C constants and equations Fowkes, [61] calculated the enthalpies of acid-base interaction between various hydrogen bonding liquids, and compared these calculated values with measured enthalpies of interaction. The calculated acid-base enthalpies agreed well with the measured interaction enthalpies, giving rise to Fowkes' claim that hydrogen bonds are a subset of acid-base interactions.

Fowkes proposed that the work of adhesion between a polymer and an inorganic substrate could be accounted for by dispersion forces and acid-base interactions [60].

$$W_A = W_A^d + W_A^{ab}$$

In a metal / polymer system, both the polymer and the metal substrate can exhibit amphoteric behavior. Bolger [49] claims that the only forces worth considering, in addition to dispersion forces, are hydrogen bonding forces, and used an acid-base mechanism to predict the relative magnitude of the hydrogen bonds. Since under ambient conditions, metal oxide surfaces are generally hydroxylated, the hydroxyl group can act as either an acid or a base.

Different adhesion theories are therefore proposed in the literature. For elastomer/metal systems, the mechanisms which can be involved are mostly the adsorption theory (wetting step and creation of an intimate contact), the molecular theory (formation of physical end/or chemical bonds between metal and polymer), and possibly the mechanical interlocking in the case of a rough metal surface.

In order to better understand the adhesion mechanisms, it is necessary to have precise information on the surface properties of materials. Surface characterization techniques can be also useful to analyse the surfaces after assemblies separation.

### **1.3. Surface characterization techniques**

Any consideration of adhesion mechanisms requires information about the physical and chemical properties of the adhering surfaces and the delamination surfaces in cases where adhesion has failed in use or as a result of mechanical testing. There are a number of surface characterization techniques utilized for investigating properties related to adhesion mechanisms and adhesion strength. These include atomic force microscopy (AFM), time-of-flight secondary ion mass spectrometry (ToF-SIMS), X-ray photoelectron spectroscopy (XPS), secondary electron microscopy (SEM), attenuated total reflectance infrared spectroscopy (ATR-IR) and other microscopy techniques plus methods sensitive to surface energy such as optical contact angle analysis. There have been numerous studies which have looked at surface properties such as roughness, polarity, chemical composition and surface free energy to describe and explain adhesion phenomena at a surface or interface using the above mentioned techniques [50]. Brief descriptions of these techniques are included below.

### 1.3.1 Atomic force microscopy (AFM)

The AFM measures the forces acting between a fine tip and a sample. The tip is attached to the free end of a cantilever and is brought very close to a surface. Attractive or repulsive forces resulting from interactions between the tip and the surface will cause a positive or negative bending of the cantilever. The bending is detected by means of a laser beam, which is reflected from the back side of the cantilever [51].

AFM is widely used to generate topographic maps of surfaces, whereby cantilever deflections arising from the interaction with surface features are recorded as a function of raster position. AFM is able to achieve atomic resolution in the vertical plane and 0.01 nm spatial resolution in the horizontal plane [50].

This resolution allows for the detection of changes to topography after surface treatment, and can be measured through roughness values, providing valuable information on contribution of surface roughness to adhesion strength.

### 1.3.2 Time-of-flight secondary ion mass spectrometry (ToF-SIMS)

Time-of-flight secondary ion mass spectrometry (TOF-SIMS) is a powerful technique that provides chemical information about the surface of a solid sample and does not need any chemical pretreatments. The significant advantage of TOF-SIMS over other techniques is imaging analysis, which allows the direct visualization of the chemical distribution on the sample surface with submicrometer spatial resolution [52].

ToF-SIMS instruments generate surface mass spectra under clean ultrahigh vacuum conditions. A pulsed, highly focused primary ion beam is directed at the surface causing the emission of secondary charged and neutral fragments from the surface and near-surface region. The primary ion source was formerly monoisotopic Ga but contemporary instruments typically use Bi cluster ion sources or C<sub>60</sub> ion sources for superior mass range and spectral yield. Positively or negatively charged secondary ions within a narrow energy band are extracted from the surface region and mass analysed using a time-of-flight analyzer. The resulting mass spectrum plots secondary ion intensity as a function of mass/charge ratio. ToF-SIMS provides elemental, isotopic and molecular information at extremely high surface

sensitivity (monolayer). This molecular information provides the chemistry at the interface, allowing for molecular insight into the adhesive reaction [50].

### 1.3.3. X-ray photoelectron spectroscopy (XPS)

X-ray Photoelectron Spectroscopy (XPS) is one of a number of surface analytical techniques that bombard the sample with photons, electrons or ions in order to excite the emission of photons, electrons or ions [53].

XPS is a surface analysis technique that is unique in providing chemical state bonding information. For example, it is widely used to determine localized bonding chemistry of carbon and to differentiate oxidation states of inorganic compounds (i.e. sulfate vs sulfide and metallic vs oxidized states of metals). It is a quantitative techniques and can detect all elements except for H and He with detection limits of approximately 0.1% atomic.

XPS is an ultra-high vacuum surface analysis technique with a sampling volume that extends from the surface sensitivity makes XPS a technique of choice for analyzing thin contamination layers and characterizing outer most surface chemistry. XPS can also be utilized for sputter depth profiling to characterize thin films by quantifying matrix-level elements (> 1% atomic) as a function of depth. The technique can accommodate in sulating as well as conducting samples. The maximum area of analysis for XPS is approximately 30  $\mu\text{m}$  [54].

As with ToFSIMS, this surface sensitivity requires that XPS instruments operate ideally at ultrahigh vacuum to minimize undesirable surface contamination. X-ray photons (generally in range 100–2500 eV), derived from monochromated laboratory X-ray sources or soft X-ray synchrotron beam lines, irradiate the sample surface and cause the emission of photoelectrons from the near surface region. The kinetic energy of these electrons is determined, typically using a hemispherical sector analyzer, and the corresponding electron binding energy calculated. The spectra produced show photoelectron intensity as a function of binding energy, mapping out the electronic structure of the parent atoms. Characteristic peaks in the spectra correspond to the electronic core levels in the atoms in the near surface region and can be used to identify the species present and quantify the relative surface composition. The elemental information along with the bonding states allow for the chemistry at the adhesive interface to be understood. XPS also facilitates quantitative correlations between

elemental and functional groups present on the surface and surface energy or adhesion strength. XPS operating principles are explained in detail in a variety of published works [50].

#### 1.3.4. Scanning electron microscopy (SEM)

The transmission electron microscope (TEM) was the first type of Electron Microscope to be developed and is patterned exactly on the light transmission microscope except that a focused beam of electrons is used instead of light to "see through" the specimen. It was developed by Max Knoll and Ernst Ruska in Germany in 1931. The first scanning electron microscope (SEM) debuted in 1938 (Von Ardenne) with the first commercial instruments around 1965. Its late development was due to the electronics involved in "scanning" the beam of electrons across the sample. Scanning electron microscope (SEM) is a type of electron microscope that images a sample by scanning it with a high-energy beam of electrons in a raster scan pattern. The electrons interact with the atoms that make up the sample producing signals that contain information about the sample's surface topography, composition, and other properties such as electrical conductivity.

The types of signals produced by a SEM include secondary electrons, back-scattered electrons (BSE), characteristic X-rays, light (cathodoluminescence), specimen current and transmitted electrons. Secondary electron detectors are common in all SEMs, but it is rare that a single machine would have detectors for all possible signals. The signals result from interactions of the electron beam with atoms at or near the surface of the sample. In the most common or standard detection mode, secondary electron imaging or SEI, the SEM can produce very high-resolution images of a sample surface, revealing details about less than 1 to 5 nm in size. Due to the very narrow electron beam, SEM micrographs have a large depth of field yielding a characteristic three-dimensional appearance useful for understanding the surface structure of a sample. Back-scattered electrons (BSE) are beam electrons that are reflected from the sample by elastic scattering. BSE are often used in analytical SEM along with the spectra made from the characteristic X-rays. Because the intensity of the BSE signal is strongly related to the atomic number ( $Z$ ) of the specimen, BSE images can provide information about the distribution of different elements in the sample. For the same reason, BSE imaging can image colloidal gold immuno-labels of 5 or 10 nm diameter which would otherwise be difficult or impossible to detect in secondary electron images in biological specimens. Characteristic X-rays are emitted when the electron beam removes an inner shell

electron from the sample, causing a higher energy electron to fill the shell and release energy. These characteristic X-rays are used to identify the composition and measure the abundance of elements in the sample [55].

SEM has the potential to generate images with a few nanometers spatial resolution, and has a relatively large depth of field, in some cases up to 100 times that of an optical microscope. This provides topographical information on the sample surface allowing for greater understanding of the reaction between surface treatment and substrate [50].

### **1.3.5. Optical contact angle analysis**

Optical contact angle analysis (OCA) is a surface sensitive technique which allows the wetting properties and surface energy of the investigated sample to be measured. In general, a polar and non-polar liquid are dispensed onto the sample surface with the angle that the liquid makes with the surface (as measured through the liquid) being recorded. Smaller contact angles indicate a more wetting surface with a higher surface energy and therefore a greater work of adhesion. As surface energy and wettability are related to adhesion, OCA provides an indirect measure of adhesion, allowing for the comparison between the work of adhesion and direct adhesion methods [50].

### **1.3.6. Attenuated total reflectance infrared spectroscopy (ATR-IR)**

ATR was developed by Fahrenfort for the determination of optical constants and as a means of obtaining intense spectra from samples which were difficult or unamenable to study by normal transmission techniques. Simultaneously Harrick developed a multireflection technique to obtain spectra from surface layers. In this case the surface was sampled many times and hence weak absorptions were magnified. In ATR the radiation incident on an interface (at angles of incidence greater than the critical angle) between the sample and an analysing crystal of higher refractive index will be totally reflected at those wavelengths where the sample shows no absorption. However, at wavelengths where the sample absorbs, part of the incident radiation will be absorbed causing an attenuation of the reflected radiation. Such an effect produces a spectrum which strongly resembles the transmission spectra, although the shape of the bands will be different [56].

ATR-IR is conducted by passing infrared radiation into an infrared transmitting crystal to achieve multiple reflections between the ATR crystal and the surface under investigation. The increased spectral sensitivity and reduced depth of analysis achieved in ATR-IR is used for surface molecular characterization. For example, it has been used to detect chemical bonds between proteins and nitrogen plasma treated polypropylene (PP/N<sub>2</sub>). This bonding increased adhesion between the (PP/N<sub>2</sub>) and the hybrid hydrogel. ATR-IR has also been used to characterize improved adhesion between polyethylene and a surface grafted acrylic acid monomer (PE-g-AAc). This study concluded that covalent bonds formed between carboxylic groups of grafted polyacrylic acid and the hardener amine group improved adhesion. Similarly, after glow discharge treatment of poly(vinylidene difluoride) ATR-IR provided information to detect the formation of oxygen-containing species on the polymer surface [50].

Surface analysis are fruitful to better predict and understand adhesion mechanisms. The adhesion performance can be evaluated through mechanical separation tests.

#### **1.4. Adhesion measurement**

Direct adhesion measurements such as pull off tests, peel tests, lap and shear tests, and scratch tests are destructive methods that measure the force required to break, tear and delaminate surfaces at the interface. Understanding the locus of failure for any system is of high importance. While many direct measurements of adhesion strength provide qualitative data, tests such as peel and pull up tests provide a quantitative measure of adhesion. However, many tests are required to provide consistent results. Further, direct methods do not provide physical interpretations of different adhesion measurements. A combination of direct adhesion measurement and surface characterization using techniques such as XPS, ToF-SIMS and contact angle measurements is an optimum way of investigating polymer adhesion. This section deals primarily with the role of direct adhesion measurement [50].

### 1.4.1 Peel test

The peel test was attentively studied by Kim and Kim (1988), Kim and Aravas (1988) and, most recently by Kinlock, Lau and Williams (1994) in order to characterize the mechanics of the test. Earlier work on this topic is cited in these papers. One of the primary aims of this general line of research has been to link the peel force or, equivalently, the macroscopic work of fracture, to the work of interface adhesion by accounting for plastic deformation accompanying the peeling process. In steady-state peeling, the peel force per unit width of film is simply related to the macroscopic work of fracture, which is effectively the sum of the work of adhesion and the plastic dissipation. Successful partitioning of these two contributions to the peel force would enable the work of adhesion to be inferred [57].

Measurement of the peel strength of an adhesive joint is usually a very good way of ensuring that adequate quality control has been maintained in the manufacture of an adhesively bonded structure. The peel test is particularly sensitive to variations in a region adjacent to the interface between adhesive and adherend, and is widely used by the aerospace industry to ensure sufficient process control has been exercised during the pretreatment and anodizing of adherends [58].

Williams, Kinloch *et al.* and Moidu *et al.* have described analyses of the peel test which permitted them to derive the energy release rate by considering each of the loss mechanisms in the peeling adherend arm in detail. Their major aim was to obtain quantitative expressions for the energy dissipated by plastic deformation due to bending of the peeling arm. Williams successfully applied his analysis to the results originally obtained by Gent and Hamed on the bending of mylar strips through 180°. Kinloch *et al.* successfully applied their analysis to the modelling of the peeling behaviour of various flexible laminates comprising polyethylene and poly(ethylene terephthalate) (PET) films bonded to aluminium foils and PET films. Moidu *et al.* successfully applied their analysis to the peeling of metal to metal adhesive joints [59].



The peel test is popular for adhesion measurements. The geometry consists of a film bonded to a thick substrate, and the test proceeds by measuring the force required to pull the film off the substrate. This peel force is then related to the properties of the interface. Under some limiting conditions, the peel force is a direct measure of the interfacial toughness. However, more generally, the peel force is affected by the geometry, the constitutive properties of the film and substrate, and the cohesive properties of the interface [60].

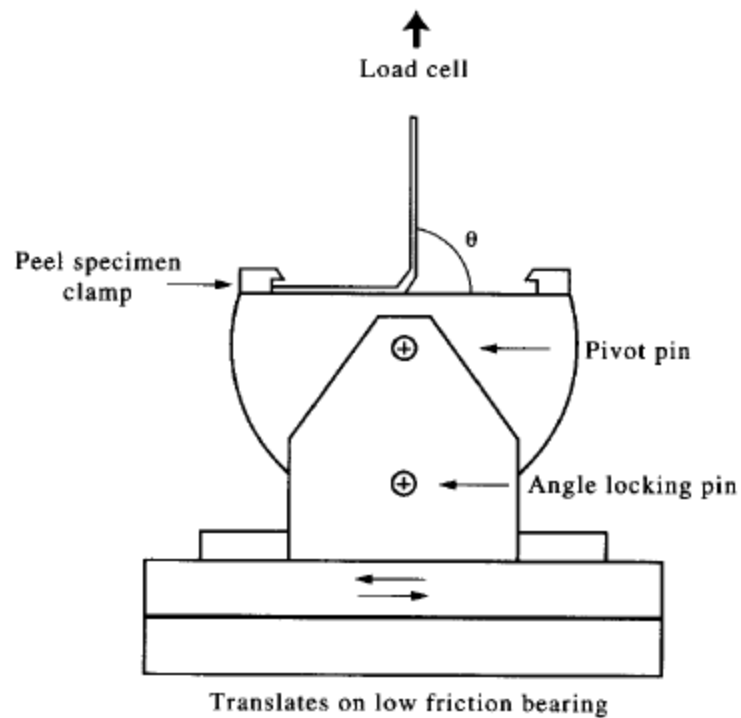
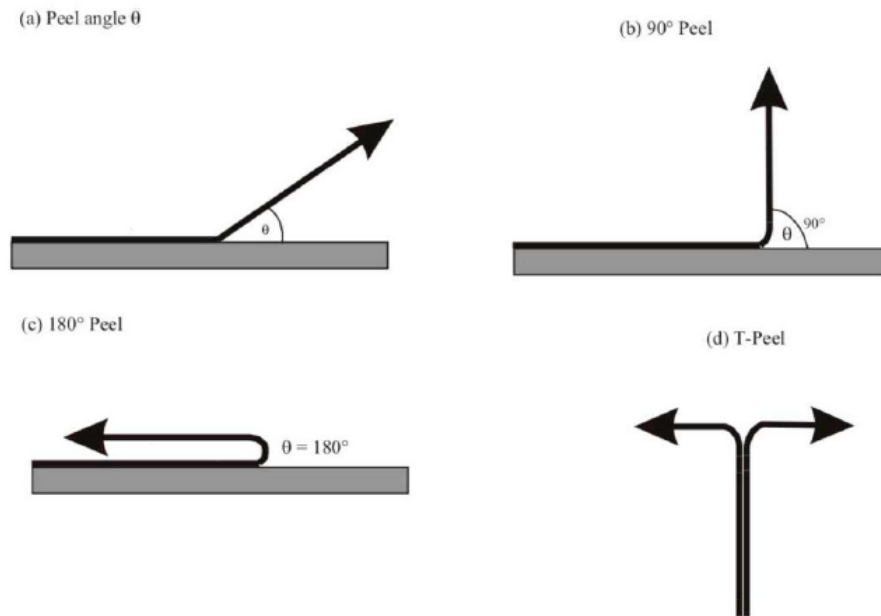


Figure 1.1 Peel testing apparatus [61]



**Figure 1.2** Basic modes of loading during fracture mechanics. [1]

### 1.4.2 Lap shear test.

The lap shear test or tensile – shear test measure the strength of the adhesive in shear. It requires the bonding together of two coated samples. A full force is applied to both parts until a film failure occurs by shearing. It is the most common adhesive test because the specimens are inexpensive, easy to fabricate, and simple to test. However, at time it is difficult to minimize or eliminate bending stresses in common shear joint specimens. Due to the nonuniform stress distribution in the adhesive arising from the joint configuration, the failure strength values are of little use for engineering design purposes.

Lap shear tests are similar to peel tests although this method of adhesion measurement is more commonly quantitative in nature [50]. A more comprehensive way of exploring and measuring adhesion phenomena is through a combination of both direct and indirect measurements by shear test in conjunctions with XPS measurements for example.

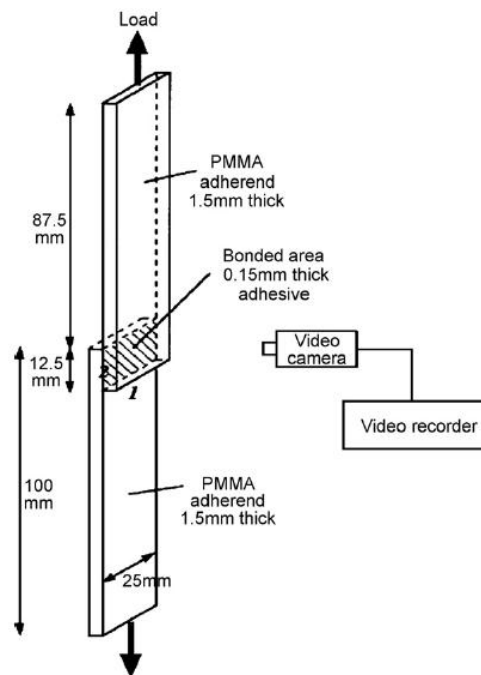


**Figure 1.3** Schematic of tensile lap shear test. [50]

### 1.4.3 Pull out test

This test is widely used to quantify fiber/matrix adherence, especially in composites materials. The specimen can be tested in two different configurations. When the shearing force reaches a critical value, pull-out takes place and the droplet is displaced along the fibre axis. The average shear stress is calculated as the maximum force divided by the embedded fibre area.

$$\tau = \frac{F}{\pi D L} \quad (1)$$

where  $F$  is the maximum load measured prior to debonding of the fibre,  $d$  is the fibre diameter and  $L$  is the embedded length.

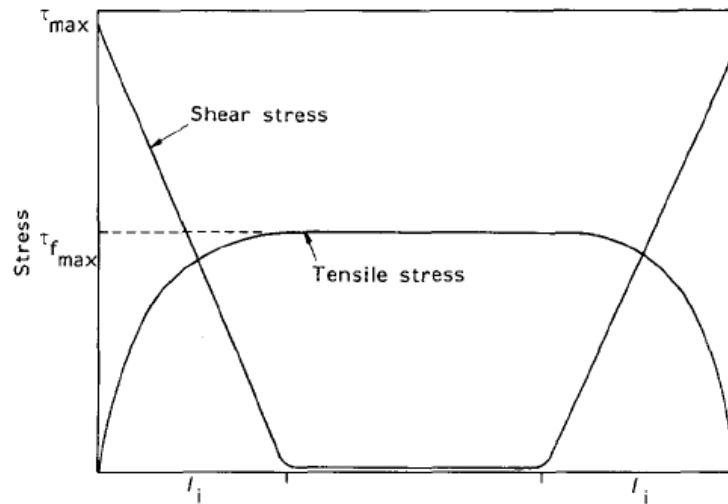


**Figure 1.4** Stress distributions for a short embedded fibre [62]

The basic assumption of the shear-lag theory is that all the tensile loads are carried by the fibre and all the shear loads are carried by the matrix, although in practice the matrix surrounding the fibre also sees some tensile stresses. The load transfer into the fibre from the matrix occurs over a length of fibre commonly called the ineffective length,  $l_i$  (Figure 1.4), which is defined when some proportion of the remote fibre load is reached. If the shear strength is calculated from Equation (1) for a fibre whose embedded length is greater than this ineffective length, then the shear strength will be underestimated. This is because a length of fibre is included over which little stress transfer is taking place. So the smaller the embedded length is the greater the estimate of the shear strength. Extending this argument the maximum shear stress will be obtained when the embedded length tends to zero, and embedded fibre length becomes too small to measure directly. However, as will be shown, it is not necessary to go to such lengths to obtain the maximum shear stress of the interface [62].

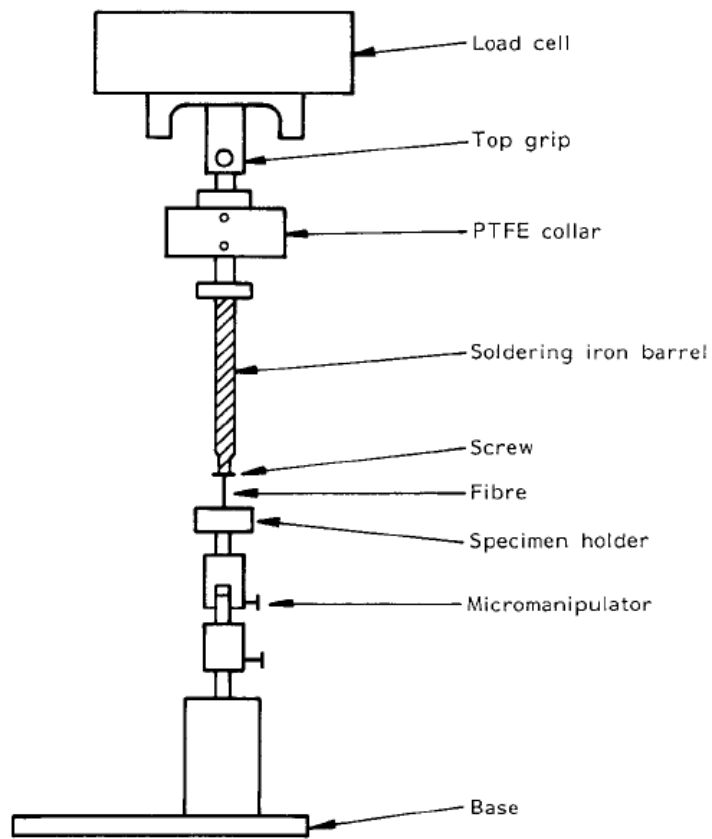


**Figure 1.5** Adaptations made to the top grip of a tensile testing machine for single fibre pull-out testing [62].

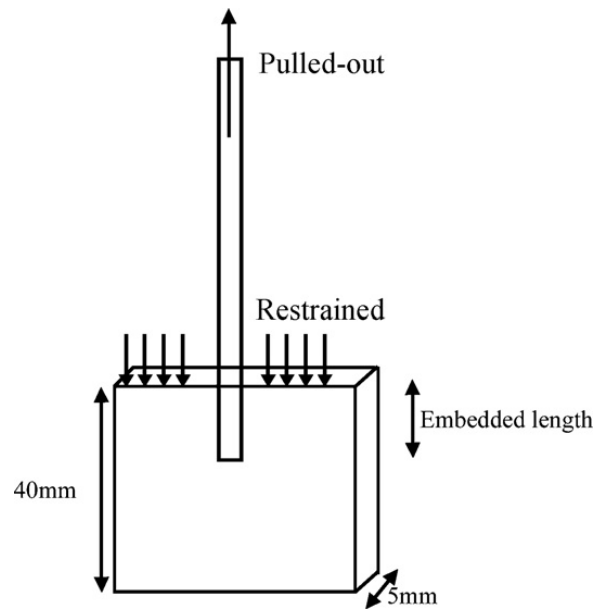


**Figure 1.6** Schematic of pull out test [50].

#### 1.4.4. Torque test

A torque method is similar to the method developed by Holloway and Walker. For this test, a small hollow, stainless steel cylinder is adhesively bonded to the surface of the test specimen. After the adhesive has cured, a larger hollow cylinder, referred to as a support table, is placed over and around the smaller cylinder. A torque wrench is attached to the top of the support table and twisted. The reading (in pound) on the torque wrench, when the small cylinder is sheared off, is then converted to pounds per square inch by dividing the reading by the bonded area. [63]

Torque tests provide good quality quantitative adhesive information. One such test was used to investigate the adhesive force at a hexamethyldisiloxane (HMDSO) gas modified polypropylene substrate. A hydrophobic polymer veneer was formed on the surface as a result of the treatment. A slotted steel stud was attached to the surface with cyanoacrylate adhesive and a torque wrench used to determine torque at failure. Shear stress (T) was calculated using the relationship,

$$T = \frac{165I}{\pi d^3} \quad (2)$$

where I is the measured torque and d the diameter of the stud . No great difference in adhesion strength was found as a function of treatment time and the failure types observed were not statistically significant [50].

#### 1.4.5. Scratch test and nanoindentation test

The scratch test is closely related to the nanoindentation test, and for simplicity, the two will be considered together. In both cases adhesion is assessed using a fine tip that is dragged across the samples surface under an increasing load, resulting in an indentation. Indentation and scratch tests are well suited to the investigation of thin films and coatings, generally producing definitive results.

Scratch test is one of the indirect methods used to test coatings adhesion to substrate. It's performed by scratching a surface with an indenter or ball to characterize the critical loads

(LC) at which failure occurs. It allows the user to determine and investigate the phenomena identified along the length of the scratch cracking deformation, delamination [64].

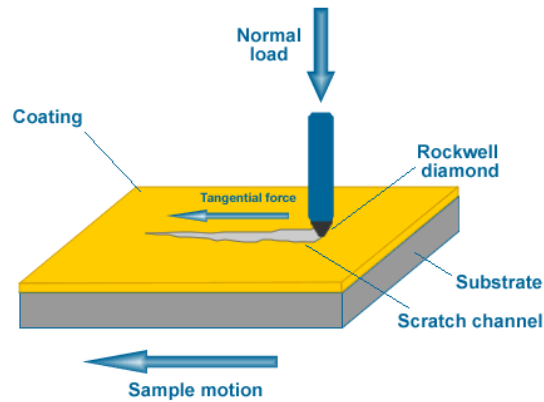


**Figure 1.7** Schematic of scratch test [64].

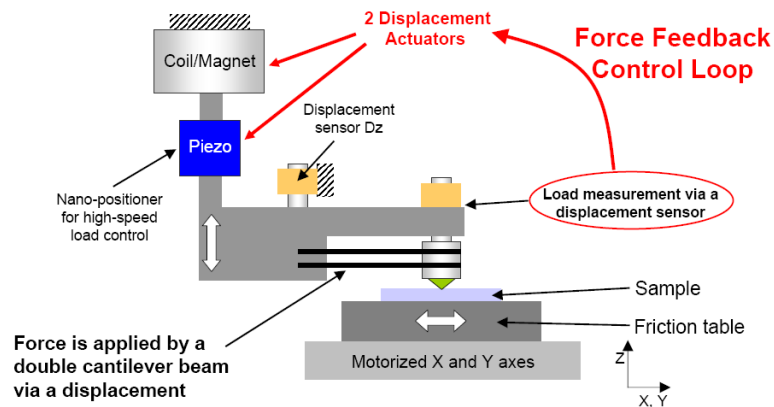


**Figure 1.8** Schematic of scratch test [64].

Nanoindenting is a new method to characterize material mechanical properties on a very small scale. Features less than 100 nm across, as well as thin films less than 5 nm thick, can be evaluated. Test methods include indentation for comparative and quantitative hardness determination and scratching for evaluation of wear resistance and thin film adhesion [78]. A prescribed load is applied to an indenter in contact with a specimen. As the load is applied, the depth of penetration is measured. The area of contact at full load is determined by the depth of the impression and the known angle or radius of the indenter. The hardness is found by

dividing the load by the area of contact. Shape of the unloading curve provides a measure of elastic modulus [64].

Nanoindentation has been used to investigate surface properties such as hardness and coating delamination force for polymers. In the exploratory work by Beake *et al.*, [65] nanoindentation was applied to thermoplastic materials (for example plasma-polymerized hexane films) which were, in general, harder and stiffer than general thermoplastics.

Failure mechanisms for polymer systems have also been used in scratch tests to explain surface condition. In a study between a gelatin coating and nitrogen plasma-treated PET surface, it was found that the failure mechanism was dependant on a series of interactions between the indenter and the coating. The study also supplemented the previous work carried out by Ochi *et al.* [66] and others in that they found that the critical load increased as a function of nitrogen plasma treatment time.

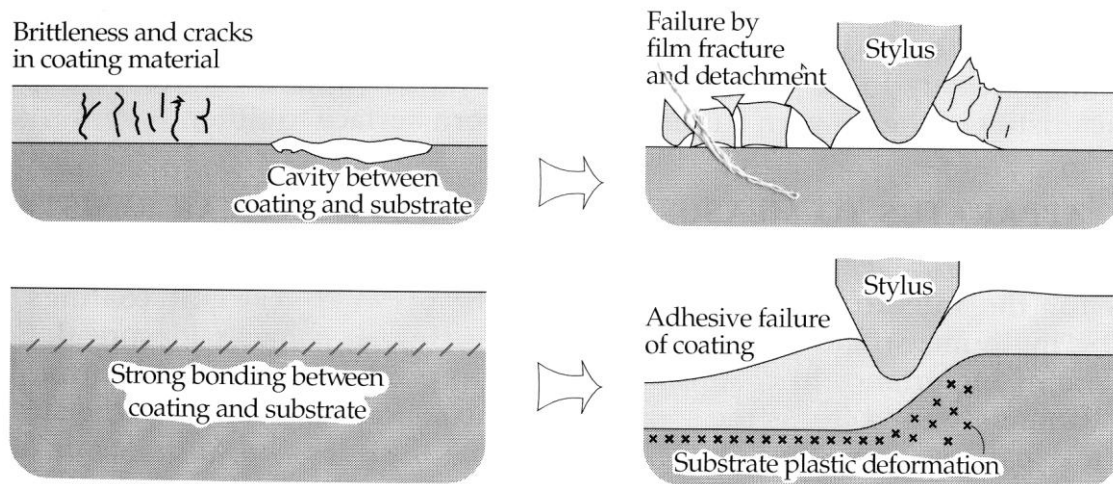


**Figure 1.9** Schematic illustration of the principle involved in scratch test of wear resistant coatings. [64]

The outcomes from indentation tests are sometimes dependant on the interactions between the indenter and the coating. Finite Element Analysis (FEA) has been used to normalise the effect the geometry of the tip has on the results by only considering the stress and not the load applied to the coatings. One such study using FEA was the investigation of



acrylic polymers coated on steel substrates. In this study it was concluded that the scratch behavior of coatings can be evaluated in a manner similar to bulk polymers.

Jardet and Morel [67] analyzed scratch parameters that relate to mechanical properties. They reported a correlation between the tensile stress-strain behaviour and scratch fracture toughness for poly(methylmethacrylate) (PMMA). Modifying the scratch test to measure not only the normal force range but also the tangential forces simultaneously allows for a complete tribological approach to surface characterization, in as much that the energy which is dissipated in the scratching process can also be measured. One such approach was undertaken by Wang and Lim who found that in a tungsten carbide (WC) particle and polymer system, the coatings containing the WC showed greater hardness and scratch resistance when compared to the pure polymer coating values.

#### 1.4.6. Pull off test or Stud/butt test

This method is used widely to test the adhesion of coatings to substrates and is also used to assess adhesives. The test is attractive as it is quick and simple to perform, requires low cost equipment and produces a quantified measure of the adhesive strength from the maximum force applied to the sample. It is critical in using the test that failure does not occur at the interface between the aluminum stub and the adhesive. The test gives good repeatability and can differentiate between good and bad surface treatments. In the case of good surface preparation, the failure tends to be cohesive in the adhesive with much greater levels of adhesion failure seen with poorer surface treatments [68].

Pull off tests, commonly known as a stud or butt test, are used to measure adhesion between a substrate and an ink or paint coating. An adhesive is applied to the paint coating and a metallic stud (aluminium) is glued onto the surface. A force is then applied perpendicular to the surface of the substrate at a constant rate. **Figure 1.10** illustrates the test schematically. The pull off test provides a superior adhesion measurement for systems such as polymer–metal interfaces.

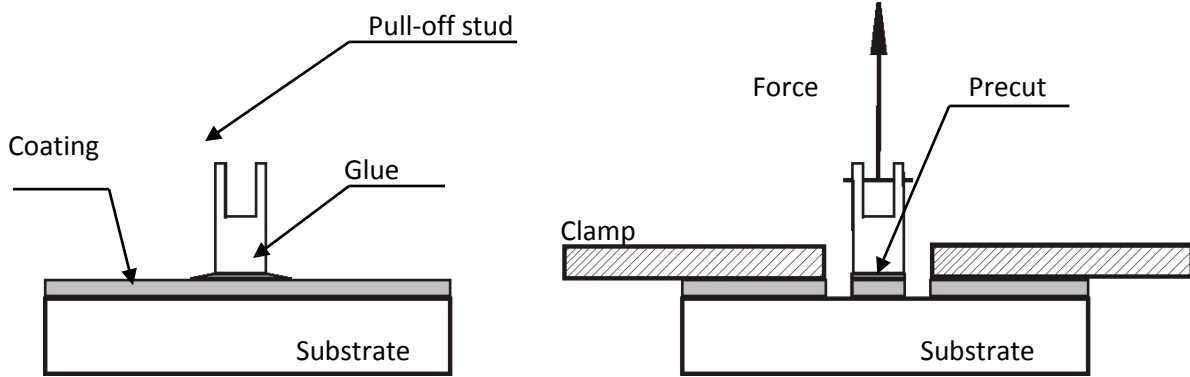


**Figure 1.10** Schematic drawing of the pull-off test specimen and b) drawing of the pull-off test specimen, with a precut, in the clamping system [69].

The pull off test is not limited to the automotive and electronic sectors. It has been applied to integrated circuits. In the work by Chiang and Hsieh, it was found that the pull off test was able to show that the adhesion strength of a resin decreased with an increase of the inorganic filler (hexagonal boron nitride hBN). The pull off test has been used directly to assess the adhesive bond strength at metal and polymer interfaces, for example in printed circuit boards. Turunen *et al.* [70] showed using pull off testing that an adhesion promoter substantially increased the durability at coating/copper interfaces.

In the development of high speed broadband services, there has been a growing interest in metal/smooth polymer composites especially the need for an improvement in their adhesive properties. Liu *et al.* found that adhesion strength of integrated circuit could be characterized using a combination of XPS and stud pull off test experiments. In model studies of epoxy/electroless copper systems, it was found that the pull off test values based on the schematic in scheme 10 correlated well with the contact angle results (in particular the polar component of the surface free energies) and XPS results [50].

The pull off test in conjunction with contact angle analysis and XPS has also been used in the investigation of the interface of polypropylene and spherical glass particles. It was found that adhesion strength was greater when the polypropylene surface was treated with hydrocarbon functional groups as opposed to fluorocarbon groups.

### 1.4.7 Wedge test or Cleavage Tests

Cleavage is also a simple means of measuring the fracture energy of an adhesive. In the cleavage test (often referred to as the Boeing wedge test following the work of Marceau *et al.* at Boeing) two metal plates are bonded by the adhesive under consideration, following the recommended procedure [71].

The Boeing wedge test is a commonly utilized method to test the durability of fractured and stressed adhesive joints when exposed to different environments [72]. This fracture test is an ASTM standard (ASTM D 3762) and utilizes a mode I specimen configuration (**Figure 1.11**). The test consists of creating an initial crack by inserting a wedge, and then following the propagation of the crack with time. The driving force for the propagation of crack comes primarily from the stiffness of the beams separated by the wedge and this driving force decreases as the crack propagates. It is important to note that in this test the cracked specimen also experiences simultaneous environmental attack at the crack site (when the specimens are placed in that environment). Upon introduction of the wedge, the crack propagates to length ‘a’. This results in creation of two new surfaces (each of area A), and release of elastic energy stored in the beams. If this released elastic energy by the beams is given by  $U_E$  and the energy to create the two new surfaces is given by  $U_S$ , then:

Release rate of elastic energy is given by, 
$$G = \partial U_E / \partial A \quad (3)$$

Energy needed to create a unit surface [84] is, 
$$W_s = \partial U_s / \partial A \quad (4)$$

The crack propagation stops when  $G=W_s$  (this is also known as Griffith’s criterion)[85]. Till ‘G’ is higher than  $W_s$ , the crack continues to propagate. The value of G, also known as the strain energy release rate (the ‘rate’ refers to ‘release of energy per unit area’ and not ‘release of energy per unit time’) is calculated to be,

$$G = \frac{3Et^3h^2}{16a^4} \quad (5)$$

where, E = young’s modulus of the beam

t = thickness of the beam

$h$  = wedge thickness

$a$  = crack length

An important assumption in this test is that adherends should not deform plastically. This is usually not a problem when using thick and stiff adherends like the ones utilized in the present study. The decreasing effective cleavage load results in the crack stopping at some equilibrium value, the value itself depends upon the system conditions. Any contributions due to the viscoelastic properties of the adhesive are not taken into account in the above calculations [74]. One of the disadvantages of the wedge test is that it is often necessary to remove the specimens from the test environment to make crack length measurements. Also, the cracks may not be easy to view or may propagate unevenly across the specimen width. The wedge test may test the adhesive strength or cohesive strength depending upon whether the crack propagates on the adhesive interface or purely in the polymer itself (cohesive failure). This test is widely utilized when comparing different surface treatments, especially when the mode of failure is interfacial.

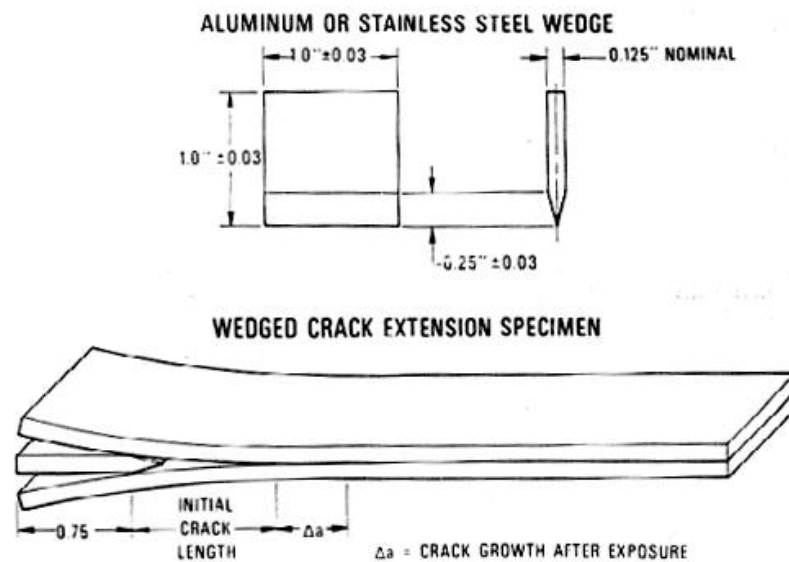


**Figure 1.11** Specimen configuration for the wedge test [73]

Several adhesion tests are proposed to quantify the adherence level. The wedge test could be well appropriate to measure polymer/metal adhesion.

## 1.5. Metal- polymer adhesion

Metal and polymers require strong bonding under two entirely different applications: (1) to form structural components and (2) to metallize polymeric substrates. For structural components, polymers serve as adhesives or binders for metals adherends. For metallization, a metal film is either deposited from a solution or in vacuum on a polymer substrate [74].

### 1.5.1 Classification of Polymers According to Their Wettabilities

In comparison with metals and metal oxides, all polymers are low surface energy materials, and surface energies range usually between 10 and 50 mJ / m<sup>2</sup>. Polymers according to their wettabilities (which are indirectly determined as Zisman's critical surface tension,  $\gamma_c$  ) into three classes:

1. low wettability ( $30 \text{ mJ} / \text{m}^2 > \gamma_c > 10 \text{ mJ} / \text{m}^2$ ) :  
Most fluoropolymers, polysiloxanes and polyolefins, etc.
2. Medium wettability ( $40 \text{ mJ} / \text{m}^2 > \gamma_c > 30 \text{ mJ} / \text{m}^2$ ) :  
Most vinylpolymes, e.g., poly(vinyl acetate), poly(styrene), poly(vinyl chloride), poly(ethyl acetate), poly(methyl methacrylate), etc.
3. High wettability ( $\gamma_c > 40 \text{ mJ} / \text{m}^2$ ) : Most condensation polymers, e.g. poly(carbonate), polyesters, nylons, epoxy resins, etc.

L.H. Lee [74] separately discuss metal-polymer adhesion according to the above three classes. Rubbers are also of either low or medium wettability and rubber-metal adhesion was discussed separately in the last section partly because the applications of rubbers are not for metallization under vacuum conditions.

## 1.5.2 Metal Adhesion to Low Wettability Polymers

- **Fluoropolymers**

For thick polymer films, the adhesion between metals and fluoropolymers is generally poor. Thus, several conventional surface modification techniques have been used.

For polytetrafluoroethylene PTFE ( $\gamma_c = 18-18.5 \text{ mJ/m}^2$ ) only the surface region is attacked by sodium naphthalene, as indicated by the color change. For the treated fluorinated ethylene-propylene copolymer FEP, Dwight and Riggs [75] have shown with ESCA the presence of unsaturations,  $> \text{C}=\text{O}$  and  $-\text{COOH}$  groups. The observed increasing wettability is due to the presence of a very thin layer of materials with the characteristics of an oxidized hydrocarbon.

The surfaces of fluoropolymers can be abraded [76] to increase mechanical interlocking. After PTFE is abraded, it can be bonded to it self and to Al. The improved adhesive strength is attributed to surface de-contamination and mechanical activation through some mechanochemical process which, in turn, can generical free radicals on the PTFE surface.

Chemical modification of the FEP surface by several metals during the deposition presents some new possibilities in improving the adhesion between thin films of fluoropolymers and metals. Lee in his review [74] presents several works on modification of polymer surface to improve adhesion of metal by deposition. The importance of both chemical and physical factors has been demonstrated. Pretreatment by reactive gas such as  $\text{O}_2$  and  $\text{CF}_4/\text{O}_2$  of PTFE surface, irradiations such as electron high - energy ion irradiations, glow discharge, increase the adhesive strength between the polymer and metal films.

Indeed, the type of metal does affect the adhesive strength between metal and PTFE. Vogel and Schonhorn have found that the tensile shear strengths of the evaporated metal films follow a decreasing order:

$$\text{Ti} > \text{Fe} > \text{Ni} > \text{Al} > \text{Au} > \text{Cu}$$

This result appears to correlate with free energy  $\Delta G_f$  and heats of formation  $\Delta H_f$  of fluorine compounds. The more negative the  $\Delta H_f$  (or  $\Delta G_f$ ), the more reactive metal is [74].

- **Polyolefins**

The adhesion between metals and thick films of polyolefins is generally poor because of low wettability and the lack of reactive groups or oxygen on the surface to achieve acid-base interaction or chemical bonding. For thick films, several common methods have been used to enhance adhesion [74].

Mechanical factors have been shown to be significant for the adhesion of low density polyethylene PE ( $\gamma_c = 29 \text{ mJ} / \text{m}^2$ ) to Al. The polymer enters the porous anionic film and creates a mechanical keying action. For electroplating the polymer (e.g. polypropylene, PP,  $\gamma_c = 29 \text{ mJ} / \text{m}^2$ ) surface is usually etched for metal ( e.g., Cu) coating. However , mechanical inter locking is not enough for achieving optimum adhesion; an additional chemical reaction between stannous ions and Cu to generate polar groups on the PP surface is needed to produce a better result.

Two commonly used methods for improving the adhesion between metals and polyolefins are corona discharge treatment (CDT) and flame treatment (FT). These treatments lead to formation of peroxides, hydroxyl, epoxy, hydroperoxy, carboxylic acid and carbonyl groups on the corona discharge treatment on PE surface. For the sample treated with CDT of an energy greater than  $4000 \text{ J/m}^2$ , water washing can only remove 10% of incorporated oxygen. Moreover, homogeneous oxidation reaches approximately  $50 \text{ \AA}$  below the polymer surface.

The flame treatment (FT) can oxidize PE surface to a depth of 40 to  $90 \text{ \AA}$  comparable to the CDT-PE surface. The oxidized surface can remain unchanged for as long as 12 months. The oxidized products on the surface are  $-\text{OH}$ ,  $-\text{C}=\text{O}$  and  $-\text{COOH}$ , with a first step producing hydroperoxide. The surface polarity is relatively more sensitive to the presence of the  $-\text{COOH}$  group [74].

For thick films, the presence of an acidic functional group on the polyolefin surface is known to enhance adhesion, presumably through the acid- base interactions.

The principles involved in the adhesion enhancement of thick film polyolefins can be readily extended to that of thin films. For example, the adhesion of Al/PE has been studied in parallel to that of Al/polyacrylic (PAA). Reactions have been postulated by DeKoven *et al*

[77] to occur at both C—O and C—C linkages with Al oxide to form carbide-like species as the final product.

Surface treatments of thin-films polyolefins with ion beam, electron beam, and plasma bombardment can enhance adhesion to metals. Without bombardment various metals yield different adhesive strengths: high for Ti, Ni, and Cr but low for Al, Cu, Ag, and Au films. Similar to PTFE, the adhesive strengths, in terms of tensile strengths, vary with metals according to the following decreasing order.

$$\text{Fe} \approx \text{Ni} > \text{Ti} > \text{Al} > \text{Au} > \text{Cu}$$

When the HDPE films are *in situ* Ar-ion bombarded, the adhesion to all metal films, except Ag and Au, increase more rapidly than the cohesive strength of HDPE. The ion bombardment presumably creates an activated and crosslinked PE surface as revealed by XPS.

The surface modification with plasma can also be applied to PE for enhancing its adhesion to metals. The adhesive strength of the vacuum-deposited Ag on PE increases in the following order: untreated < Ar-plasma, O<sub>2</sub>-plasma < N<sub>2</sub>-plasma treated PE. Chemical interactions have been manifested by identifying the Ag—O—C and Ag—N—C species with XPS. These species presumably act as nucleation and chemical reaction sites.

- **Polysiloxanes**

Poly(dimethyl siloxane), PDMS ( $\gamma_c = 24 \text{ mJ} / \text{m}^2$ ), is another low wettability polymer. Bodö and Sundgren [78] have studied the effect of surface modification of PDMS on its adhesion to Ti. Two pretreatment methods have been used: (1) Ar<sup>+</sup> bombardment and (2) O<sub>2</sub>-plasma treatment. Both methods lead to crosslinking of the surface and an increase in the polymer strength. The XPS results indicate the presence of Ti—C and Ti—O bonds, respectively. The ion bombardment of the polymer film also tends to affect the crystal growth of Ti from a three- dimensional to a two- dimensional mode.



### 1.5.3 Metal Adhesion to Medium Wettability Polymers.

Polymers with a critical surface tension between 30 and 40 mJ / m<sup>2</sup> may be considered to be of medium wettability. In this group, there are mostly vinyl polymers as shown in **Table 1.1**.

**Table 1.1** Medium Wettability Polymers <sup>a</sup>

Polymer	Abbreviation	$\gamma_c$ (mJ / m <sup>2</sup> )
Poly(vinyl methyl ether)	PVME	29-30
Poly(propylene oxide)	PPO	32
Poly (ethyl methacrylate)	PEMA	33
Poly(ethyl acrylate)	PEA	33-35
Poly(styrene)	PS	33-36
Poly(vinyl acetate)	PVAc	37
Poly(vinyl alcohol)	PVA	37
Poly(methyl methacrylate)	PMMA	39
Poly(vinyl chloride)	PVC	39
Poly(vinylidene chloride)	PVCl <sub>2</sub>	40

<sup>a</sup> From L.H. Lee, *J.Appl. Polym. Sci.* **12**, 719(1968)[74]

One of the metal-electroplated plastics is the ABS(acrylonitrile-butadiene-styrene) copolymer. Morphologically, the copolymer is a two- phase material. During the solution etching of the copolymer, the grafted rubber particles are dissolved out to leave spherical holes behind. The activation and chemical deposition of the metal takes place predominantly inside the wall of those holes. The filling of those holes with metal is the major step of electroplating. Thus, the mechanism involved appears to be mechanical interlocking. However, a chemical activation step is necessary to catalyze the deposition of Ag<sup>+</sup>, Pd<sup>2+</sup>, or Sn<sup>2+</sup> on the inner wall surface. The final step is the electrodeposition of Cu or Ni metal. Other

polymers, e.g., modified polypropylene (PP) and modified poly(phenylene oxide) (PPO), have also been electroplated.

Thin films of ABS polymer can also be electroplated without electroless plating. A Cu thin film has been reported by Tsukada and Hosokawa [79] to deposit on the ABS polymer by an internal-magnet magnetron sputtering system. Oxygen-plasma treatment of the polymer surface improves the adhesion, presumably owing to the change of topography and to chemically modified surface as detected by ESCA analysis.

Burkstrand [80] has established that the adhesion between styrene and metals can be achieved by oxidation of the polymer. His results indicate that a metal complex of the M—O—C type is responsible for the increase in adhesive strengths to Cu, Ni, or Cr.

Later, Burkstrand [81] concluded that if a polymer already contains an oxygen it is not necessary to oxidize the polymer and form the complex. For example, in the case of polyvinyl alcohol (PVA), a similar complex to that in the oxidized polystyrene has been identified at the interface as with other oxygen-containing polymers, e.g. poly(ethylene oxide) (PEO), poly(vinyl methyl ether) (PVME), poly(vinyl acetate) (PVAc), and poly(methyl methacrylate) (PMMA).

#### 1.5.4 Metal Adhesion to High Wettability Polymers.

Most condensation polymers and some vinyl polymers with a critical surface tension  $>40$  mJ/m<sup>2</sup> can be considered to be of high wettability. These polymers are presented in **Table 1.2**. In general, the adhesion of these polymers to most metals is good, though their surface energies are still much lower than those of oxides and metals. The wettability is still a problem if a metal is deposited on a solid polymer. On the other hand, if a molten polymer is coated on a solid metal, a spontaneous wetting should result.

**Table 1.2** High Wettability Polymers <sup>a</sup>

Polymer	Abbreviation	$\gamma_c(\text{mJ}/\text{m}^2)$
Poly(carbonate)	PC	42
Poly(6-aminocaproic acid)	Nylon 6	42
Poly(ethylene terephthalate)	PET	43
Poly(acrylonitrile)	PAN	44
Poly(hexamethylene adipamide)	Nylon 6, 6	46
Epoxy resins	Epoxide	43

<sup>a</sup> From L.H. Lee, *J. Appl. Polym. Sci.* **12**, 719(1968) [74]

As in the case of surface modification of polyolefins, corona discharge treatment (CDT) has been a common practice for improving the adhesion of thick films of PET. Lederer *et al.* [82] have observed the effect of corona treatment on chemical and physical changes on the PET surface. The chemical change is determined as the increase in polarity by the adsorption of radioactive calcium ions and by the contact angle on the surface. An increase of functional groups has been estimated to be approximately  $2 \times 10^{13}$  sites/cm<sup>2</sup>. Briggs *et al.* [83] have identified with XPS the reactive groups of -OH and -COOH on the PET surface. Pochan *et al.* [84] have demonstrated that about 4% of O<sub>2</sub> is added to the PET surface with dry-air corona and 75% of the oxidation products are hydroperoxide, epoxy, hydroxyl, carboxylic, and isolated carbonyl species. Both chemical and physical factors serve to enhance the adhesion of metals to CDT - PET.

For the adhesion between Ni and polyacrylonitrile, Boiziau *et al.* [85] concluded that the monomer, acrylonitrile, VCN, can graft onto Ni to form PAN. This graft polymerization assumes a form of the acid-base interaction between the monomer and metal surface. Monomer is presumably adsorbed on the metal surface by anchoring both the double bond and the nucleophile (C=N) and then the polymerization takes place by stabilizing interfacial bonds.

Polyimides are versatile high-temperature polymers which have been used for both thick-film and thin-film applications. For thick-film coating, the internal reflectance IR spectroscopy or Mössbauer technique have been used to study the interaction between Co and

polyimide. The results indicated polyimide bonds to the cobalt substrate by means of carboxylate groups with  $\text{CO}^{2+}$  ions in the oxide film at the interface [74].

Chou and Tang [86] have employed XPS to study the interactions between metals and thin polyimide films during the metallization in UHY. The results indicate that Cr and Ni react with the pendant oxygen on the polyimide surface but Cu and Ag do not.

Among metal-polyimide reactions, the interaction involving Cr is the most well studied. Chromium is one of the more reactive transition metals, and the chemical interaction has been identified to be the formation of a charge-transfer complex between Cr and not the carbonyl group but the  $\pi$  system of the PMDA (pyromellitic dianhydride-oxydianiline) unit of polyimide. Recently Lee has postulated an acid-base interaction [74].

Different works have studied the reactions between polyimide and several reactive metals. All concluded to a reactive of metal with the  $-\text{C}=\text{O}$  group of polyimide leading to stronger M-O bonds complexes.

Following the general trend in metal reactivities, Cu and Au are also unreactive with PI. However, as a component part for microelectronics, Cu is more attractive partially due to its lower cost than most metals. Thus, there has been a great deal of work toward achieving the adhesion between Cu and PI.

One of the methods involves the oxygen-reactive ion-beam bombardment of the polymer surface. The adhesive strength can be increased by a factor of 25. A second method is to apply a thin Cr interlayer to adhere Cu and PI together [74].

The above difficult bonding situation can be completely reversed, if polyimide is deposited on Cu from solution. First of all, wetting is favored by placing a lower surface tension liquid on a high surface energy solid. Chambers *et al.* [87] have shown that an oxide layer of CuO is formed at the interface about one hour after the coating. CuO can enhance the acid-base interaction by raising the acid strength of Cu resulting in a higher.

### 1.5.5 Metal-Rubber Adhesion

Like vinyl polymers, most rubbers are of low to medium wettability (**Table 1.3**), thus they are difficult to adhere to metals. To achieve metal-rubber adhesion, the rubbers have to be modified through chemical reactions with halogens, or cyclization, or copolymerization with polar monomers, e.g., those containing cyano- or carboxylic acid groups. For example, after poly (1, 3-butadiene) is transformed into poly (2-chloro-1,3-butadiene), the wettability increases from 31 to 38 mJ/m<sup>2</sup> [74].

**Table 1.3** Wettabilities of Rubbers<sup>a</sup>

Rubbers	Abbreviation	$\gamma_c$ ( mJ / m <sup>2</sup> )
Isobutene-isoprene copolymer	Butyl	27
Ethylene-propylene rubber	EP	28
Poly(isoprene), trans	PIP (trans)	30
Poly(1,3-butadiene). trans	PB (trans)	31
Poly(isoprene), cis	PIP (cis)	31
Poly(1,3-butadiene), cis	PB (cis)	32
Styrene-butadiene copolymer (25:75)	SBR	33
Cyclized poly(isoprene)	-	34
Poly( epichlorohydrin)	-	35
Rubber hydrochloride	-	36
Chlorosulfonated polyethylene	CSPE	37
Butadiene- acrylonitrile	BN	37
Chlorinated poly(isoprene)	-	37
poly(isoprene) Chloroprene	-	38

<sup>a</sup> From L.H. Lee, *J. Polym. Sci. A-2*, **5**, 1103(1967) [74]

- **Natural Rubber Steel- Adhesion**

During the last forty-five years, the adhesion between natural rubber (NR) and brassplated steel (for the steel cord tire application) has been well studied. Without the plated brass, there is no adhesion between NR and steel (**Table 1.4**). Interestingly, sulfur, the crosslinking (or vulcanizing) agent in the NR, actually also functions as the crossbridging agent between NR and brass to form the  $\text{Cu}_x\text{S}/\text{ZnS}$  interphase. In the model (**Figure 1.12**), the brass develops a strong adhesive bond to NR through the in situ growth of a thin (50 nm) copper sulfide film on the brass surface before crosslinking sets in. Since this sulfide film is porous, the rubber chains become entangled throughout this film.

**Table 1.4** Adhesion of Various Materials to Natural Rubber <sup>a,b</sup>

Material	Adhesion level <sup>d</sup>	Interface	Remarks
Iron, steel	0	-	No adhesion
Copper	0	Excess $\text{Cu}_2\text{S}$	Some adhesion if undercured
Copper-plated steel <sup>e</sup>	700 - 900	-	Good adhesion if thickness < 50nm
$\text{Cu}_2\text{S}$ – coated steel <sup>f</sup>	700 – 800	-	Good adhesion with fresh $\text{Cu}_2\text{S}$
Zince	100 – 200	Some $\text{ZnS}$	Poor adhesion
Copper-plated zince <sup>e</sup>	700 – 800	$\text{Cu}_2\text{S}$	Good adhesion if thickness <50 nm
Brass 70/30	700 - 1200	$\text{Cu}_2\text{S}$ and some $\text{ZnS}$	Good adhesion depends on surface preparation

<sup>a</sup> From W. 1. van Goij, Rubber Chern. Techno/. 52,605(1979).[74]

<sup>b</sup> Compound of type A; cured 25 min at 150°C.

<sup>c</sup> Sheets of 0.5 mm thickness.

<sup>d</sup> N/64 mm<sup>2</sup>.

<sup>e</sup> Electroless immersion plating.

<sup>f</sup> Copper-plated steel sulfidized by S in paraffin.

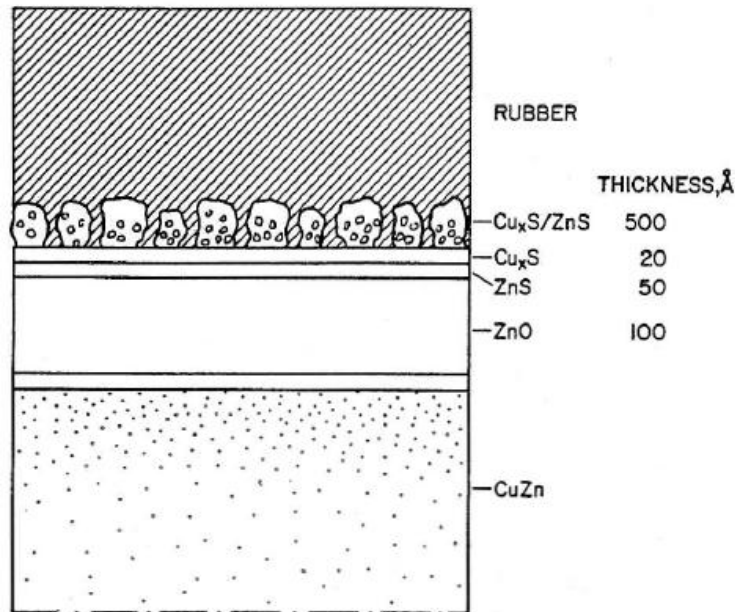


**Figure 1.12.** Schematic of interfacial sulfide in natural rubber-brass bonding showing mechanical interlocking [74].

- **Natural Rubber – Nickel Alloy Adhesion**

In the last several years, a new coating containing one of Ni-Cu-Zn alloys has been developed to replace the brass coating. These ternary alloys are less sensitive to dezincification than ordinary brass. Furthermore, these alloys do not form a conducting oxide layer and, consequently, the formation of the  $\text{Cu}_x\text{S}$  layer can be suppressed. The formulation of these alloys can affect adhesion. For example, the optimum Co content is approximately between 0.05 and 0.2 phr (part per hundred of the metal). In the rubber formulation, 4 phr of the insoluble sulfur gives a good overall performance [74].

In brief, the ternary alloy-coated cord can equal and, in the case of salt water immersion, surpass the adhesion of low copper content brass-coated cord. Therefore, the use of ternary alloys should be one of the important developments for the future tire cord technology.

- **Polybutadiene-Cobalt Interaction**

The interaction between polybutadiene (PB) and cobalt has been studied by Leidheiser *et al.* with the  $^{57}\text{Co}$  emission Mössbauer technique. The results indicate that the interfacial contact is through a layer of oxide and hydrous oxide, and the oxide on Co does not thicken during the baking process. On the steel side, the thermal treatment at 200°C causes a significant amount of conversion of  $\text{Fe}^{3+}$  to  $\text{Fe}^{2+}$  at the oxide coating interface. The latter part of PB/Fe reaction has been verified by Watts *et al.* In this case, PB acts like a reducing agent [74].

## 1.6. Chemical structure of Natural Rubber based adhesives

In spite of its limited resistance to oxidation and to a wide range of chemicals and solvents, and poor ozone and weathering performance, Natural Rubber (NR) is the most widely used material for adhesive applications, particularly for pressure-sensitive adhesives (PSA) mainly because it presents a high initial tack and good strength. Tackifier resins may be added to increase oxidation and heat resistance and to improve wetting properties. Moreover, the chemical modification of NR has been widely considered as a way to compensate these drawbacks. Among the modified NR products, we focus this part on graft and block copolymers with polar polymers and Epoxidized Natural Rubber (ENR) which can improve adhesion of NR adhesives on polar surfaces.

### 1.6.1. Natural Rubber based adhesive blends

Leong *et al.* [88] described the viscoelastic properties of NR pressure-sensitive adhesive using acrylic resin as a tackifier. The acrylic resin prepared by free radical polymerization, was blended with the rubber in various ratio. The authors found that the shear and peel strengths increased as the percentage of acrylic tackifier increased up to a maximum at 40%. The blends with increasing peel and shear strengths (10 to 40% acrylic resin in NR) have low shear storage modulus. This shows that the adhesive samples have good wetting properties at bonding. Fujita *et al.* [89] have studied the effects of miscibility and viscoelasticity on shear creep resistance of NR based pressure sensitive adhesives. They found that the shear creep of miscible pressure sensitive adhesive systems tended to decrease as the



tackifier content is increased, whereas the shear creep of an immiscible adhesive system varies with the tackifier used.

The more studied adhesives from modified NR are the ENR-based materials.

### 1.6.2. Epoxidized Natural Rubber based adhesive blends

C. Nakason *et al.* [90] have described the use of ENR for para rubber wood particleboard instead of the formaldehyde based resins. The adhesion was improved by reducing the molecular weight of ENR. This may be attributed to the greater ability of the lowest molecular weight ENR ( $1.10 \times 10^5 \text{ g.mol}^{-1}$ ), to wet or cover the wood particle surfaces.

Poh *et al.* have performed some studies on the adhesion behavior of Epoxidized Natural Rubber-based pressure sensitive adhesives. They described the peel and shear strength of pressure sensitive adhesives prepared from ENR25 and ENR50 (having 25 and 50% of epoxidation) [91], and from SMR10/ENR25, SMR10/ENR50 and ENR25/ENR50 blends [92]. Coumarone-indene resin was used as tackifier. Results show that maximum peel strength occurs at 40 phr of tackifier for both ENRs. ENR25 consistently indicates higher peel strength and shear strength than ENR50 because of the greater flexibility and compatibility with resin in the former. Generally, peel and shear strength increases with coating thickness. They have also investigated effects of different fillers such as zinc oxide [93], calcium carbonate [94] and silica [95] on adhesive properties of ENR-based adhesives. They found a maximum value of 40 phr for zinc oxide, 30 phr of calcium carbonate and 40 phr for silica corresponding to the maximum wettability and compatibility of adhesive on the substrate at the respective filler loadings. In addition, they have studied the effect of molecular weight of ENR on the shear strength, loop tack and viscosity of ENR based pressure sensitive adhesives [96-99]. They found that shear strength and loop tack increase with increasing molecular weight of ENR until optimum values of  $6.63 \times 10^4$  and  $4.14 \times 10^4$  for ENR25 and ENR50 respectively.

### 1.6.3. Graft and block copolymers

Another way to enhance polarity of NR for adhesives application were the graft and block copolymerizations with polar polymers.

In the technology of rubber, Heveaplus MG rubbers are used for adhesives application. They are made by polymerizing methyl methacrylate in the presence of natural rubber latex. The polymethylmethacrylate (PMMA) chains are thereby grafted to the rubber molecules. Two commercial grades are available: MG 30 and MG 49 containing 30% and 49%, respectively, of PMMA. The solutions of Heveaplus MG are used as adhesives or bonding agents to bond rubber to polyvinyl chloride (PVC), leather, textiles and metals.

The graft copolymerization of MMA onto NR has been performed by free-radical polymerization in solution [100] or latex states [101-103]. The effects of the initiator concentration, reaction temperature, monomer concentration and reaction time on the monomer conversion and grafting efficiency were investigated. The authors focus on thermoplastic elastomers applications, and improve mechanical properties and compatibility of the blends of NR and PMMA by addition of this graft copolymer.

Block copolymers have also great potential for specialty and high-technology applications as thin films, adhesives, and surfactants. Particularly the Styrene-Isoprene-Styrene (SIS) block copolymer is widely used in pressure-sensitive adhesive formulations. Kim *et al.* [104] described the effect of substrate and tackifier on peel strength of SIS-based hot-melt pressure-sensitive adhesives. High peel strength was observed in the case of stainless steel and glass substrates. Medium peel strength was observed with Bakelite, PVC and PP, and low peel strength in the case of PE and Teflon surfaces. Ni *et al.* [105] studied the influence of the PI block microstructure in the triblock copolymer poly(styrene-*b*-isoprene-*b*-styrene) on the dynamic wetting behaviors. It was found that the receding contact angle ( $\theta_r$ ) of SIS containing 3,4-units was far higher than that of SIS with 1,4-units. This demonstrates the possibility to modulate the surface structure and properties of SIS by adjusting the chemical structure of polyisoprene segments.

## 1.7. Conclusion

In this bibliographic part, we have survey general theories of adhesion, and the different techniques used to characterize the surfaces properties and the adhesion strengths. The optical contact analysis is a simple technique allowing to know the wetting of a surface and so to access to its potentiality of adhesion. We have employed this method to characterize the synthesized polymers. Among the different techniques of direct adhesion measurement described in this part, we have selected the wedge test because it is well adapted to rigid substrate such as steel, and also easy to perform.

The Natural Rubber is a choice material for adhesive properties because it has a natural good tack property and because it comes from a renewable resource. As seen in the literature, the adhesion properties of NR may be enhanced by increasing the polarity of its chemical structure. We have choose the simple and well known epoxidation reaction at different level to modified the polarity of the hydroxytelechelic polyisoprene used to synthesize the NR-based polyurethane which may be the based adhesive formulation of our work. Short bibliographic parts will be presented at the beginning of the next chapters about the hydroxytelechelic polyisoprene and the polyurethanes used for adhesive formulations.

## References

- [1] N. Marhmoood. *Investigations on the Adhesion of Polyurethane Foams on Thermoplastic Material Systems*. **2005**.
- [2] K. L. Mittal, *Adhesion measurement of films and coatings*, VSP, Utrecht, **1995**, 5
- [3] P. Benjamin, C. Weaver, *Proc. Roy. Soc. A*, **1961**, 261, 516.
- [4] A. J. Kinloch, C. C. Lau, J. G. Williams, *Int. J. Fracture*, **1994**, 66, 45.
- [5] C. Poisson, V. Hervais, M.F. Lacrampe, P. Krawczak. *J. Appl Polym Sci*, **2006**, 101(1), 118.
- [6] R. F Charles. *Handbook of Wood Chemistry and Wood Composites*, **2005**, 221
- [7] R-Y. Qin, H.P. Schreiber. *Colloids and Surfaces*, **1999**, 156, 85.
- [8] A. J. Kinloch, *J. Mater. Sci.*, **1980**, 15, 2141.
- [9] K. W. Allen, *Int. J. Adhes. Adhes.*, **1993**, 13, 67.
- [10] D. E. Packham, *Adhes. Aspects Polym. Coat. Proc. Symp.*, 1, Plenum Press, New York, NY, **1983**
- [11] D. E. Packham. and C. Johnston, *Int. J. Adhes. Adhes.*, **1994**, 14
- [12] H.R. Brown. *Materials Forum*, **2000**, 24, 49.
- [13] K. Bright, B. W. Malpass., D. E. Packham., *Nature*, **1969**, 223, 1360.
- [14] D. J. Arrowsmith, *Trans. Instit. Met. Finish.*, **1970**, 48, 88.
- [15] J. D. Venables, *J. Mater. Sci.*, **1985**, 19, 2431.
- [16] J. R. Evans, D. E. Packham., *J. Adhes.*, **1979**, 10, 177.
- [17] T. Wang, H. N. Vazirani., *J. Adhes.*, **1972**, 4, 353.
- [18] R.P. Wool., *Adhesive Science and Engineering—2: Surfaces, Chemistry and Applications*. Elsevier, Amsterdam, chap. 8, **2002**, 351.
- [19] K. W. Allen, *J. Adhes.*, **1987**, 21, 261.
- [20] K. W. Allen, *Int. J. Adhes. Adhes.*, **1993**, 13, 67
- [21] S. S. Voyutskii, *Adhes. Age*, **1960**, 5(4), 30.
- [22] J. N. Anand, *J. Adhes.*, **1973**, 5, 265.
- [23] P. G. De Gennes, *J. Chem. Phys.*, **1971**, 55, 572.

- [24] M. Doi., S. F. Edwards, *J. Chem. Soc. Fara. Trans 2: Mol. Chem. Phys.*, **1978**, 74(10), 1789
- [25] W. W. Graessley., *Adv. Polymer Sci.*, **1982**, 47, 76
- [26] K. Jud., H. H. Kausch., J. G. Williams, *J. Mater. Sci.*, **1981**, 16, 204.
- [27] B. V. Deryaguin., *Research*, **1955**, 8, 70.
- [28] C .Weaver., *Farad. Special Discussions*, **1975**, 2, 18.
- [29] S. M. Skinner., R. L. Savage., J. E. Rutzler. *J. Appl. Phys.*, **1953**, 24, 439.
- [30] B. N. Chapman., in *Aspects of Adhesion Alner*, D. J. ed. University of London Press, London, **1970**, 43.
- [31] L.H. Sharpe. *The Interfacial Interactions in Polymeric Composites*, **1993**, 230, 1.
- [32] A.J. Kinloch. *J. Mat Sci*, **1980**, 15, 66.
- [33] M. Mutsuda., H. Komada. *J. Appl Polym Sci*, **2005**, 95(1), 9.
- [34] R. Bailey., J.E. Castle. *J. Mat Sci*, **1977**, 12(10), 2049.
- [35] M. Gettings, A.J. Kinloch. *J. Mat Sci*, **1977**, 12(12), 2511.
- [36] V.E. Basin. *Progress in Organic Coatings*, **1984**, 12(3), 213–50.
- [37] M.A Chen, H.Z. Li, X.M. Zhang. *Int. J. Adhes Adhes*, **2007**, 27(3), 87
- [38] S.S. Voyutskii. *Autoadhesion and adhesion of high polymers*. Interscience Publishers; **1963**
- [39] A.R. Hutchinson, S. Iglauer. *Int. J. Adhes Adhes*, **2006**, 26(7), 555.
- [40] G. L. Dennis., C. Paul., A. Pizzi., K. L. Mittal., In *Hand Book of Adhesive Technology* ed. Marcel Dekker: New York, **1994**, Chapter. 24
- [41] W. A. Zisman. *Ind. Eng Chem.*, **1963**, 55, 18.
- [42] J. Schultz, K. T. Sutsumi, and J. B. Donnet, *J. Colloid Interface Sci.*, **1977**, 59, 27.
- [43] A. Carré and J. Schultz, *J. Adhes.*, **1983**, 15, 151.
- [44] L-H. Lee, *J. Colloid Interface Sci*, **1968**, 27, 751
- [45] R. E. Baier, E. G. Shafrin, and W. A. Zisman. *Science*, **1968**, 162, 1360.
- [46] F. M. Fowkes, *J. Adhes.*, **1972**, 4, 155.
- [47] F. M. Fowkes, *Physiochem. Aspects Polym. Surf. Proc. Int. Symp.*, **1983**, 2, 583.

- [48] R. S. Drago, G. C. Vogel, and T. E. Needham, *J. Am. Chem. Soc.*, **1970**, *93*, 6014
- [49] J. C. Bolger, *Adhes. Aspects Polym. Coat. Proc. Symp.*, 1, Plenum Press, New York, NY, **1983**, 3.
- [50] F. Awaja, M. Gilbert, G. Kellya., B. Foxa., P. J. Pigram. *Progress in Polymer Science*, **2009**, *34*, 950.
- [51] Park Scientific Instruments. *A practical guide to scanning probe microscopy*. **1997**
- [52] K. Saito, T. Mitsutani, T. Imai, Y. Matsushita, K. Fukushima. *Analytical Chemistry*, **2008**, *80*, 1552.
- [53] [http://csacs.mcgill.ca/francais/docs/CHEM634/XPS\\_Paynter\\_t.pdf](http://csacs.mcgill.ca/francais/docs/CHEM634/XPS_Paynter_t.pdf)
- [54] <http://www.eaglabs.com/en-US/services/esca.html>
- [55] [http://en.wikipedia.org/wiki/Scanning\\_electron\\_microscope](http://en.wikipedia.org/wiki/Scanning_electron_microscope)
- [56] N. A. Puttnam, S. Lee and B. H. Baxter, *J. Soc. Cosmetic Chemists*, **1965**, *16*, 607.
- [57] Y. Wei. and J. W. Hutchinsun. *Int. J. of Fract*, **1998**, *93*, 315.
- [58] J.P. Sargent, *Int.J. Adhes Adhes*, **1994**
- [59] A.J. Price t and J.P. Sargent., *Int.J. Adhes Adhes*, **1997**, 17
- [60] M.D. Thouless, Q.D. Yang., *Int.J. Adhes Adhes*, **2008**, *28*, 176.
- [61] J.W. Cook, S. Edge and D.E. Packham, *Int.J. Adhes Adhes*, **1997**, *17*, 335.
- [62] M.J. Pitkethy, J.B. Doble., *Composites*, **1990**, *21*, 391.
- [63] M.W. Holloway, P.A. Walker, *JOCCA*, **1964**, *10*, 812.
- [64] J. Savkova. Centre des Matériaux, MINES ParisTech
- [65] B.D. Beake., S. Zheng., M.R. Alexander. *J. Mat Sci* , **2002**, *37*, 3821.
- [66] M. Ochi, R. Takahashi, A.Terauchi, *Polymer*, **2001**, *42*, 5151.
- [67] V. Jardet, P. Morel, *Progress in Organic Coatings*, **2003**, *48*, 31.
- [68] B. Duncan, and B. Broughton. *Characterising Strength of Adhesion*, NPL Measurement Good Practice Guide No 72, **2004**
- [69] N. Mahmood, K. Busse, J. Kressler. *Polym. Mat. Sci. and Eng.* **2004**, *90*, 831.
- [70] M.P.K. Turunen, P. Marjamäki, M. Paajanen, J. Lahtinen, J.K. Kivilahti., *Microelectronics Reliability*, **2004**, *44*, 993.
- [71] J. Cognard. *Int.J.Adhes adhes*. **1986**, *6*, 215.

- [72] R.D. Ed. Adams. *Engineered Materials Handbook, Adhesives and Sealants*, Vol. 3, Materials Park, OH: ASM International, **1995**, 325.
- [73] J. Cognard. *J. Adhes*, **1987**, 22, 97.
- [74] L.H. Lee. *Fundamental of adhesion*, **1991**, 50.
- [75] D. Dwight and W. M. Riggs, *J. Colloid Interface Sci.*, **1974**, 47, 650
- [76] M. Brenman, *Polym. Eng. Sci*, **1976**, 16, 745.
- [77] B.M. Dekoven, P.L. Hagans, *Appl. Surf-sci.*, **1986**, 27, 199.
- [78] P. Bodö and J.-E. Sundgren, *J. Appl. Phys.*, **1986**, 60, 1161.
- [79] T. Tsukada, N. Hosokawa, *J. Vac. Sci. Technol.*, **1976**, 16, 348.
- [80] J.M. Burkstrand, *Appl. Phys. Lett.*, **1978**, 33, 387.
- [81] J.M. Burkstrand *Phys. Rev. B*, **1979**, 20, 4853.
- [82] B. Lederer, M. Sotton, A. Baszkin, L. Ter-Minassian-Saraga, *Polymer*, **1977**, 18, 675.
- [83] D. Briggs, D.G. Rance, C.R. Kendall, A.R. Blythe, *Polymer*, **1980**, 21, 895.
- [84] J.M. Pochan, L.J. Gerenser, J.F. Elman, *Polymer*, **1986**, 27, 1058.
- [85] C. Boiziau, G. Lecayan, *Int. J. Adhes. Adhes.*, **1986**, 6, 207.
- [86] N.J. Chou, C.H. Tang, *J. Vac. Sci. Technol.*, **1984**, A2, 751.
- [87] S.A. Chambers, K.K. Chakravorty, *J. Vac. Sci. Technol.*, **1988**, A6, 3008.
- [88] Y.C. Leong, L.M.S. Lee, S.N. Gan, *J. Appl. Polym. Sci.*, **2003**, 88, 2118.
- [89] M. Fujita, A. Takemura, H. Ono, M. Kajiyama, S. Hayashi, H. Mizumachi, *J. Appl. Polym. Sci.*, **2000**, 75, 1535.
- [90] B. Thongnuanchan, K. Nokkaew, A. Kaesaman, C. Nakason, *Polymer Engineering and Science*, **2007**, 421
- [91] B.T. Poh, H.K. Kwo, *J. Appl. Polym. Sci.*, **2007**, 105, 680.
- [92] B.T. Poh, A.L. Lim, *J. Appl. Polym. Sci.*, **2008**, 109, 115.
- [93] B.T. Poh, S.K. Chow, *J. Appl. Polym. Sci.*, **2007**, 106, 333.
- [94] B.T. Poh, P.G. Lee, S.C. Chuah, *eXPRESS Polym Letters*, **2008**, 2, 398.
- [95] I. Khan, B.T. Poh, *J. Appl. Polym. Sci.*, **2010**, 118, 3439.
- [96] B.T. Poh, K.W. Yee, H.B. Lim, *J. Appl. Polym. Sci.*, **2008**, 110, 4079.

- [97] B.T. Poh, A.T. Yong, *J. Appl. Polym. Sci.*, **2009**, *114*, 3976.
- [98] B.T. Poh, A.T. Yong, *J. Appl. Polym. Sci.*, **2010**, *115*, 1120.
- [99] I. Khan, B.T. Poh, *Materials and Design*, **2011**, *32*, 2513.
- [100] D. Derouet, Q.N. Tran, J.L. Leblanc, *J. Appl. Polym. Sci.*, **2009**, *112*, 788.
- [101] Z. Oommen, S. Thomas, *J. Appl. Polym. Sci.*, **1997**, *65*, 1245.
- [102] L. Thiraphattaraphun, S. Kiatkamjornwong, P. Prasassarakich, S. Damronglerd, *J. Appl. Polym. Sci.*, **2001**, *81*, 428.
- [103] W. Arayaprane, P. Prasassarakich, G.L. Rempel, *J. Appl. Polym. Sci.*, **2003**, *89*, 63.
- [104] D-J. Kim, H-J. Kim, G-H. Yoon, *J. Adhes. Adhes.*, **2005**, *25*, 288.
- [105] H. Ni, X. Wang, *Surf. Sci.*, **2007**, *601*, 1560.



***Chapter 2- Synthesis and characterization of  
telechelic cis -1, 4-polyisoprene***

## 2.1 Introduction

Telechelic oligomers with terminal carbonyl and/or carboxylic groups can be obtained by specific oxidative double bond cleavage of 1,4-butadiene, 1,4-polyisoprene or other unsaturated units in polymers. Epoxidized polymers can also lead to heterotelechelic or homotelechelic oligomers by substitute cleavage of epoxide units with suitable oxidative reagent [1].

In this chapter, telechelic cis-1,4-polyisoprene is prepared by oxidative degradation of epoxidized cis-1,4-polyisoprene using periodic acid as selective oxidizing agent. The cleavage leads to oligomers with aldehyde and ketone chain ends and with polydispersity index near 2. This method has been developed in our laboratory [1, 14, 15, 17, 18]. Firstly, epoxidized cis-1,4-polyisoprene was prepared using epoxidizing agent, m-chloroperbenzoic acid, subsequently chain cleavage with periodic acid was produced. Secondly, the functional groups modification of carbonyltelechelic cis-1,4-polyisoprene to hydroxytelechelic cis-1,4-polyisoprene for using as precursor for polyurethane was accomplished.

The modification of isoprene unit of hydroxyltelechelic oligomers by epoxidation was also carried out. Products in each step were characterized by Fourier Transform Infrared Spectroscopy (FTIR), Nuclear Magnetic Resonance spectroscopy ( $^1\text{H}$ -,  $^{13}\text{C}$ - NMR). The average molecular weights and polydispersity index of telechelic cis-1,4-polyisoprene were determined by Size Exclusion Chromatography (SEC).

To introduce this work, a bibliographic part on telechelic polyisoprenes, their preparation and their reactivity is presented.

## 2.2 Bibliographic part on Telechelic polyisoprene

### 2.2.1. Definition

The term “telechelic” was proposed originally by Ura-neck, Hsieh and Buck for low molecular weight polymers bearing two functional end groups. Nowadays, this term is also applied to oligomers having two or more terminal groups [1]. Telechelic liquid natural rubber

(TLNR) can be defined as a low molecular weight oligomer having number average molecular weight approximately 100-10000 and containing reactive terminal groups capable for using in further chain extension and crosslinking. TLNR still consists of isoprene units, basic structure of natural rubber (NR). The main difference from NR is that TLNR has reactive groups at the chain end, as denoted by X and Y. X and Y may, or may not, be similar. Although research on the production of TLNR began in the early 1970s, commercial TLNR is still not widely available. Most TLNR used in research are prepared especially in the laboratory [2].

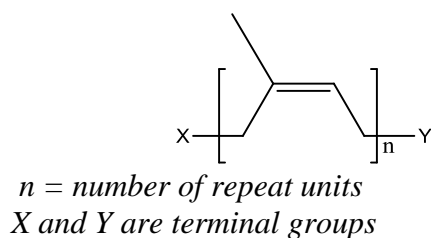


**Figure 2.1** Chemical structure of telechelic liquid natural rubber

### 2.2.2. Obtaining of telechelic polyisoprene by controlled degradation.

Normally, the methods of controlled degradation of the NR backbone proceed via oxidative chain scissions by either chemical or photochemical routes. The methods can be classified into five main categories, i.e., redox, photochemical, oxidation at high temperature and pressure, specific oxidative cleavage of double bonds and metathesis degradation. Details of these main categories are discussed below.

- **.Oxidation in the presence of redox system**

This method utilizes an appropriate mixture of oxidizing and reducing agents (redox couple). The redox couple can cleave polymer chains with the introduction of reactive terminal groups on the resulting oligomers. Thus, an oxidizing agent such as an organic peroxide, hydrogen peroxide, atmospheric oxygen or ferric chloride-oxygen, coupled with reducing agent such as an aromatic hydrazine or sulphanilic acid were employed to depolymerise NR to yield TLNR. The redox system type employed determines the bearing phenylhydrazone groups i.e. carbonyl or hydroxyl terminal. The depolymerization can be carried out either in an organic solvent or directly in the latex phase. The depolymerization reaction of NR in the latex phase using phenylhydrazine as reducing agent and atmospheric

oxygen as an oxidizing agent is more favoured owing to it being economically viable in an industrial scale. A reaction mechanism was proposed by Boccaccio and de Livonnière [3] as shown in **Figure 2.2**.

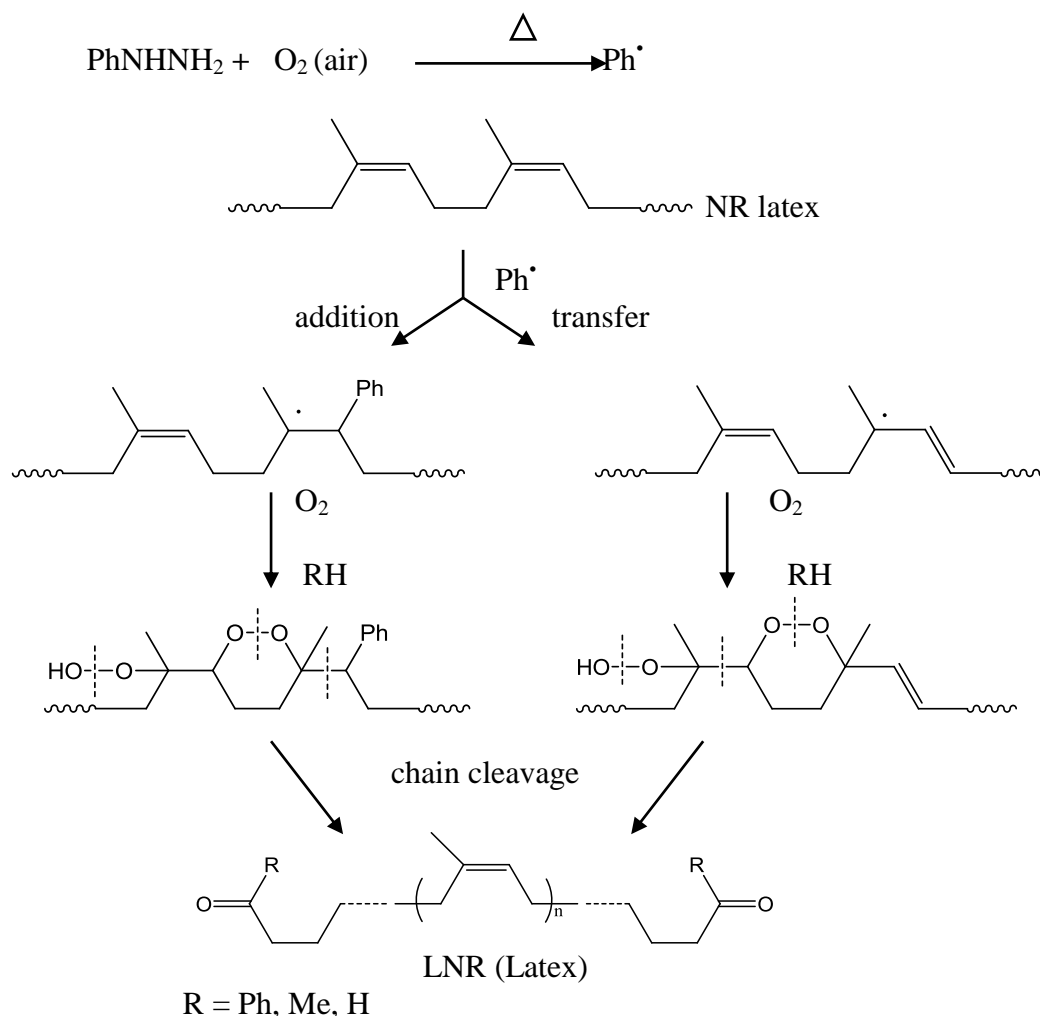


**Figure 2.2** Mechanism of the oxidizing cleavage by atmospheric oxygen in the presence of phenylhydrazine at the carbon-carbon double bond of the natural rubber in latex phase

Tangpakdee *et al.* [4] have studied an oxidative degradation reaction of deproteinized natural rubber using different initiators, AIBN, potassium persulfate ( $\text{K}_2\text{S}_2\text{O}_8$ ) and benzoyl peroxide in the presence of a carbonyl product such as acetone formaldehyde or propanal. They demonstrated that  $\text{K}_2\text{S}_2\text{O}_8$ /propanal system is most effective for NR degradation at  $60^\circ\text{C}$ . The mechanism that they proposed is the oxidation of chain by radical initiator followed by the reaction of propanal with aldehyde end group. The obtained TLNR contained aldehyde and ketone groups.

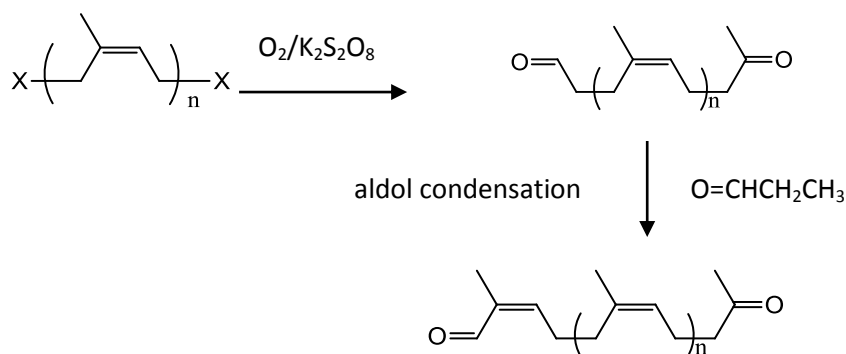


**Figure 2.3** The degradation reaction of deproteinized natural rubber in the presence of  $\text{K}_2\text{S}_2\text{O}_8$  and propanal

- **Oxidation by photochemical method**

Control degradation of NR by photochemical chain scission for preparation of TLNR was first explored by Cunneen [5]. NR was irradiated with UV light in presence of nitrobenzene as a photosensitizer to give carboxy-terminated natural rubber (CTNR) having  $\overline{M}_n$  of about 3000 g/mol. The degradation of NR in solid state was studied but not appears to have further development. The controlled degradation of NR in solution was also studied by Ravindran *et al* [6]. NR depolymerization in toluene by UV light in the presence of hydrogen peroxide and methanol or tetrahydrofuran gives HTNR having  $\overline{M}_n$  of 8700 or 5000 g.mol<sup>-1</sup>, respectively. They also found that sunlight is almost as effective as UV light in degradation of NR in toluene.

However, the concentration of NR in solution is limited at 10%. The mechanism of the degradation proceeds via hydroxyl radicals ( $\text{HO}^\bullet$ ) issued from the homolytic cleavage of hydrogen peroxide (**Figure 2.4**).

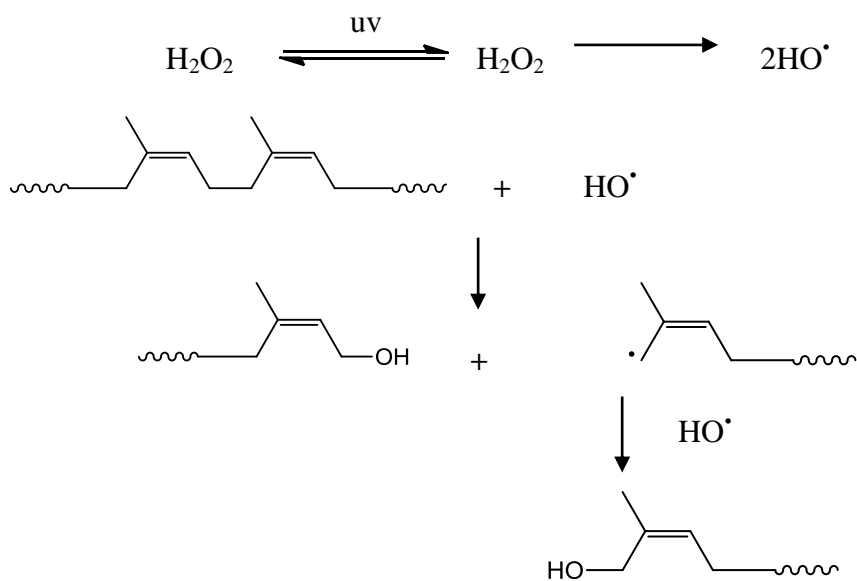


**Figure 2.4** The proposed mechanism of cis-1, 4-polyisoprene degradation reaction by hydrogen peroxide/UV radiation

Later, the degradation of NR from fresh latex with 20% DRC (Dry Rubber Content) by sunlight and hydrogen peroxide was also reported but there are no information of type and functionality [2]. In another case, NR was depolymerized by swelled in solution in the presence of benzophenone (photosensitizer) and exposed to sunlight for a day to give TLNR. The mechanism of the reaction (**Figure 2.5**) involves chain scissions leading to hydroxyle, hydroperoxide and ketone end groups [2]

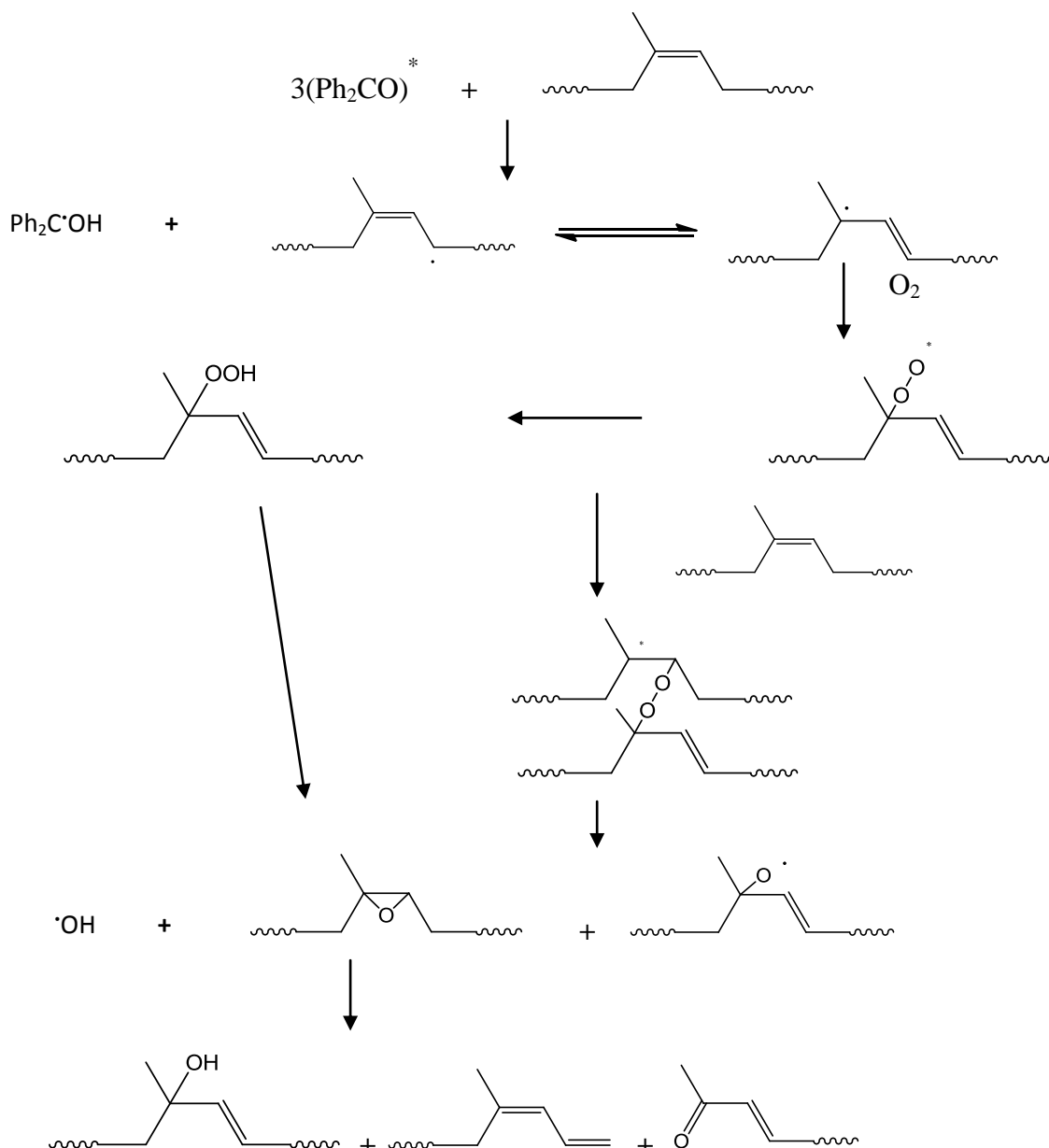


**Figure 2.5** The proposed mechanism of cis-1,4-polyisoprene degradation reaction by Benzophenone /UV radiations

- **Oxidation at high temperatures and high pressures**

In this method, masticated NR in toluene containing 30-40% hydrogen peroxide was heated at 150°C in reactor at a pressure of 200-300 psi to yield HTNR having  $\overline{M}_n$  between 2500 and 3000 g.mol<sup>-1</sup>. Unfortunately, analytical data indicate that the efficiency of functionalization of HTNR by this method is low. This low efficiency is caused by side reactions. A mechanism of reaction was proposed as shown in **Figure 2.6** [7].

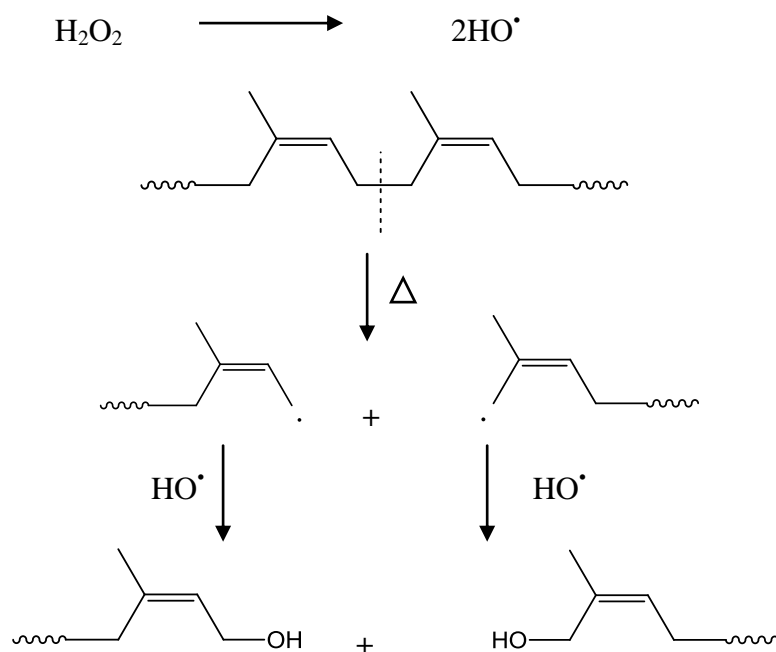


**Figure 2.6** The proposed mechanism of degradation of cis-1,4-polyisoprene by hydrogen peroxide at high temperature and high pressure

- Oxidation by cleavage reagent specific to double bonds
  - Ozonolysis

The term “ozonolysis” refers to the cleavage of bonds by ozone leading to the formation of peroxy or non-peroxy products, whereas the term “ozonization” refers merely to the process of treatment of a compound with ozone. Mechanism of ozone attack on C=C bonds of polydiene rubber backbones, causing chain scission and yielding various peroxidic products was proposed by Criegee (**Figure 2.7**) [8]. The reaction between C=C bonds and ozone leads to the unstable molozonide formation. This unstable species can easily cleave to a stable carbonyl compound (aldehyde or ketone) and an unstable carbonyl oxide (zwitterion). The carbonyl oxide then undergoes reaction leading to final, stable products. Degradation of unsaturated rubber by ozone results in a decrease in molecular weight and increase in species containing oxygenated functions such as aldehyde, ketone, acid and peroxide.



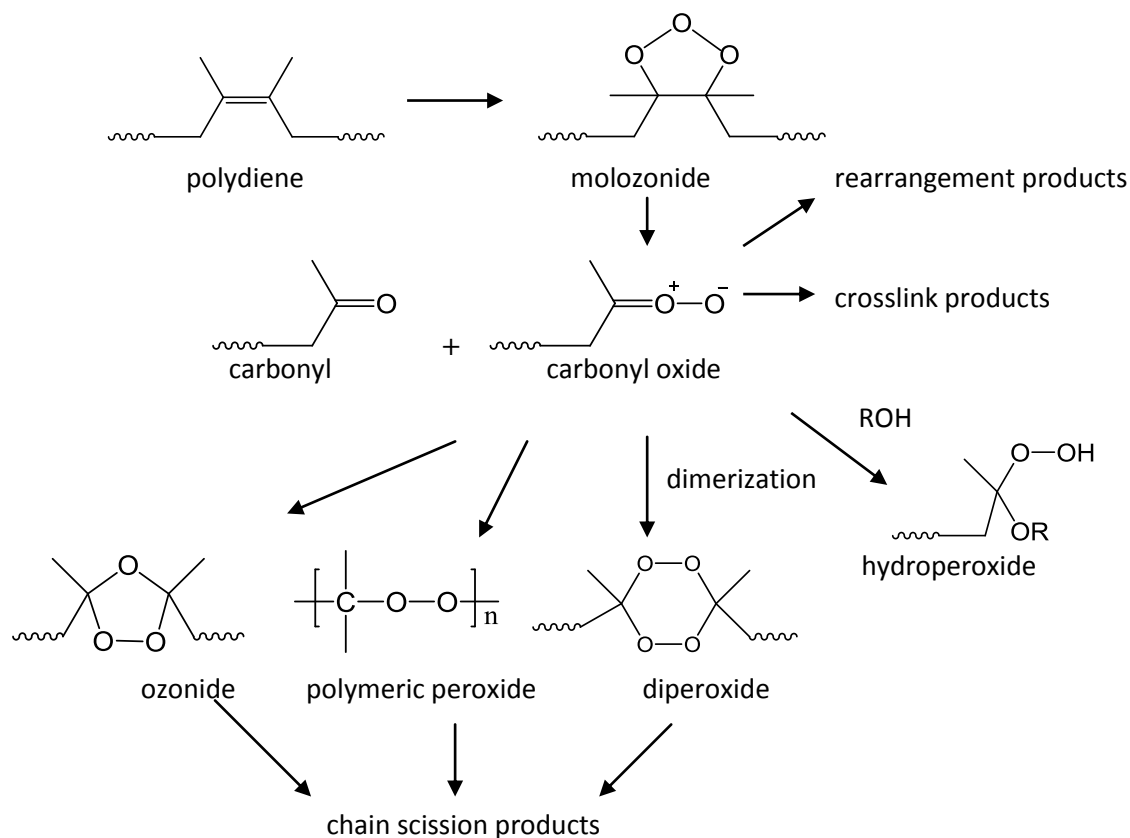


**Figure 2.7** Mechanism of reaction of ozone at double bond of polydienes

Tanaka *et al.* showed that controlled ozonolysis of trans- and cis-1,4-polyisoprene and 1,4-polybutadiene resulted in selective chain scission and produced HTNRs having 11 and 10 units and HTBDs having 12 and 13 repeat units with very narrow polydispersities of 1.01-1.06 [9]. Montaudo *et al.* [10] reported that ozonolysis of cis-1,4-polyisoprene in hexane at ice-bath temperature without further treatment with either oxidizing or reducing agents can lead to the formation of telechelic oligomers bearing only ketone and carboxylic acid end groups with no oligomeric ozonides being detected. Whereas, ozonolysis of cis-1,4-polyisoprene in carbon tetrachloride reported by Anachkov [11], leads to the basic ozonolysis products: ozonide, ketones and aldehydes.

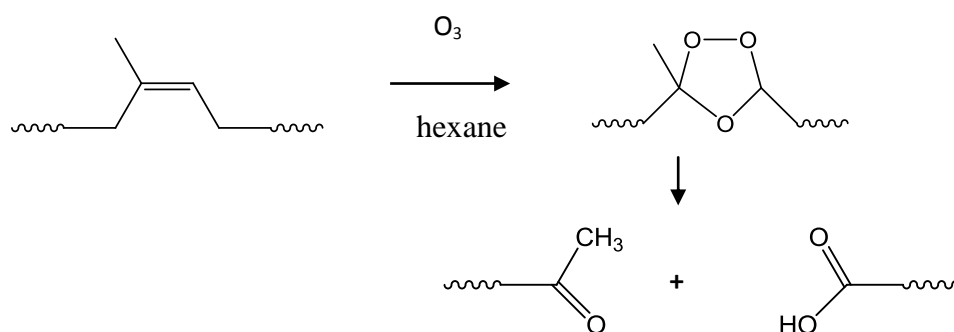


**Figure 2.8** Ozonolysis of cis-1,4-polyisoprene in hexane

- **Cleavage by periodic acid or transition compounds**

Guizard *et al.* developed the method to specifically double bonds cleavage to obtain bifunctional oligomers. Ruthenium tetraoxide was used in the presence of peracid as co-oxidant. Chain scission occurs at unsaturated site rather than entirely randomly [12]. Lead tetraacetate,  $Pb(OAc)_4$  and periodic acid ( $H_5IO_6$ ) are interesting for degradation of polyisoprenic chains. Typically, both reagents cause cleavage of vic-glycols to yield carbonyl compounds. Burfield and Gan [13] found that  $Pb(OAc)_4$  causes degradation of hydrolyzed epoxidized synthetic rubber faster than that of epoxidized synthetic rubber. Synthetic polyisoprene sample which presumably contains no 1,2-diols, was also slowly degraded by  $Pb(OAc)_4$ . They also found that  $H_5IO_6$  could be used to degrade NR and acid hydrolyzed NR. In the case of NR, it is believed that the chain degradation occurs in the presence of a few 1, 2- diol units in the molecular chain.

Reyx and Campistron used  $H_5IO_6$  for preparation of telechelic liquid natural rubber. They found that epoxide content of starting rubber decreased from 25 to 8% after degradation reaction. The NMR spectrum showed the presence of aldehyde and ketone moieties, residual oxiranes, and secondary furanic and cyclic structures [14].

Gillier-Ritoit *et al.* [15] investigated chain degradation of polyisoprene and epoxidized polyisoprene using  $H_5IO_6$  in organic solvent. The degrade PI gave  $^1H$ -NMR characteristics similar to those of degraded epoxidized polyisoprene. The degraded rubber containing aldehyde and ketone terminal groups, but the reaction is slower than in case of epoxidized polyisoprene. They found that in epoxidized polyisoprene, the  $H_5IO_6$  cleavage of polymer chain occurs nearly instantaneously, while  $H_5IO_6$  cleavage of double bonds of

polyisoprene is slower process. It appears that two equivalents of  $H_5IO_6$  are needed for cleavage of one double bond in polyisoprene. They proposed that the cleavage result from two steps. Firstly,  $H_5IO_6$  reacts with a double bond to give an epoxide or  $\alpha$ -glycol. Secondly, the epoxide or  $\alpha$ -glycol is cleaved by reacting with the second equivalent of  $H_5IO_6$  (**Figure 2.9**).

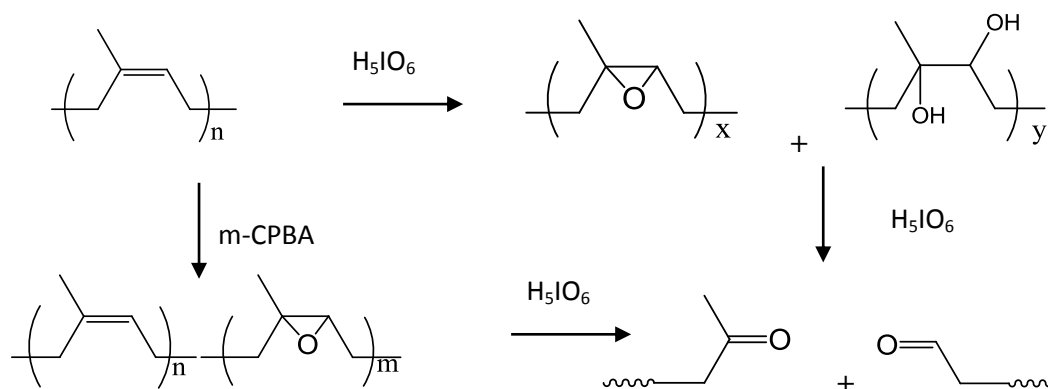


**Figure 2.9** The degradation of cis-1,4-polyisoprene and epoxidized cis-1,4-polyisoprene using  $H_5IO_6$

Mauler *et al.* investigated that degradation of cis-1,4-polyisoprene by using  $H_5IO_6$ /ultrasonic radiation (sonochemical) is more efficient than the use of radiation or chemical degradation alone. The presence of ultrasound irradiation accelerates the chemical degradation process leading to lower molecular weight products [16].

The degradation of deproteinized epoxidized NR using  $H_5IO_6$  was performed by Phinyocheep *et al.*. The epoxidation of deproteinized NR was carried out in latex phase using performic acid formed in situ by reaction of hydrogen peroxide and formic acid. The epoxidized NR was then degraded by  $H_5IO_6$ . In all ENR samples obtained, there was no observation of NMR signals corresponding to products of side reactions such as formation of diol and furan, as previous mention. After treatment with  $H_5IO_6$ , they still found epoxides and also the new signals of carbonyl and hydroxyl functional groups and the molecular weight decreased. Therefore, they proposed reaction pathway as shown in the **Figure 2.10** [17].

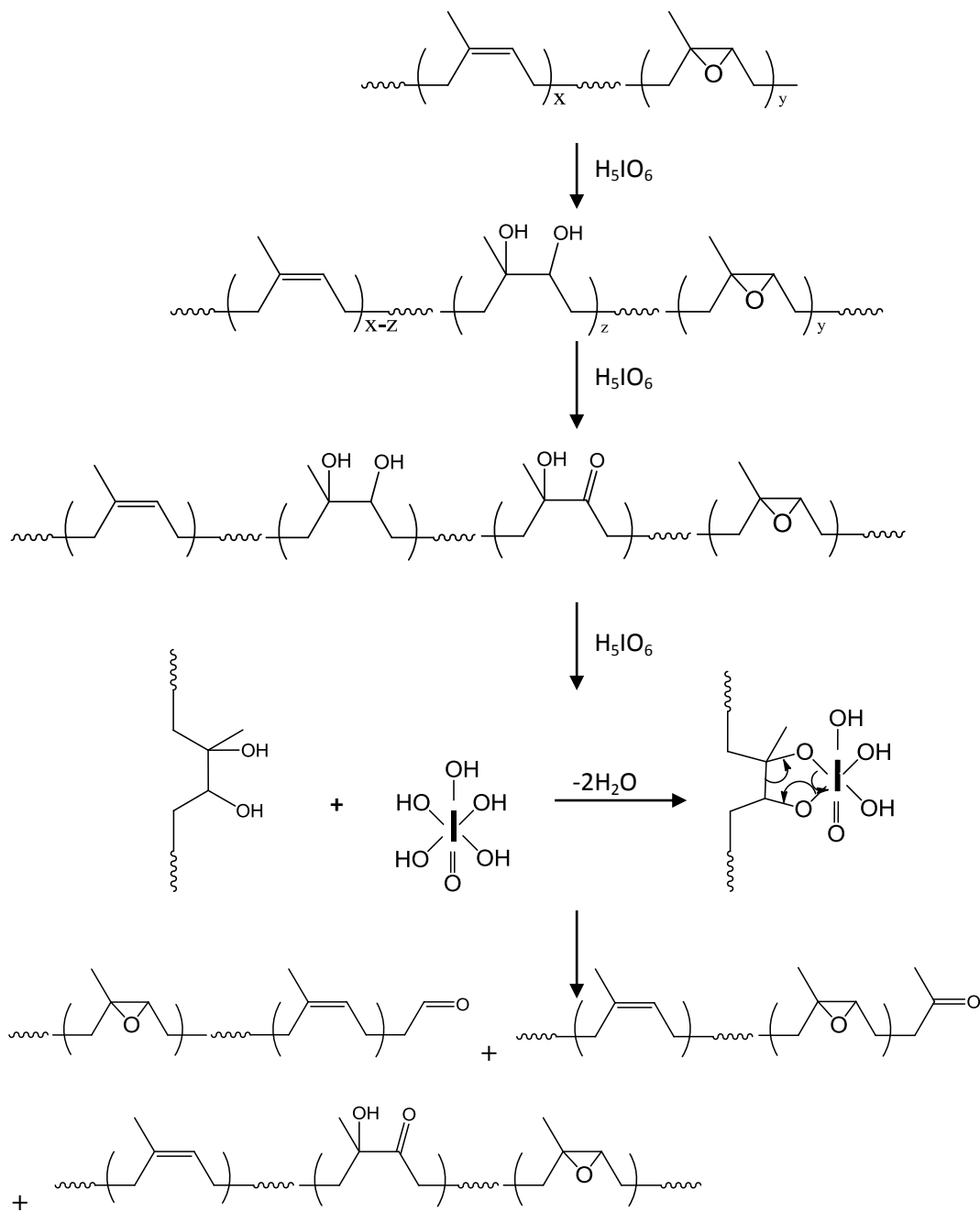


**Figure 2.10** Proposed reaction pathway of oxidative degradation of epoxidized rubber by periodic acid

Kébir *et al.* [18] studied new telechelic cis-1,4-polyisoprene oligomers bearing hydroxyl groups at the end of the polyisoprene backbone and possessing controlled molecular weights, to use as soft segments in the elaboration of polyurethane elastomers. Besides, the hydroxytelechelic cis-1,4-polyisoprene (HTPI) has a well define structure obtained through a controlled methodology as shown in **Figure 2.11**. These oligomers were chemically modified leading to hydrogenated and epoxidized oligoisoprenes based polyurethanes.

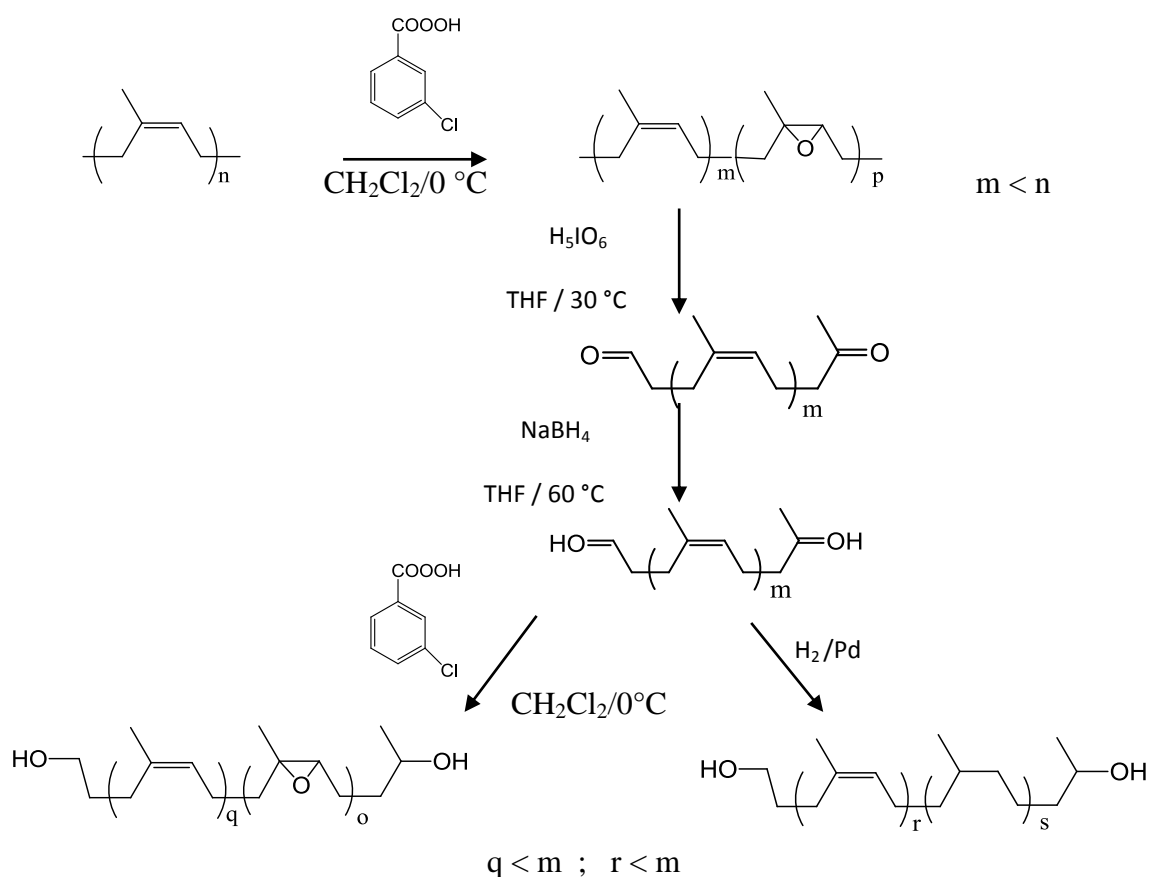


**Figure 2.11** Preparation and following modifications of hydroxytelechelic cis-1,4-polyisoprene

- **Metathesis degradation**

Depolymerization agents or chain transfer agents and catalysts especially Lewis acid catalysts, Schrock and Grubbs carbenes were used in metathesis depolymerization of polyalkenamers including polydienes, resulting oligomers and telechelic oligomers.

Use of Lewis acid catalyst such as  $WCl_6/Sn(CH_3)_4$  can lead to side reactions. Therefore, Marmo *et al.* reported the synthesis of mass-exact telechelic polybutadiene oligomer by metathesis degradation of cis-1, 4- polybutadiene using allylsilane monoene and alkyldienes complex catalyst [19]. They also synthesized the diester, disilyl ether and diamide telechelic polybutadiene oligomers via cyclic dienes metathesis depolymerization. The characterisation of the obtained products showed that these telechelic oligomers were perfectly difunctional. The proposed mechanism describes a first stage proceeding through

intermolecular cyclization of 1, 4-polybutadiene, then macrocyclic butadiene cross-metathesis proceeds with functionalized monoene to form linear difunctional telechelic oligomers [20].

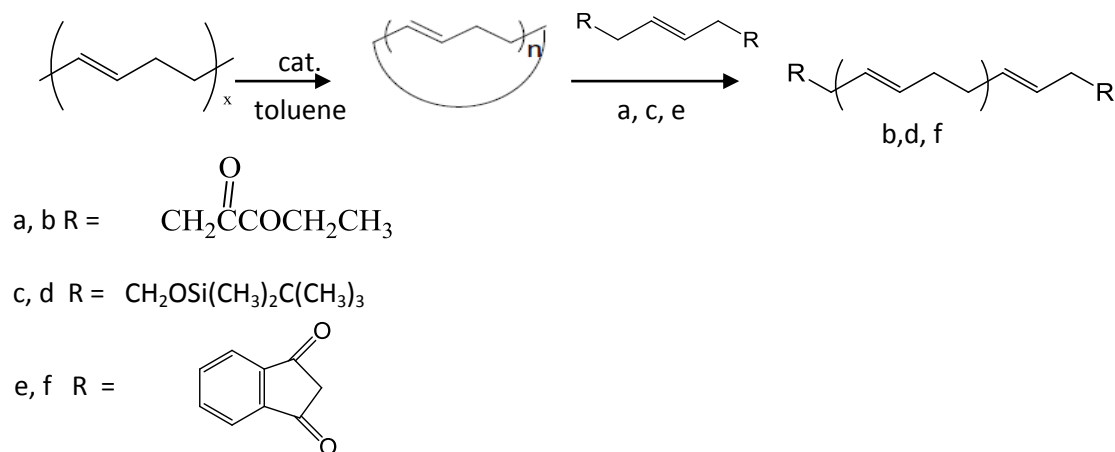


**Figure 2.12** Depolymerization of 1,4-polybutadiene with diethyl 4-octene-1,8-dioate (a), bis(*t*-butyldimethylsilyl)-3-hexene-1,6-diol diether (c), and 2-butene-1,4-diylbis(phthalimide) (e)

However, there is not much work using this technique in degradation of polyisoprene for a present. Our laboratory interested in preparing telechelic polydienes. Thanki *et al.* performed metathetic alkenolysis of partially epoxidized cis-1,4-polybutadiene using Grubbs' ruthenium benzylidene compound as catalyst and 4-octene as depolymerizing agent as shown in **Figure 2.13**. They found that when the molar ratio of monomer unit to catalyst decreases, yield of oligomer increases linearly [21].

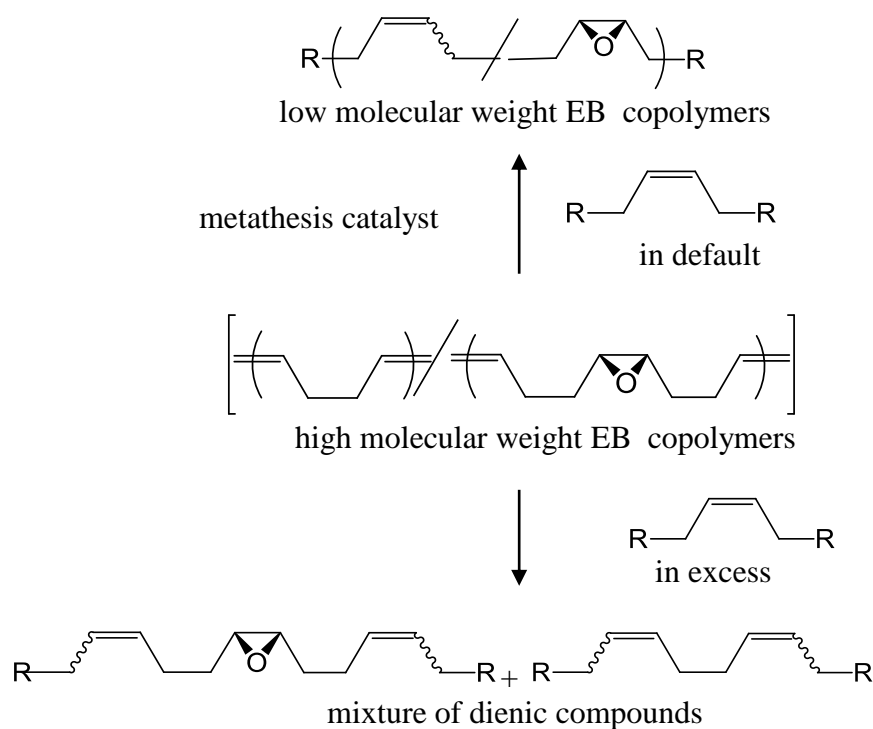


**Figure 2.13** Metathesis alkenolysis of partially epoxidized polybutadiene

Solanky *et al.* studied a new approach for obtaining end-functionalized acetyloxy polyisoprene in a controlled manner through a metathesis methodology using second generation Grubbs catalyst and chain transfer agent from cis-1,4-polyisoprene. Oligomers of molecular weight range 8000-40000 g.mol<sup>-1</sup> were obtained in very good yields, while lower molecular weight oligomers were obtained in moderate yields. Moreover, they have prepared telechelic natural rubber with molecular weight 38000 from deproteinized natural rubber in latex phase [22].

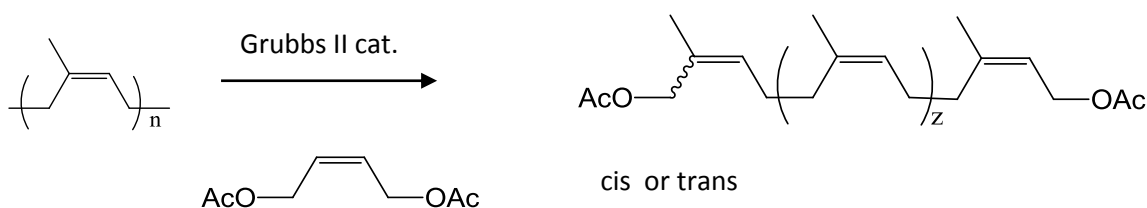


**Figure 2.14** Structure of the product obtained by metathesis degradation of polyisoprene

### 2.2.3 Reactivity of telechelic liquid natural rubber.

TLNRs possess not only isoprene units in the main chains, but also reactive end groups at the chain terminals. Therefore, they can undergo various reactions at the double bonds of isoprene units and various chain extension reactions.

- **Modification of backbone**

Generally, the structure of TLNR is very close to that of an alkene. Therefore its chemical reactivity is influenced by the presence of carbon-carbon double bonds. Moreover, the presence of the methyl group at the carbon-carbon double bonds, electrophilic group, increases the reactivity further compared to those of the carbon-carbon double bonds in polybutadienes.

- **Maleinization**

The reaction of TLNR with maleic anhydride was reported to yield a product having adhesive properties. It is well-known that the double bonds of NR can undergo ‘ene’ reactions as shown in **Figure 2.15**.

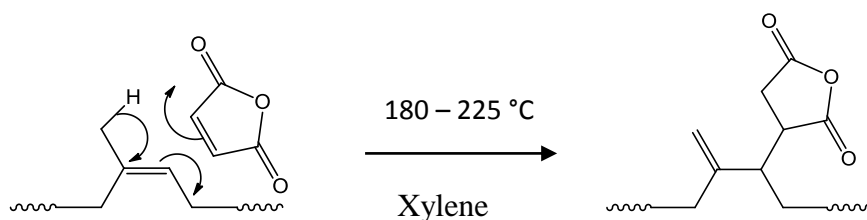
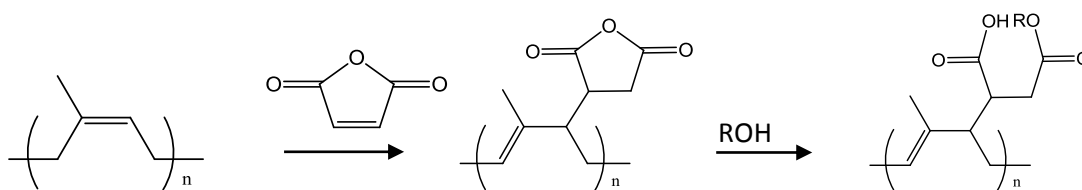


**Figure 2.15** Mechanism of maleinization reaction

In a further study, modifications of TLNR with maleic anhydride followed by subsequent reaction with photo-reactive alcohols such as 2-hydroxyethylacrylate (HEA) and 2-hydroxyethyl cinnamate (HEC) were found to give TLNR, respectively, having pendent succinic anhydride functionality, which was ultraviolet curable. These reactions are shown in **Figure 2.16** [23].





Where R =  $-\text{CH}_2\text{CH}_2\text{OCOCH}=\text{C}_6\text{H}_5$  (cinnamate group)  
 $-\text{CH}_2\text{CH}_2\text{OCOCH}=\text{CH}_2$  (acrylate group)

**Figure 2.16** Modification of telechelic natural rubber for ultraviolet application

- **Chlorination**

TLNR can be chlorinated to give chlorinated TLNR containing 65%-68% chlorine [24]. The reaction proceeds as shown in Scheme 2.17. The product obtained can be used as an anti-corrosion adhesive and its characteristics are comparable to those of the adhesives which are available commercially.

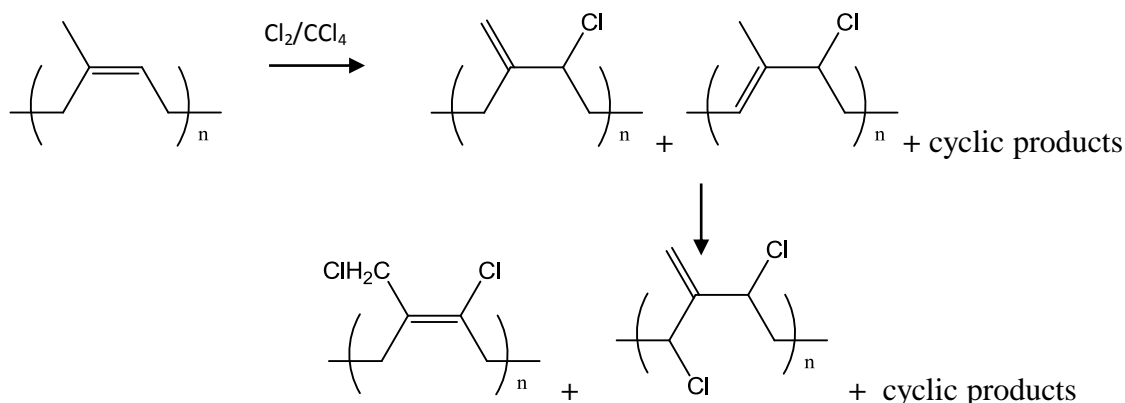


**Figure 2.17** Reaction of chlorination on TLNR

- **Grafting**

The modification of TLNR could be the grafting of monomers onto the TLNR backbone to give a graft copolymer. It was reported that chemical grafting of styrene and methyl methacrylate onto TLNR of  $M_n$  10000-20000 g/mol by radical polymerization (using peroxy or diazo compounds as initiator) gives 43% graft polystyrene and 49% graft poly(methyl methacrylate), respectively[25]. Unfortunately, the mechanical properties of the vulcanizates obtained from these grafted TLNRs are inferior compared with those of NR vulcanizates.

Polystyrene (30%-50%) graft copolymer was found to give a thermoplastic rubber suitable for use as heat-resistant adhesive [26].

- **Epoxidation**

In this process, backbone double bonds are converted into oxiranes (epoxides) using an organic peracid. It has been reported that TLNR can be epoxidized in situ in the latex form, using organic peracids derived from formic or acetic acids, in two-step reactions. In the first step, peracid is formed by reaction between the acid and hydrogen peroxide. Then, in the second step, the peracid is reacted with TLNR to give telechelic epoxidized liquid natural rubber (TELNR). The reaction was proposed by Kwart and Hoffman as shown in **Figure 2.18** [27].

Our laboratory was also successful in preparation of epoxidation of hydroxyl telechelic cis-1,4- polyisoprene with *m*-chloroperbenzoic acid in solvent phase [18].

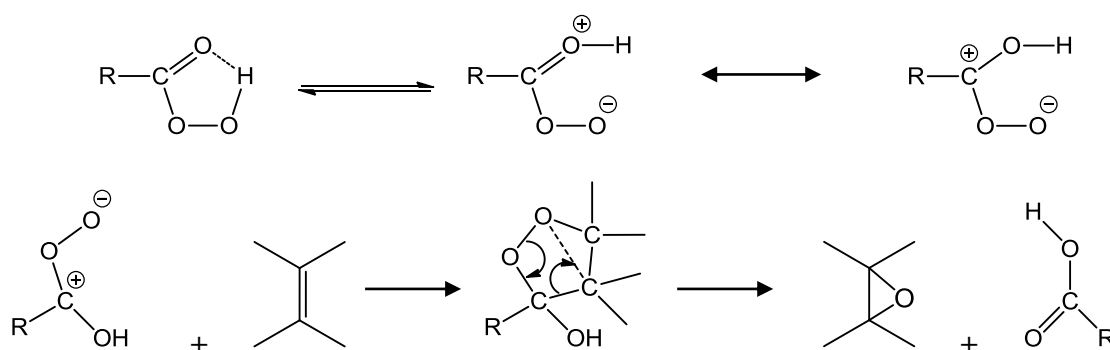


**Figure 2.18** Mechanism of epoxidation reaction on isoprene unit from peracid

ELNRs are the starting products and their chemical modification may allow new properties and technological interests. Indeed, the presence of carbon–carbon double bonds, or oxirane rings on the rubber backbone is of great interest because of the number of chemical reactions that can be used to add reagents. The reactivity of the epoxide groups toward carboxylic acids [28, 29], amines [30], phosphoric acid derivatives [31] and alcohols [32] is well known as shown in **Figure 2.19**. Some recent studies have shown the importance of these compounds in the synthesis of higher value added materials.

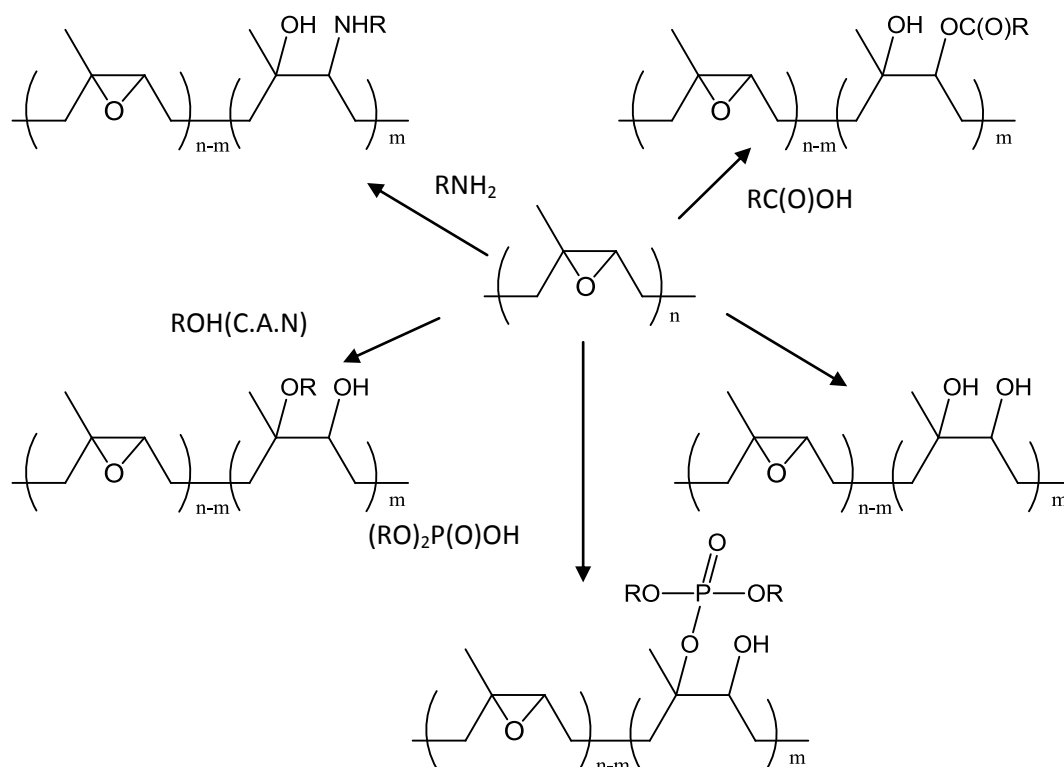


**Figure 2.19** Possibilities of chemical transformations via epoxide groups

- **Hydrogenation**

Almost hydrogenation is a useful method for the reduction of unsaturations in diene polymers. It can be performed with elemental hydrogen in the presence of a transition metal catalyst [33, 34] or by a noncatalytic method [36]. Our laboratory was successful in preparation of hydrogenated hydroxyl telechelic cis-1,4-polyisoprene (HTPI) under hydrogen pressure with catalyst in acetate medium as shown in **Figure 2.20** [18].

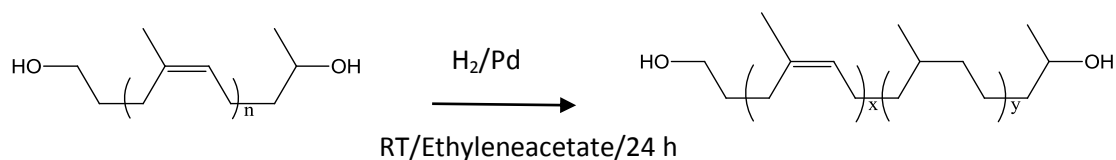


**Figure 2.20** Hydrogenation of HTPI

### 2.2.4 Modification of functional end –groups of telechelic natural rubber

The possibility of chemical modification of TLNR bearing phenylhydrazone chain-ends were proposed as shown in **Figure 2.21** [1].

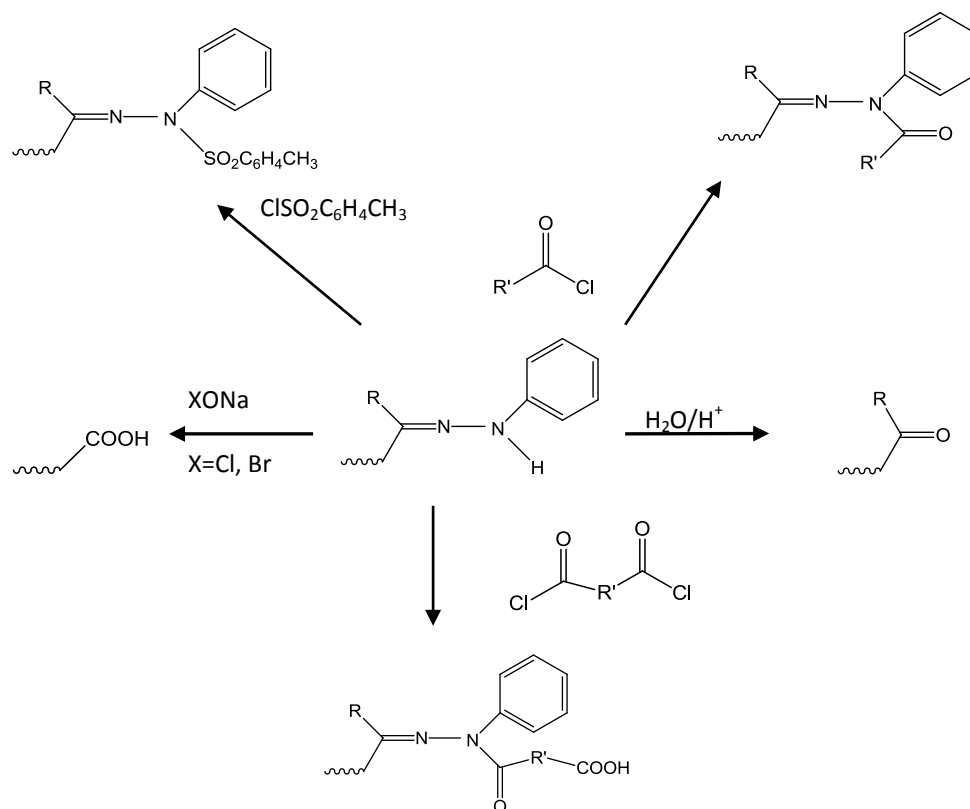


**Figure 2.21** Possible reactions of chemical modification of phenylhydrazone end-groups

Our laboratory studied the chemical modifications of carbonyl oligoisoprenes which can lead to hydroxyl or amino end-groups [18, 36, 37]. It was found that new well defined hydroxyl or amino telechelic cis-1,4- oligoisoprenes have been obtained in a mass range of 1600–2300 g/mol. For successful synthesis of these amino telechelic oligoisoprenes, two approaches were described. The first approach involved a standard mesylate displacement by sodium azide followed by smooth reduction using triphenylphosphine. The second pathway implied a reductive amination sequence. Primary and secondary amine functions have thus been selectively obtained at both oligomer chain-ends depending on reaction conditions. These reactions are showed in **Figure 2.22**.

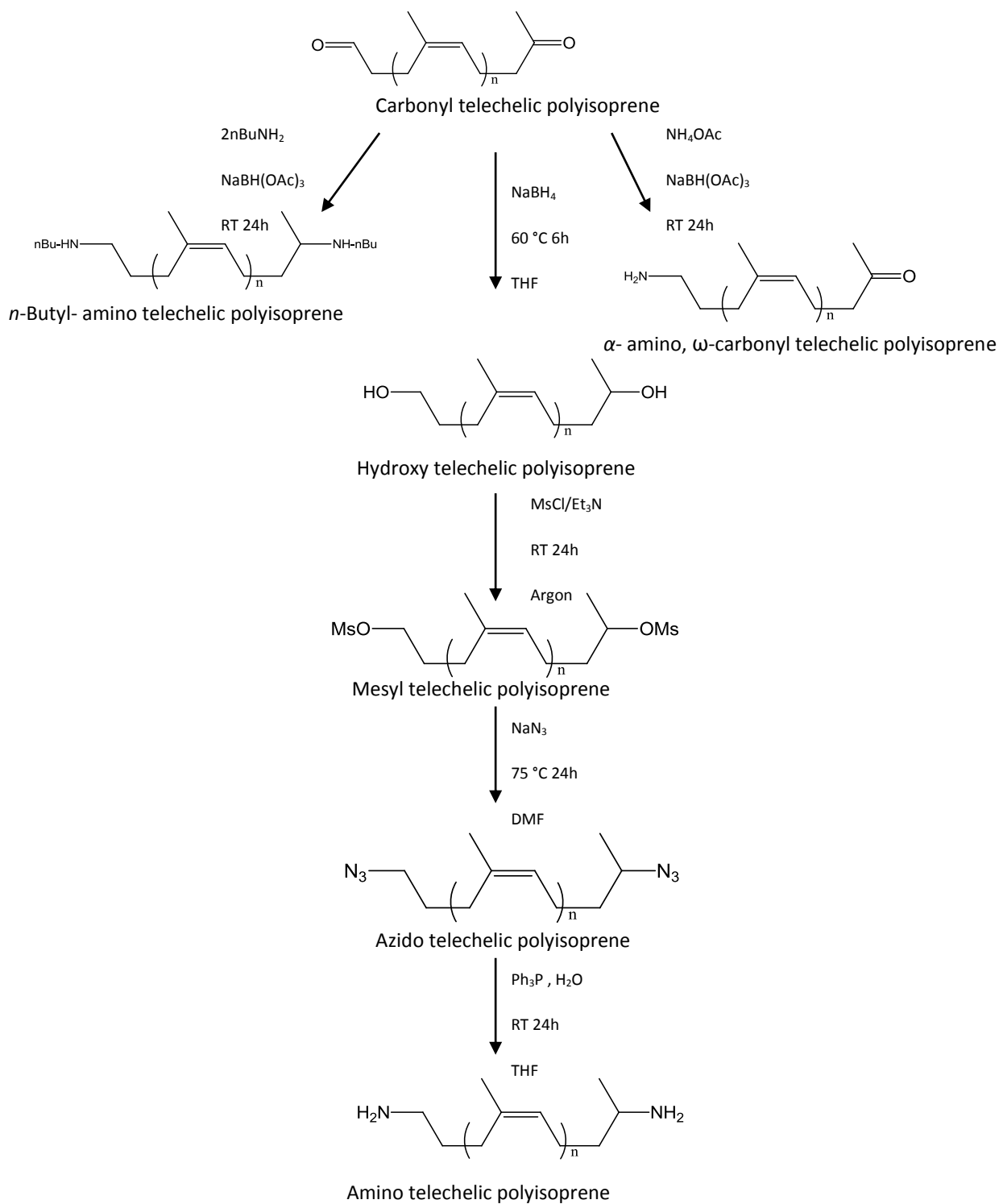


**Figure 2.22** Reaction pathways for amination of carbonyltelechelic oligoisoprene

### 2.2.5 Chain extension reaction of telechelic natural rubber

The chain extension reactions of TLNR can lead to polyurethane block copolymers (Figure 2.23) for both thermoplastic and elastomers applications. Different mechanical properties of polyurethane elastomers can be obtained by varying isocyanate functions natural, molecular weight of oligomers and the ratio of (NCO)/(OH) [38, 39].

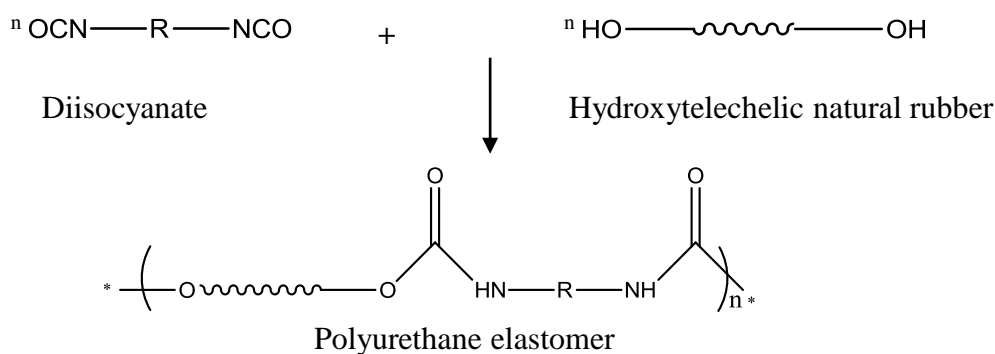


**Figure 2.23** Synthesis of polyurethane.

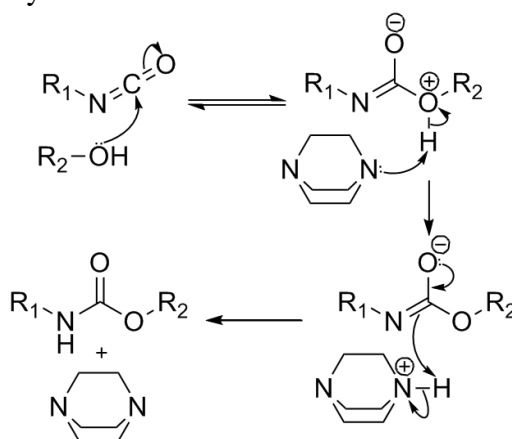


**Figure 2.24** Polyurethane reaction mechanism catalyzed by tertiary amine.

### Conclusion on the bibliographic part

This literature survey allows us to describe first the different methods of preparation of telechelic polyisoprene by degradation of natural rubber or high molecular weight polyisoprene. All the methods utilizing radical mechanism (oxidation in the presence of redox system, photochemical method, oxidation at high temperatures and pressures) lead to not well controlled degradation. Ozone and lead tetraacetate are toxic products not used easily in an industrial scale. For these reasons, we have chosen the cleavage by periodic acid which allows good control of the molecular weights and of the functionality of the obtained oligomers.

In a second part, we have described the reactivity of the telechelic polyisoprenes, focusing on the reactions leading to the increasing of the adhesive properties, more particularly the epoxidation and secondary modification via epoxide groups, and to the reactions at the chain-ends, especially the synthesis of hydroxytelechelic polyisoprenes precursors of polyurethanes. In the next part of this chapter describing our works, we present the controlled degradation of the cis-1,4- polyisoprene in two steps, in order to have a good control of the average molecular weights and of the functionality of the oligomers. Then, reduction of the carbonyl chain-ends is described, allowing to obtain hydroxytelechelic polyisoprenes. Then, different modifications of the chains are described.

### 2.3. Oxidative degradation of cis-1, 4-polyisoprene

The controlled degradation of cis-1,4-polyisoprene consists of two steps. Firstly, oxidation of carbon-carbon double bonds is performed using m-chloroperbenzoic acid. Secondly, a selective cleavage at the oxirane ring in epoxidized product is carried out by periodic acid as shown in **Figure 2.25**.

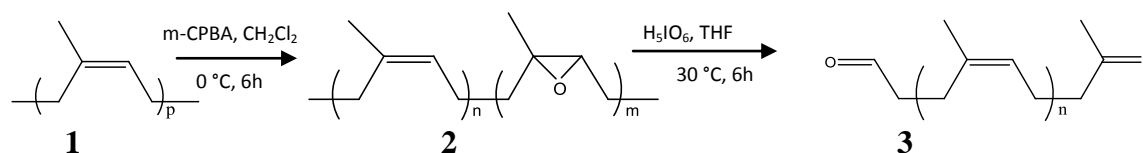


**Figure 2.25** Controlled degradation reaction of cis-1, 4-polyisoprene

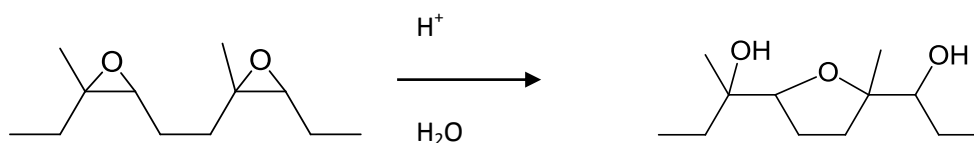
Cis-1,4-polyisoprene **1** was purified by dissolving in dichloromethane and precipitating in excess volume of methanol. <sup>1</sup>H-NMR spectrum of purified cis-1,4-polyisoprene as shown in appendix 1.1, confirmed the purity and stereoregularity of cis-1,4-polyisoprene.

#### 2.3.1. Epoxidation of cis-1,4-polyisoprene

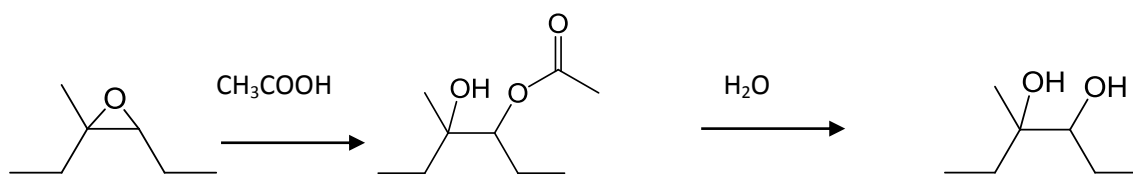
Epoxidation of unsaturated polymer consists of the transformation partially or totally of carbon-carbon double bonds to oxirane rings (epoxides). In our case, we have used metachloroperbenzoic acid as the epoxidation reagent.

The secondary reactions that can occur in this kind of reaction [40, 41] are:

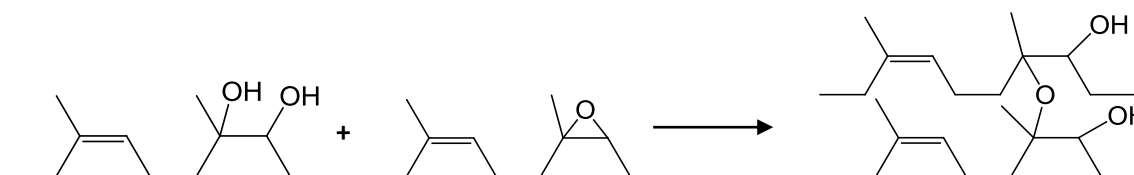
- Furanisation; the reaction giving a cyclic furan unit starts from the two adjacent oxirane rings.



- Formation of ester alcohol and diol in acid medium:



- Crosslinked reaction: formation of ether linkage between chains



In the epoxidation reaction, the reagent were added dropwise to cis-1,4- polyisoprene **1** solution in dichloromethane at 0°C. This method allows us to obtain the amount of epoxidation following the proportion of isoprene unit and m-CPBA with the satisfying yield (93-97%).

The characterization of the epoxidized product by  $^1\text{H-NMR}$  was shown in Figure 2.25. The presence of methylenic and methylic protons at the epoxide ring was indicated by a triplet peak at 2.68 ppm and a singlet peak at 1.29 ppm, respectively. However, in this case, signals of OH group were not observed, These signals would indicate the products of the oxirane ring opening secondary reaction, at chemical shift about 3 and 4 ppm. By  $^{13}\text{C}$  NMR characterisation (**Figure 2.27**), peaks at 60.88 and 64.57 correspond to carbon of epoxide ring.

The percentage of epoxidation can be estimated from the ratio of integration peaks of proton at the epoxide ring ( $\delta = 2.68$  ppm) ( $I_{\text{epoxide}}$ ) and ethylenic proton ( $\delta=5.12$  ppm) ( $I_{\text{C=CH}}$ ) of isoprene unit following equation:



$$\tau = I_{\text{epoxide}} * 100 / ( I_{\text{epoxide}} + I_{\text{C=CH}} )$$

The percentage of epoxidation of product obtained is nearly the same as the calculated one according to the amount of added m-CPBA (~10% molar in this case)( Table 1 in experimental part).

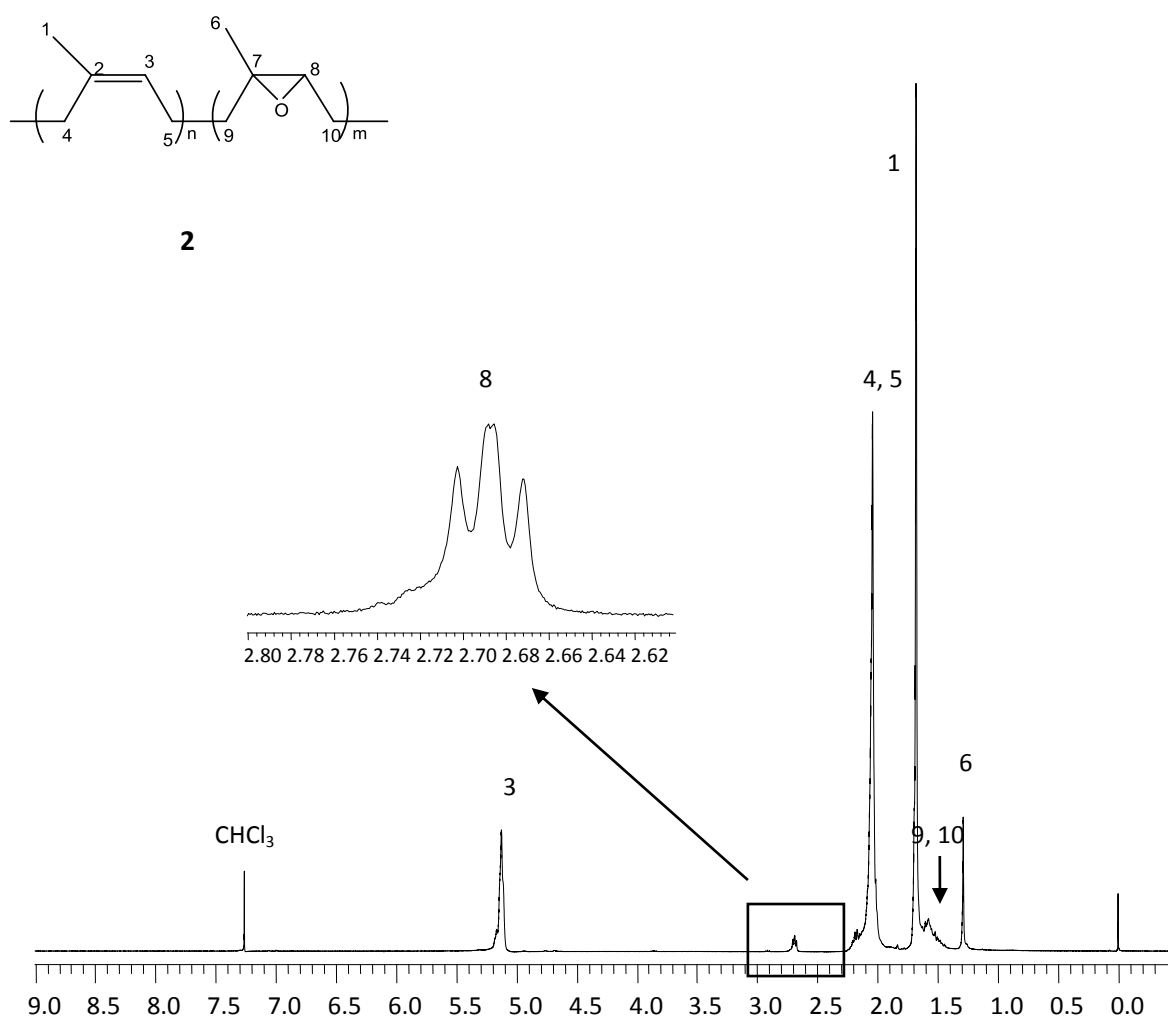


**Figure 2.26**  $^1\text{H-NMR}$  spectrum of epoxidized cis-1,4-polyisoprene 2

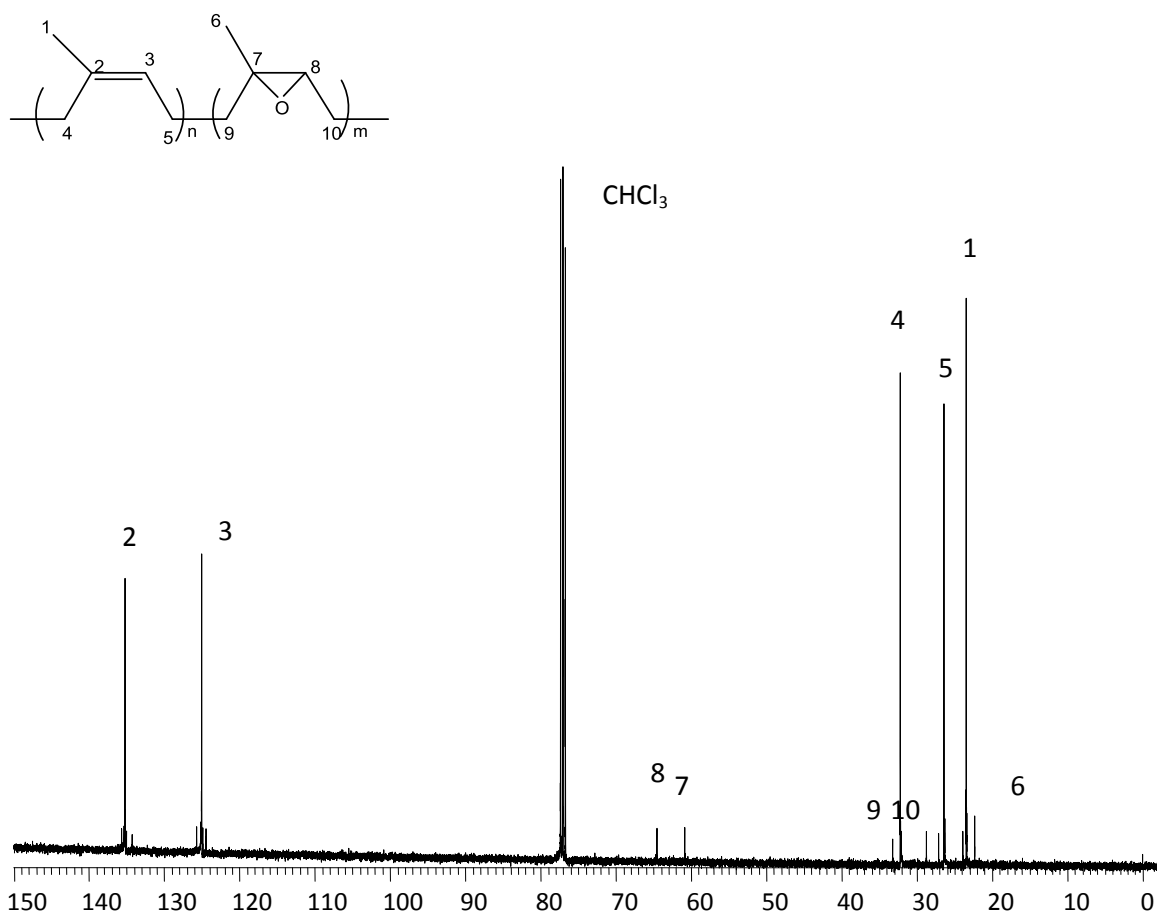


**Figure 2.27**  $^{13}\text{C}$ -NMR spectrum of epoxidized cis-1, 4-polyisoprene 2

### 2.3.2. Cleavage of epoxidized cis-1,4-polyisoprene 2 in organic medium

The oxirane rings are very reactive toward chemical reactions involving hydrogen donor molecules, thus many chemical modifications can be done from this site, especially cleavage. The cleavage of polyisoprene in organic phase and latex phase using periodic acid has been studied in our laboratory [1, 14, 15, 16, 18]. Periodic acid causes the cleavage of the carbon - carbon bond of the oxirane ring forming shorter chain with the formation of aldehyde and ketone functional groups at the chain ends.

Periodic acid was added dropwise into the solution of epoxidized cis-1,4-polyisoprene 2 in THF. The reaction was performed at 30°C during 6 hours. The degradation product is yellow viscous liquid with yielding 52-86% (Table 2 in experimental part).

The characterization of the product by  $^1\text{H-NMR}$  (Figure 2.28) shows the disappearing of the oxirane unit signals at 2.68 and 1.29 ppm. There are the new peaks at 9.78, 2.49 and 2.35 ppm corresponding to protons at the aldehyde group and  $\text{CH}_2$  at  $\alpha$  and  $\beta$  positions next to the aldehyde end group, respectively. A peak representing methylic protons at ketonic group appears at 2.13 ppm, and  $\text{CH}_2$  at  $\alpha$  and  $\beta$  positions next to ketonic end group at 2.43 and 2.26 respectively.

The integration of peak of proton at aldehyde function at 9.78 ppm ( $I_{\text{CHO}}$ ) or of those of methylenic protons between 2.26 and 2.49 ppm near carbonyl end groups compared with ethylenic proton in isoprene repeat unit ( $I_{\text{C=CH}}$ ) permits us to calculate number average molecular weight of telechelic cis-1,4-oligoisoprene according to the following equation;

$$\overline{M}_n (\text{CTPI}) = [I_{\text{C=CH}} / I_{\text{CHO}}] \times 68 + 100$$

The  $\overline{M}_n$  calculated from  $^1\text{H NMR}$  is  $900 \text{ g}\cdot\text{mol}^{-1}$  for the degradation of 10% epoxidized cis-1,4-polyisoprene.

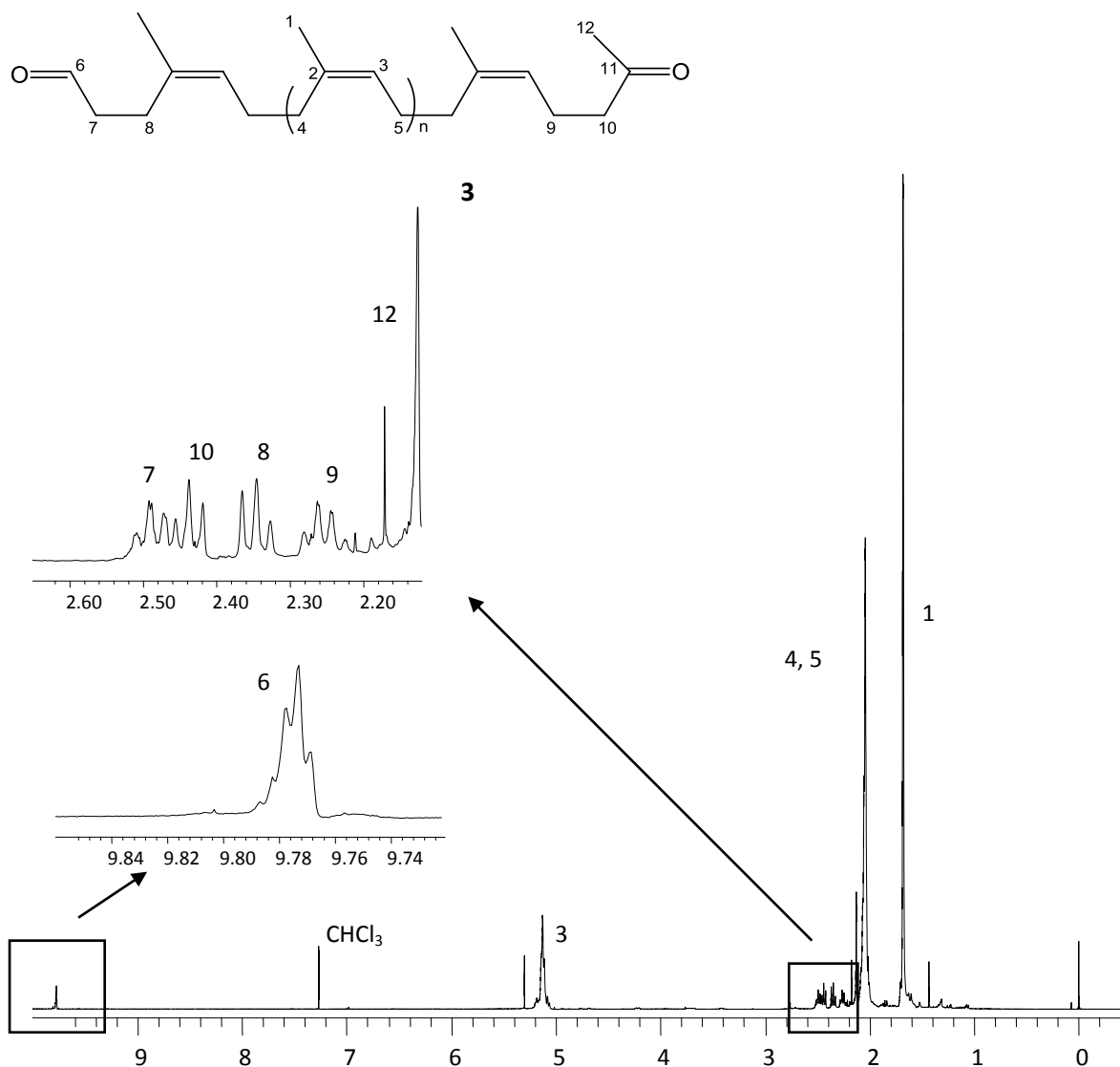


**Figure 2.28** <sup>1</sup>H-NMR spectrum of carbonyltelechelic cis-1,4-polyisoprene (CTPI) **3**

The <sup>13</sup>C NMR analysis (Figure 2.28) shows the disappearing of carbon signals at epoxide unit (60.88 and 64.57 ppm) and appearing of peaks corresponding to aldehyde and ketone carbons at 202.17 and 208.72 ppm respectively.

From FTIR spectra, the characteristic stretching peak of carbonyl group at 1720 cm<sup>-1</sup> was observed.

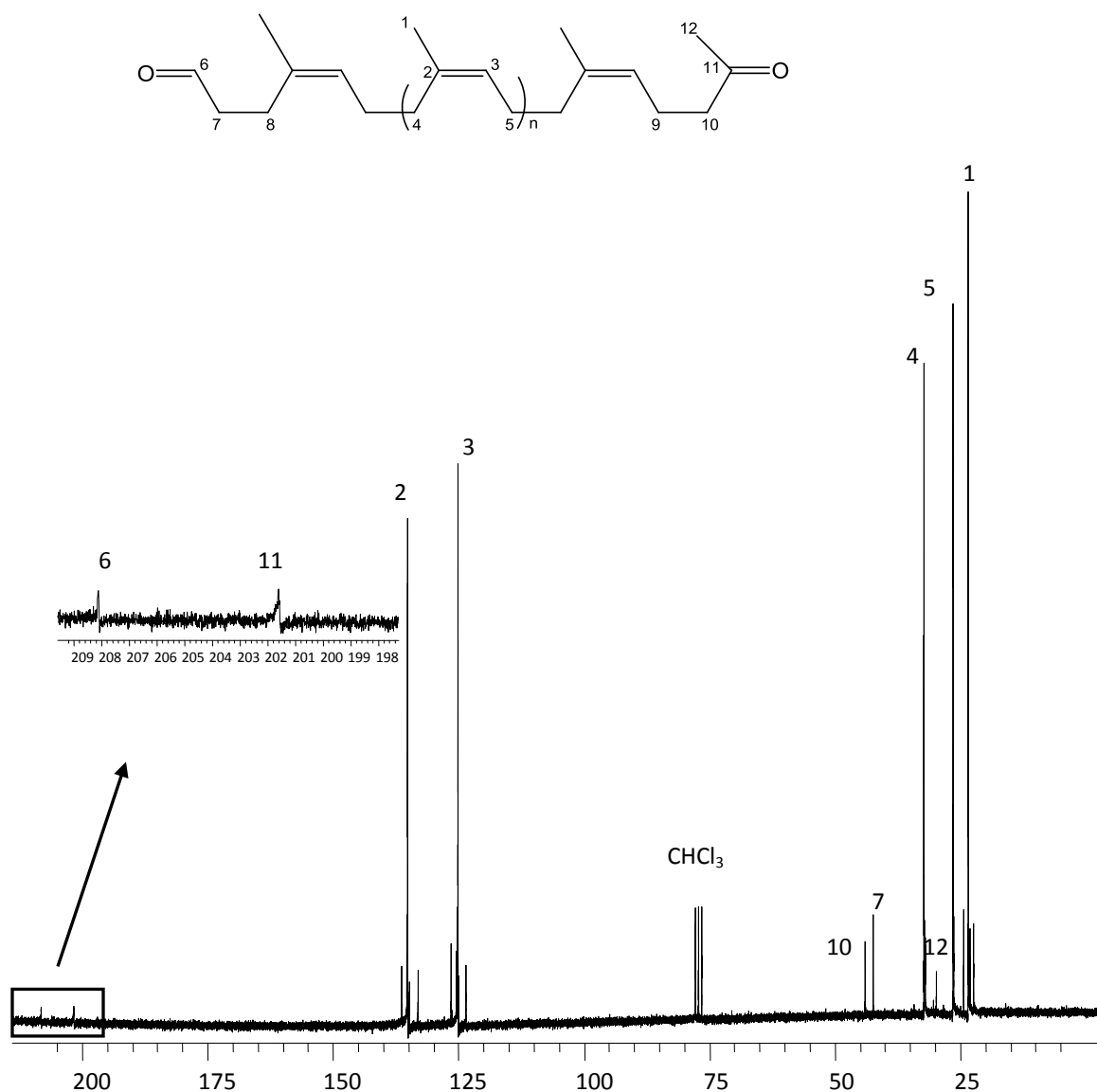


**Figure 2.29**  $^{13}\text{C}$ -NMR spectrum of carbonyltelechelic cis-1,4-polyisoprene (CTPI) **3**

Average molecular weights ( $\overline{M}_n$  and  $\overline{M}_w$ ) and polydispersity index of product was determined by Size Exclusion Chromatography (SEC) using polystyrene standard calibration. The value of  $\overline{M}_n$  obtained directly from this technique ( $1400 \text{ g}\cdot\text{mol}^{-1}$ ) is much higher than value calculated from NMR. The actual  $\overline{M}_n$  value for polyisoprene is converted from average molecular weight value obtained from SEC (polystyrene standard calibration) using Benoît factor, 0.67 [42]. The relationship is;  $\overline{M}_n(\text{PI}) = 0.67 \overline{M}_n(\text{PS})$ , where  $\overline{M}_n(\text{PS})$  is the real average molecular weight from standard polystyrene and  $\overline{M}_n(\text{PI})$  is real average molecular

weight of cis-1,4-polyisoprene corresponding. The value obtained from this equation ( $940 \text{ g}\cdot\text{mol}^{-1}$ ) is close to value obtained from  $^1\text{H-NMR}$  ( $900 \text{ g}\cdot\text{mol}^{-1}$ ).

#### 2.4. Synthesis and characterization of hydroxytelechelic polyisoprene precursor of polyurethane.

Synthesis of hydroxytelechelic cis-1,4-polyisoprene **4** from carbonyltelechelic cis-1,4-polyisoprene **3** was achieved using sodium borohydride as the specific reduction agent at  $60^\circ\text{C}$  for 6 hours. The metal hydride reduces carbonyl function groups into alcohol groups without effect on the carbon-carbon double bond. The reaction pathway was shown in **Figure 2.30**.

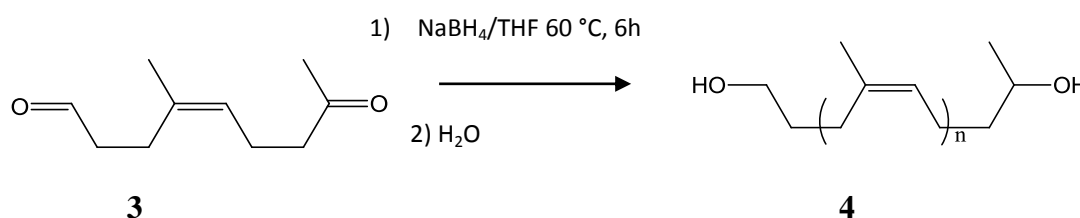


**Figure 2.30** Synthesis reaction of hydroxytelechelic cis-1, 4-polyisoprene **4**

The  $^1\text{H-NMR}$  spectrum (**Figure 2.31**), allows observing that the characteristic peaks of aldehyde and methylketone protons at 9.78 and 2.13 ppm respectively, and those of the methylenic protons in  $\alpha$  and  $\beta$  positions from carbonyl end groups have disappeared. The triplet and multiplet peaks corresponding to  $\text{CH}_2$  and  $\text{CH}$  next to hydroxyl groups at the chain ends were noted at 3.63 and 3.80 ppm, respectively. Moreover, a doublet peak of methyl protons of secondary alcohol was remarked at 1.18 ppm.

Number average molecular weight of hydroxytelechelic cis-1,4-polyisoprene can be calculated from following equation:

$$\overline{M}_n = [I_{\text{C}=\text{CH}}/I_{\text{CHOH}}] \times 68 + 104$$

Where  $I_{\text{C}=\text{CH}}$  = signal integration of ethylenic proton

$I_{\text{CHOH}}$  = signal integration of CH proton in  $\alpha$ -position of hydroxyl group

The number average molecular weight calculated from  $^1\text{H-NMR}$  is  $1100 \text{ g}\cdot\text{mol}^{-1}$  which corresponds to the value obtained from SEC.

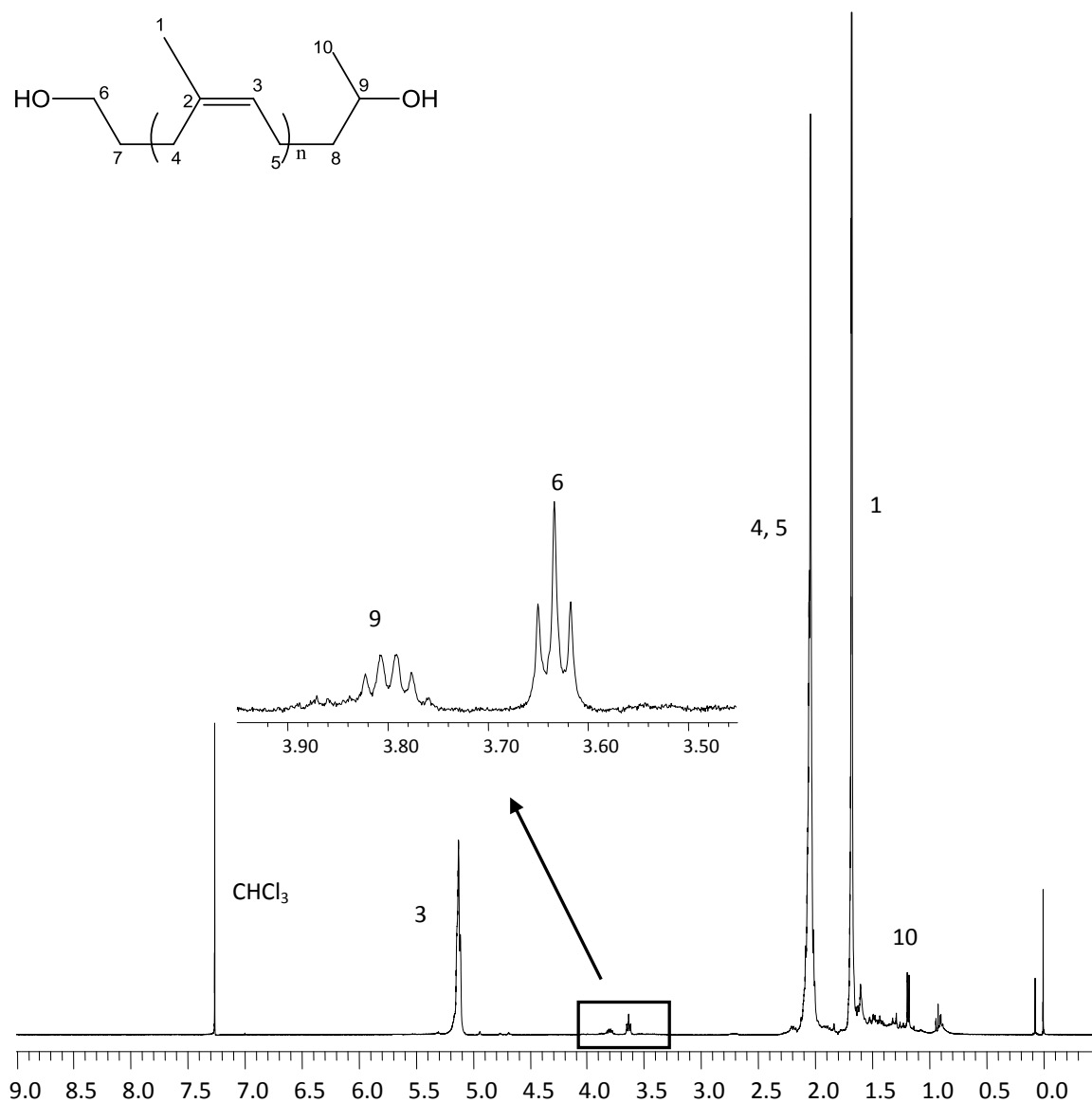


**Figure 2.31**  $^1\text{H-NMR}$  spectrum of hydroxytelechelic cis-1, 4-polyisoprene (HTPI) 4

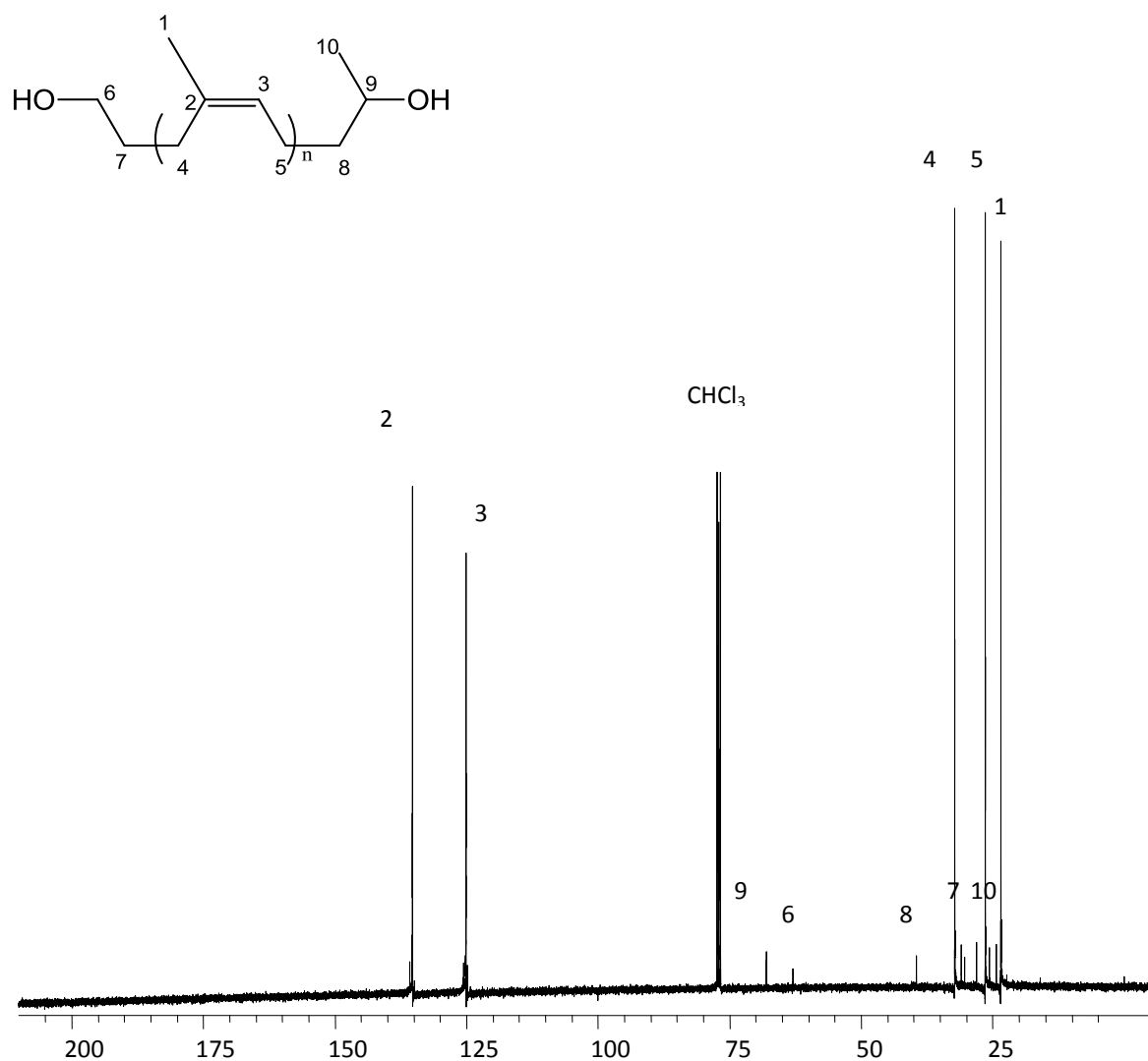


**Figure 2.32**  $^{13}\text{C}$ -NMR spectrum of hydroxytelechelic cis-1, 4-polyisoprene **4**.

By  $^{13}\text{C}$ -NMR characterization (Figure 2.32), we observed appearing of peaks at 62.93 and 67.96 ppm corresponding respectively to  $\text{CH}_2$  and  $\text{CH}$  of primary and secondary alcohols. Also, peak of methylic carbon at secondary alcohol appears at 24.24 ppm.

From FTIR spectra, we perceived the disappearing of  $\text{C}=\text{O}$  stretching band at  $1720\text{ cm}^{-1}$  and appearing of  $\text{O-H}$  stretching at  $3350\text{ cm}^{-1}$ .



## 2.5. Modification of hydroxytelechelic cis-1,4-polyisoprene precursor of polyurethanes.

The modifications of hydroxytelechelic cis-1,4-polyisoprene main chain were carried out by epoxidation as shown in **Figure 2.33**.

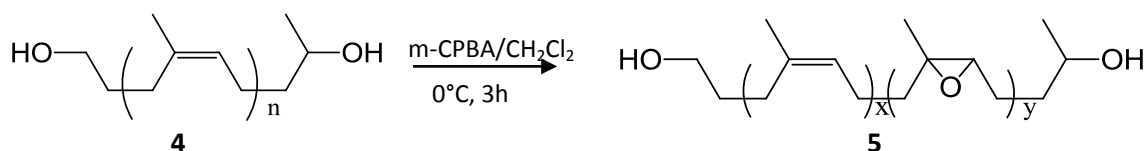


**Figure 2.33** Main chain modification of hydroxytelechelic cis-1,4-polyisoprene **4**

### 2.5.1. Epoxidation of hydroxytelechelic cis-1,4-polyisoprene **4**

Epoxidized hydroxytelechelic cis-1, 4-polyisoprene **5** with different percentages corresponding to different proportions of isoprene unit and epoxidizing reagent were performed at 0°C in CH<sub>2</sub>Cl<sub>2</sub> for 3 h using m-CPBA as the epoxidizing agent.

**Table 2.1** Experimental conditions and characteristics of hydroxyl telechelic polyisoprene after epoxidation.

Entry	Code	HTPI	Eq.M ol HTPI	Eq.mol m- CPBA	Mass (g)	Yield (%)	$\bar{M}_n$ (NMR)	$\bar{M}_n$ (SEC)	PDI	%E
<b>1</b>	EH1	HTPI10	1	0.1	3.53	83	1194	1000	1.67	6.3
<b>2</b>	EH2	HTPI10	1	0.3	3.22	86	1306	1000	1.69	27.7
<b>3</b>	EH3	HTPI10	1	0.5	2.8	84	1474	1000	1.64	61.3
<b>4</b>	EH4	HTPI11	1	0.3	2.0	85	1708	1100	1.56	34.8
<b>5</b>	EH5	HTPI11	1	0.5	2.1	82	1936	1100	1.69	60.1
<b>6</b>	EH6	HTPI11	1	0.1	1.84	83	1718	1000	1.7	10.2
<b>7</b>	EH7	HTPI12	1	0.1	1.85	85	-	7200	1.82	9.2
<b>8</b>	EH8	HTPI12	1	0.3	2.17	84	-	6200	2.17	38
<b>9</b>	EH9	HTPI12	1	0.5	2.10	87	-	7600	1.83	62.5
<b>10</b>	EH10	HTPI13	1	0.1	3.1	90	1090	900	1.56	9.8
<b>11</b>	EH11	HTPI13	1	0.3	3.0	97	1150	1000	1.55	28.5
<b>12</b>	EH12	HTPI13	1	0.5	3.17	87	1220	1000	1.43	43.0
<b>13</b>	EH13	HTPI14	1	0.1	4.0	90	-	4100	2.5	8.2

<b>14</b>	EH14	HTPI14	1	0.3	4.0	89	-	4000	1.95	24.6
<b>15</b>	EH15	HTPI14	1	0.5	3.4	86	-	4000	1.97	47.6

E(%) = percent of epoxidation determined according  $^1\text{H}$  NMR spectrums, Eq.Mol HTPI = Equivalent mole of Hydroxytelechelic polyisoprene, Eq.mol m-CPBA = Equivalent mole of meta- chloroperbenzoic acid, Yield (%) = polymer recovery yields,  $M_n$  (NMR) = determined with NMR,  $M_n$  (SEC) = determined with SEC using polystyrene standards and correcting with Benoit factor (0.67 for polyisoprene), PDI = polydispersity index

Different tries were performed using Eq.mol m-CPBA of 0.1(entries 1,6,7,10,13) 0.3(entries 2,4,8,11,14) and 0.5(entries 3,5,9,12,15) in order to have sufficient samples to do adhesive tests. Good reproducibility in the limits of the NMR precision is observed optimization of the recovery yield was performed (82-97%).

From  $^1\text{H}$ -NMR spectrum (Figure 2.34), peaks of protons at the epoxidized isoprene units were detected at 2.68 ( $\text{CH}_{\text{oxirane ring}}$ ) and 1.29 ppm ( $\text{CH}_3\text{C}_{\text{oxirane ring}}$ ). Intensity of signal at 2.68 ppm increases as percentage of epoxidation increases while intensity of ethylenic protons at 5.12 ppm decreases.

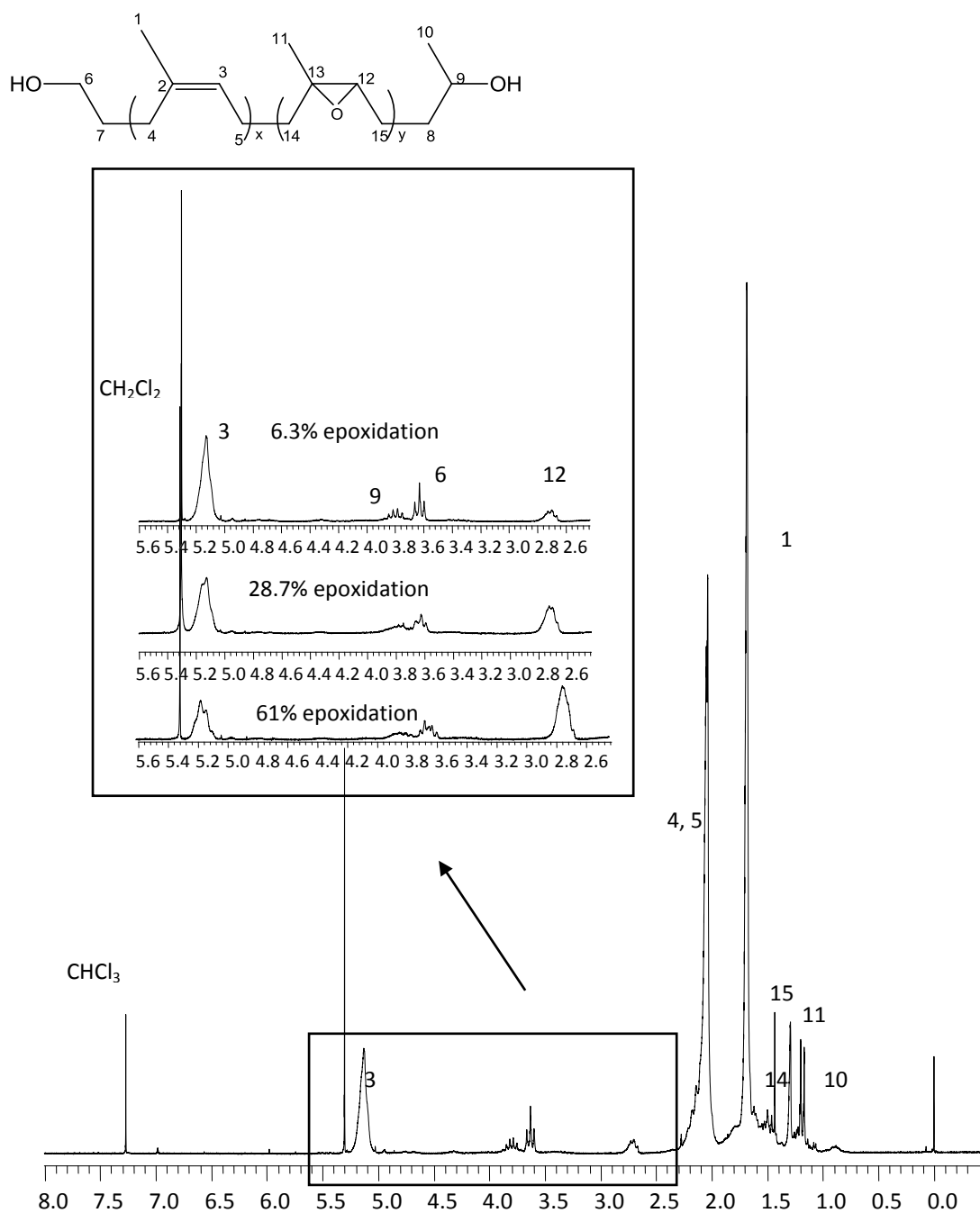


**Figure 2.34**  $^1\text{H-NMR}$  spectrum of 6.3 % epoxidized hydroxytelechelic cis-1,4-polyisoprene compared to those of 28.7% and 61% epoxidized oligomers

In addition,  $^{13}\text{C-NMR}$  spectrum confirmed the presence of peaks corresponding to carbons at oxirane ring at chemical shift 59.77 ppm ( $\text{CH}_3\text{C}_{\text{oxirane ring}}$ ) and 63.47 ppm ( $\text{CH}_{\text{oxirane ring}}$ ). (Figure 2.35).

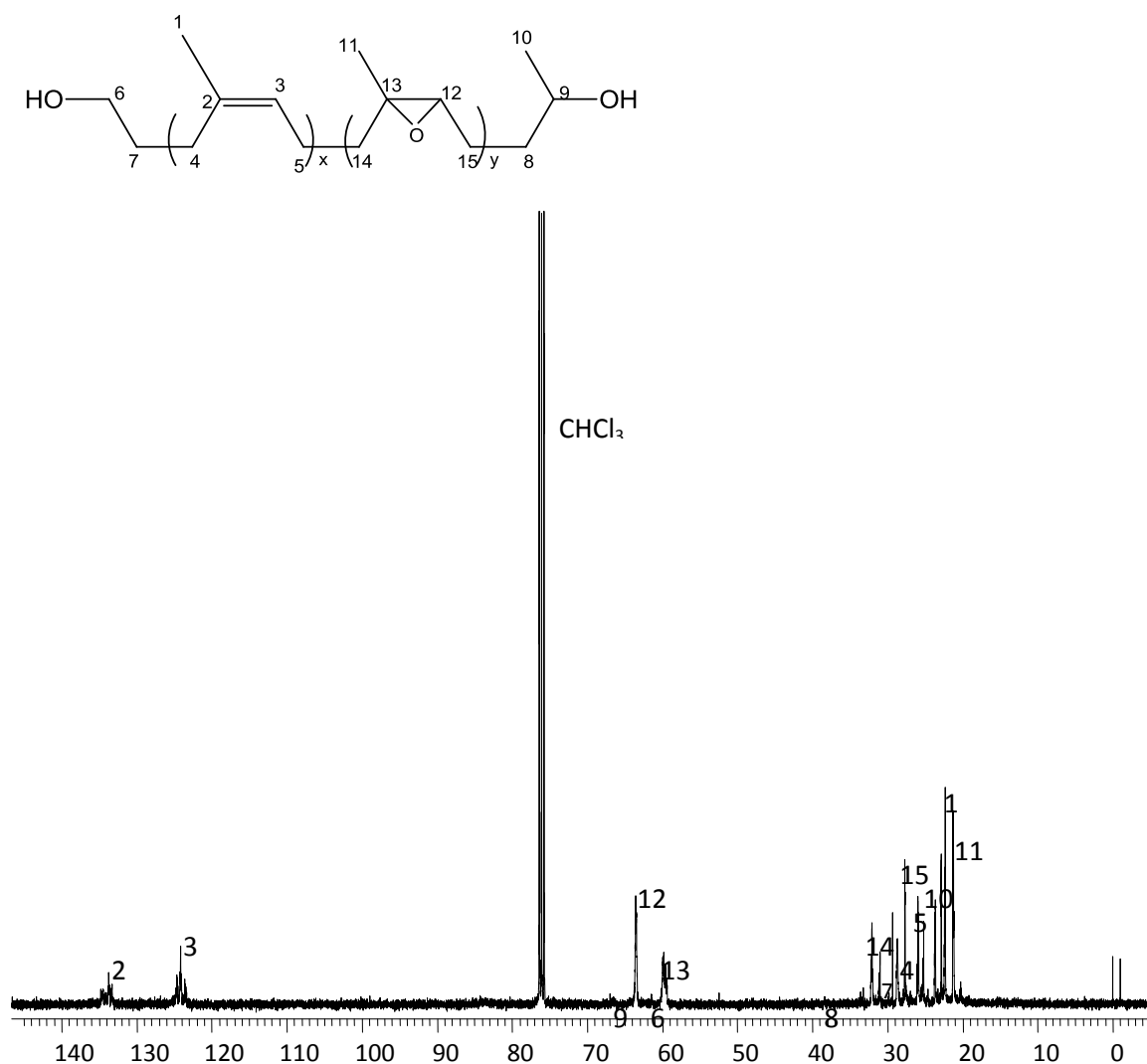


**Figure 2.35**  $^{13}\text{C}$ -NMR spectrum of epoxidized hydroxytelechelic cis-1,4-polyisoprene 5

IR analysis of oligomers has been also performed. Assignment of infrared absorption bands for the hydroxytelechelic oligomers and for the epoxidized hydroxytelechelic oligomers are detailed in the Table 2.2 and 2.3 respectively.

**Table 2.2** Assignment of infrared absorption bands for the hydroxytelechelic segment

Wave number (cm <sup>-1</sup> )	Assignment [43]
3336-3344	$\nu_{OH}$
3035	$\nu_{C=C-H}$
2960-2726	$\nu_{CH_2, CH_3}$ ( $CH_3$ asymmetric stretching)
1664	$\nu_{C=C}$
1448	$\nu_{CH_2, CH_3}$ cis-1,4-isoprene
1376	$\nu_{CH_2, CH_3}$ cis-1,4-isoprene
1127	$\nu_{CH_2, CH_3}$ cis-1,4-isoprene
834	$\delta_{C=C-H}$

**Table 2.3** Assignment of infrared absorption bands for the epoxidized hydroxytelechelic segment (EH)

Wave number (cm <sup>-1</sup> )	Assignment [18]and [43]
3450	$\nu_{OH}$
3035	$\nu_{C=C-H}$
2960-2726	$\nu_{CH_2, CH_3}$
1664	$\nu_{C=C}$
1448	$\nu_{CH_2, CH_3}$ cis-1,4-isoprene
1376	$\nu_{CH_2, CH_3}$ cis-1,4-isoprene
1250	-C-O of epoxide units
1127	$\nu_{CH_2, CH_3}$ cis-1,4-isoprene
1065-1082	C-C-O stretching
870	$\nu_{C-O}$ (epoxide)
834	$\delta_{C=C-H}$

FTIR analysis (**Figure 2.36**), allow us to observe increasing intensity of  $\delta_{C-O}$  (epoxide) (872 cm<sup>-1</sup>) band as percentage of epoxidation increases, in the other hand, intensity of  $\nu_{C=C}$  and  $\delta_{C=C-H}$  bands at 1664 and 837 cm<sup>-1</sup> decreases.

A spectra normalization has been made on  $\nu_{CH_2, CH_3}$  bands in order to quantitatively compare the intensities of the other bands.

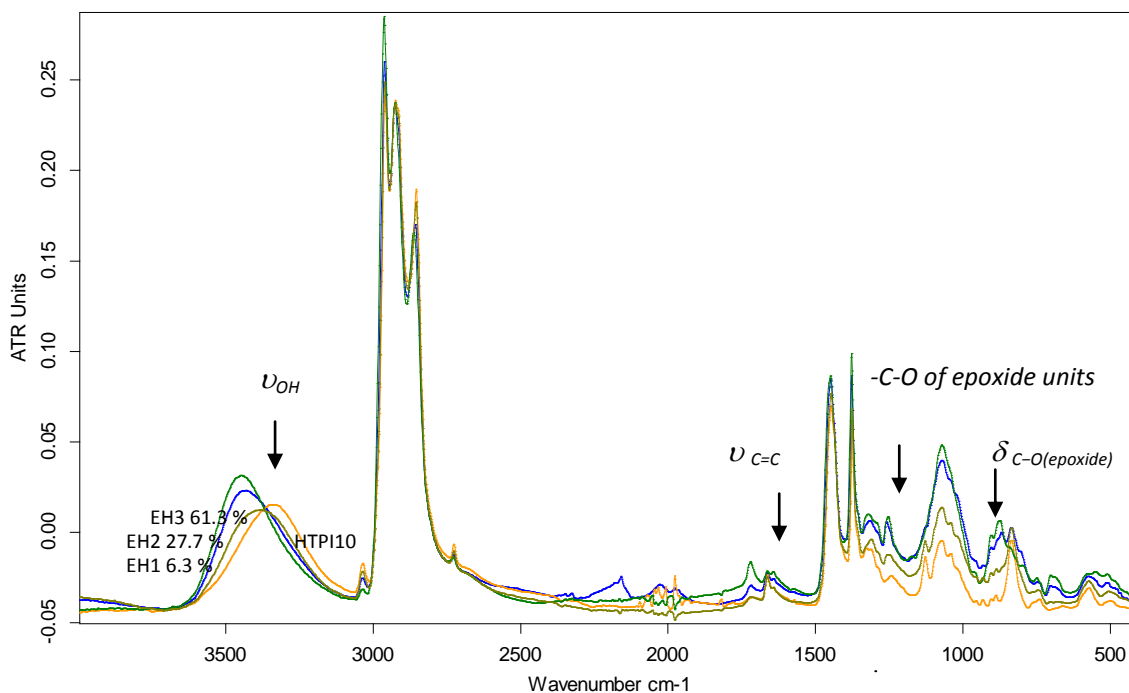
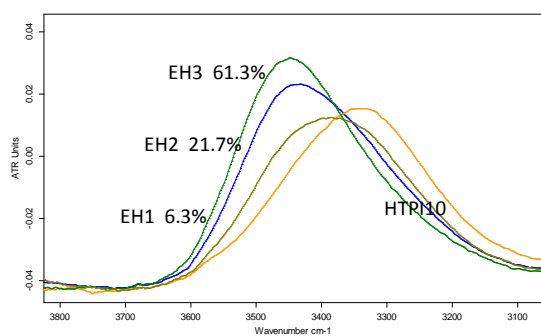


**Figure 2.36** Comparison between ATR FT-IR spectra of HTPI10 EH1 EH2 and EH3

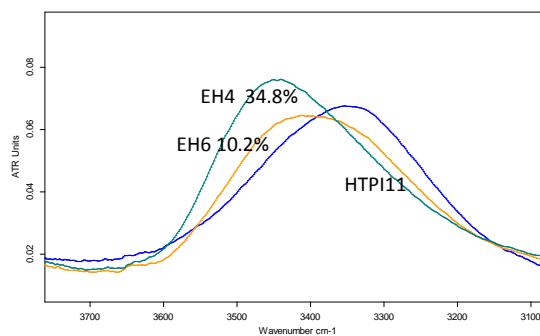
Moreover, it was observed that the oligomers (HTPI or EHTPI) molecular weight increase leads to a decrease of the band intensity of the O-H band (**Figure 2.37**, c and d).

a) Oligomers ( $\overline{M}_n$  1000, various in % epoxide)    b) Oligomers ( $\overline{M}_n$  1000, various in % epoxide)



C:\DATA\kaspi\EH1.0	EH1	ATR DTGS	18/01/2015
C:\DATA\kaspi\EH2.0	EH2	ATR DTGS	18/01/2015
C:\DATA\kaspi\HTPI10.0	HTPI10	ATR DTGS	18/01/2015
C:\DATA\kaspi\EH3.0	EH3	ATR DTGS	18/01/2015

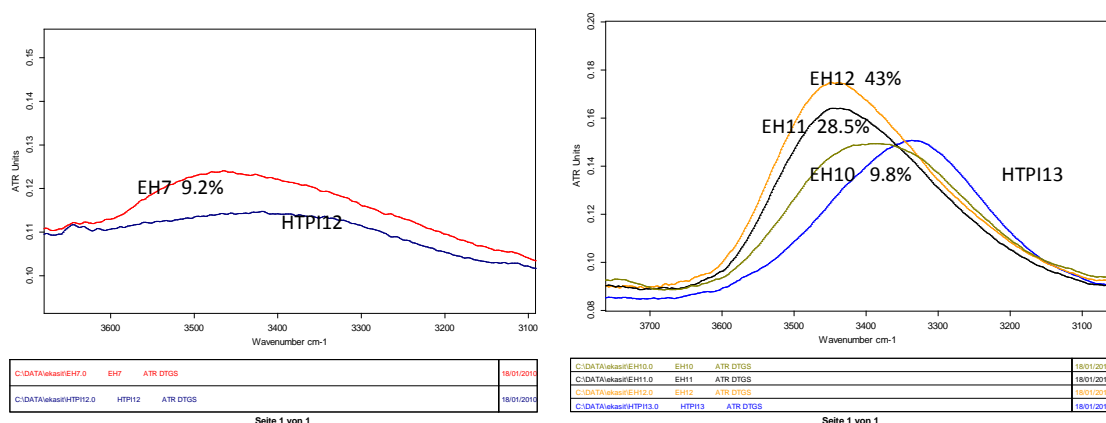
Seite 1 von 1



C:\DATA\kaspi\EH4.0	EH4	ATR DTGS	18/01/2015
C:\DATA\kaspi\EH6.0	EH6	ATR DTGS	18/01/2015
C:\DATA\kaspi\HTPI11.0	HTPI11	ATR DTGS	18/01/2015

Seite 1 von 1

c) Oligomers ( $\overline{M}_n$  8000, various in % epoxide)    d) Oligomers ( $\overline{M}_n$  900, various in % epoxide)



e) Oligomers ( $\bar{M}_n$  4000, various in % epoxide) f) HTPI (various  $\bar{M}_n$ )

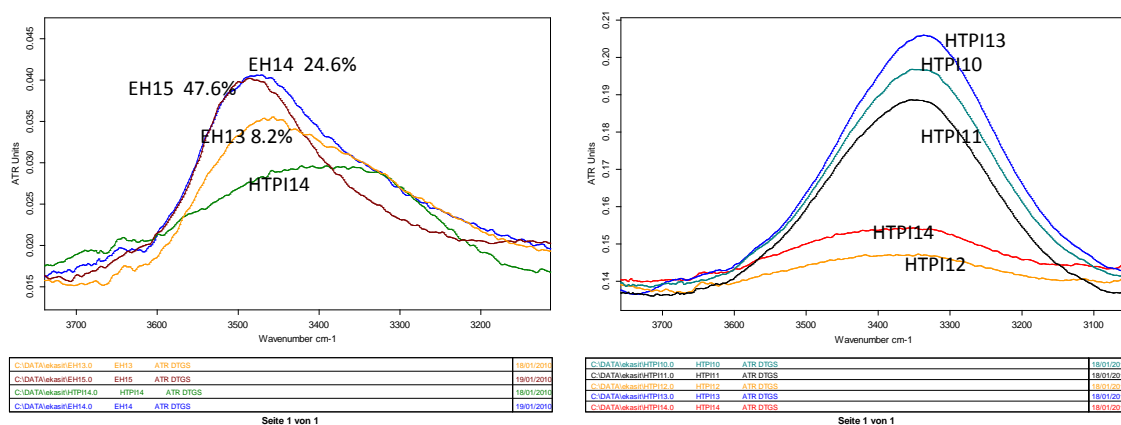
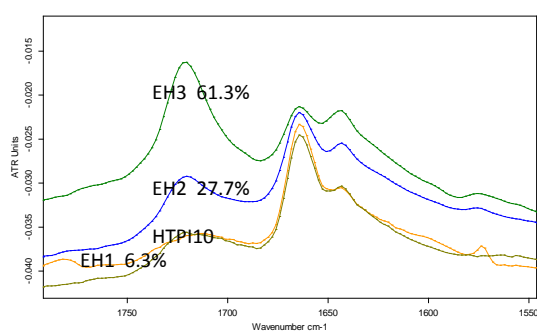


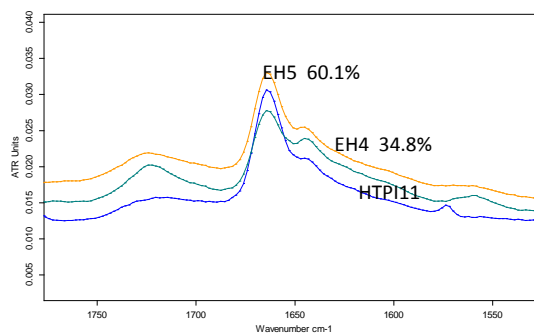
**Figure 2.37** Comparison ATR FT-IR spectra at 3450 cm<sup>-1</sup> between a) HTPI10 EH1 EH2 and EH3 b) HTPI11 EH4 and EH6 c) HTPI12 and EH7 d) HTPI13 EH10 EH11 and EH12 e) HTPI14 EH13 EH14 and EH15 f) HTPI (various  $\bar{M}_n$ )

Comparison of the spectra of different epoxidized polyisoprenes allows us to observe that the O-H band is shift from 3330 cm<sup>-1</sup> for non epoxidized oligomer (HTPI) to around 3450 cm<sup>-1</sup> for the EHTPI with 61.3% of oxirane along the chain. That observed shift may be due to hydrogen bonds between the hydrogen of the hydroxyl groups and the oxygen of the oxirane rings.

a) Oligomers ( $\overline{M}_n$  1000, various in % epoxide) b) Oligomers ( $\overline{M}_n$  1000, various in % epoxide)

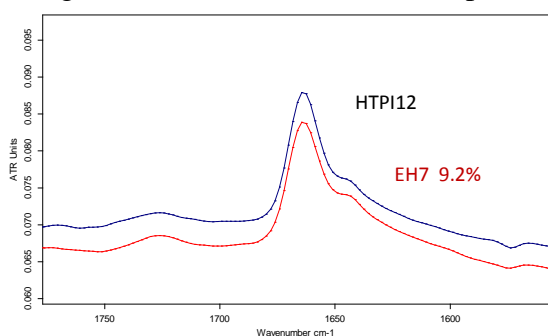


C:\DATA\akast\EH1.0	EH1	ATR DTGS	18/01/2014
C:\DATA\akast\EH3.0	EH3	ATR DTGS	18/01/2014
C:\DATA\akast\HTP110.0	HTP110	ATR DTGS	18/01/2014
C:\DATA\akast\EH2.0	EH2	ATR DTGS	18/01/2014

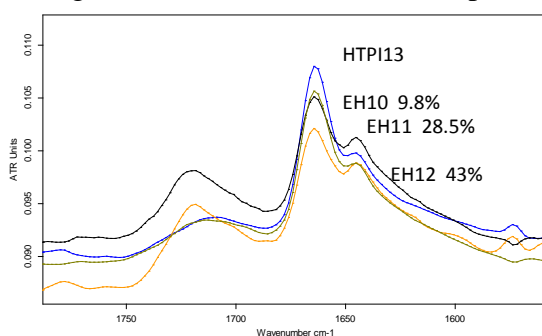


C:\DATA\akast\EH4.0	EH4	ATR DTGS	18/01/2014
C:\DATA\akast\EH6.0	EH6	ATR DTGS	18/01/2014
C:\DATA\akast\HTP111.0	HTP111	ATR DTGS	18/01/2014

c) Oligomers ( $\overline{M}_n$  8000, various in % epoxide) d) Oligomers ( $\overline{M}_n$  900, various in % epoxide)

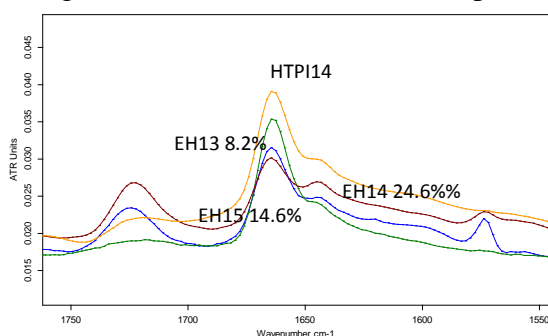


C:\DATA\akast\EH7.0	EH7	ATR DTGS	18/01/2014
C:\DATA\akast\HTP112.0	HTP112	ATR DTGS	18/01/2014



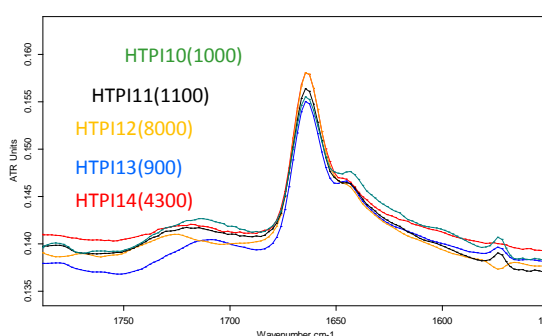
C:\DATA\akast\EH10.0	EH10	ATR DTGS	18/01/2014
C:\DATA\akast\EH11.0	EH11	ATR DTGS	18/01/2014
C:\DATA\akast\EH12.0	EH12	ATR DTGS	18/01/2014
C:\DATA\akast\HTP113.0	HTP113	ATR DTGS	18/01/2014

e) Oligomers ( $\overline{M}_n$  4000, various in % epoxide)



C:\DATA\akast\EH13.0	EH13	ATR DTGS	18/01/2014
C:\DATA\akast\EH15.0	EH15	ATR DTGS	18/01/2014
C:\DATA\akast\HTP114.0	HTP114	ATR DTGS	18/01/2014
C:\DATA\akast\EH14.0	EH14	ATR DTGS	18/01/2014

f) HTPI (various  $\overline{M}_n$ )



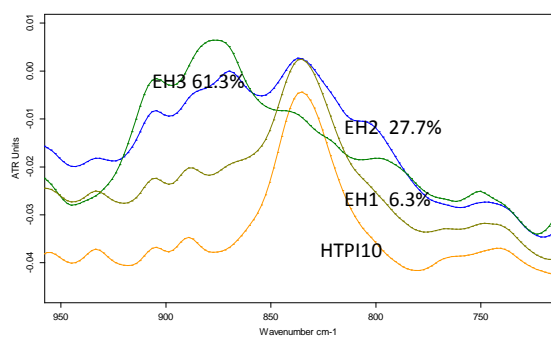
C:\DATA\akast\HTP110.0	HTP110	ATR DTGS	18/01/2014
C:\DATA\akast\HTP111.0	HTP111	ATR DTGS	18/01/2014
C:\DATA\akast\HTP112.0	HTP112	ATR DTGS	18/01/2014
C:\DATA\akast\HTP113.0	HTP113	ATR DTGS	18/01/2014
C:\DATA\akast\HTP114.0	HTP114	ATR DTGS	18/01/2014

**Figure 2.38** Comparison ATR FT-IR spectra at  $1664\text{ cm}^{-1}$  between ATR FT-IR spectra of a) HTP110 EH1 EH2 and EH3 b) HTP111 EH4 and EH6 c) HTP112 and EH7 d) HTP113 EH10 EH11 and EH12 e) HTP114 EH13 EH14 and EH15 f) HTPI (various  $\overline{M}_n$ ).

Focusing on the band at  $1664\text{ cm}^{-1}$  attributed to  $\nu_{C=C}$ , (**Figure 2.38**), it was observed as expected that when the percentage of epoxide increases the intensity of this band decreases (**Figure 2.38 d**), for example).

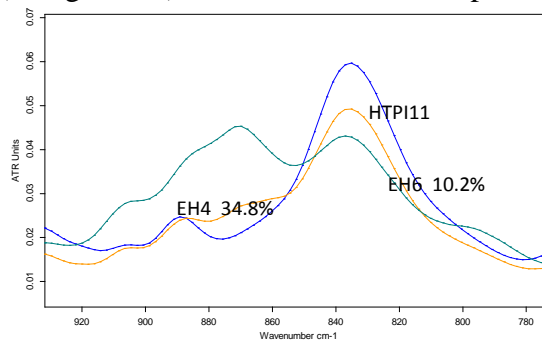


a) Oligomers ( $\overline{M}_n$  1000, various in % epoxide) b) Oligomers ( $\overline{M}_n$  1000, various in % epoxide)



C:\DATA\kasaf\EH3.0	EH3	ATR DTGS	18/01/2014
C:\DATA\kasaf\EH2.0	EH2	ATR DTGS	18/01/2014
C:\DATA\kasaf\HTP10.0	HTP10	ATR DTGS	18/01/2014
C:\DATA\kasaf\EH1.0	EH1	ATR DTGS	18/01/2014

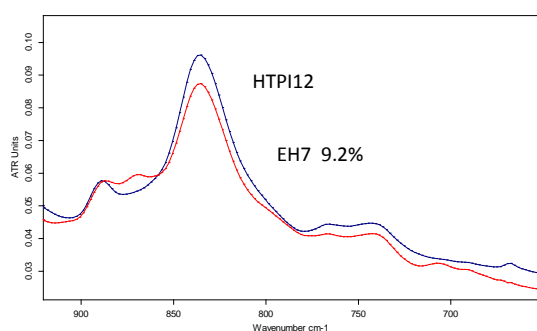
Seite 1 von 1



C:\DATA\kasaf\EH4.0	EH4	ATR DTGS	18/01/2014
C:\DATA\kasaf\EH6.0	EH6	ATR DTGS	18/01/2014
C:\DATA\kasaf\HTP11.0	HTP11	ATR DTGS	18/01/2014

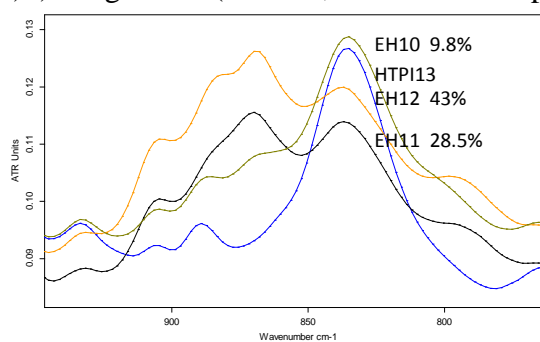
Seite 1 von 1

c) Oligomers ( $\overline{M}_n$  8000, various in % epoxide) d) Oligomers ( $\overline{M}_n$  900, various in % epoxide)



C:\DATA\kasaf\EH7.0	EH7	ATR DTGS	18/01/2014
C:\DATA\kasaf\HTP12.0	HTP12	ATR DTGS	18/01/2014

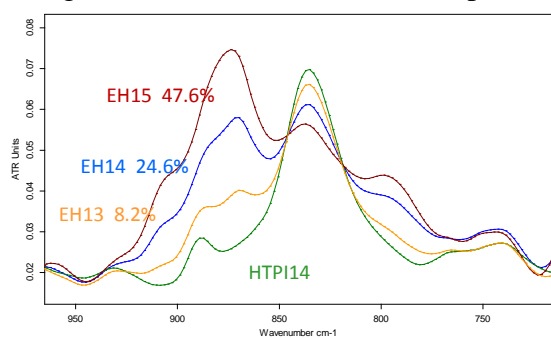
Seite 1 von 1



C:\DATA\kasaf\EH10.0	EH10	ATR DTGS	18/01/2014
C:\DATA\kasaf\EH11.0	EH11	ATR DTGS	18/01/2014
C:\DATA\kasaf\EH12.0	EH12	ATR DTGS	18/01/2014
C:\DATA\kasaf\HTP13.0	HTP13	ATR DTGS	18/01/2014

Seite 1 von 1

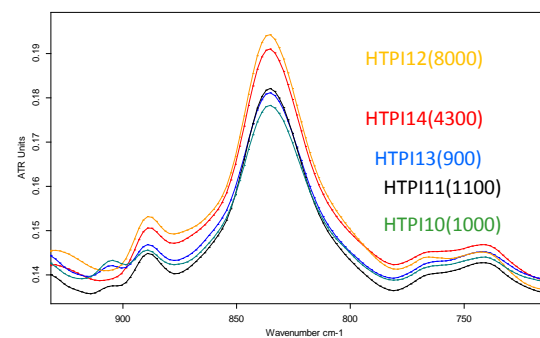
e) Oligomers ( $\overline{M}_n$  4000, various in % epoxide)



C:\DATA\kasaf\EH15.0	EH15	ATR DTGS	18/01/2014
C:\DATA\kasaf\EH14.0	EH14	ATR DTGS	18/01/2014
C:\DATA\kasaf\HTP14.0	HTP14	ATR DTGS	18/01/2014
C:\DATA\kasaf\EH13.0	EH13	ATR DTGS	18/01/2014

Seite 1 von 1

f) HTPI (various  $\overline{M}_n$ )



C:\DATA\kasaf\HTP10.0	HTP10	ATR DTGS	18/01/2014
C:\DATA\kasaf\HTP11.0	HTP11	ATR DTGS	18/01/2014
C:\DATA\kasaf\HTP12.0	HTP12	ATR DTGS	18/01/2014
C:\DATA\kasaf\HTP13.0	HTP13	ATR DTGS	18/01/2014
C:\DATA\kasaf\HTP14.0	HTP14	ATR DTGS	18/01/2014

Seite 1 von 1

**Figure 2.39** Comparison ATR FT-IR spectra at  $870\text{--}830\text{ cm}^{-1}$  between ATR FT-IR spectra of a) HTP10 EH1 EH2 and EH3 b) HTP11 EH4 and EH6 c) HTP12 and EH7 d) HTP13 EH10 EH11 and EH12 e) HTP14 EH13 EH14 and EH15 f) HTPI (various  $\overline{M}_n$ )

Figure 2.39 confirms that the band at  $870\text{ cm}^{-1}$  attributed to  $\nu_{C-O(\text{epoxide})}$ , increases when the percentage of epoxidation increases.

## 2.6 Conclusion

Telechelic cis-1,4-polyisoprene were obtained by controlled degradation of Natural Rubber following a two step process. Partial epoxidation was performed using m-CPBA, and cleavage of the oxirane rings was obtained with periodic acid. Oligomers with aldehyde and ketone chain-ends were obtained with good yields, and no secondary reactions have been detected, in the limit of the precision of the NMR spectroscopy. Carbonyltelechelic oligomers with  $\overline{M}_n$  calculated from  $^1\text{H}$  NMR of  $900 \text{ g}\cdot\text{mol}^{-1}$ , were obtained from 10% epoxidized natural rubber. For this sample, SEC analysis gave a  $\overline{M}_n$  of  $940 \text{ g}\cdot\text{mol}^{-1}$ , with a polydispersity index about 1.9. Different average molecular weights were performed varying the epoxidation ratio. Reduction of the carbonyl chain ends by sodium borohydride leads to the hydroxytelechelic cis-1,4-polyisoprene. Chain modification of these oligomers was done by epoxidation at different ratios. These modified hydroxytelechelic epoxidized oligomers were used as diol precursors in polyurethane synthesis.

## References

- [1] J.C. Brosse, I. Campistron, D. Derouet, A. El Hamdaoui, S. Houdayer, S. Gillier- Ritoit, J. *Appl. Polym. Sci.*, **2000**, 78, 1461.
- [2] H.M. Nor, J.R. Ebdon, *Prog. Sci.*, **1998**, 23, 143.
- [3] G. Boccaccio, H. de Livonnier, *Actual. Chim.*, **1991**, 2, 100.
- [4] J. Tangpakdee, M. Mizokoski, A. Endo, Y. Tanaka, *Rubber Chem. Technol.*, **1998**, 71, 795.
- [5] J.I. Cunneen, *NR Technol.* **1973**, 4, 65.
- [6] T. Ravindran, M.R. Gopinathan, J.D. Francis, *Makromol. Chem. Rapid Commun.* **1986**, 7, 159.
- [7] S.K. Gupta, M.R. Kurup, E. Devadoss, R. Muthiah, S. Thomas, *J. Appl. Polym. Sci.* **1985**, 30, 1095.
- [8] R. Criegé, *Angew. Chem. Internat. Edit*, **1975**, 14, 745.
- [9] Y. Tanaka, Y. Shimizu, P. Boochthum, M. Shimizu, R. Mita, *Polymer*, **1993**, 34, 1098.
- [10] G. Montaudo, E. Scamporrino, D. Vitalini, R. Rapisardi, *J. Polym. Sci. Polym. Chem.; Part A*, **1992**, 30, 525.
- [11] M.P. Anachkov, S.K. Rakovski, R.V. Stefanova, *Polym. Degrad. Stab.*, **2000**, 67, 355.
- [12] C. Guizard, H. Cheradamme, *Eur. Polym. J.*, **1981**, 17, 121.
- [13] D. Burfield, S.N. Gan, *Polymer*, **1977**, 18, 607.
- [14] D. Reyx, I. Campistron, *Die Angew. Makromol. Chem.*, **1997**, 247, 197.
- [15] S. Gillier-Ritoit, D. Reyx, A. Laguerre, I. Campistron, R.P. Singh, *J. Appl. Polym. Sci.*, **2003**, 87, 42.
- [16] R.S. Mauler, F.M. Guaragna, D.L. Gobbi, D. Samios, *Eur. Polym. J.*, **1997**, 33, 399.
- [17] P. Phinyocheep, C.W. Phetphaisit, D. Derouet, I. Campistron, J.C. Brosse, *J. Appl. Polym. Sci.*, **2005**, 95, 6.
- [18] N.Kébir, I. Campistron, A. Laguerre, J.-F. Pilard, C. Bunel, J.-P Couvercelle, and C. Gondard, *Polymer*, **2005**, 46(18), 6869.
- [19] J.C. Marmo, K.B. Wagener, *Macromolecules*, **1993**, 26, 2137.
- [20] J.C. Marmo, K.B. Wagener, *Macromolecules*, **1995**, 28, 2602.
- [21] P.N. Thanki, D. Reyx, I. Campistron, A. Laguerre, R. P. Singh, *Eur. Polym. J.*, **2004**, 40, 2611
- [22] S. S. Solanky, I. Campistron, A. Laguerre, J.-P. Pilard, *Macromol. Chem. Phys.*, **2005**, 206, 1057.
- [23] D.Derouet, P. Phinyocheep, J.C. Brosse, and , G.Boccaccio., *Eur. Polym. J.*, **1990** 26(12), 1301.
- [24] J.B. Pande, D. Raghunath and C.S. Ramakrishnan., *Makromol. Chem.*, **1956**, 20(1), 181.
- [25] J.C. Brosse, G. Boccaccio and R. Pautra., *Processing Symp.*, Malays. Rubb. Res. Dev. Board, Kuala Lumpur Malaysia., **1981**, 195.
- [26] R. Pautra and J. Marteau, **1976**. US 3957737.
- [27] H. Kwart, and D.M Hoffman., *J. Org. Chem.*, **1966**, 31(2), 419.
- [28] J.C Brosse, J.C Soutif, and C.P Pinazzi, *Makromol. Chem.*, **1979**, 180(9), 2109.
- [29] J.C. Soutif, and J.C. Brosse, *Makromol. Chem.*, **1984**, 185(5), 839.

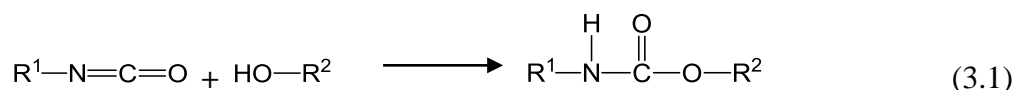
- [30] S. Jayawardena, D. Reyx, D. Durand, and C.P. Pinazzi, *Makromol. Chem.*, **1984**, *185(10)*, 2089.
- [31] D. Derouet, F. Morvan, and J.C. Brosse, *Eur. Polym. J.*, **2001**, *37(7)*, 1297.
- [32] D. Derouet, J.C. Brosse, and A.Challioui, *Eur. Polym. J.*, **2001**, *37(7)*, 1315.
- [33] N. Hinchiranan, K. Charmondusit, P. Prasassarakich, and G.L. Rempel., *J. Appl. Polym. Sci.*, **2006**, *100(5)*, 4219.
- [34] R. Tangthongkul, P. Prasassarakich, and G.L. Rempel, *J. Appl. Polym. Sci.*, **2005**, *97(6)*, 2399.
- [35] J. Samran, P. Phinyocheep, P. Daniel, and S. Kittipoom., *J. Appl. Polym. Sci.*, **2005**, *95(1)*, 16.
- [36] N. Kébir, I. Campistron, A. Laguerre, J.F. Pilard, C. Bunel, and J.P. Couvercelle, *e-Polymers*, **2006**, 48.
- [37] G. Morandi, N. Kebir, I. Campistron, F. Gohier, A. Laguerre, and J.F. Pilard, *Tetrahedron Lett.*, **2007**, *48(43)*, 7726.
- [38] S. Gopakumar, and M.R.G.Nair, *Polym. Eng. Sci.*, **2006**, *46(12)*, 1812.
- [39] T. Ravindran, M.R.G. Nayar, and D.J. Francis, *J. Appl. Polym. Sci.*, **1991**, *42(2)* 325.
- [40] N. Kebir, *Elaboration de nouveaux polyuréthanes à partir de cis-1,4-oligoisoprènes hétérocarbonyltéléchéliques issus de la dégradation contrôlée du cis-1,4-polyisoprène de haute masse. Etude de leurs propriétés mécaniques, thermiques et biocides*, thèse de l'Université du Maine, Le Mans, **2005**.
- [41] M.C.S. Perera, J.A. Elix, J.H. Bradbury, *J. Polym. Sci, Part A* **1988**, *26(2)*, 637.
- [42] J.P. Busnel, *Polymer*, **1982**, *23*, 139.
- [43] D.Derouet, J-C Brosse and A. Challioui, *Eur Polym J.*, **2001**, *37*, 1327.

***Chapter 3 - Synthesis and characterization of  
polyurethane base on cis-1,4- polyisoprene***

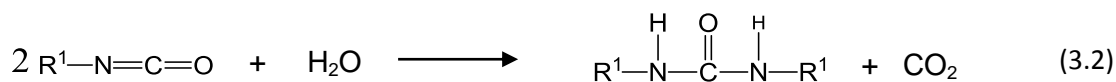
### 3.1 Introduction

Polyurethane polymers are essential components for many composites, coatings, paints, lacquers and for structural adhesives that are used for example in metal adhesive joints. The performances of such compound material including their strength and durability, depend strongly on the properties of the interphase that evolves during the polymerisation as a boundary layer due to the specific interactions between the reactive polymer system and the substrate surface. The properties of this boundary layer and the processes that lead to its formation are not well understood so far although they are considered to play a key role for the relevant technical properties [1].

Normally, polyurethane forms as a reaction product of the polyaddition of di- or multifunctional isocyanates and di- or multifunctional alcohols, according to Eq. (3.1).



The difunctional isomers of the toluene diisocyanate (TDI) and of the methylene diphenyl diisocyanate (MDI) are the technically most important isocyanate hardeners. Di- or multifunctional polyester or polyether polyols are usually used as hydroxyl components. The functionality, chain length, or molecular weights of the polyol molecules determine the properties of the final polymer. Linear thermoplastic polyurethanes result from difunctional components. If chain extenders (e.g., 1,4-butanediol) are added to difunctional polyesters or polyethers, thermoplastic polyurethanes become inhomogeneous and separate into hard and soft domains as a consequence of strong intermolecular interactions (hydrogen bonding of urethane groups). For a polyurethane elastomer that is cross-linked to a low extent, the phase separation is avoided and the bulk of that polymer is homogeneous. Due to the omnipresence of more or less amounts of water in the atmosphere or adsorbed on surfaces, its reaction with isocyanates [Eq. (3.2)] may also be relevant for the chemistry of polyurethanes, especially in thin films and coatings [1].



It is important to note that the water molecules also act as chain extenders and that the reaction product urea is also capable to build strong hydrogen bonds that could give rise to phase separation. Only few informations can be found in the literature on the adhesive interactions of polyurethanes and metal surfaces. Though it is well known that many inorganic substances have a catalytic influence on the formation of urethane groups [2] or on the reactivity of the isocyanate group in general[3].

In this study, adhesion of thin films of polyurethane (PU) systems based on hydroxytelechelic polyisoprene and epoxydized hydroxytelechelic polyisoprene, was investigated on the glass and steel. Their  $\overline{M}_n$  and % epoxide is thereby varied to give access to microstructure gradients even though all relevant measuring techniques (e.g. IR spectroscopy, DSC, TGA). In this way, the resulting chemical structure and the morphology of the polymer films differs.

## 3.2 Bibliographic part on polyurethane

### 3.2.1 History and Development of Polyurethanes

Polyurethanes are formed by a simple polyaddition reaction. They are a unique class of polymers that have a wide range of applications as diverse as coatings, adhesives, elastomers, fibers and foams. The first basic diisocyanate polyaddition reactions were discovered by Otto Bayer and coworkers at I. G. Farben industrie, Germany in 1937 [4] This discovery responses to the competitive challenge arising from Carother's work on polyamides, or nylons, at E. I. du Pont. The successful development of high molecular weight polyamides at E. I. du Pont stimulated Bayer to investigate similar materials that were not covered by Du Pont's patents. The initial work was to react an aliphatic isocyanate with a diamine to form polyureas that were infusible, but very hydrophilic. Further research on this subject demonstrated that when an aliphatic isocyanate reacted with a glycol, a new material with interesting properties for production of plastics and fibers could be made. Du Pont and ICI soon recognized the desirable elastic properties of polyurethanes. The industrial scale production of polyurethane started in 1940. But subsequent market growth of these materials

was seriously impacted by World War II. A noticeable improvement in the elastomeric properties PU waited until 1952, when polyisocyanate, especially toluene diisocyanate (TDI), become commercially available. In 1952–1954, Bayer developed different polyester–polyisocyanate system. In 1958, Schollenberger of BF Goodrich introduced a new virtually crosslinked thermoplastic PU elastomer. At approximately the same time, Dupont introduced a Spandex fibre called Lycra, which is a PU based on polytetramethylene glycol (PTMG), 4,4'-diphenylmethane diisocyanate (MDI) and ethylene diamine. By the early 1960s, BF Goodrich produced Estane, Mobay marketed Texin, and Upjohn marketed Palleshane in the USA. Bayer and Elastgran marketed Desmopan and Elastollan, respectively in Europe [5].

In addition to elastomers, polyurethanes can also be produced as foams (rigid and flexible), adhesives, binders, coatings, and paints. Because of their unique properties, polyurethanes have found a wide variety of applications in the automotive, furniture, construction, and foot wear industries, as seating, exterior panels, structural foam, housing for electric equipment, shoe and boot soles, and refrigerator insulation [5].

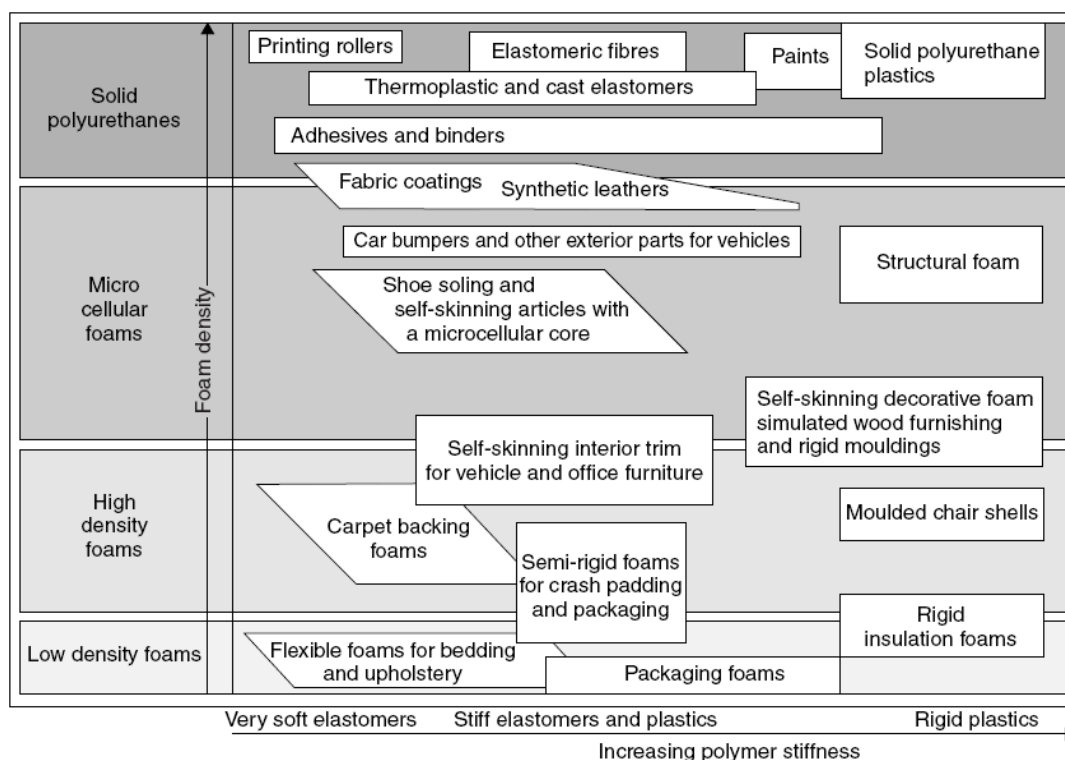


Figure 3.1 Property matrixes for polyurethanes. [6]



### 3.2.2 Raw Materials in polyurethane synthesis

Polyurethanes are linear polymers that have a molecular backbone containing carbamate groups ( $-\text{NHCO}_2$ ). These groups, called urethane, are produced through an addition reaction between a diisocyanate and a polyol. The reaction rapidly yields high molecular weight materials. Polyurethanes typically also contain other functional groups in the molecule including esters, ethers or urea groups. A variety of raw materials are used to produce polyurethanes. These include monomers, prepolymers, stabilizers which protect the integrity of the polymer, and colorants [7].

#### 3.2.2.1 Isocyanates

Isocyanates are mainly constituents of hard segments of polyurethanes. With increasing symmetry of the isocyanate, the following properties increase: the ability of the polyurethane to crystallize, microphase separation, modulus of elasticity, tensile strength, hardness. From isocyanates of a more regular structure and with an aromatic backbone structure, improvement of the strength of polyurethane is obtained. Many publications studied the effect of the isocyanate structure on the polyurethane properties.

Both aliphatic and aromatic isocyanates can be used to synthesize polyurethanes. The presence of an aromatic isocyanate in the hard segment produces a stiffer polymer chain with higher melting point. The two most commonly used isocyanates are toluene diisocyanate (TDI) and 4,4'-diphenylmethane diisocyanate (MDI). TDI is less expensive than MDI, but MDI has superior reactivity, and polymers based on MDI may possess better physical properties. TDI is usually prepared as an isomeric mixture of 2,4-TDI and 2,6-TDI. MDI is crystallisable while 2,4-TDI does not crystallize in the solid state. Other aromatic diisocyanates, such as naphthalene diisocyanate (NDI) and bitoluene diisocyanate (TODI) also can result in high-performance polymers, but at a higher cost than MDI based materials. MDI is available in several forms based on two types of product, purified monomeric MDI and polymeric MDI [6, 8].

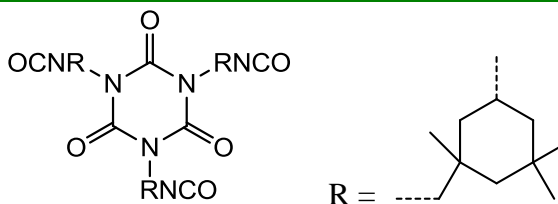
Typical aliphatic diisocyanates include 1,6-hexane diisocyanate (HDI), isophorone diisocyanate (IPDI) and methylene bis(p-cyclohexyl isocyanate) ( $\text{H}_{12}\text{MDI}$ ). Because aromatic diisocyanates and polymers made from them are somewhere unstable toward light and

become yellow with time, aliphatic isocyanates have found wider use in coating applications, than aromatic containing materials. In addition to greater light stability, polyurethanes based on aliphatic isocyanates possess increased resistance to hydrolysis and thermal degradation. Unfortunately, this is sometime accompanied by a decrease in the mechanical properties of the material. The chemical structures of commonly used diisocyanates used in polyurethane synthesis are shown below, in **Table 3.1** [8].

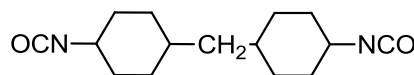
**Table 3.1** Isocyanates used for making polyurethanes

Name	Structure
2,4- , 2,6- toluene diisocyanate (TDI)	
4,4' - methylenediphenyl diisocyanate (MDI)	
1, 5- naphthalene diisocyanate (NDI)	
<i>p</i> - phenylene diisocyanate (PPDI)	
1, 6 – hexamethylene diisocyanate (HDI)	
Cyclohexyl diisocyanate (CHDI)	
Isophorone diisocyanate (IPDI)	

Isocyanurate of isophorone diisocyanate  
(I-IPDI)



4, 4' -dicyclohexylmethane diisocyanate  
(H<sub>12</sub>MDI)



Kébir *et al.* studied the influence of the structure and amount of different isocyanates in polyurethanes based on hydroxyl telechelic cis-1,4-polyisoprene (HTPI) on mechanical behavior and thermal properties. They reported that the diisocyanate structure (TDI, MDI, H<sub>12</sub>MDI) had no notable effect on the behavior of the polyurethanes properties. On the contrary, I-IPDI showed higher crosslink and higher hard segments amount. Moreover, the increase of the isocyanate equivalent ratio ( $[NCO]/[OH] = 1.75$ ) (I-IPDI), enhanced an increase of  $E'$  at the rubbery plateau and a decrease of  $\tan \delta$  max. The following order of thermal stability depending on the isocyanate structure is observed: PU(TDI) < PU(H<sub>12</sub>MDI) < PU(I-IPDI)[9].

### 3.2.2.2 Polyols

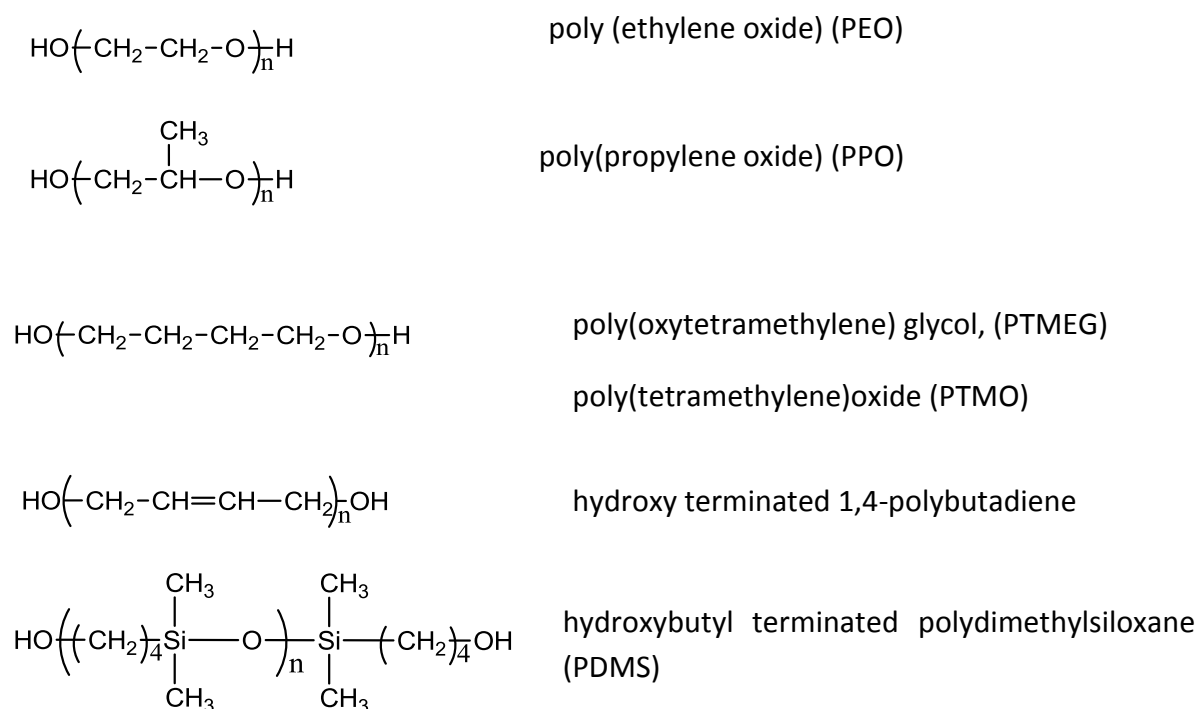
The next materials that have important role in polyurethane structure are polyols. The polyol flexible segments impart flexibility to polyurethane and are responsible to their high elongation at break, low temperature resistance and low  $T_g$ . The best strength properties of polyurethane are achieved by using polyols of symmetrical structure.

Polyols are hydroxyl terminated macromolecules, with molecular weights ranging from 250 to 8000. The structure of polyol is an important factor in determining the properties of polyurethane. A wide range of polyols are used for the manufacture of polyurethanes. However, most of them fall under two classes: hydroxyl terminated polyethers and hydroxyl terminated polyesters [7].

Traditionally, polyurethanes have been produced with polyester and polyether soft segments. Polyurethanes synthesized from polyesters possess relatively good physical properties; however, they are susceptible to hydrolytic cleavage of the ester linkage.

Polyether-based polyurethanes exhibit a relative high resistance to hydrolytic cleavage, when compared with polyester urethanes, and are favoured for used in applications where hydrolytic stability is required. The polyether that results in polyurethane with the best physical properties is polytetramethylene oxide and polytetramethylene glycol (PTMO and PTMEG) [8, 10].

The newer materials from renewable sources for the polymer manufacture in the future in the place of synthetic raw materials for example polyisoprene, we can obtain from natural rubber. Besides, polyurethane was synthesized from common used diol, it is possible to prepare it from hydroxytelechelic polyisoprene. Burel *et al.* have prepared PU network from commercial hydrogenated hydroxy-terminated polyisoprene (EPOL<sup>®</sup>, Atofina)[11]. Furthermore, Kébir *et al.* successfully prepared PU with polyisoprene backbone and they are able to control and modulate PUs structure to obtain lower or higher thermal-mechanical properties than one of commercial polydiene based PU [12, 13].

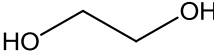
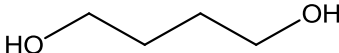
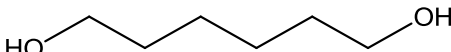
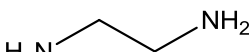


**Figure 3.2** Some commonly used polyols.

### 3.2.2.3 Chain Extenders

Chain extenders are low molecular weight hydroxyl or amine terminated compounds that play an important role in polymer morphology. The choice of chain extender and diisocyanate determines the characteristics of the hard segment and to a large extent the physical properties of polyurethane. The most important chain extenders are linear diols such as ethylene glycol, 1,4-butanediol, 1,6-hexanediol, and hydroquinone bis(2-hydroxyethyl) ether. These diols form well crystallized hard segments with isocyanates. Diamines react faster than diols with isocyanates and result in the formation of the hard segment with a higher density of secondary bonding, high hard segment  $T_g$ , and high thermal stability of the polymer. Table 3.2 lists some common chain extenders [7].

**Table 3.2** Chain extenders

Polyol	Structure
Ethylene glycol	
1,4 - butanediol	
1, 6- hexanediol	
Ethylene diamine	

Kébir *et al* studied the influence of chain extenders on properties of polyurethanes based on HTPI with toluene diisocyanates. It was found that the increase of the chain extender equivalent ratio leads to an increase of  $E'$  at the rubbery plateau, an increase of length of the rubbery plateau and a decrease of  $\tan\delta$  max due to the increase of the hard segments ratio in the polyurethane. 1, 6-Hexanediol leads to polyurethane with higher value of  $E'$  at the rubbery plateau, and failure temperatures were observed for tetraethylene glycol and 1,4- phenylene dimethanol. The following order of thermal stability depending on the nature of the chain extender is observed: PU (tetraethylene glycol) < PU (n-alkanediol) < PU (glycol) < PU (1,4-diphenyl dimethanol)[9].

#### 3.2.2.4 Additives

In addition to isocyanates and polyols, the basic materials for making polyurethanes, a wide range of auxiliary chemicals may be added to control and modify both the polyurethane reaction and the properties of final polymers.

#### 3.2.2.5 Catalysts

A number of catalysts can be used for the reaction of isocyanates with water and polyols and these include aliphatic and aromatic tertiary amines, and organometallic compounds, although compounds of mercury or lead are also used. Alkali metal salts of carboxylic acids and phenols, and symmetrical triazine derivatives are used to promote the polymerization of isocyanates. The tertiary amines are the catalyst most widely used in making PU foams. The catalytic activity depends on their structure and basicity. The organometallic catalysts are also used to accelerate the urethane formation. The most popular organometallic catalysts are stannous octoate and dibutyltin dilaurate [6].

### 3.2.3 Method of synthesis of polyurethanes

Polyurethane polymerization reaction contains features of both addition and condensation polymerization. Although no small molecule is eliminated during polymerization, the reaction between the diol and the diisocyanate can be classified as a condensation polymerization reaction. The kinetic of the polymerization reaction more closely resembles that of condensation polymerization than addition polymerization.

#### 3.2.3.1 One step method

The one step process is the quickest and easiest of the manufacturing techniques. A functional or multifunctional liquid isocyanate and liquid diol are mixed in a mould, and allowed to react as shown in Figure 3.3. A lightly crosslinked structure can be synthesized with careful selection of the precursors. Curing of material from one-step procedure produces an elastomer.

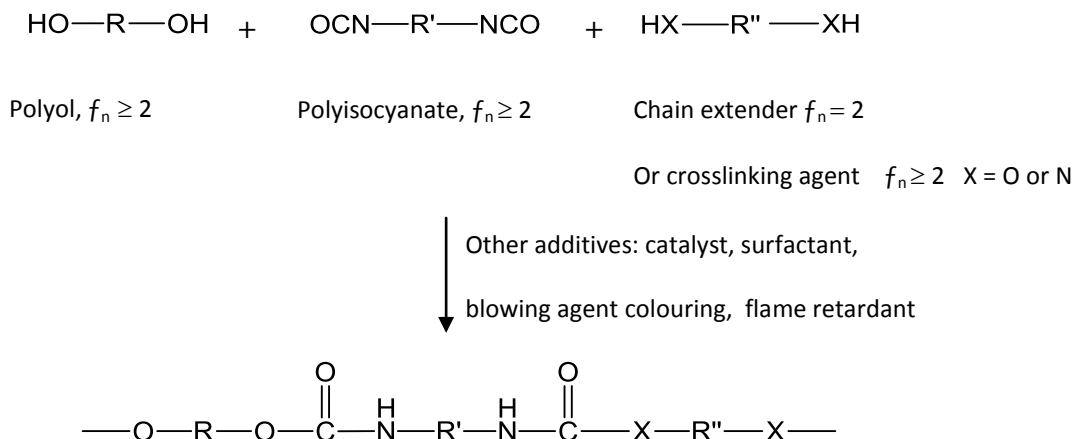


**Figure 3.3** One step polyurethane synthesis.

### 3.2.3.2 Two steps method

Synthesis via more than one step gives greater control over the chemistry of the reaction, influencing the structure, physical properties, reactivity and processability of the finished product. It is commonly referred to as the prepolymer method. The first step involves synthesis of a prepolymer from diol in excess diisocyanate to produce an isocyanate terminated molecule (Figure 3.4). The prepolymer generally has a low molecular weight and is either a viscous liquid or a low melting solid. Subsequent reaction of this prepolymer with a diol or diamine chain extender constitutes the second step, which produces a multiblock copolymer of the  $(AB)_n$  type[8].

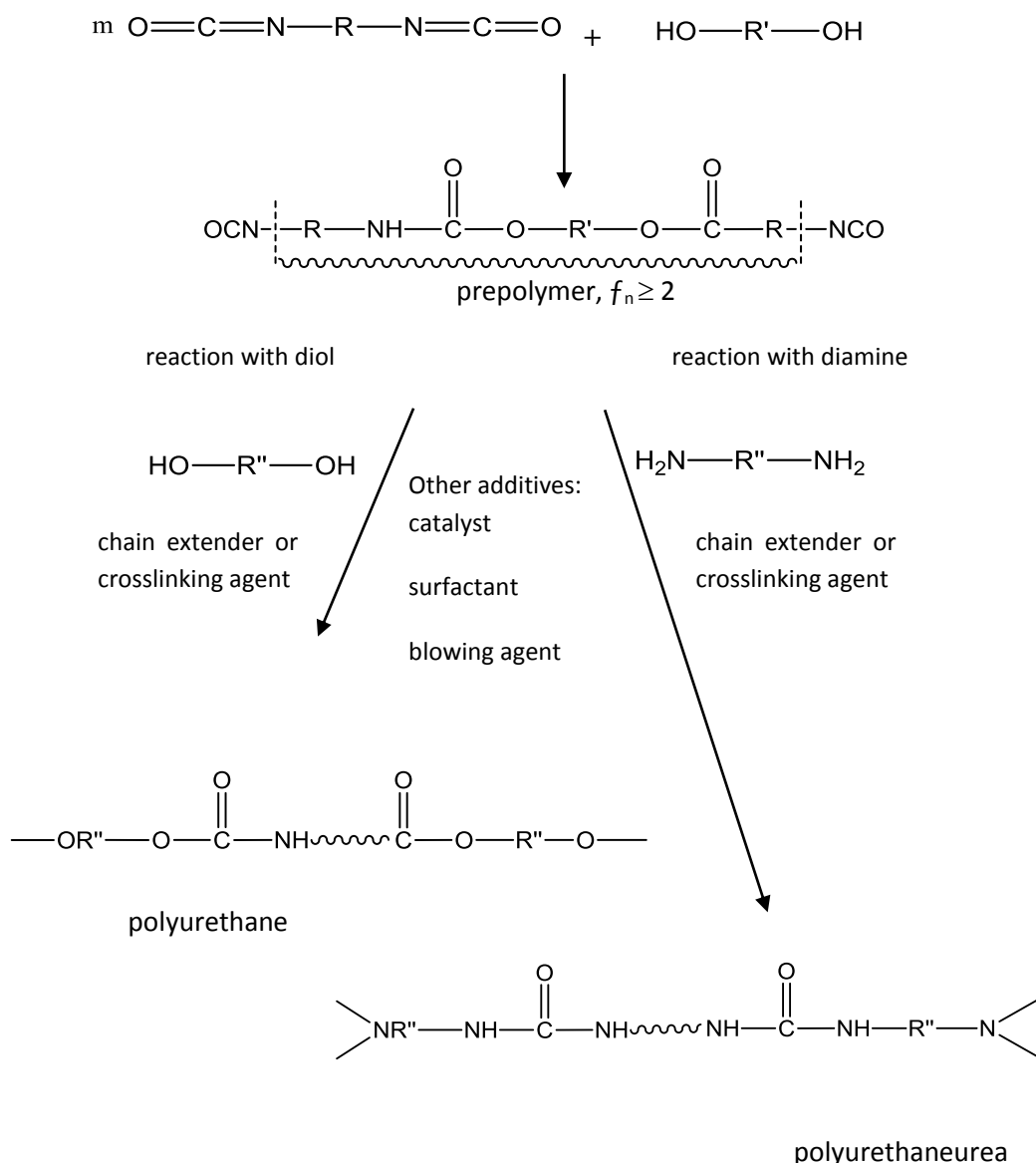


**Figure 3.4** Two steps polyurethane synthesis [8].

### 3.2.4 Properties of polyurethanes

Polyurethanes are segmented polymers which are built from alternating hard and soft segments. Polyurethane properties are the resultant of the overlap, often in a fairly complex manner, of a number of parameters related to molecular structure. The parameters involved are segmental flexibility, size of flexible and rigid segments, together with the ratio of both kinds of segment in the polymer, hydrogen and, van der waals bonds, size and symmetry of the aromatic rings, intertwining of chains, segment orientation, crosslink bonds, microphase separation and crystallization. Polyurethane structure chain is showed in Figure 3.5.



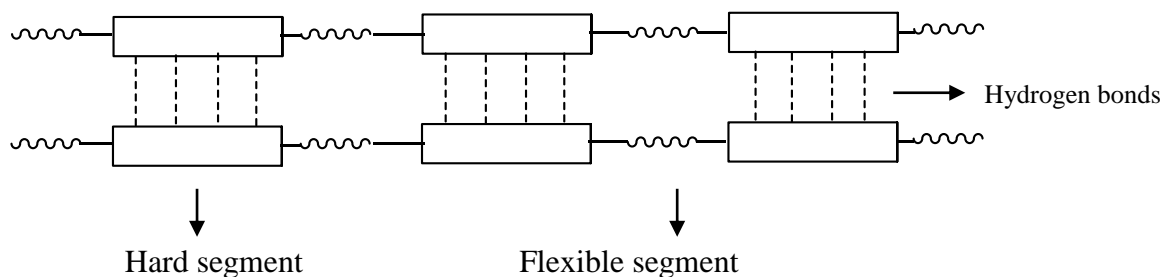


**Figure 3.5** Structure of linear segmented polyurethane chain [14].

### 3.2.4.1 Structure Property Relationship

These polymers can be considered in terms of long (1000 - 2000 nm) flexible segments and much shorter (150 nm) rigid units which are chemically and hydrogen bonded together. This segmented polymer structure has three basic building blocks: the polyol, the diisocyanate and the chain extender. The desired properties can be obtained by controlling the type and concentration of the present segments.

Polyurethanes can contain a high concentration of polar groups (polar hard segment and less polar flexible segment), that results from isocyanate-hydroxyl reactions, as well as ester, urea and other groups. Hard and flexible (soft) segment incompatibility causes phase separation since heat of mixing is positive. The final properties of polyurethanes are determined by the extent of interactions between these polar groups. The rigid segments in polyurethanes particularly affect the modulus, hardness and tear strength, and determine the upper-use temperature by their ability to remain at elevated temperatures.

The flexible blocks primarily influence the elastic nature of the product and its low-temperature performance, and they make important contributions towards the hardness, tear strength and modulus. Such strong polar interactions in polyurethanes can lead to a supramolecular organization into aggregated structures, which may be in the form of glassy domains or crystallites. Aliphatic polyethers or aliphatic polyesters are the usual materials used as flexible segments in polyurethane elastomers production. These have glass transition temperatures below room temperature and are low melting point solids or liquids. Polyethers have weaker interchain interface forces than polyesters, and generally give elastomers with inadequate physical properties. Rigid segments properties determine the interchain interactions in the elastomers to a large extent and so determine the network structure in these

materials. Preferred diisocyanates are those having large molecular structural bulk resulting in interchain steric hindrance and these have the highest levels of modulus, tear and tensile strengths. Elastomers based on aliphatic isocyanates generally had superior mechanical properties. This pattern of behavior applies to both polyester and polyether based urethane elastomers [15].

### 3.2.4.2 Parameters influencing physical properties

- **Hydrogen Bonding**

Hydrogen bonding results from the attraction of hydrogen atoms in one molecule with an oxygen or nitrogen atom in another molecule. The hydrogen bond is the strongest secondary chemical bond with a strength estimated to about 20-50 kJ/mol. Hydrogen bonding in polyurethanes plays an important role in determining the degree of phase separation. N-H group is the proton donor whereas the carbonyl and the etheric oxygen are the proton acceptors. Hydrogen bonding in urethane chains was illustrated in Figure 3.6. The FTIR analysis differentiate the hydrogen bonded N-H and free N-H, and also gave information about the presence of urethane carbonyl C=O and urea carbonyl C=O [16].

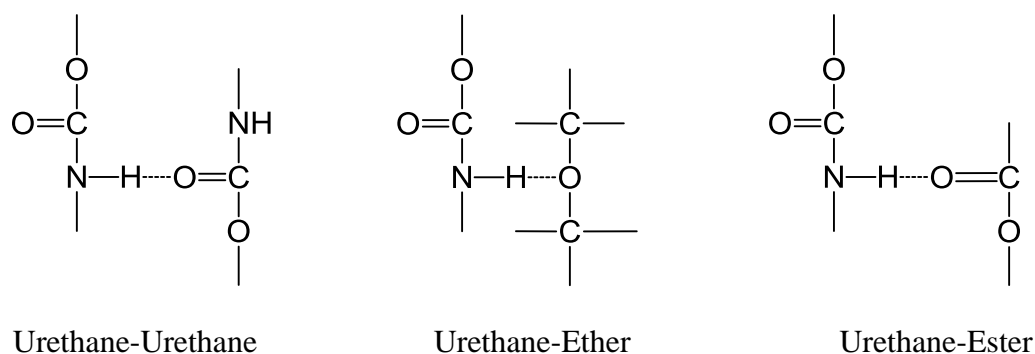


**Figure 3.6** Hydrogen bonding interaction in polyurethanes

- **Molecular interactions**

Values of the cohesion forces for individual bonds that typically occur in polyurethane are given in Table 3.3

**Table 3.3** Cohesion energy of constituent groups of polyurethanes [14].

Group	Cohesion energy (kJ mol <sup>-1</sup> )	Molar volume (cm <sup>3</sup> mol <sup>-1</sup> )
-CH <sub>2</sub> -	2.85	21.8
-O-	4.2	7.3
-CO-	11.1	21.6
-COO-	12.1	28.9
-C <sub>6</sub> H <sub>4</sub> -	16.9	83.9
-CONH-	35.6	36.2
-OCONH-	36.5	43.5
-NHCONH-	50-100	-

The barrier to rotation of a single C-C bond is 12.6 kJ mol/mol. The bonds mentioned in Table 3.3 may be divided into two groups: those for which the value is below 12.6 kJ/mol, are free to rotate, thus forming flexible chains (segments) which render the polyurethane flexibility. In the other hand those for which the value lies above 12.6 kJ/mol with hindered or no free rotation, which form rigid segments. However, the ether bond exhibits a stronger cohesion than methylene bond, imparts greater flexibility to polymer on account of the ball-joint effect of the ether oxygen atom. The aromatic ring makes the polymer chain stiff by being incorporated into the rigid segments. These stiffening remain even at elevated temperature. The ester bond also participates in a considerable degree in hydrogen bonding with the urethane groups which is significant especially at room temperature.

The urethane group, although its cohesion barely exceeds that of the amide group due to its extra oxygen atom, imparts rather minor stiffness to the polymers. The greatest cohesion is found in the urea group, as it contains two NH moieties capable of hydrogen bonding. The

urethane groups in polyurethane form hydrogen bonds mainly owing to interaction of the NH groups with the urethane and urea carbonyl functions, and to a lesser extent with ester and ether groups [14].

- **Segment and domain structure**

Properties of polyurethane depend on several factors such as the composition of soft or flexible segment, hard or rigid segment. Hard segments of polyurethane are composed of isocyanate residues, extenders, urethane groups, and possibly also of urea and ionic groups, if present in the polymer. The flexible segments consist of methylene and ether or ester groups. Their glass transition temperature ( $T_g$ ) are commonly below  $-30\text{ }^\circ\text{C}$ . They account for 60-80% of flexible polyurethanes composition [14]. Table 3.4 illustrates the effect of the length of the glycol derived hydrocarbon segment on the  $T_g$  and melting point (m.p.) of the linear polyurethanes synthesis from isocyanate and glycol. The highest  $T_g$  values are observed for polyurethanes containing the largest number of aromatic rings: in such polyurethanes the relation between  $T_g$  and aliphatic chain length is also the strongest.

**Table 3.4** Glass transition temperature and melting point of glycol  $\text{HO}(\text{CH}_2)_x\text{OH}$  based polyurethane made from different isocyanates [17].

Glycol	$T_g(^\circ\text{C})$			Melting point ( $^\circ\text{C}$ )	
	HDI	MDI	TDI	HDI	MDI
x					
2	56	139	52	166	>decomp.
3	55	119	72	163	241
4	59	109	42	182	248
5	58	95	52	157	192
6	59	91	32	171	200

TDI = Toluene diisocyanates, HDI = Hexamethylene diisocyanates, MDI = Methylene diphenyl diisocyanates

The highest m.p. of rigid segments is observed in the 1, 4-butylene glycol extended polyurethanes. The rigid segment m.p. increases with their size (the number of repeating units) and with their ordering (crystallinity) as shown in Table 3.5

**Table 3.5** Characteristics of MDI and 1, 4-butanediol derived rigid segment [18].

Repeating units	Molecular weight of oligomer	Melting point (°C)	
		Before annealing	After annealing
1	430	118-125	133
2	770	183-187	190
3	1110	208-213	213
5	1790	233	237

The more the hard segment content in polyurethane, the greater are its elastic modulus, rigidity, abrasion resistance and maximum permissible service temperature. The more the flexible segments in a polymer, the greater are its flexibility, elongation at break, and resistance to low temperatures and the lower its hardness, elastic modulus [19].

- **Crystallization**

Crystallization in polymers is promoted by linearity, close and regular fit of polymer chains, strong intermolecular forces, and stiff units in the chain which restrict rotation. In many ways the effect of crystallization are similar to those of crosslinking: reduction of solubility, flexibility, elasticity, and elongation, and increase of hardness, tensile strength and melting point. The bonding of one chain to another by crystalline forces is different from that by true crosslinking in that the crystalline portion of the polymer may be disruption reversibly by heat [20].

### 3.2.4.3 Thermal stability

Thermal properties of polyurethane depend on the structure of block copolymer, and on the glass transition and melt temperature of crystalline structure of soft and hard segments [21]. There are several transition points in polyurethane [14].

- In the temperature range of -90 to -80 °C there is the glass transition temperature,  $T_g$ , related to the flexible segment i.e., polyether chains in polyether urethane.
- In the temperature range of -45 to -12 °C there is the  $T_g$  that refers to the polyester chains in polyesterurethanes.
- In the 20-60 °C temperature range, the physical properties of linear polyurethanes remain virtually unaffected, while up to 100 °C they halve.

The modulus of elasticity varies with temperature: below the  $T_g$  of the flexible segments, the polymer behaves as a rigid plastic, whereas above  $T_g$ , it behaves as an elastomer.

The elastic plateau remains at the same level but at a modulus which increases with the content of rigid segment in the polymer. Over the range 80-150 °C (depending on the degree of ordering of the polymer) cleavage of the hydrogen bonds between the NH groups of the urethane bond and the oxygen atoms of the flexible segments occurs. In the range 130-170 °C cleavage of the majority of urethane hydrogen bonds take place and the remainder break only above 197 °C. In the temperature 100-130 °C the allophanate and biuret bonds dissociate. At 183-247 °C the rigid segments domains vanish. Polyurethanes decomposition is initiated in the rigid segments. These decomposition products in the rigid segments undergo further conversion to stable solid products. The next stage of decomposition refers to the flexible segments and urethane group linked to an aliphatic group. In the third stage, ester groups in flexible segments undergo decomposition. The presence of aromatic rings in the polymer chain has a stabilizing effect and reduces the tendency to form volatile decomposition products. The rigid segments stabilize the decomposition of the flexible segments.

The decomposition temperatures of the urethane bonds were also considered to depend on the urethane bond structure: Ar-NHCOOAr bonds decomposed at 120 °C, R-NHCOOAr at 180 °C, Ar-NHCOOR at 200 °C, and R-NHCOOR bonds decomposed at 250 °C, where Ar is an aromatic substituents and R is aliphatic [22].

The thermal stability of an urethane bond formed by reaction of RNCO with R'OH to give RNHOOR' increases in the order (R = tert-butyl > cyclohexyl > n-alkyl > benzyl > phenyl > p-nitrophenyl) (R' = aryl > aralkyl > cycloalkyl > n-alkyl > sec-alkyl > tert-alkyl).

Cyclic systems of greater thermal stability are formed in untypical reaction of isocyanate groups with esters, anhydrides, and epoxy compounds. The thermal stabilities of particular groups in polyurethanes are in the following order:  $-\text{COO}- > -\text{COC}- > -\text{NHCONH}- > -\text{NHCOO}- > -\text{NHCONCNH}- \geq -\text{NHCONCOO}-$  [14]. The limiting thermal resistance of the flexible segments of polyurethanes corresponds to about 250 °C, whereas the polyester urethanes start decomposing about 300 °C.

The higher temperature decomposition was caused by higher ester group content. However, the flexible segments of unsaturated oligoester exhibited lower thermal stability. Chemical crosslinking effects on thermal stability of polyurethanes are also considered. The thermal stabilities of these types of chemical crosslinking are in the order: crosslinking from trimerization of excess isocyanates > crosslinking from trifunctional of polyols > crosslinking from excess of isocyanates with urethane or urea groups of polyurethane. A general indication of presence of covalent crosslinking is the infusibility and insolubility of the polyurethane in powerful solvents such as DMF [14]. Thermal stability data of individual bonds present in polyurethane are collated in Table 3.6

**Table 3.6** Thermal stability of groups formed by the isocyanate reaction [14]

Name of group	Decomposition temperature (°C)
Isocyanurate ring	> 270
Carbodiimide group	>270
Urea group	180-250
Urethane group	150-250
Biuret group	120-180
Allophanate group	20-180
Uretidinedione	120-170

### 3.2.4.4 Surface Properties of Polyurethane

These properties include surface tension, surface chemical composition, surface morphology, hydrophilicity. To analyze the surface, a variety of physical techniques are available as illustrated in Table 3.7

Many investigators have extensively studied surface properties of segmented polyurethanes. Due to microphase separation between the hard and soft segments, segmented polyurethanes exhibit unique bulk and surface properties. Slight changes in synthetic methods, chemical composition, and process conditions can lead to variations in chemical and physical properties of polyurethanes. This reflects on the properties of the surface as well, which may be also different from the bulk [5].

**Table 3.7** Selected Surface Analysis Methods [5]

Acronym	Method
ESCA (or XPS)	Electron Spectroscopy for Chemical Analysis (X-Ray Photoelectron Spectroscopy)
AES (or SAM)	Auger Electron Spectroscopy (Scanning Auger Microprobe)
SIMS	Secondary Ion Mass Spectroscopy
ISS	Ion Scattering Spectroscopy
LEED	Low-Energy Electron Diffraction
STM	Scanning Tunneling Microscopy
AFM	Atomic Force Microscopy
ATR-IR	Attenuated Total Reflectance-Infrared
	Contact Angle Methods



## Conclusion

The bibliographic part describes in a first time the more used raw materials in polyurethane synthesis: isocyanates, polyols, chain extenders, additives and catalysts. Among the different polyols used, we focused on the polydienes-based polyols and more particularly on the polyisoprene-based polyols, according to the aims of this work.

Effect of the chemical structure on the physical properties has been enlightened and the structure properties relationship was examined in function of different parameters as hydrogen bonding, cohesion forces of the different bonds, composition in flexible and rigid segments. Physical, thermal and surface properties of polyurethanes were reviewed, always in function of their chemical structures.

In the second part of this chapter, synthesis and characterization of different natural rubber-based polyurethanes is presented. Thermal properties are compared in function of the chemical structure of the PU.

### 3.3. Synthesis of linear and crosslinked polyurethanes

The synthesis of polyurethanes involves the classical one-shot polyaddition reaction of alcohol groups of telechelic oligomers with isocyanate groups in the presence of a catalyst [23]. In our study, we have prepared polyurethane films in the same procedure. Hydroxytelechelic cis-1,4-polyisoprene, **4**, (different samples with different values of  $\overline{M}_n$ ) or epoxidized hydroxytelechelic cis-1,4-polyisoprene, **5**, (different proportions of % epoxidation and  $\overline{M}_n$ ) were dissolved in THF. Catalyst and isocyanate (TDI or I-IPDI) were then added into reaction solution. PU obtained from TDI are linear, and PU obtained from I-IPDI are crosslinked (Figure 3.7).

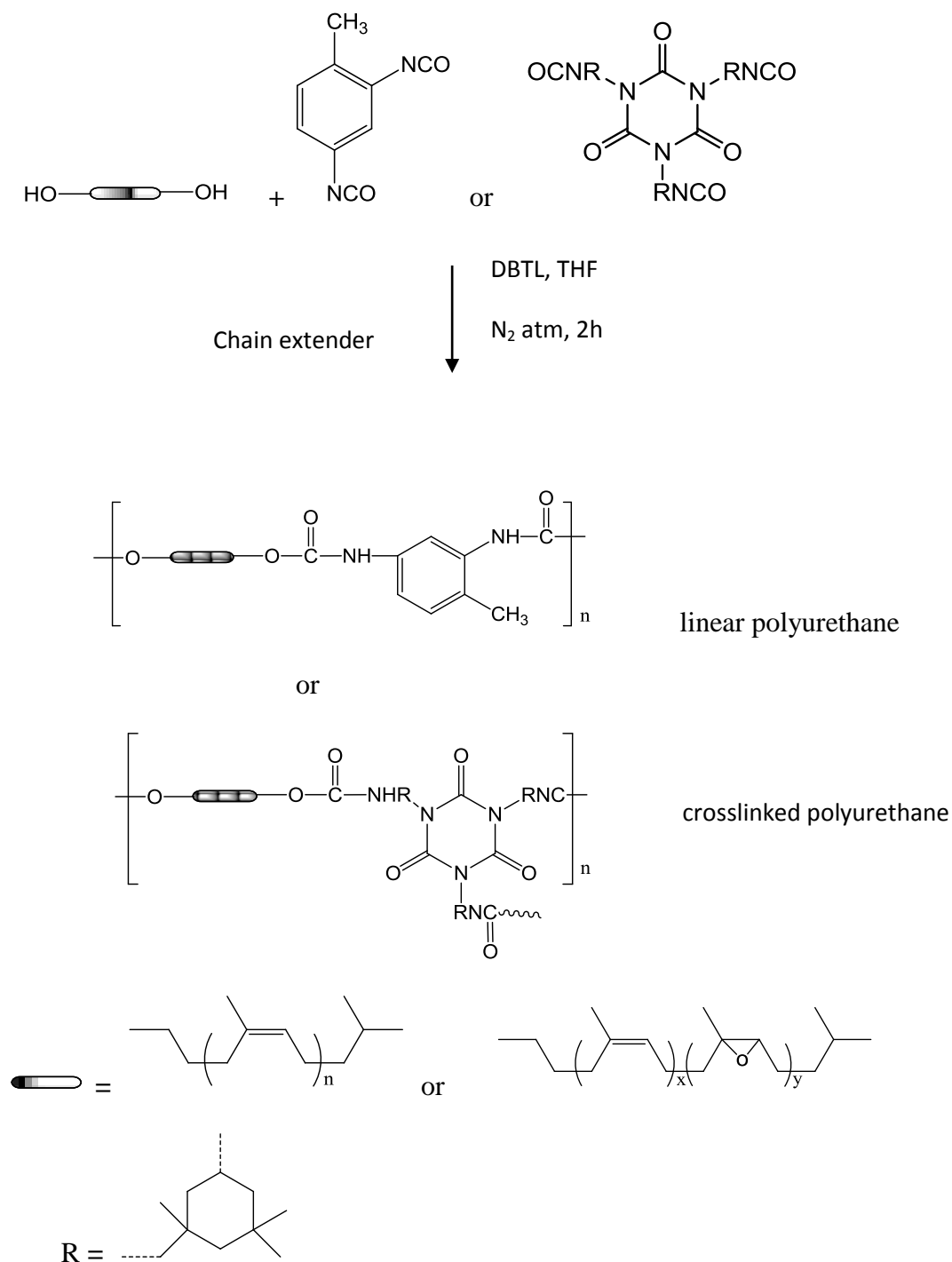


**Figure 3.7** Synthesis of linear and crosslinked polyurethanes.

Films were obtained by casting technique under nitrogen atmosphere at room temperature and subsequently cured at 60°C for 12 h. They were characterized by FTIR, DSC and TGA.

The compositions of the different linear and crosslinked polyurethanes are detailed in Table 3.8, with indications on the nature (epoxized or not) of the diol precursor and its

average molecular weight, on the nature of the isocyanate and of the chain extender for some samples. Linear polyurethanes are synthesized by reaction of different hydroxytelechelic polyisoprenes (with a different average molecular weights and different proportions of epoxidation), with a difunctional isocyanate : the 2,4-toluene diisocyanate (TDI).

Only 3 samples of crosslinked polyurethanes have been synthesized by reaction of diol precursor with isocyanurate of isophorone diisocyanate (I-IPDI). (three first lines of the table 3.8) and 2 samples of PU synthesized with glycerol (PU 14, PU15).

**Table 3.8** Composition of the synthesized polyurethanes.

Notation	Precursors ( $\overline{M}_n$ , %epoxide) /Isocyanate /Chain extender
PU(HTPI)	HTPI(1000)/ I-IPDI
PU(EHTPI10)	EHTPI10(1000, % E = 13)/I-IPDI
PU(EHTPI50)	EHTPI50(1100, % E = 60.5%)/I-IPDI
PU2	HTPI10(1000)/TDI
PU3	EH1(1000, %E = 6.3)/TDI
PU4	EH2(1000, %E = 27.7)/TDI
PU5	EH3(1000, %E = 60.1)/TDI
PU6	HTPI10(1000) + EH1(1000, %E = 6.3)/TDI
PU7	HTPI10(1000) + EH2(1000, %E = 27.7)/TDI
PU8	HTPI10(1000) + EH3(1000, %E = 60.1)/TDI
PU11	HTPI10(1000) /TDI / D-glucose
PU12	EH1(1000, %E = 6.3)/TDI / D-glucose
PU13	EH3(1000, %E = 60.1)/TDI /1,4 butanediol
PU14	EH4(1100, %E=34.8)/TDI / glycerol
PU15	EH5(1100, %E = 60.1) /TDI / glycerol
PU16	EH5(1100, %E = 60.1)/TDI
PU17	HTPI11(1000) + EH5(1100, %E = 60.1)/TDI
PU18	HTPI11(1000) + EH4(1100, %E = 34.8)/TDI
PU19	HTPI11(1000) + EH6(1000, %E=10.2)/TDI

PU20	EH4(1100, %E=34.8)/TDI
PU21	HTPI13(900)+EH12(1000, %E = 43)/TDI
PU22	EH10(900, %E = 9.8)/TDI
PU23	EH12(1000, %E = 43)/TDI
PU25	EH7(7200, %E = 9.2)/TDI
PU26	EH9(7600, %E = 62.9)/TDI
PU27	HTPI12(8000)/TDI
PU28	EH8(6200, %E = 38)/TDI
PU29	HTPI14(4300)/TDI
PU30	EH13(4100, %E = 8.2)/TDI
PU31	EH14(4000, %E = 24.6)/TDI
PU32	EH15(4000, %E = 47.6)/TDI
PU33	HTPI13(900)/TDI
PU34	HTPI13(900)/TDI /D-glucose
PU35	EH10(900, %E = 9.8) /TDI /D-glucose
PU36	EH11(1000, %E = 28.5)/TDI
PU37	EH11(1000, %E = 28.5)/TDI /D-glucose
PU38	EH12(1000, %E = 43)/TDI /D-glucose
PU39	HTPI13(900)+EH11(900, %E = 9.8)/TDI
PU40	HTPI14(4300)/TDI
PU41	EH14(4000, %E = 24.6)/TDI
PU42	HTPI12(8000)/TDI
PU43	HTPI14(4300)/TDI
PU44	EH6(1000, %E = 10.2)/TDI
PU45	HTPI13(900)/TDI
PU46	EH7(7200, %E = 9.2)/TDI
PU47	HTPI10 (1000)/TDI
PU48	EH1(1000, %E = 6.3)/TDI

---

Table 3.9, 3.10 and 3.11 collect the structural characteristics of the diol precursors used to synthesized the different PU samples (codes listed in the last column) obtained by reaction with TDI.

**Table 3.9** Chemical structure and molecular weight of the diol precursors HTPI and EHTPI

Code	$\overline{M}_n$ (calc) a) (g.mol <sup>-1</sup> )	$\overline{M}_n$ (SEC) b) (g.mol <sup>-1</sup> )	%E c)	PU sample
HTPI10		1000	0	PU2, PU47
EH1	$\overline{M}_n$ 1000	1000	6.3	PU3
EH2		1000	27.7	PU4
EH3		1000	61.3	PU5
HTPI11		1000	0	-
EH4		1100	34.8	PU20
EH5		1100	60.1	PU16
EH6		1000	10.2	PU44
HTPI12		8000	0	PU27, PU42
EH7	$\overline{M}_n$ 8000	7200	9.2	PU25, PU46
EH8		6200	38	PU28
EH9		7600	62.5	PU26
HTPI13		900	0	PU33, PU45
EH10	$\overline{M}_n$ 900	900	9.8	PU22
EH11		1000	28.5	-
EH12		1000	43.0	PU23
HTPI14		4300	0	PU29, PU40, PU43
EH13	$\overline{M}_n$ 4000	4100	8.2	PU30
EH14		4000	24.6	PU31, PU41
EH15		4000	47.6	PU32

- a)  $\overline{M}_n$  calculated according to the used ratio [PI]/[m-CPBA] in the oxidative degradation step.  
 b)  $\overline{M}_n$  (SEC) = number average molecular weight determined by SEC calibrated with polystyrene standards  
 c) percent epoxidation determined by  $^1\text{H}$  NMR

**Table 3.10** Chemical structures and molecular weights of the diol precursors HTPI and EHTPI in mixture with D-glucose.

Code	$\overline{M}_n$ (calc) a) (g.mol <sup>-1</sup> )	$\overline{M}_n$ (SEC) b) (g.mol <sup>-1</sup> )	%E c)	PU sample
HTPI10+D-glucose		1000	-	PU11
EH1+D-glucose	$\overline{M}_n$ 1000	1000	6.3	PU12
HTPI13+D - glucose		900	-	PU34
EH10+D - glucose	$\overline{M}_n$ 900	900	9.8	PU36
EH11+D - glucose		1000	28.5	PU37
EH12+D - glucose		1000	43.0	PU38

- a)  $\overline{M}_n$  calculated according to the used ratio [PI]/[m-CPBA] in the oxidative degradation step.  
 b)  $\overline{M}_n$  (SEC) = number average molecular weight determined by SEC calibrated with polystyrene standards  
 c) percent epoxidation determined by  $^1\text{H}$ NMR

In the table 3.10, number-average molecular weights and percentages of epoxidation are listed for diol precursors used in mixture with D-glucose. Linear polyurethanes are also obtained by reaction with TDI, as for the polyurethanes listed in the table 3.11 where the described diol precursors are mixtures of hydroxytelechelic polyisoprene (HTPI) and epoxidized hydroxytelechelic polyisoprene (EH).

**Table 3.11** Chemical structures and molecular weights of the diol precursors HTPI and EHTPI in mixture with EHTPI (HTPI/EH = 90/10)

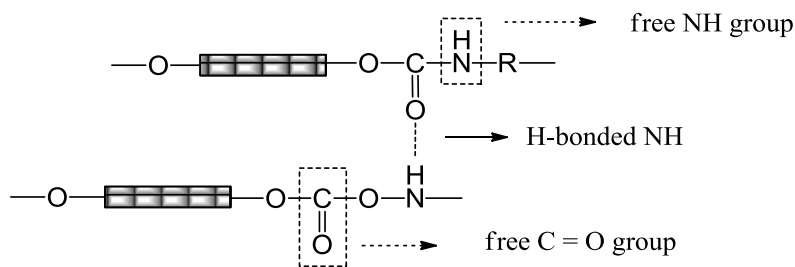
Code	$\overline{M}_n$ (calc) a) (g.mol <sup>-1</sup> )	$\overline{M}_n$ (SEC) b) (g.mol <sup>-1</sup> )	%E c)	PU sample
HTPI10+EH1		1000	6.3	PU6
HTPI10+EH2	$\overline{M}_n$ 1000	1000	27.7	PU7
HTPI10+EH3		1000	61.3	PU8
HTPI11+EH5		1000	60.1	PU17
HTPI11+EH4		1000	34.8	PU18
HTPI11+EH6		1000	10.2	PU19
HTPI13+EH12	$\overline{M}_n$ 900	900	43	PU21
HTPI13+EH11		900	28.5	PU39

a)  $M_n$  calculated according to the used ratio [PI]/[m-CPBA] in the oxidative degradation step. b)  $M_n$  (SEC) = number average molecular weight determined by SEC calibrated with polystyrene standards c) percent epoxidation determined by <sup>1</sup>H NMR

### 3.3.1 ATR-FTIR Analysis Results

FTIR is a well established analytical technique for functional group analysis and to study the hydrogen bonding and phase separation behavior of polyurethanes. The frequency shifts in hydrogen bonded N-H and carbonyl peaks relative to free N-H and C=O peaks determine the extent of hydrogen bonding and microphase separation between hard and soft segments [24-26]. If hydrogen bonding exists only within the hard segment domains (due to the hydrogen donor N-H group), phase separation occurs. On the other hand, if they can be formed between the hard and the soft segments via oxygen atom of oxirane rings, the interphase hydrogen bonding enhances the degree of phase mixing (Figure 3.8) [27] Characteristic IR absorption frequencies of polyurethanes are listed in Table 3.12

a)



b)

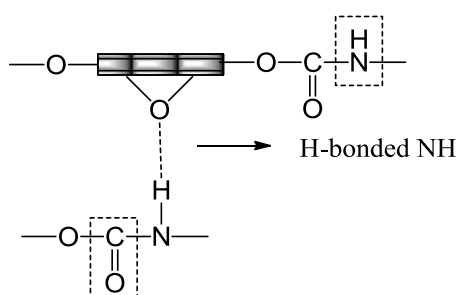


**Figure 3.8** Hydrogen interactions between two hard segments a), and between hard and soft segments b)

**Table 3.12** FTIR-ATR band assignments for polyurethanes

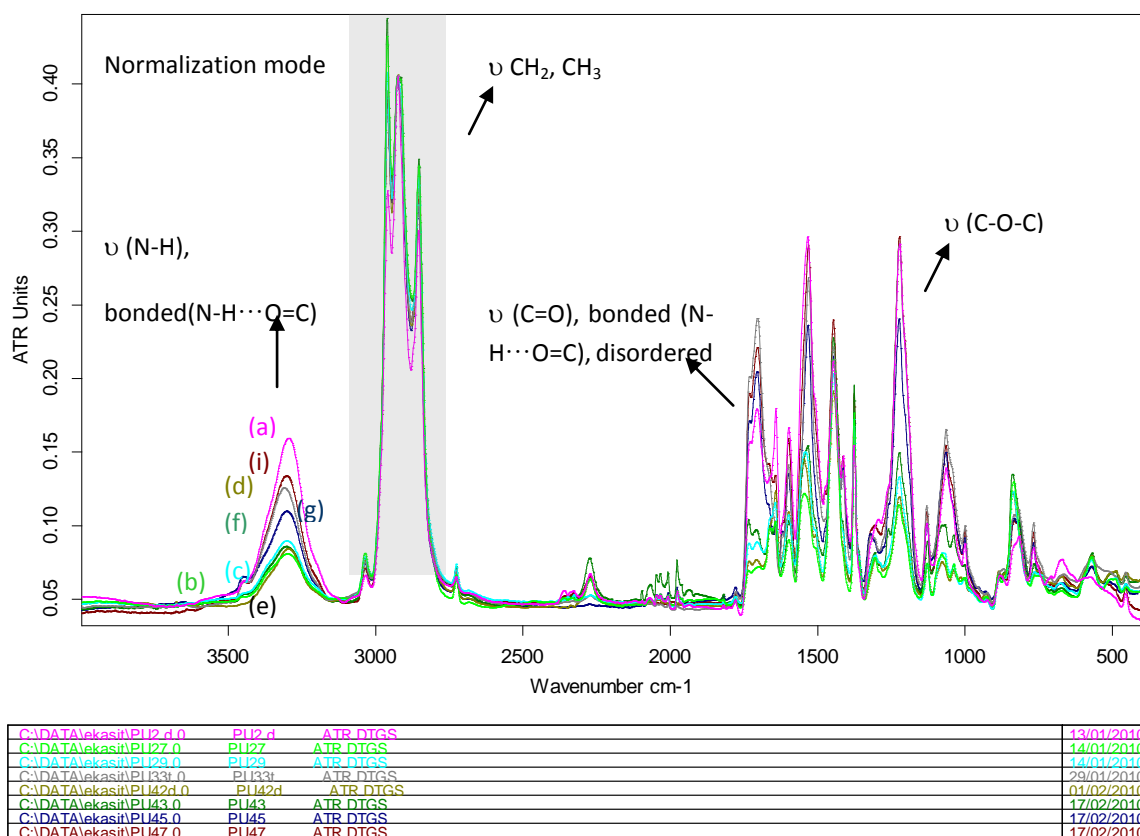
Frequency (cm <sup>-1</sup> )	Group	Assignment <sup>a</sup>
3400-3500	N-H	$\nu(\text{N-H})$ , free N-H
3310-3350	N-H	$\nu(\text{N-H})$ , bonded (N-H...O=C)
3260-3300	N-H	$\nu(\text{N-H})$ , bonded (N-H...O)
2890-3050	C-H	$\nu_a(\text{CH}_2)$
2850-2880	C-H	$\nu_s(\text{CH}_2)$
2240-2270	Residual N=C=O	$\nu(\text{NCO})$
1720-1740	C=O	$\nu(\text{C=O})$ , free C=O
1700-1715	C=O	$\nu(\text{C=O})$ , bonded (N-H...O=C),



		disordered
1670-1685	C=O	$\nu$ (C=O), bonded (N-H...O=C), ordered
1600-1610	C=C	$\nu$ (C=C), aromatic ring
1500-1550	Amide II	$\delta$ (C-N-H) + $\delta$ (C-N)
1430-1500	C-H	$\delta$ (CH <sub>2</sub> )
1410-1420	C-C	$\nu$ (C-C), aromatic ring
1360-1400	C-H	$\omega$ (CH <sub>2</sub> )
1200-1300	Amide III	$\delta$ (N-H) + $\delta$ (C-N)
1100-1120	C-O-C	$\nu$ (C-O-C), oxirane (soft segment)
1050-1080	C-O-C	$\nu$ (C-O-C), hard segment
1000-1020	C-H	r(C-H)
810-820	C-H	$\gamma$ (C-H), aromatic ring
765-770	C=O	$\gamma$ (C=O)

<sup>a</sup>  $\nu$  =stretching, a=asymmetric, s= symmetric,  $\delta$  = bending,  $\omega$  = wagging, r=rocking ,  $\gamma$  = out of plane bending or twisting.

The effect of different structural parameters of the synthesized polyurethanes has been studied focusing on two special regions of the IR spectra: the C=O stretching vibration from 1600 to 1800  $\text{cm}^{-1}$  and the NH stretching vibration near 3300  $\text{cm}^{-1}$ . It was established [24] that the peak at 1730  $\text{cm}^{-1}$  is assigned to the free carbonyl bond vibration and the one near 1700  $\text{cm}^{-1}$  to carbonyl groups hydrogen bonded to N-H groups. Higher absorbance observed for the 1700  $\text{cm}^{-1}$  peak relative to 1730  $\text{cm}^{-1}$  is characteristic of a phase-separated structure of polyurethane. The NH stretching vibration should give also complementary information. The frequency of N-H groups free from hydrogen bonding is at 3450  $\text{cm}^{-1}$ . The authors [24] have assigned 3330 and 3295  $\text{cm}^{-1}$  bands to N-H groups hydrogen bonded to C=O groups and the ether oxygen, respectively, in the case of poly(propylene oxide) as soft segment. The same NH hydrogen bonded to oxygen atom of oxirane ring, in our case of epoxidized natural rubber as soft segment, may be observed.

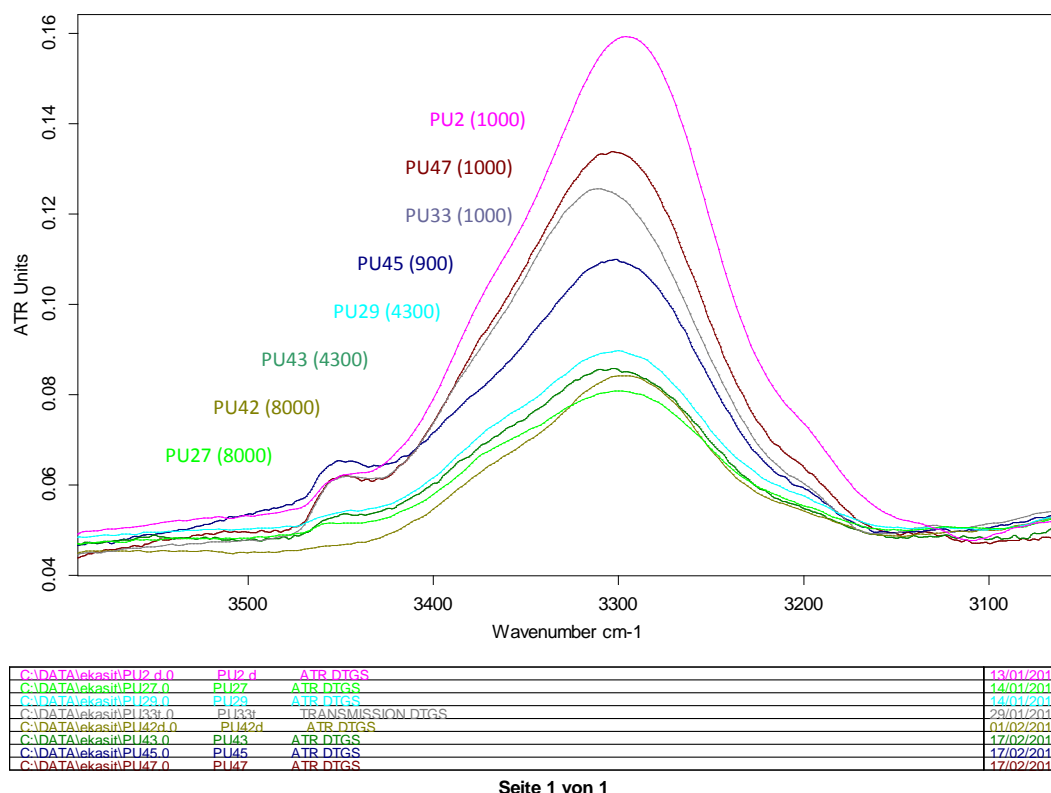


Seite 1 von 1

**Figure 3.9** Comparison between ATR FT-IR spectra of PU(HTPI varied  $\overline{M}_n$ ) (a) PU2(HTPI 1000 g.mol<sup>-1</sup>), (b) PU27(HTPI 8000 g.mol<sup>-1</sup>), (c) PU29(HTPI 4300 g.mol<sup>-1</sup>), (d) PU33(HTPI g.mol<sup>-1</sup>), (e) PU42(HTPI 8000 g.mol<sup>-1</sup>), (f) PU43(HTPI g.mol<sup>-1</sup>), (g) PU 45(HTPI 900 g.mol<sup>-1</sup>) and (i) PU 47(HTPI 1000 g.mol<sup>-1</sup>)

### 3.3.1.1 Effect of varied molecular weights of diol precursor:

Characteristic IR spectrum of HTPI based polyurethane shows bands at 3287-3294 cm<sup>-1</sup> (NH stretching vibrations), at 2726-2960 cm<sup>-1</sup> (CH stretching vibrations, reference band), at 1600-1800 cm<sup>-1</sup> (C=O stretching vibrations), at 1534 cm<sup>-1</sup> (NH in plane bending), and at 1070 cm<sup>-1</sup> (C-O-C stretching vibration). As the major concern of this work focus on hydrogen bonding and their relation to the segregation of hard and soft segments, two especial regions are of main interest: the C=O stretching vibration from 1700 to 1800 cm<sup>-1</sup> and the NH stretching vibration at 3295 cm<sup>-1</sup> (Figure 3.9).

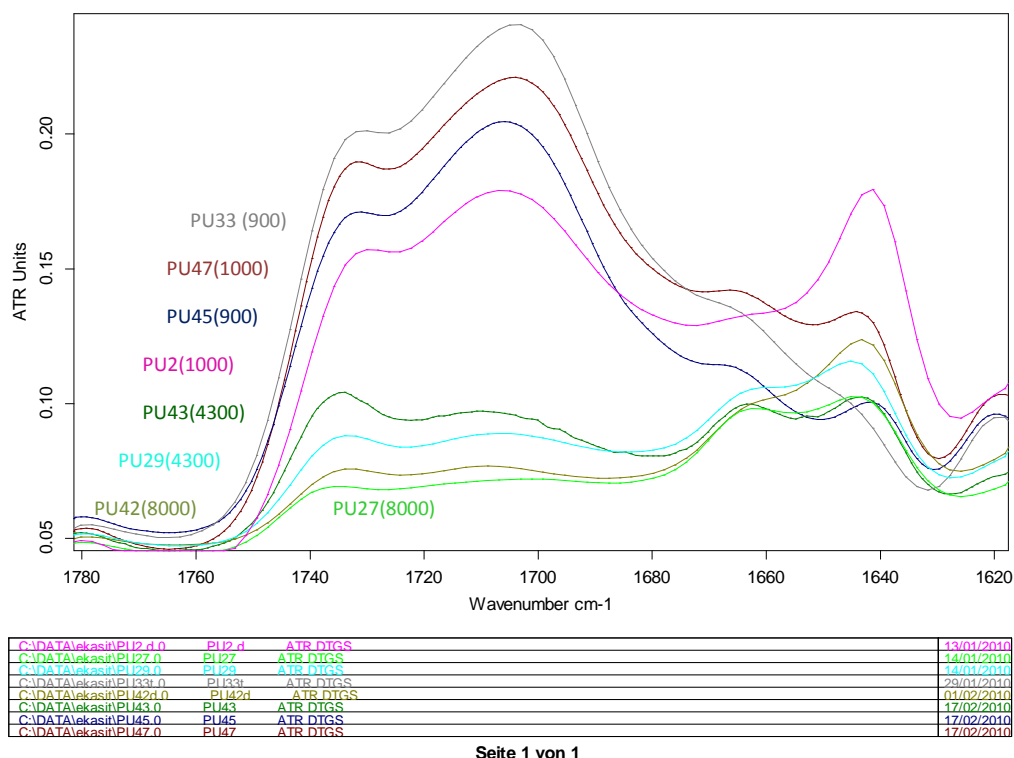


Seite 1 von 1

**Figure 3.10** Comparison between ATR FT-IR spectra at 3200-3500  $\text{cm}^{-1}$  of PU films

Figure 3.10 shows the ATR-FTIR spectra of NH stretching region for the PU with different  $\overline{M}_n$  in HTPI soft segments. For all of them, the NH stretching vibration exhibits a strong absorption peak centered at around 3294  $\text{cm}^{-1}$ . Some authors [24] have reported that the stretching vibration of NH- -O- hydrogen bond occurs at 3295  $\text{cm}^{-1}$  while other [28] verified this same absorption at lower frequency. Christenson *et al.*, [28] for example, observed this band at 3258-3265  $\text{cm}^{-1}$ . Latter, Teo *et al.* [29] reported that the NH--O- hydrogen bond appears at around 3264-3280  $\text{cm}^{-1}$ .

In our case, we observe higher intensity of this characteristic band at 3296  $\text{cm}^{-1}$  for the lower molecular weights of HTPI used (1000-900  $\text{g}\cdot\text{mol}^{-1}$ ). It is well explained by the higher proportions of urethane hard segments relative to polyisoprene soft segment. This band corresponds to hydrogen bonding between hard segments. We can observe a weak band near 3450  $\text{cm}^{-1}$  which could be a characteristic band of vibrations of free NH. It may be explained also by a higher content of hard segments in the case of lower molecular weight diol precursor. Region of C=O vibrations around 1700-1750  $\text{cm}^{-1}$  may give more information on the ratio of C=O bonded to NH and free C=O bonds.



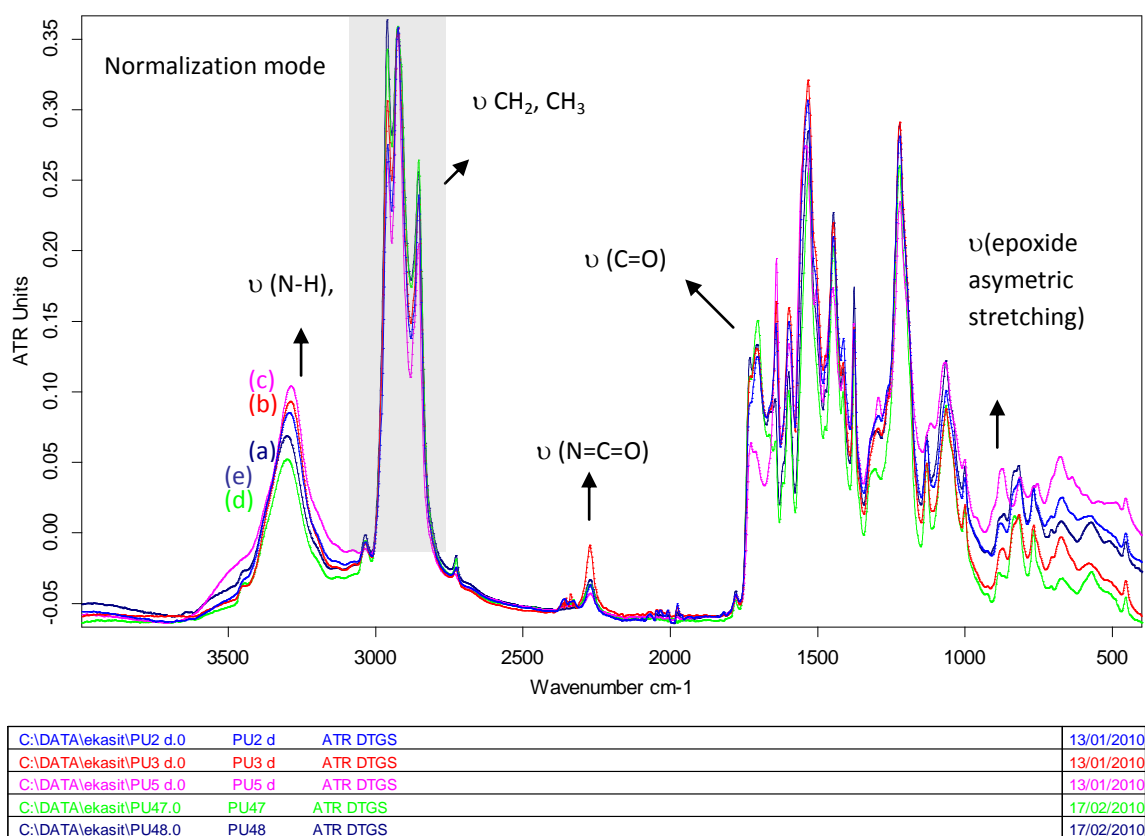
**Figure 3.11** Comparison between ATR FT-IR spectra at 1740-1640  $\text{cm}^{-1}$  of PU films with different  $M_n$  HTPI

Figure 3.11 presents the C=O stretching region around 1700 – 1750  $\text{cm}^{-1}$ . Multiple absorption bands are observed, which would reflect the complex properties of hydrogen bonding. Almost spectra are characterized by a major band centered at approximately 1708  $\text{cm}^{-1}$ , which is ascribed to hydrogen-bonded urethane and shoulder at about 1727  $\text{cm}^{-1}$  attributed to free C=O urethane groups. By comparison between the band at 1708  $\text{cm}^{-1}$  relative to hydrogen bonded C=O, and the band at 1727  $\text{cm}^{-1}$  relative to free C=O, we observe higher proportion of hydrogen bonded C=O versus free C=O, as the average molecular weight of the PI precursors is lower. Free C=O bonds are in higher proportion in the obtained polyurethane with high molecular weight diol PI precursors( PU43, PU29, PU42, PU27) with average molecular weights of 4300 and 8000  $\text{g}\cdot\text{mol}^{-1}$ .

In this case steric hindrance of this high molecular weight soft segment may decrease the probability of hydrogen bonding between the urethane hard segment. For high  $M_n$ , the lower urethane content will also decrease the probability of interactions between these functions. At 1640  $\text{cm}^{-1}$ , we observe the characteristic band of vibration of C=C bond of the polyisoprene soft segments. As expected, intensity of this band is higher in the case of polyurethanes with high average molecular weight PI soft segments.

## 3.3.1.2 Effect of varied epoxidized diol precursors.

Examples of FTIR spectra of synthesized polyurethanes are shown in Figure 3.12. The  $CH_{asym}$  and  $CH_{sym}$  stretching vibration peaks of the HTPI and EH soft segments located at 2959 and 2854  $cm^{-1}$ , respectively are chose as reference bands.

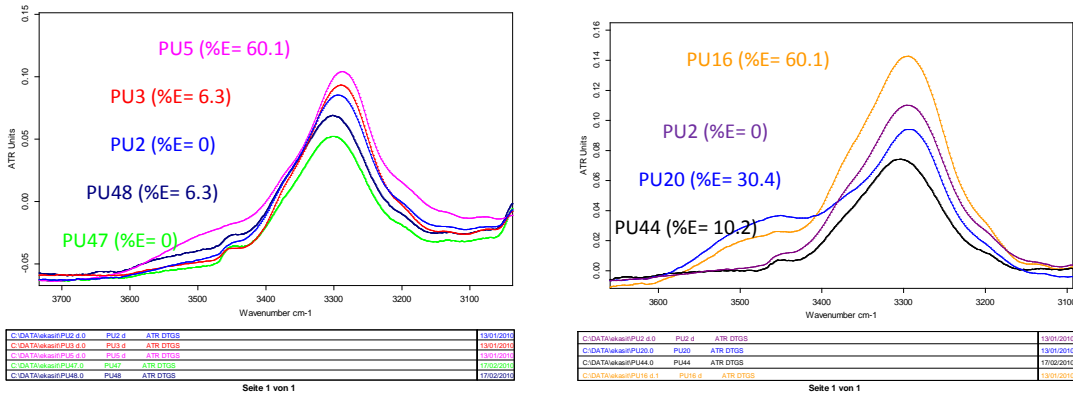


Seite 1 von 1

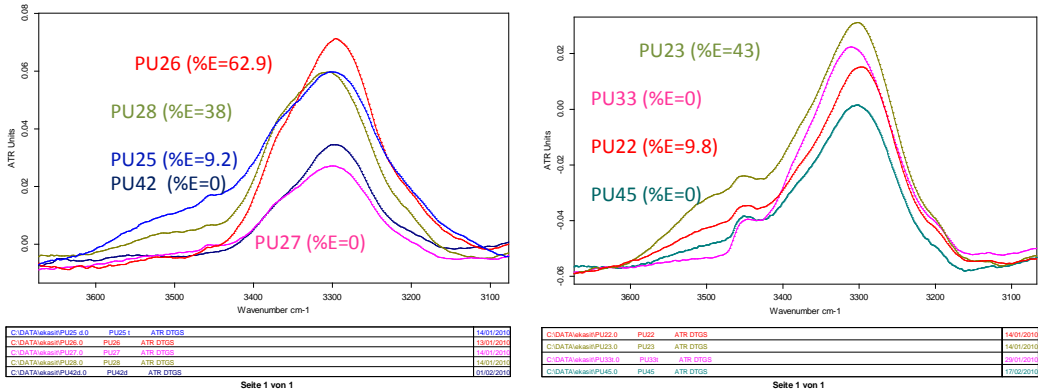
**Figure 3.12** Comparison between ATR FT-IR spectra of PU(HTPI10  $\overline{M}_n$  1000, varied %E) (a) PU2(HTPI10, %E = 0), (b) PU3(EH1, %E = 6.3), (c) PU5 (EH3, %E = 60.1), (d) PU47(HTPI10, %E = 0) and (e) PU48(EH1, %E = 6.3)

Two main spectra regions like previously are of main interest in this study: the NH stretching vibration from 3287 to 3294  $cm^{-1}$  as well as the carbonyl stretching vibration from 1680 to 1730  $cm^{-1}$ . Epoxide bands stretching appears at 870  $cm^{-1}$ .

1)PU(HTPI10  $\overline{M}_n$  = 1000, Varied % epoxide) 2)PU(HTPI11  $\overline{M}_n$  = 1000, Varied % epoxide)



3) PU(HTPI12  $\overline{M}_n = 8000$ , Varied % epoxide) 4) PU(HTPI13  $\overline{M}_n = 900$ , Varied % epoxide)



5) PU(HTPI14  $\overline{M}_n = 4300$ , Varied % epoxide)

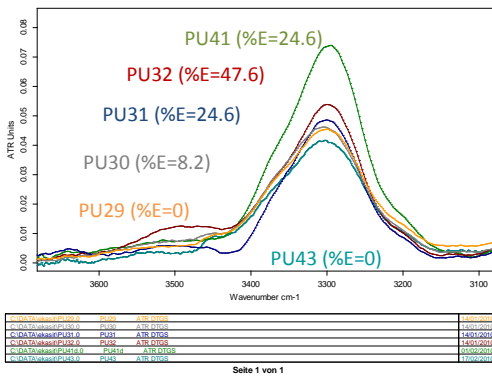
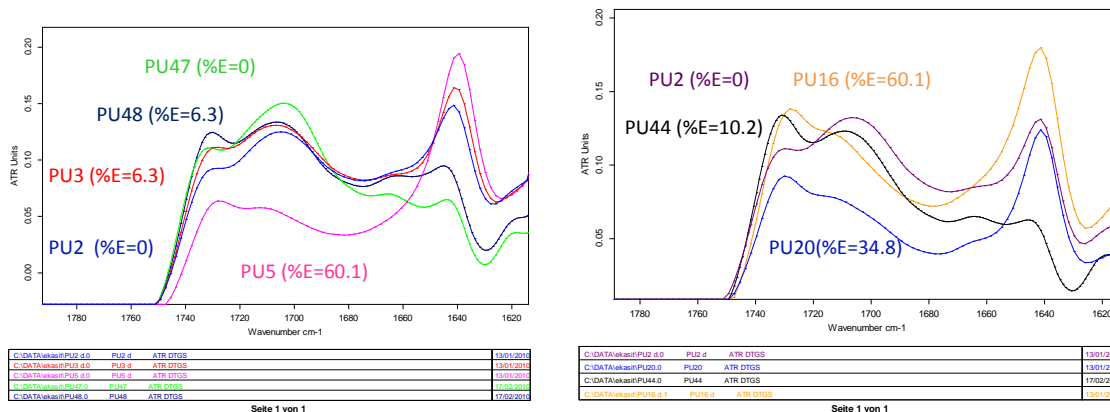
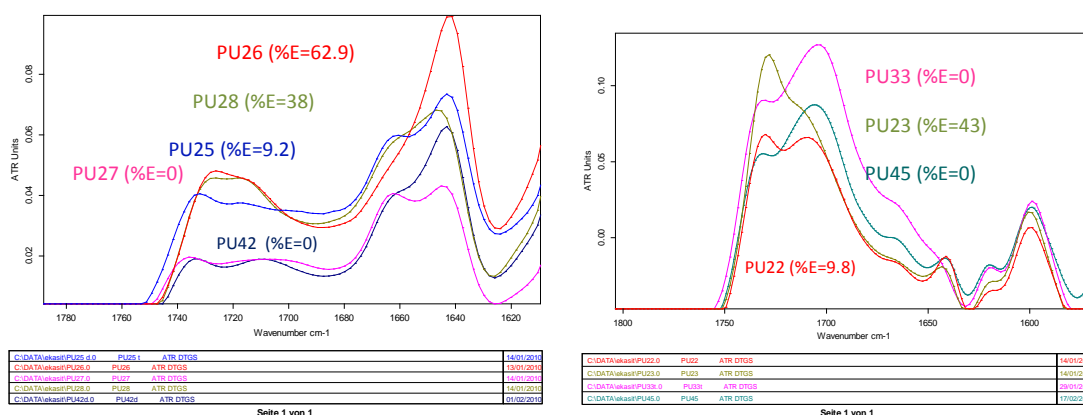


**Figure 3.13** Comparison between ATR FT-IR spectra at 3292 cm<sup>-1</sup> of different EHTPI-based PU films.

1) PU(HTPI10  $\overline{M}_n = 1000$ , Varied % epoxide) 2) PU(HTPI11  $\overline{M}_n = 1000$ , Varied % epoxide)



3) PU(HTPI12  $\bar{M}_n = 8000$ , Varied % epoxide) 4) PU(HTPI13  $\bar{M}_n = 900$ , Varied % epoxide)



5) PU(HTPI14  $\bar{M}_n = 4300$ , Varied % epoxide)

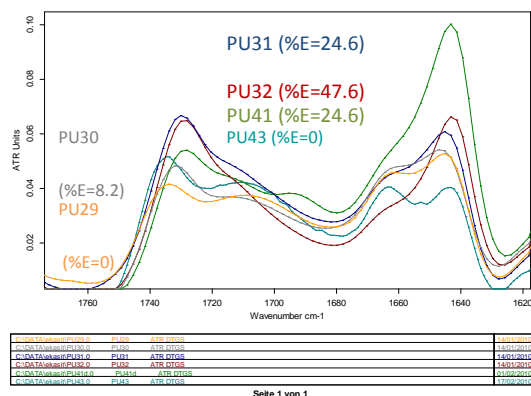


**Figure 3.14** Comparison between ATR FT-IR spectra at 1740-1640 cm<sup>-1</sup> of different EHTPI-based PU films.

From the comparison between the ATR FT-IR spectra of PU different epoxidized HTPI-based PU films, it was found that the NH stretching vibration exhibits a strong absorption peak centered at around 3294 cm<sup>-1</sup>, (which corresponds to the stretching vibration

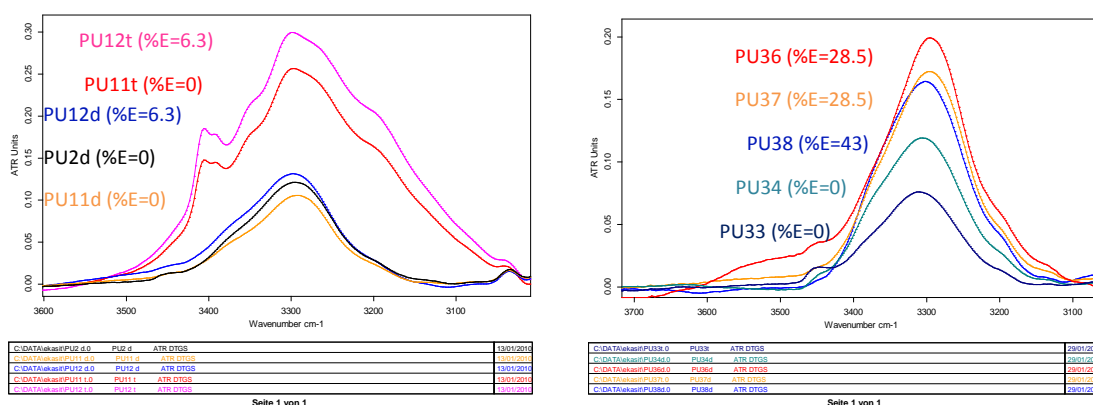
of the NH- -O- hydrogen bond), while the free NH stretching vibration appears as a weak shoulder at about  $3445\text{ cm}^{-1}$ . Note that there appears shoulder or peak at  $3268\text{ cm}^{-1}$  in PU base on EH. This may be a characteristic band of the N-H with hydrogen bond with oxirane groups. We observe less relative proportions of free NH versus N-H hydrogen bonded with increasing proportions of epoxidation in the soft segments.

Figure 3.14 presents the C=O stretching region. It shows that the spectra of PU based on EH are characterized by a major band centered at approximately  $1727\text{ cm}^{-1}$  attributed to free C=O urethane groups, and shoulder at about  $1708\text{ cm}^{-1}$  which is ascribed to hydrogen-bonded urethane. For the PU based on HTPI, the major band is centered at approximately  $1708\text{ cm}^{-1}$ , corresponding to hydrogen bond C=O. This may indicate a preferential hydrogen bonding of NH with oxygen of oxirane groups along the chains allowing more free C=O.

### 3.3.1.3 Effect of varied diol precursors in presence of D-glucose.

1) PU(oligomers  $\overline{M}_n$  1000 + D-glucose)

2) PU(oligomers  $\overline{M}_n$  900 + D-glucose)



**Figure 3.15** Comparison between ATR FT-IR spectra at  $3292\text{ cm}^{-1}$  of PU(oligomers  $M_n$  1000 + D-glucose) (a) PU2d(HTPI10), (b) PU11d(HTPI10/D-glucose), (c) PU12 d (EH10/ D-glucose), (d) PU11t(HTPI10/D-glucose) and (e) PU12 t (EH10/ D-glucose), d= surface with air and t= surface with glass

Figure 3.15 shows the region of the IR spectra corresponding to the N-H bond vibrations. PU11 (base on HTPI10 + D- glucose) and PU12 (base on EH1 + D- glucose) spectra show the band of -NH at  $3296\text{ cm}^{-1}$  attributed to NH hydrogen bonded, and a shoulder at  $3450\text{ cm}^{-1}$  attributed to NH free stretching. Comparison between PU11d (d= surface on air) and PU11t (t= surface on glass) shows that PU11t have the higher intensity at  $3287\text{ cm}^{-1}$



(attributed to –NH hydrogen bonded), than PU11d. Same observation is made in the case of PU12.

For the lower molecular weight precursor – based polyurethanes, we observe increased NH free band when % epoxidation of soft segment increases. For all the spectra, comparing with the other one without glucose, the characteristic band of N-H free vibrations at  $3450\text{ cm}^{-1}$  is very low and quite disappears. This may be explained by supplementary hydrogen bonding with glucose. On Figure 3.16, in the region of the spectra corresponding to C=O bond vibrations, we observe the same proportions between C=O free bond and C=O---H bonded than for the same PU without glucose.

1) PU(oligomers  $\overline{M}_n$  1000 + D-glucose)

2) PU(oligomers  $\overline{M}_n$  900 + D-glucose)

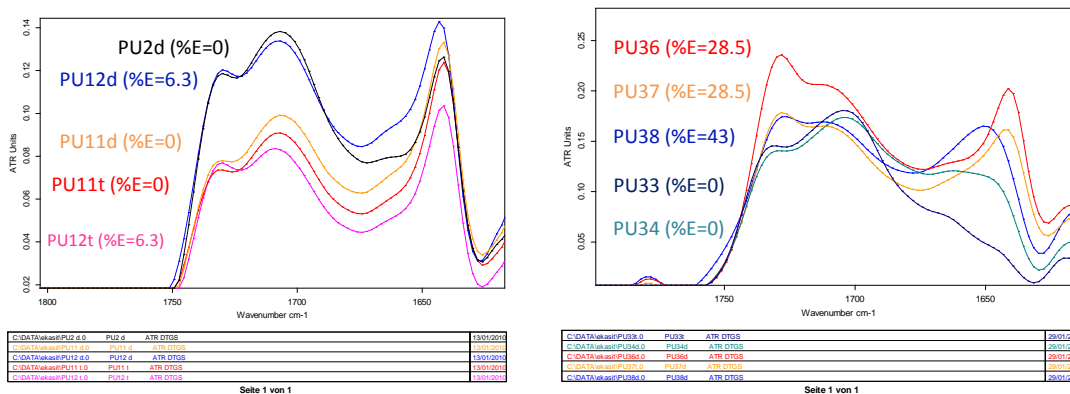
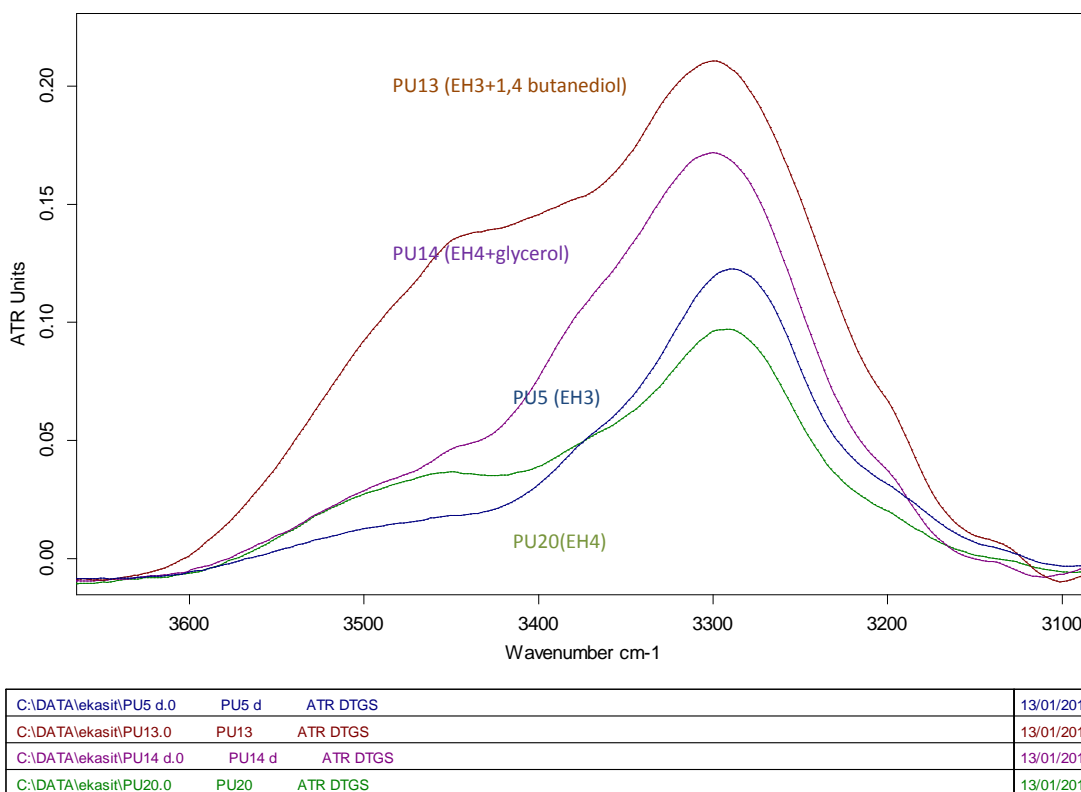


**Figure 3.16** Comparison between ATR FT-IR spectra at  $3292\text{ cm}^{-1}$  of PU(oligomers  $\overline{M}_n$  900 + D-glucose) (a) PU33(HTPI13), (b) PU34 (HTPI13/ D-glucose), (c) PU36(EH1) , (d) PU37(EH11/D-glucose) and (e) PU38(EH12/D-glucose)

Residual band at  $2250\text{ cm}^{-1}$  attributed to –NCO of TDI is observed for some PI + D-glucose based PU. Comparison of the band at  $3290\text{ cm}^{-1}$  shows an order of intensity of PU36d(EH11) > PU37d(EH11+D-glucose) > PU38d(EH12 +D-glucose) > PU34d(HTPI13+D-glucose) > PU33t(HTPI900). This may be an effect of residual isocyanate which should increase the proportions of NH hydrogen bonding with oxygen of isocyanate groups.

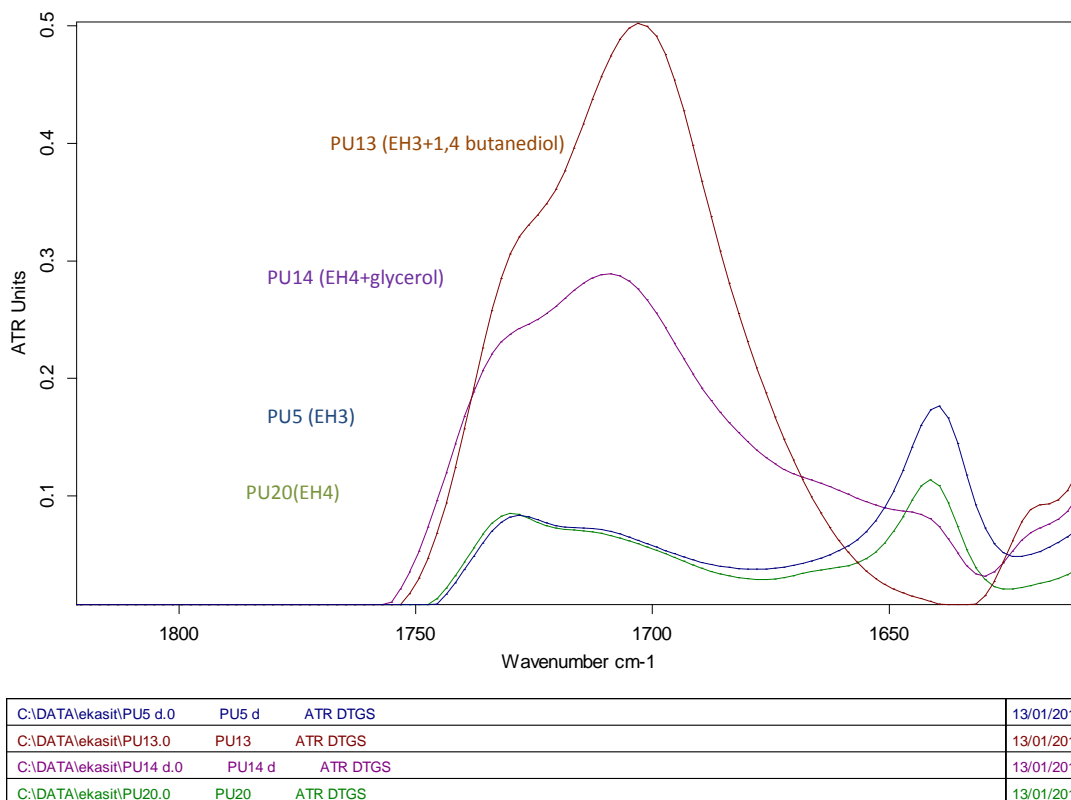
## 3.3.1.4 Effect of varied chain-extenders



Seite 1 von 1

**Figure 3.17** Comparison between ATR FT-IR spectra at 3300-3400  $\text{cm}^{-1}$  of PU (EH / chain extender)

1,4- butanediol and glycerol were added as chain extenders in some formulations (PU13, PU14 and PU15, Table 3.8). Comparison of formulations with, and without chain extender was performed using IR analysis, focusing on NH band near 3300-3400  $\text{cm}^{-1}$  (Figure 3.17), and C=O band near 1700  $\text{cm}^{-1}$  (Figure 3.18). As previously described in 3.3.1.2, the intensity of the band at 3300  $\text{cm}^{-1}$  characteristic of N-H hydrogen bonded is higher in PU with epoxidized precursor (PU13, PU14) compared to non epoxidized analogs (PU5, PU20). A shoulder at 3450  $\text{cm}^{-1}$  (characteristic of NH free bands) is observed, especially in the case of the 1,4 – butanediol added formulation. But remaining not reacted alcohol functions may interfere in this region of the IR spectrum, and no clear conclusions may be done.



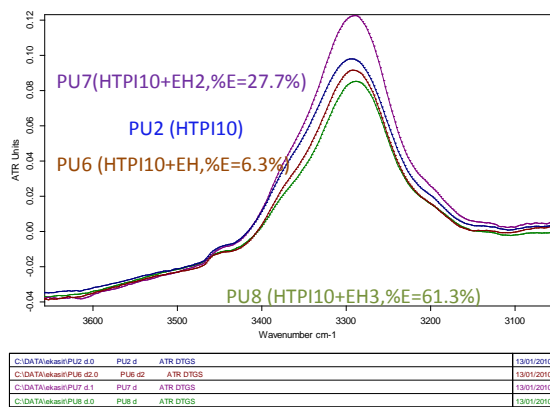
Seite 1 von 1

**Figure 3.18** Comparison between ATR FT-IR spectra at  $1700\text{ cm}^{-1}$  of PU (EH / chain extender) (a) PU5(EH3), (b) PU13(EH3/1,4 butanediol), (c) PU14( EH3/ glycerol) and (d) PU20 (EH4)

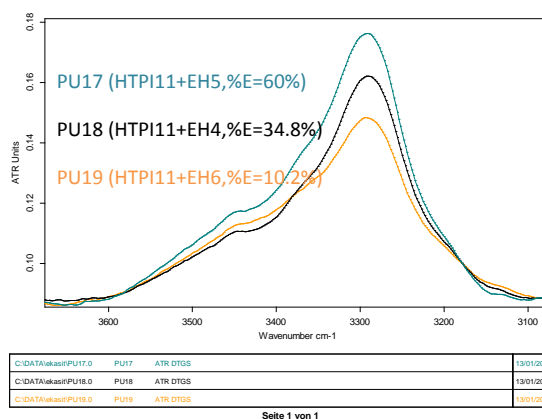
In the  $1700\text{ cm}^{-1}$  region, more clear observations are possible. Increasing amount of C=O hydrogen bonded ( $1708\text{ cm}^{-1}$ ) is observed with increasing amount of epoxy groups as previously described in 3.3.1.2. When chain extender is added in the formulation, we observe increase of the C=O hydrogen bonded band versus free C=O band. This may be explained by the increasing proportion of urethane groups compared to PI soft segment with addition of the extender. Moreover, it is more effective in the case of 1,4-butanediol, perhaps because reaction with glycerol which is a triol, produce reticulation and stiffness of the network, leading to less possibilities of bonding between the urethane functions.

### 3.3.1.5 Effect of mixing HTPI and EH

1) PU( $\overline{M}_n$  1000 + EH)



2) PU( $\overline{M}_n$  1000 + EH)



3) PU( $\overline{M}_n$  900 + EH)

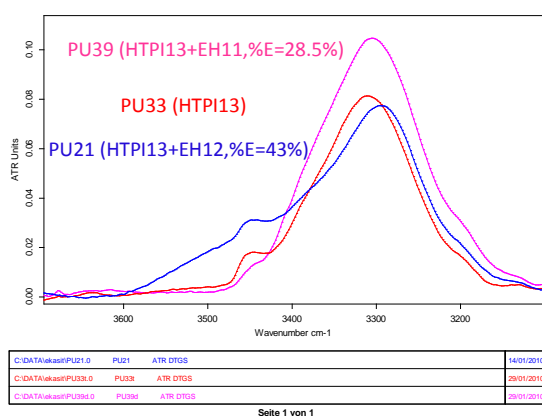
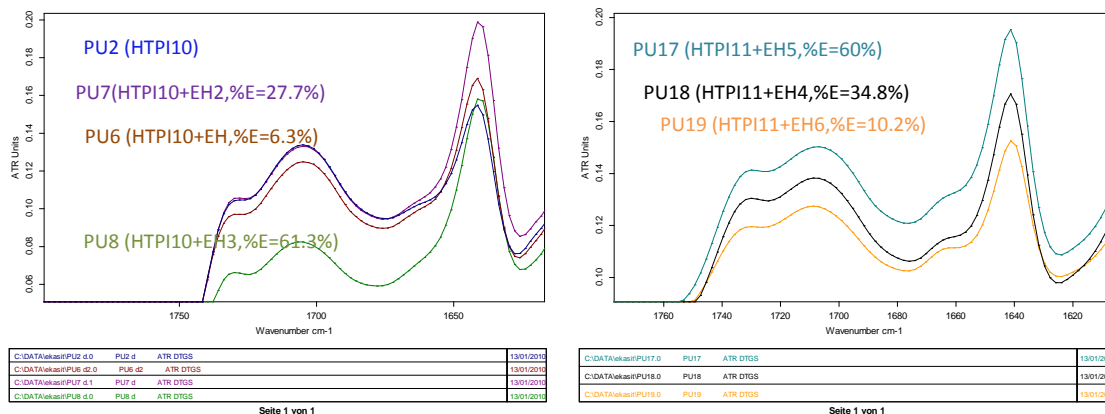


**Figure 3.19** Comparison between ATR FT-IR spectra at  $3290\text{ cm}^{-1}$  of PU ( $\overline{M}_n$  1000 + EH) (a) PU17 (HTPI11+EH5), (b) PU 18(HTPI11+EH4) and (c) PU 19(HTPI11+EH6)

Comparison of the intensity of the band at  $3290\text{ cm}^{-1}$  attributed to  $\text{-NH}$  (Figure 3.19), and of the intensity of the band at  $1708\text{ cm}^{-1}$  attributed to  $\text{C=O}$  stretching vibrations (Figure 3.20), shows the order of intensity of PU17(HTPI11+EH5, %E=60.1) > PU18(HTPI11+EH4, %E=34.8) > PU19 (HTPI11+EH6, %E=10.2) for example, for  $\overline{M}_n$  1000 HTPI precursor. It is the same effect than previously described in paragraph 3.3.1.2.

1) PU( $\overline{M}_n$  1000 + EH)

2) PU( $\overline{M}_n$  1000 + EH)



### 3) PU(HTPI13 $\overline{M}_n$ 900 + EH)

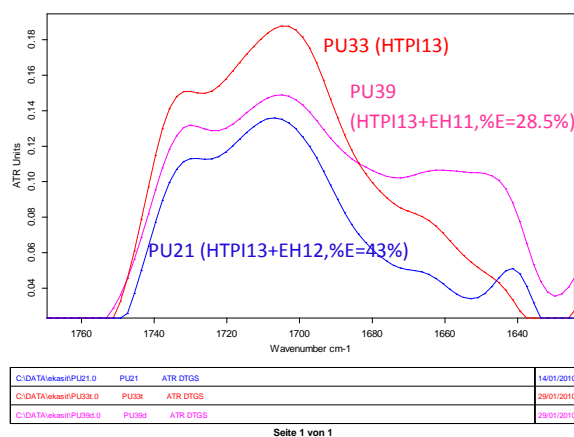


**Figure 3.20** Comparison between ATR FT-IR spectra at  $1690\text{ cm}^{-1}$  of PU (HTPI11  $\overline{M}_n$  1000 + EH) (a) PU17 (HTPI11+EH5), (b) PU 18(HTPI11+EH4) and (c) PU 19(HTPI11+EH6)

The absorb peak at  $1640\text{ cm}^{-1}$  is attributed to the vibration of carbon-carbon double bonds. Intensity of this band decrease compared to the C=O bond at  $1700 - 1720\text{ cm}^{-1}$  with the decreasing  $\overline{M}_n$  of the PI precursors.

### 3.3.2 Thermal properties of polyurethane

Table 3.13 presents the glass transition temperature ( $T_g$ ), determined from DSC analysis for the different PU.

**Table 3.13** Composition and  $T_g$  of polyurethanes

Notation	Precursors( $M_n$ , %epoxide) /Chain extainder	% Hard block <sup>a</sup>	% Catalyst <sup>b</sup>	$T_g$ (°C)
PU(HTPI)	HTPI(1000)/ I-IPDI	-	-	-37
PU(EHTPI10)	EHTPI10(1000, % E = 13)/I-IPDI	-	-	-21
PU(EHTPI50)	EHTPI50(1100, 60.5%)/I-IPDI	-	-	25
PU2	HTPI10(1000)/TDI	17.4	3.8	-55
PU3	EH1(1000, %E = 6.3)/TDI	17.2	3.9	-31
PU4	EH2(1000, %E = 27.7)/TDI	16.4	1.6	-20
PU5	EH3(1000, %E = 60.1)/TDI	14.4	3.1	-14
PU6	HTPI10(1000) + EH1(1000, %E = 6.3)/TDI	17.2	4.4	-52
PU7	HTPI10(1000) + EH2(1000, %E = 27.7)/TDI	18.4	3.7	-40
PU8	HTPI10(1000) + EH3(1000, %E = 60.1)/TDI	17.1	3.6	-29
PU11	HTPI10(1000) /TDI / D-glucose	17.3	3.7	-48
PU12	EH1(1000, %E = 6.3)/TDI / D-glucose	17.2	3.7	-43
PU13	EH3(1000, %E = 60.1)/TDI /1,4 butanediol	14.6	3.1	-23
PU14	EH4(1100, %E=34.8)/TDI / glycerol	31	2.2	-41
PU15	EH5(1100, %E = 60.1) /TDI / glycerol	33.7	1.7	-20
PU16	EH5(1100, %E = 60.1)/TDI	11.5	2.5	-11
PU17	HTPI11(1000) + EH5(1100, %E = 60.1)/TDI	13.1	2.8	-43
PU18	HTPI11(1000) + EH4(1100, %E = 34.8)/TDI	13.1	2.9	-52
PU19	HTPI11(1000) + EH6(1000, %E=10.2)/TDI	12.9	2.8	-61
PU20	EH4(1100, %E=34.8)/TDI	12.9	2.9	-32
PU21	HTPI13(900)+EH12(1000, %E = 43)/TDI	21.3	4.4	*
PU22	EH10(900, %E = 9.8)/TDI	17.7	4.1	*
PU23	EH12(1000, %E = 43)/TDI	17.3	4.2	*
PU25	EH7(7200, %E = 9.2)/TDI	12.4	1.5	-54
PU26	EH9(7600, %E = 62.9)/TDI	12.4	1.5	-14

PU27	HTPI12(8000)/TDI	8.1	1.2	-61
PU28	EH8(6200, %E = 38)/TDI	10.1	1.5	-30
PU29	HTPI14(4300)/TDI	10.5	2.4	-63
PU30	EH13(4100, %E = 8.2 )/TDI	10.1	2.3	-53
PU31	EH14(4000, %E = 24.6)/TDI	10.1	2.3	*
PU32	EH15(4000, %E = 47.6)/TDI	10.5	2.4	*
PU33	HTPI13(900)/TDI	19.7	4.3	-46
PU34	HTPI13(900)/TDI /D-glucose	31	6.8	-32
PU35	EH10(900, %E = 9.8) /TDI /D-glucose	45	9.6	-22
PU36	EH11(1000, %E = 28.5)/TDI	24	5.2	-19
PU37	EH11(1000, %E = 28.5)/TDI /D-glucose	31.8	7	-22
PU38	EH12(1000, %E = 43)/TDI /D-glucose	31.8	7	-21
PU39	HTPI13(900)+EH11(900, %E = 9.8)/TDI	32.5	7.1	*
PU40	HTPI14(4300)/TDI	13.4	2.8	-64
PU41	EH14(4000, %E = 24.6)/TDI	15.6	3.5	-37
PU42	HTPI12(8000)/TDI	8.4	2	-64
PU43	HTPI14(4300)/TDI	10.6	2.3	-60
PU44	EH6(1000, %E = 10.2)/TDI	19.1	4.3	-44
PU45	HTPI13(900)/TDI	21.4	4.4	-51
PU46	EH7(7200, %E = 9.2)/TDI	6.7	1.4	-55
PU47	HTPI10 (1000)/TDI	19.8	4.3	-46
PU48	EH1(1000, %E = 6.3)/TDI	19.7	4.3	-30

<sup>a</sup> % Hard segment = [wt. of (TDI)/ wt. of (TDI + oligomer + catalyst)] × 100

<sup>b</sup> % Catalyst = [wt. of (catalyst)/ wt. of (TDI + oligomer + catalyst)] × 100

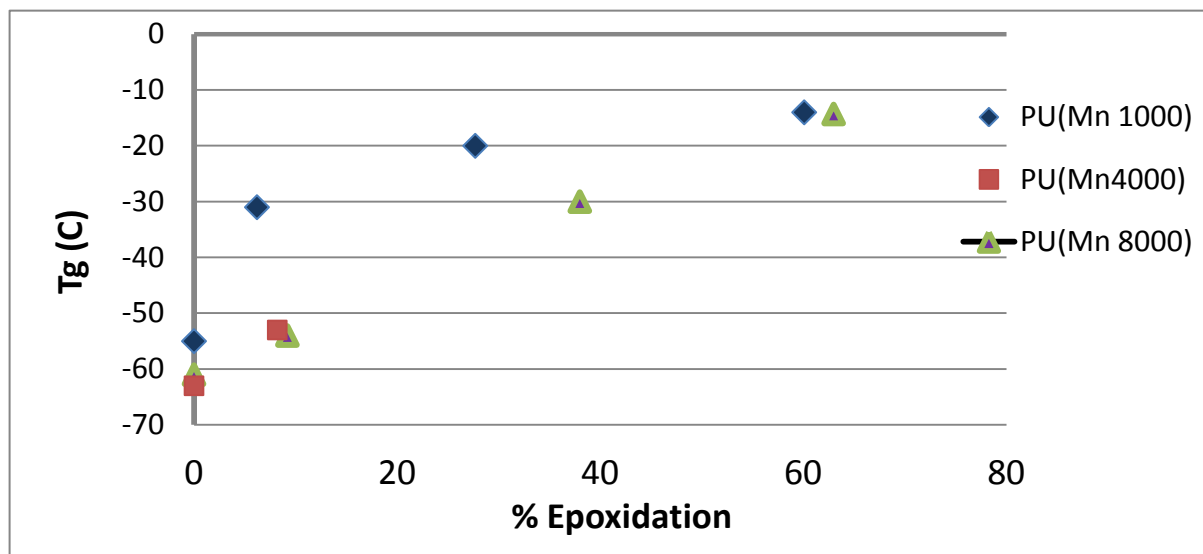


**Figure 3.21** The relationship of  $T_g$  and percentages of epoxidation of polyurethane films different  $M_n$  of PI

For all the formulations of PU done with NR- based diol precursors, only one  $T_g$  was observed,  $T_g$  depends on the proportion of epoxide groups in the mixture( from  $-64^\circ\text{C}$  for HTPI precursor without oxiranes, to  $25^\circ\text{C}$  for EHTPI with 60.5% of oxirane(Table 3.13).

$T_g$  of polyurethane films increases linearly with the increasing percentage of epoxidation as shown in Fig 3.21. This is due to the bulky effect of oxirane rings in the polyurethane main chain, hence higher energy was needed for chain mobility. This  $T_g$  increase could also be the results of intermolecular interactions (hydrogen bonds...), as showed previously by FTIR analysis.

PU obtained from I-IPDI, which are crosslinked, exhibit a higher  $T_g$  ( $-37^\circ\text{C}$  for HTPI(1000)/ I-IPDI (crosslinked), compared to  $-55^\circ\text{C}$  for HTPI10(1000)/TDI (linear). This effect is due to the reduction of mobility induced by the crosslinking. The influence of epoxidation induced a similar effect for crosslinked PU compared to those observed for linear PU : an increase of epoxidation leads to an increase of  $T_g$ .

TGA analysis have been performed on PU in order to determine their thermal stability (degradation temperature). Table 3.14 presents the degradation temperatures and corresponding weight loss of PU.



**Table 3.14** Thermal degradation data of linear polyurethanes

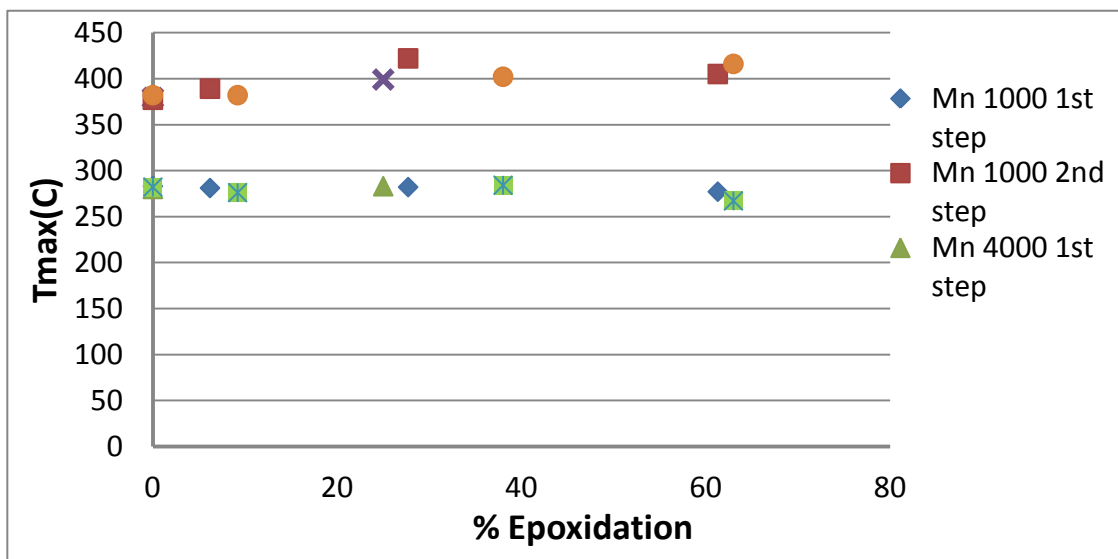
Code	Degradation	T <sub>g</sub> (°C)	T <sub>id</sub> (°C)	T <sub>fd</sub> (°C)	1 <sup>st</sup> Step		2 <sup>st</sup> Step		3rd step	
					T <sub>max</sub> (°C)	% Weight loss	T <sub>max</sub> (°C)	% Weight loss	T <sub>max</sub> (°C)	% Weight loss
PU2	2 steps	-55	119.2	506.6	282.6	27.3	377.2	62.5	-	-
PU3	2 steps	-31	97	500	281.1	25	389.1	66	-	-
PU4	2 steps	-20	117	501.5	281.8	28	421.6	78	-	-
PU5	2 steps	-14	134.7	508.9	277.4	27	405.3	72	-	-
PU6	2 steps	-52	127.3	483.7	281.8	24.1	381.7	63	-	-
PU7	2 steps	-40	98.5	538.4	287	27.1	379.4	62	-	-
PU8	2 steps	-29	140.6	488.9	285.5	26	378.7	61.5	-	-
PU11	3 steps	-48	119.2	546.6	185.7	4.5	262.6	25	375	61
PU12	3 steps	-43	116.2	548.8	180.6	3.2	281.8	30.5	445.3	89.6
PU13	2 steps	-23	80	520.7	275.9	32.9	397.9	74.2	-	-
PU14	2 steps	-41	99.6	534	288.5	28.1	392.8	63.3	-	-
PU15	2 steps	-20	49.7	517.7	281.1	27.3	409.8	72.8	-	-
PU16	2 steps	-11	119	487.4	282.6	24.9	400.2	68.2	-	-
PU17	2 steps	-43	87.4	481.5	289.2	17.5	375.8	53.9	-	-
PU18	2 steps	-52	79.2	471.2	282.6	18.3	375.8	56.7	-	-
PU19	2 steps	-61	89.6	485.2	281.9	14.6	375.8	53.5	-	-
PU20	2 steps	-32	72.6	483.7	286.3	16.5	394.3	61.3	-	-
PU21	2 steps	*	156.1	483.7	288.5	11	378	51.3	-	-
PU22	2 steps	*	91.1	492.6	290.7	12.3	382.4	51.5	-	-
PU25	2 steps	-54	71.9	486	276	10.3	381.7	51.2	-	-
PU26	2 steps	-14	77	503.7	266.4	10	415.7	70	-	-
PU27	2 steps	-61	139.2	475	281.9	7.2	381.7	51.6	-	-
PU28	2 steps	-30	71.9	500	284.1	10	402.1	57	-	-
PU33	2 steps	-46	134	494.1	290.8	16.4	378.2	59	-	-
PU34	3 steps	-32	102.2	511.8	200.5	4.6	294.5	28.6	380.2	60.4

PU35	3 steps	-22	95.5	511.1	202	8.3	283.4	30.5	378.7	57.4
PU36	2 steps	-19	119.2	507.4	287.8	21	397.9	65.5	-	-
PU37	3 steps	-22	70.4	498.5	180.6	3.2	280.4	31.1	406.8	70.6
PU38	3 steps	-21	70	523.7	191.7	7	273.7	32	423.9	73.4
PU41	2 steps	-37	119.9	471.1	283.3	22.1	398.7	58.9	-	-
PU43	2 steps	-60	146.6	474.1	280.4	7.9	379.5	54.1	-	-
PU44	2 steps	-44	112	484.5	282.1	18.3	377.3	54.5	-	-
PU45	2 steps	-51	96	486.7	283.4	15.9	378.0	58	-	-
PU46	2 steps	-55	120	477.1	278.2	7.5	376.5	55.3	-	-
PU47	3 steps	-46	118.9	493.9	226.3	6.6	292.5	23.7	366.1	60.3
PU48	2 steps	-30	96.9	487.9	291.7	21	364.2	55	-	-

$T_{id}$  = Initial decomposition temperature

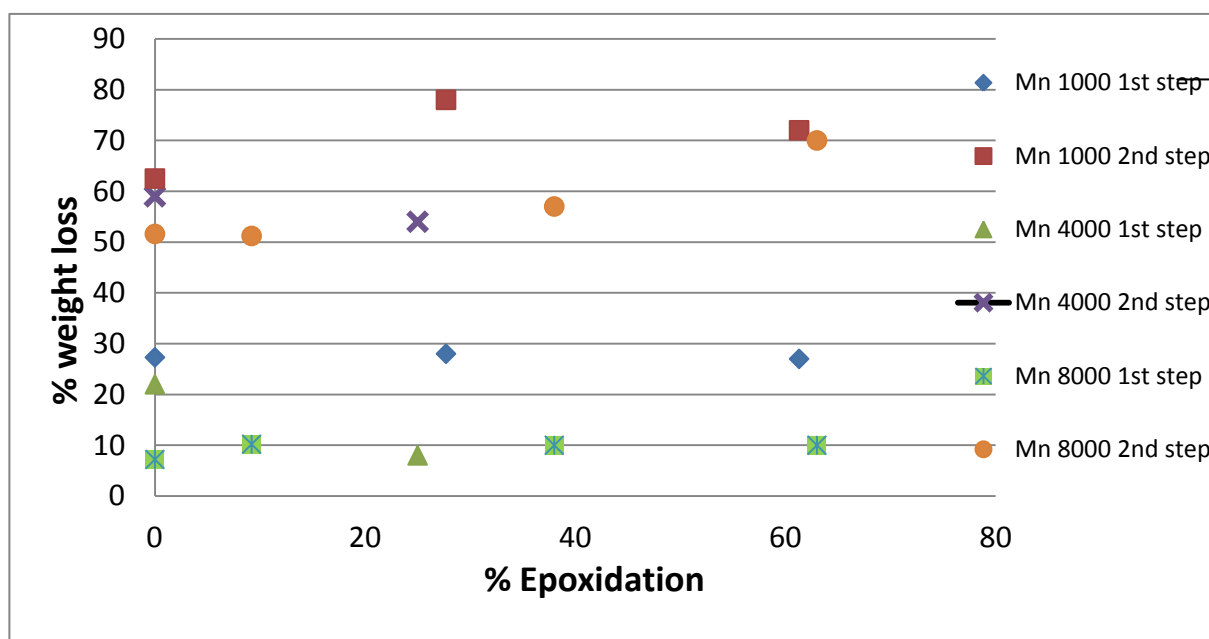
$T_{fd}$  = Final decomposition temperature

Table 3.14 shows weight loss, and characteristic temperatures ( $T_{max}$ ), determined from the minimum of the peak observed on the derived curve, for each polyurethane and for each step. All the TGA curves are presented in Appendix 2. They were obtained at a heating rate of  $10^{\circ} \text{C mn}^{-1}$ , from room temperature to  $600^{\circ} \text{C}$  under nitrogen atmosphere. A two-step degradation was observed for all polyurethanes (except for polyurethanes base on D-glucose which have 3 steps). The curves indicate that all polyurethanes remain stable up to  $260^{\circ} \text{C}$ , after that the first step of degradation occurs. This first step corresponds mainly to the urethane degradation. The second steps correspond perfectly to the soft segment degradations. Otherwise, as observed for oligomers, the third steps do not occur under a nitrogen atmosphere [1].



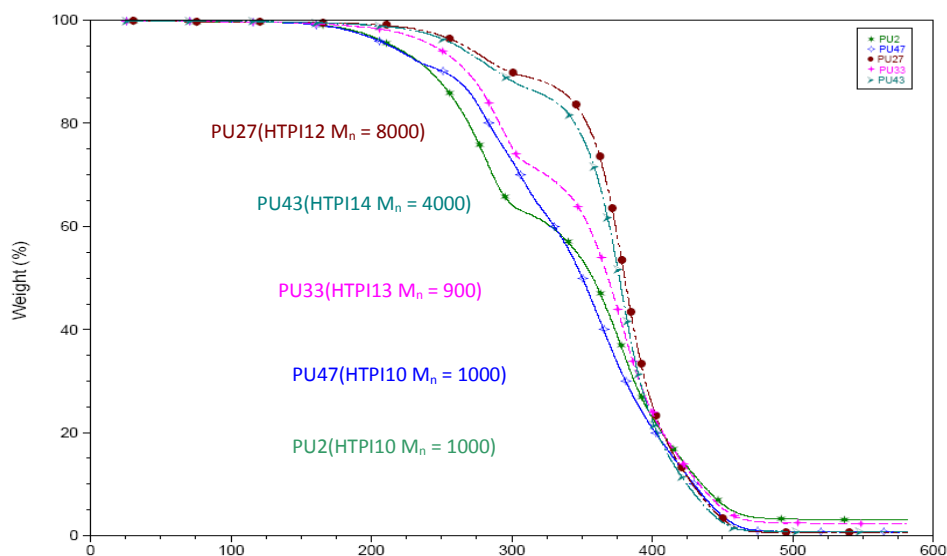
**Figure 3.22** The relationship of percentages of epoxidation of polyurethane films and thermal decomposition data ( $T_{max}$  1<sup>st</sup> step and 2<sup>nd</sup> step) different  $M_n$  of PI.

Figure 3.22 shows the relationship between the  $T_{max}$  1<sup>st</sup> step and 2<sup>nd</sup> step and the % epoxidation of polyurethane films. As it can be seen  $T_{max}$  of all films slightly increases as the percentage of epoxidation increases and it decreases after 30% epoxidation. For the different molecular weights of the precursors, for the 1<sup>st</sup> step and 2<sup>nd</sup> step, it seems that the more stable PU is obtained with a percentage of epoxidation of the diol PI precursor near 30%.



**Figure 3.23** The relationship of percentages of epoxidation of polyurethane films different  $M_n$  of PI and %weight loss ( 1<sup>st</sup> step and 2<sup>nd</sup> step)

The relationship of % epoxidation and %weight loss presented in Figure 3.23, shows increasing %weight loss with increasing %epoxidation. The higher weight loss is observed for a 30% epoxidized HTPI based PU.



**Figure 3.24** TGA thermograms of polyurethanes with different  $\overline{M}_n$  of HTPI

TGA of polyurethanes with different  $M_n$  of HTPI were analyzed comparatively for verification of degradation steps of polymers (Figure 3.24). The analysis showed two decomposition steps of samples corresponding to the two present phases. The first step (110-310°C) is attributed to the degradation of the hard segments and the second step (310-400°C) is related to the degradation of soft segments from polyisoprene block.

The thermal stability of PU( $\overline{M}_n$  = 8000) and PU( $\overline{M}_n$  = 4000) are higher than PU( $\overline{M}_n$  = 1000). Initial degradation temperature ( $T_{id}$ ) and 1<sup>st</sup> step maximum degradation rate temperature ( $T_{max}$ ) are higher whereas the degradation rate is lower. Same observations are done for different epoxidized NR-based PU (Annex 2.1-2.14).

All samples exhibited also the two degradation stages located at 280 and 390 °C. The weight losses for the first and second stages were 15 and 60% w/w, respectively. In this sense, it has been reported that the first weight loss during thermal degradation of PU is due to the degradation of the hard segment as a consequence of the relatively low thermal stability of the urethane groups whereas the second weight loss has been associated to soft segment decomposition [12]. Furthermore, it has been suggested that the amount of weight loss at each degradation stage may be used as a quantitative measurement of the hard and soft content in the PU. We observe that the increasing percentage of epoxidation of the soft segment lead to a lower rate of degradation in the second step and a higher  $T_{max}$ . An other interesting result is the fact that the PU are stable at least until 260°C. This information is important for industrial adhesive applications, where assemblies can be submitted to high temperatures. This stability will also avoid the emission of volatile organic compounds, and consequently limit toxicological impact.

### 3.4 Conclusion

A large serie of PU samples has been synthesized from cis-1,4- oligoisoprene diols obtained by controlled oxidative degradation of high molecular weight polyisoprene as described in chapter 2. Characterization of these PU by FT-IR allows to determine the effect of different factors (such as the average molecular weight and the percent of epoxidation of PI diols precursors, the presence of the D-glucose and varied chain-extendors), on the relative proportions of hydrogen bonding between the urethane hard segments, and between urethane segments and soft segments via the oxirane groups. More free C=O of urethane is observed in the case of more epoxidized PI diols precursors. It means that N-H groups of the urethane make preferential hydrogen bonding with oxygen of oxirane, leading to more free C=O bond of the urethane groups. DSC analysis indicates a significant increase of Tg when epoxidation level is increased. Such higher Tg could have an effect on adhesive properties. Thermal analysis shows that the obtained PU remain stable up to 260 °C. The more stable are those with the higher molecular weight diols precursors with a degree of epoxidation near 30 %.

## References

- [1] C. Wehlack, W. Possart, J. K. Kruger and U. Muller, *Soft Mater.* **2007**, 5, 87.
- [2] A. Farkas and G.A. Mills . *Advanced Catalysis.*, **1962**, 13, 393.
- [3] P. Thomas, (ed.) *Waterborne & Solvent Based Surface Coating Resins and their Applications*; John Wiley & Sons: Chichester: New York., **1998**.
- [4] O. Bayer , *Angew. Chem.*, **1947**, A59, 257
- [5] F. Wang. Doctoral dissertation; *polydimethylsiloxane modification of segmented thermoplastic polyurethanes and polyureas*. Virginia Polytechnic Institute and State University; **1998**.
- [6] G. Woods. *The ICI Polyurethanes Book*; John Wiley and Sons, New York, **1990**.
- [7] P. J. Vipin. Doctoral dissertation; *Studies on Synthesis and Characterization of Thermoplastic Polyurethane-urea Copolymers*. University of Pune , **2009**.
- [8] N.M.K. Lamba, K. A. Woodhouse, *Polyurethane in biomedical applications*, CRC Press, Florida, **1998**
- [9] N. Kébir, I. Campistron, A. Laguerre, , J.F.Pilard, , C. Bunel, and J.P.Couvercelle, *e-Polymers.*, **2006**, 48.
- [10] M. Seki, K. Sato, *Makromol. Chem.*, **1992**, 193, 2971.
- [11] F. Burel, A. Feldman, C. Bunel, *Polymer* , **2005**, 46, 483.
- [12] N. Kebir, I. Campistron, A. Laguerre, J.-F. Pilard, C. Bunel, J.-P. Couvercelle, C. Gondard, *Polymer*, **2005**, 46, 6869.
- [13] N. Kebir, G. Morandi, I. Campistron, A. Laguerre, J.-F. Pilard, *Polymer.*, **2005**, 46, 6844.
- [14] Z. Wirpsza , *Polyurethanes: Chemistry, Technology and Applications*. Ellis Horwood, New York., **1993**
- [15] C. Hepburn, *Polyurethane elastomers*, 2<sup>nd</sup> edition, **1992**.
- [16] S. Keskin. Doctoral dissertation; *Synthesis and characterization of copolymers of diisocyanates and dialcohol*. Middle East Technical University, **2008**
- [17] A. Noshay, and J.E. McGrath, *Block copolymers*. Academic Press, New York., **1977**
- [18] Z.Y. Qin, C.W. Macosko and S.T Wellinghoff. *Macromolecules*, **1985**, 18(3), 553.
- [19] R.J Zdrahala, R.M. Gerkin, S.L Hager, and F.E. Critchfield, *J. Appl. Polym. Sci.*, **1979**, 24(9), 2041.

- [20] J.H. Saunders, and K.C. Frisch, E. Robert. Krieger. Publishing Company, Inc., Florida., **1962**.
- [21] P. Król., Prog. Mat. Sci., **2007**, 52(6), 915.
- [22] B.A. Dombrow. Polyurethanes. Reinhold Publishing Corporation, New York, **1965**
- [23] N. Kebir, *Elaboration de nouveaux polyuréthanes à partir de cis-1,4-oligoisoprènes hétérocarbonyltéléchéliques issus de la dégradation contrôlée du cis-1,4-polyisoprène de haute masse. Etude de leurs propriétés mécaniques, thermiques et biocides*, thèse de l'Université du Maine, Le Mans, **2005**.
- [24] H.S. Lee, S.L Hsu. *Macromolecules*, **1989**, 22, 1100 .
- [25] C.M. Brunette, S.L. Hsu, W.J. MacKnight. *Macromolecules*, **1982**, 15, 71
- [26] I. Yilgor, E. Yilgor. *Polymer Reviews*, **2007**, 47, 487.
- [27] O. Olabisi. Handbook of thermoplastics, Chapter 16 Thermoplastic polyurethanes, Marcel Dekker, **1997**, 386-390
- [28] C. P. Christenson , M. A. Harthcock, M. D Meadows, H. L Spell and W. L Howard, *J.Polym. Sci., Part B: Polym. Phys.* **1986**, 24, 1401.
- [29] L.-S. Teo, C.-Y Chen, J.-F Kuo., *Macromoleculs*, **1997**, 30, 1793.

***Chapter 4 - Adhesive Properties of  
Polyurethane Prepared from  
Hydroxytelechelic cis-1,4-Polyisoprene***



## **4.1 Introduction**

The objective of the chapter is to quantify the adherence of steel/polyurethane/steel assemblies. Surface properties of polyurethane films were firstly investigated by wettability. A wedge test was then used to quantify adherence level of assemblies. The final crack length was measured for different polyurethanes prepared from hydroxytelechelic cis-1,4-polyisoprenes of various molecular weight and epoxydation degree. Microscopy analysis was used to precisely localize the locus of failure. Adhesive behaviour is then discussed as a function of isoprene molecular weight and epoxidation degree.

The adherence level corresponds to the energy required to separate the adhesive and the substrate during a mechanical test. During the adherence test, the join failure could be the consequence of interfacial bonds break (in the case of interfacial rupture), adhesive chains slippage and/or adhesive chains rupture (in the case of a cohesive rupture).

In all cases, interfacial interactions assure the stress transfer between the adhesive and the substrate. During the separation, a part of the energy is then dissipated by friction, due to internal molecular motions. This viscoelastic dissipation leads to a greater measured adherence value compared to the real adhesion energy.

A good wetting is therefore the first required criterion, leading to the formation of interfacial interactions. Both number and nature of these interactions will directly affect the adhesion energy. The presence of polar functions on the adhesive and substrate will favour the wetting and the creation of interfacial bonds.

The development of intimate molecular contact at an interface is a necessary condition for good adhesion, which explain that polymers (viscous liquids during application) are able to assure a good substrate wetting.

Surface energy measurements are able to give information about the nature of physical interfacial interactions (van der Waals interactions and hydrogen or acid-base bonds), even if this parameters is not sufficient to induce a high adherence.

For example, chemical (or covalent) bonds can also occur, depending on the reactivity of both adhesive and substrate.

This chapter will present and discuss surface energy values of PU prepared from the different oligomers, and then adherence level of steel/PU/steel assemblies.

## 4.2 Wettability measurements

Surface energy of PU films is determined by wettability measurement. The contact angle of different liquids drops (water, polar liquid and diiodomethane or  $\alpha$ -bromonaphtalene, non polar liquids) is measured with an automated Kruss apparatus. Table 4.1 presents the surface tension values of the liquids used for wettability measurements.

**Table 4.1** Surface tension of liquids [1].

Standard liquids	Surface tension values [mJ/m <sup>2</sup> ]		
	$\gamma_L$	$\gamma_L^d$	$\gamma_L^p$
Distilled water	72.8	21.8	51
Diiodomethane	50.8	50.8	0
$\alpha$ -Bromonaphtalene	44.4	44.4	0

Table 4.2 presents the surface energy of the PU films prepared from HTPI (hydroxytelechelic cis-1,4-polyisoprene) and EH (epoxidized hydroxytelechelic cis-1,4-polyisoprene). The dispersive component  $\gamma_s^D$  and polar (or non dispersive) component  $\gamma_s^P$  of the surface energy  $\gamma_s$  have been calculated using  $\alpha$ -bromonaphthalene and diodomethane for  $\gamma_s^D$  and water for  $\gamma_s^P$  [2]

**Table 4.2** Surface energy values of PU films for different  $M_n$  and % epoxidation of oligomers.

$\overline{M}_n$	Oligomers	$\overline{M}_n$ (SEC)	%E	$\gamma_s^P$	$\gamma_s^D$	$\gamma_s = \gamma_s^P + \gamma_s^D$
$\text{g.mol}^{-1}$				$\text{mJ/m}^2$	$\text{mJ/m}^2$	$\text{mJ/m}^2$
				[ $\pm 1$ ]	[ $\pm 1$ ]	[ $\pm 2$ ]
	HTPI10	1000	0	0.2	42	<b>42</b>
	EH1	1000	6	0.1	43	<b>43</b>
	EH3	1000	61	0.5	47	<b>48</b>
$\overline{M}_n$ 1000						
	EH4	1100	35	1.8	42	<b>44</b>
	EH5	1100	60	0.7	44	<b>45</b>
	EH6	1000	10	0.5	45	<b>45</b>
$\overline{M}_n$ 8000						
	HTPI12	8000	0	0.5	29	<b>29</b>
	EH7	7200	9	0.4	28	<b>28</b>
	EH8	6200	38	2.5	43	<b>46</b>

	EH9	7600	63	0.2	40	<b>40</b>
	HTPI13	900	0	0.3	36	<b>37</b>
$\overline{M}_n$ 900	EH10	900	10	0.3	39	<b>39</b>
	EH12	1000	43	0.8	44	<b>45</b>
	HTPI14	4300	0	0.1	40	<b>40</b>
	EH13	4100	8	0.2	41	<b>41</b>
$\overline{M}_n$ 4000	EH14	4000	25	0.1	43	<b>43</b>
	EH15	4000	48	0.4	45	<b>45</b>

Surface energy values are globally closed whatever the molecular weight and epoxidation degree, ranging from 37 to 46 mJ/m<sup>2</sup> with an experimental error estimated to  $\pm 2$ .

However, lower values are obtained for the higher molecular weight polymers ( $\overline{M}_n = 8000$ ), containing a low epoxidation degree. This low surface energy value, typical of non-polar polymers such as polyolefins, could be explained by the longer chains (and therefore lower chains polar ends content), which behaves like a hydrocarbonated chains. Increasing the epoxidation degree will increase the surface energy, due to the presence of more reactive groups.

The effect of chains length is then negligible from 900 to 4000, and become detectable for higher length (8000) and low epoxidation.

The effect of epoxidation degree is globally low, with a very slight increase of surface energy with epoxidation degree increase, as illustrated on Figure 4.1.

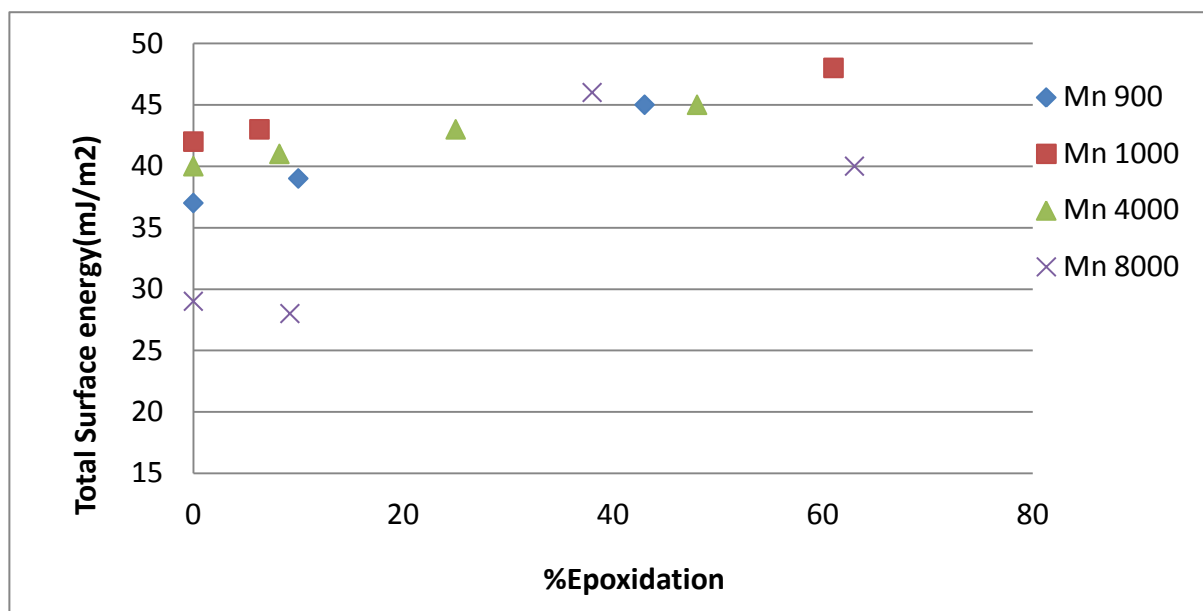


**Figure 4.1** Evolution of the total surface energy[ $\pm 2$ ] of PU films with the epoxidation degree, for different oligomer molecular weights.

The effect of epoxidation degree on polar component is also very low (ranging from 0 to 3 mJ/m<sup>2</sup>, with an experimental error estimated to 1). However, the higher polar components are measured for an epoxidation degree close to 35-40%, as illustrated on Figure 4.2.

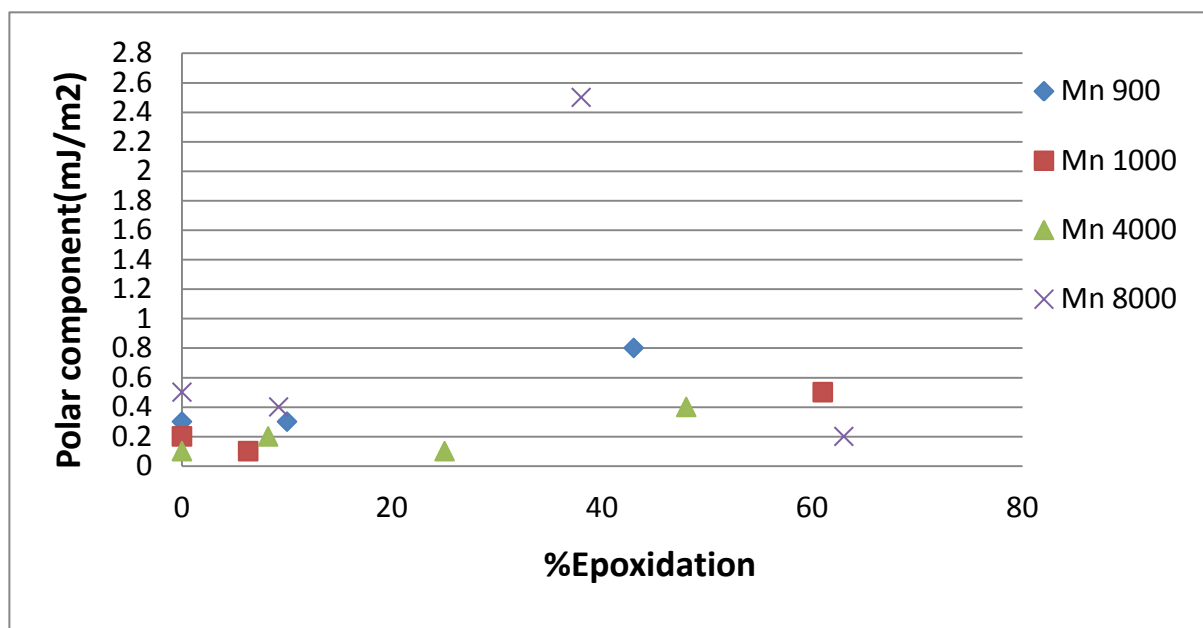


**Figure 4.2** Evolution of the polar component of the surface energy [ $\pm 1$ ] of PU films with the epoxidation degree, for different oligomer molecular weights.

This higher polar component measured for 40% of epoxidation will be correlated with adherence performance in the next part.

To resume, the effect of molecular weight of HTPI on surface energy is negligible, excepted for higher  $\overline{M}_n$ , and epoxidation degree of EH has a slight influence.

Surface energy has been also determined for PU films based on HTPI (hydroxytelechelic cis-1,4-polyisoprene) and EH (epoxidized hydroxytelechelic cis-1,4-polyisoprene) + D-glucose. Results are presented on Table 4.3.

**Table 4.3** Surface energy values of PU films based on HTPI + D -glucose

$\overline{M}_n$ g/mol	Oligomers/Chain extender	$\overline{M}_n$ (SEC)	%E	PU sample	$\gamma_s^P$ mJ/m <sup>2</sup> [± 1]	$\gamma_s^D$ mJ/m <sup>2</sup> [± 1]	$\gamma_s = \gamma_s^P + \gamma_s^D$ mJ/m <sup>2</sup> [± 2]
	HTPI10+D-glucose	1000	0	PU11	3	43	<b>46</b>
$\overline{M}_n$ 1000	EH1+D-glucose	1000	6	PU12	3	43	<b>46</b>
	HTPI13+D - glucose	900	0	PU34	0.2	44	<b>44</b>
$\overline{M}_n$ 900	EH10+D - glucose	900	10	PU36	2	47	<b>49</b>
	EH11+D - glucose	1000	28	PU37	2	48	<b>50</b>
	EH12+D - glucose	1000	43	PU38	2	47	<b>49</b>

Table 4.3 shows that both total surface energy and polar component values of PU based on HTPI + D –glucose are globally higher compared to PU obtained from previous oligomers. This could be explained by the polarity of glucose (hydroxyl groups). The effect of molecular weight and epoxidation level is negligible.

Surface energy of polyurethanes prepared from HTPI and EH oligomers blends are presented in Table 4.4.

**Table 4.4** Surface energy values of polyurethanes base on HTPI + EH blends

$\overline{M}_n$	Code	$\overline{M}_n$ (SEC)	%E	$\gamma_s^P$	$\gamma_s^D$	$\gamma_s = \gamma_s^P + \gamma_s^D$
$\text{g.mol}^{-1}$				$\text{mJ/m}^2$	$\text{mJ/m}^2$	$\text{mJ/m}^2$
				[ $\pm 1$ ]	[ $\pm 1$ ]	[ $\pm 2$ ]
	HTPI10+EH1	1000	6	0	43	<b>43</b>
	HTPI10+EH2	1000	28	0.2	44	<b>44</b>
$\overline{M}_n$ 1000	HTPI10+EH3	1000	61	0.5	44	<b>44</b>
	HTPI11+EH5	1000	60	0.8	44	<b>45</b>
	HTPI11+EH4	1000	35	2.1	43	<b>46</b>
	HTPI11+EH6	1000	10	0.7	44	<b>45</b>
	HTPI13+EH12	900	43	0.4	38	<b>38</b>
$\overline{M}_n$ 900	HTPI13+EH11	900	28	0.8	45	<b>46</b>

The effect of molecular weight and expoxidation level is negligible. Surface energy values are in the same range as PU obtained from EH oligomers.

To resume, wettability measurements indicates quite similar surface energy values for the different PU, excepted for the higher Mn. PU based on HTPI + D –glucose exhibit higher polar component due to the hydroxyl groups of glucose. Now adherence tests will be performed on steel/PU/steel assemblies by using a wedge test.

### 4.3 Wedge test results



The assemblies are submitted to a deformation in mode I by introducing a wedge at 20°C, in ambient conditions. The wedge introduction induces a crack propagation until equilibrium, as shown on Figure 4.3. The final equilibrium is then measured.

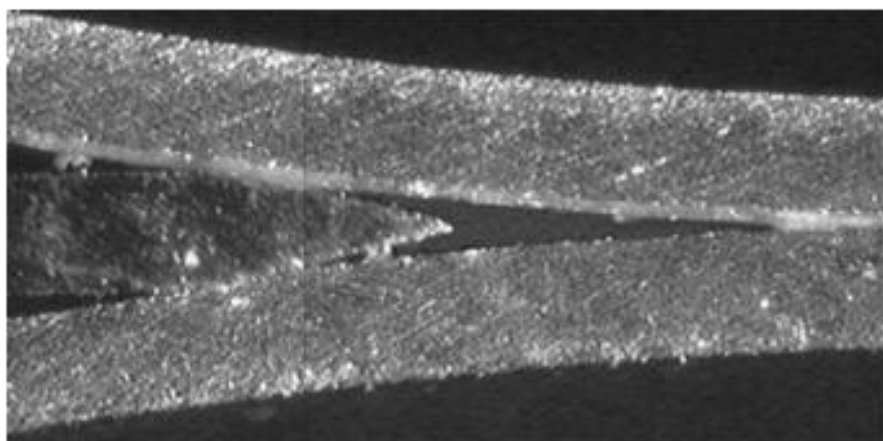


**Figure 4.3** Crack length inside the assemblies at equilibrium

If the deformation of the steel substrate is purely elastic, and if no energy is stored in the polymer layer, the equilibrium is reached when the rate of loss of elastic energy by the metal substrates is equal to the failure energy of the assembly (per unit area).

The failure energy  $G$  can then be calculated from the crack length using the following equation [3]

$$G = \frac{3E\delta^2h^3}{16L^4}$$

where  $E$  is the Young's modulus of the steel substrate ( $2.1 \times 10^{11}$  Pa),  $h$  is the substrate thickness (0.4 mm),  $\delta$  the wedge height (0.4 mm) and  $L$  the crack length.

Previous equation shows that adherence energy  $G$  is directly linked to the crack length (the substrate thickness  $h$  and the wedge height  $\delta$  are indeed constant). We can then directly

compare the crack length to evaluate the adhesive performances of the different assemblies: a high crack length corresponds to a low adherence and inversely.

In a first step, the adherence performance of all PU has been evaluated, in order to select the best polymers for an adhesion application. The worst adhesive behaviour will be firstly presented. Poor adhesive performances, with a total delamination, have been observed for PU based on HTPI + D –glucose, as shown on Table 4.5.

**Table 4.5** The crack length of PU films based on HTPI and EH + D –glucose.

Notation	Oligomers ( $\bar{M}_n$ , % epoxide) /Chain extainer	Crack Length(mm) [ $\pm 1$ ]
PU34	HTPI13(900) + D-glucose	<b>17</b>
PU35	EH10(900, %E = 9.8)	delamination
PU36	EH10(900, %E = 9.8) + D-glucose	delamination
PU37	EH11(1000, %E = 28.5) +D-glucose	delamination
PU38	EH12(1000, %E = 43) +D-glucose	delamination

Steel surfaces were analysed after failure by optical miscoscopy (x 100) in order to assess the locus of failure. For assemblies with a total delamination, microscopy has been performed on the “steel side”, i.e the surface on which a polymer layer is apparently not present (on the opposite side, the steel is covered by the polymer layer). For these assemblies with poor adhesion, the rupture seems to be interfacial (it occurs at a polymer/steel interface). Microscopy confirms the interfacial rupture for all the delaminated assemblies, as illustrated on Figure 4.4 for PU35.

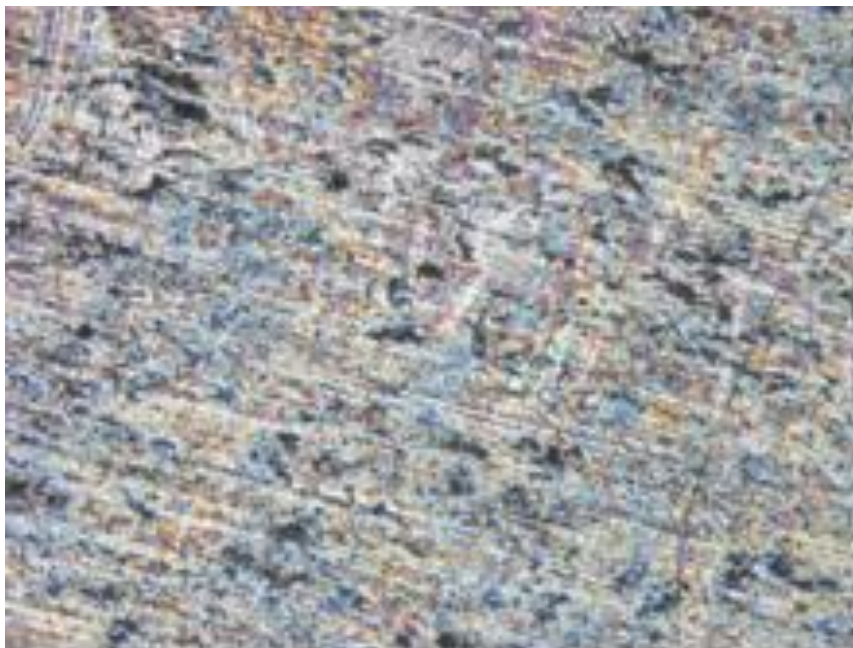


**Figure 4.4** Optical microscopy image of steel surface (200 $\mu$ m) after a total delamination (PU35)

Figure 4.4 corresponds to a steel surface, without any residual polymer layer. Similar images have been obtained for the other delaminated assemblies (PU36 to 35).

However, PU based on HTPI + D –glucose (PU34), without any epoxy groups, shows a high adhesive performance, with a crack length equal to 17 mm. Epoxy groups seem then to induce a decrease of adherence.

For PU34, which exhibits a high adhesion, the failure occurs inside the polymer layer (cohesive failure), as shown on Figure 4.5.

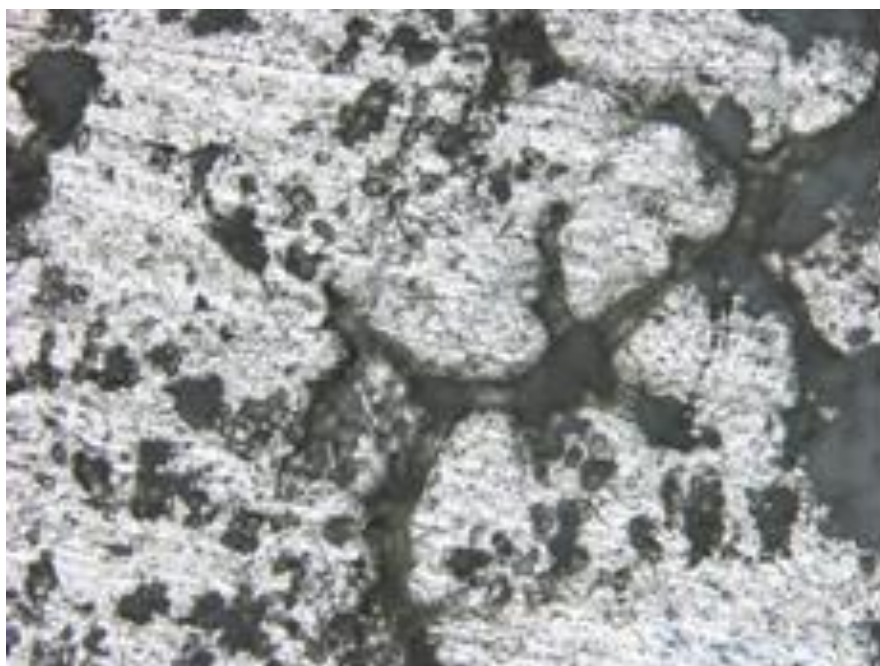


**Figure 4.5** Optical microscopy image of steel surface (200µm) after wedge test (PU34)

Residual polymer can be detected on both steel sides, after wedge test, confirming the cohesive rupture inside the polymer.

Adherence of PU prepared from HTPI (hydroxytelechelic cis-1,4-polyisoprene) and EH (epoxidized hydroxytelechelic cis-1,4-polyisoprene) blends have been also quantified by wedge test. These polymers present a very low adherence, with a total delamination, whatever the epoxy content, as illustrated on Table 4.6.

**Table 4.6** The crack length of PU films based on HTPI and EH blends

Notation	Oligomers ( $M_n$ , % epoxide) /Chain extainder	Crack Length (mm)
PU6	HTPI10(1000) + EH1(1000, %E = 6.3)	delamination
PU17	HTPI11(1000) + EH5(1100, %E = 60.1)	delamination
PU18	HTPI11(1000) + EH4(1100, %E = 34.8)	delamination
PU19	HTPI11(1000) + EH6(1000, %E=10.2)	delamination

For all these delaminated assemblies, the failure occurs at the steel/polymer interface, as illustrated, for PU 19, on Figure 4.6 which confirms the interfacial rupture.

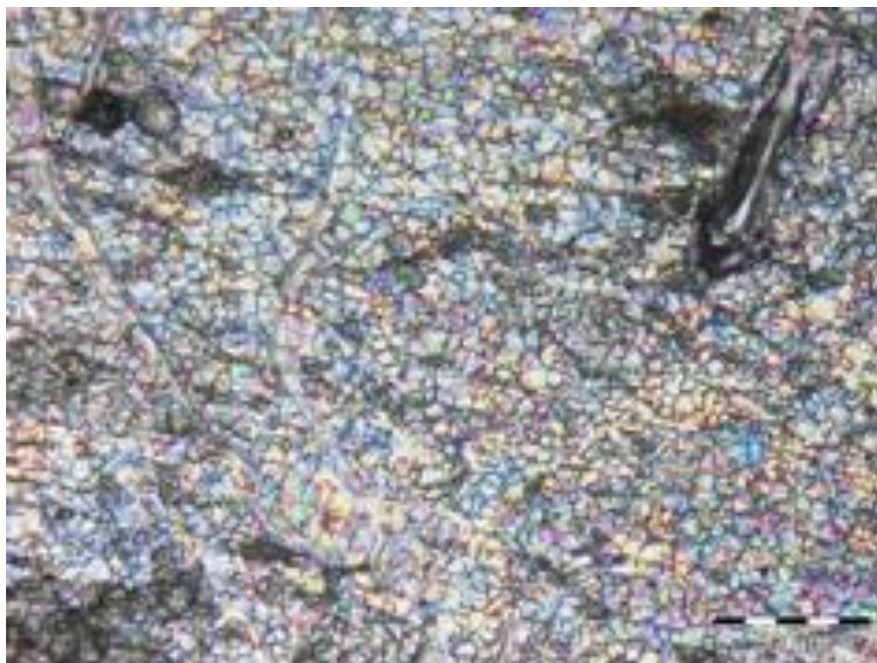


**Figure 4.6** Optical microscopy image of steel surface (200 $\mu$ m) after a total delamination (PU19)

As it was observed for PU based on EH+ D –glucose, epoxy groups do not favour adhesion, while PU prepared from only HTPI (without epoxy group) presents a high adherence, with a crack length equal to 16 mm (PU2), as indicated on Table 4.7 below.

**Table 4.7** The crack length of PU films based on HTPI and EH

Notation	Oligomers ( $M_n$ , % epoxide) /Chain extender	Crack Length (mm)
PU2	HTPI10(1000)	<b>16</b>
PU3	EH1(1000, %E = 6)	delamination
PU22	EH10 (900, %E = 10)	delamination
PU4	EH2 (1000, %E = 28)	<b>22</b>

PU23	EH12 (1000, %E = 43)	<b>18</b>
PU29	HTPI14 (4300)	<b>19</b>
PU30	EH13(4100, %E = 8 )	delamination
PU31	EH14 (4000, %E = 25)	<b>19</b>
PU32	EH15 (4000, %E = 48)	<b>17</b>

---

Table 4.7 shows that PU based on EH (epoxidized hydroxytelechelic cis-1,4-polyisoprene) exhibit a very poor adhesion (delamination) for low epoxidation degrees, and then adhesion increases with epoxy content.

However, a higher epoxy content is not favorable, a delamination being observed for high epoxy content (60%). The optimum epoxy content is then closed to 40%.

The effect of molecular weight is slight (nevertheless, a higher  $\overline{M}_n$  of HTPI induces globally a better adherence for epoxidation degree between 25 and 50%).

However, it is important to notice that when the epoxidation degree is between 25 and 48%, the adherence level is higher, but still lower than the adherence obtained for PU based on pure HTPI (without any epoxy group).

For all the delaminated assemblies, the failure occurs at the steel/polymer interface, as illustrated, for PU22, on Figure 4.7 which confirms the interfacial rupture.

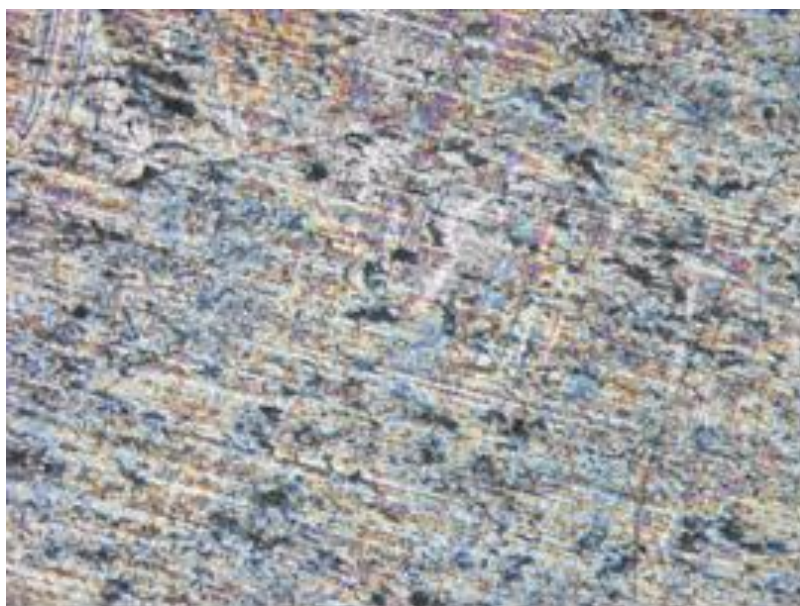


**Figure 4.7** Optical microscopy image of steel surface (200µm) after a total delamination (PU22)

For PU which exhibits a high adhesion, the failure occurs inside the polymer layer (cohesive failure), as shown on Figure 4.8 for PU2.



**Figure 4.8** Optical microscopy image of steel surface(200µm) after wedge test (PU2)

Residual polymer can be detected on both steel sides, after wedge test, confirming the cohesive rupture inside the polymer.

#### **4.4 Conclusion**

Surface energy values of PU prepared from the different oligomers was investigated by wettability measurement (contact angle technique), and then adherence level of steel/PU/steel assemblies was determined by wedge test.

Epoxidation is then able to induce a delamination (for low and high degrees), but is not really able to increase adhesion compared to non-epoxidized oligomer, even in the optimized range of 30-40%.

This optimum range of 30-40% was also identified for surface energy values, for which a higher polar component was measured for epoxidation degree close to 40%, even if a direct relation between both properties is difficult to establish.

The negative effect of epoxidation could be explained by the increase of T<sub>g</sub> with epoxidation degree, especially for high epoxidation (T<sub>g</sub> close to -11°C for 60% of epoxidation, against -60°C for pure HTPI, without any epoxidation). A higher T<sub>g</sub> will decrease the viscoelastic dissipation during separation, and consequently favor the crack propagation. Furthermore, complex chemical reactions during polymerization with isocyanate could occur between epoxy groups and other functions, with consequence of polymer reactivity towards steel.



## References

- [1] P. Krol, B. Krol , *J. of the European Ceramic Society* , **2006**, 26, 2241.
- [2] F.M. Fowkes, *Ind. Eng. Chem.*, **1964**, 56 (12), 40.
- [3] J. Cognard, *J. Adhe.*, **1986**, 20, 1.

## ***General conclusion***

The objective of our research work was the study of the adhesion properties of cis-1,4-polyisoprene-based polyurethanes on metal surface. In order to use Natural Rubber as renewable source material, hydroxytelechelic cis-1,4-polyisoprene(HTPI) was chosen to be used as diol precursor for polyurethanes synthesis. HTPI was obtained successfully by reduction of carbonyltelechelic cis-1,4-polyisoprene(CTPI) issued from the oxidative degradation of high molecular weight polyisoprene by successive steps of epoxidation and cleavage by periodic acid. Various chain structure modifications such as  $M_n$  and different percentages of epoxidation allow to prepare different well defined precursors for polyurethane synthesis.

The characterization of these PU by FT-IR allow to determine the effect of different factors such as the average molecular weight and the percent of epoxidation of PI diols precursors, the presence of the D-glucose and varied chain-extendors on the relative proportions of hydrogen bonding between the urethane hard segments, and between urethane segments and soft segments via the oxirane groups. More free C=O of urethane is observed in the case of more epoxidized PI diols precursors. It means that N-H groups of the urethane make preferential hydrogen bonding with oxygen of oxirane, leading to more free C=O bond of the urethane group. Thermal analysis shows that the obtained PU remain stable up to 260 °C. The more stable are those with the higher molecular weight diols precursors with a degree of epoxidation near 30 %.

Adherence performance of the obtained PU was investigated, focusing on various epoxidation degrees and diol precursors oligomers molecular weights. Wettability measurement by contact angle technique allows to determine the surface energy of the PU. Lower values are obtained for the higher molecular weight HTPI-based PU with low epoxidation degree. Slight increase of surface energy with increase of the epoxidation degree is observed.

Adhesion level was estimated by wedge test on steel/PU/steel assemblies. The pure HTPI samples (without any epoxy group) present a very high adhesion level. Epoxidation degrees close to 30-40% allow to obtain interesting adhesive performance, but higher epoxidation level induces delamination and is not really able to increase adhesion. Elsewhere, the effect of molecular weight is slight (nevertheless, a higher  $\overline{M}_n$  of HTPI induces globally a

better adherence). The adherence level is similar to those measured for structural adhesive used in car or aeronautic industry. The wedge test is a severe adherence test, and the low crack propagation observed for some formulations underlines promising industrial developments for this new polymers.

These low crack lengths (high adherence level) suggest also that strong interactions (probably covalent bonds) have been created between steel and polymer. The surface of stainless steel has a complex composition, which includes the presence of oxides ( $\text{Fe}_2\text{O}_3$ ,  $\text{Cr}_2\text{O}_3$ ,  $\text{NiO}$ ,  $\text{MoO}_3$ ) and hydroxides (mainly  $\text{FeOH}$ ). These polar groups are able to chemically react with PU (especially with isocyanate group, and also epoxy group).

It would be interesting, in a further study, to try to identify the nature of PU/steel bonds, in order to better optimize the polymer formulation. Durability studies would be also fruitful, especially ageing in water or humid conditions, which are usually very severe and damaging for adhesion.

The chemical modification of hydroxytelechelic oligoisoprenes used as precursors of PU, is then able to produce new high performance adhesives using environmentally friendly sources such as natural rubber latex.

## ***Experimental part***

## 1. Chemical products

### 1.1. Polymer:

Cis-1,4-polyisoprene (80% cis,  $\overline{M}_w = 800,000$ , Acros Organics)

### 1.2. Solvents

Dichloromethane ( $\text{CH}_2\text{Cl}_2$ ), chloroform ( $\text{CHCl}_3$ ), methanol ( $\text{CH}_3\text{OH}$ ), ethanol ( $\text{CH}_3\text{CH}_2\text{OH}$ ), ethyl acetate ( $\text{CH}_3\text{CH}_2\text{CO}_2\text{CH}_3$ ), acetone ( $\text{CH}_3\text{COCH}_3$ ), water ( $\text{H}_2\text{O}$ ) were used after distillation. Tetrahydrofuran was used after distillation under nitrogen atmosphere in presence of Na/benzophenone for PU synthesis. Tetrahydrofuran was used as received (commercial grade)

### 1.3. Reagents

Reagents following were used without further purification:

- *meta*-chloroperbenzoic acid, m-CPBA ( $\text{C}_7\text{H}_5\text{ClO}_3$ , 77%, Aldrich)
- Sodium borohydride ( $\text{NaBH}_4$ , 99%, Acros Organics)
- Periodic acid ( $\text{H}_5\text{IO}_6$ , Acros Organics, 99+%)
- Toluene-2, 4-diisocyanate, TDI ( $\text{C}_9\text{H}_6\text{N}_2\text{O}_2$ , 80%, Janssen Chimica)
- Dibutyltin dilaurate, DBTL ( $[\text{CH}_3(\text{CH}_2)_{10}\text{CO}_2]_2\text{Sn}[(\text{CH}_2)_3\text{CH}_3]_2$ , 95%, Aldrich)
- Isocyanurate of isophone diisocyanate, I-IPDI (VESTANAT<sup>®</sup> 1890/100, Degussa-Hüls,  $\overline{M}_n = 825 \text{ g}\cdot\text{mol}^{-1}$ , 16% NCO (w/w),  $f_w(\text{NCO}) = 3.43$ )
- Glycerol (99%,  $\text{C}_3\text{H}_8\text{O}_3$ , Riedel de Haen.)
- 1,4-Butanediol (99%,  $\text{C}_4\text{H}_{10}\text{O}_2$ , Acros organics)

## 1.4. Others

- Potassium carbonate ( $K_2CO_3$ , 97%, Prolabo)
- Sodium hydroxide (NaOH, Acros Organics)
- Sodium chloride (NaCl)
- Sodium bicarbonate ( $NaHCO_3$ , Prolabo)
- Sodium thiosulfate ( $Na_2S_2O_3$ , 98.5%, Acros Organics)
- Magnesium sulfate ( $MgSO_4$ , Fisher Chemicals, 99.7%)
- Silica gel size 40-63  $\mu m$  ( $SiO_6$ )
- Deuterated chloroform (99.8%, 0.03% TMS, Merck)
- Steel substrate: stainless steel 316 L, thickness=0.4 mm

## 2. Materials and instruments

### 2.1. Nuclear Magnetic Resonance (NMR)

NMR spectra were recorded on Bruker 400 Fourier Transform spectrometer at 400.13 MHz for  $^1H$  NMR and at 100.62 MHz for  $^{13}C$  NMR. Chemical shifts are reported in part per million (ppm) downfield from the singlet peak of tetramethylsilane (TMS) using as internal reference.

### 2.2. Size Exclusive Chromatography (SEC)

Number average molecular weight, weight average molecular weight and polydispersity of different samples were measured by Size Exclusive Chromatography on system equipped with Spectra SYSTEM AS1000 autosampler, with a guard column (Polymer Laboratories, PL gel 5  $\mu m$  Guard column, 50x7.5mm) followed by two columns (Polymer Laboratories; 2 PL gel 5  $\mu m$  MIXED-D columns, 2x300x7.5 mm) and two detectors of SpectraSYSTEM RI-150 and Spectra SYSTEM UV 2000. Tetrahydrofuran was used as eluent with flow rate 1 mL.min<sup>-1</sup> at 35°C. Polystyrene standards (580-483 x 103 g.mol<sup>-1</sup>) were

used to calibrate the SEC. Polystyrene standardized weights, named PS eq., were corrected by the Benoit factor,  $\overline{M}_{nSEC} PI = 0.67 \times \overline{M}_{nSEC} PS$ .

### 2.3. Fourier Transform Infrared spectroscopy (FTIR)

IR spectra were recorded on a FTIR Spectrophotometer (Nicolet AVATAR 370 DTGS), equipped with a diamond ATR device (attenuated total reflection). Spectra were obtained from 100 scans (solid mode) and 50 scans (liquid mode) between 4000 and 500  $\text{cm}^{-1}$ .

The transmission mode was also used to characterize liquid samples by placing sample between two pellets of KBr.

FTIR-ATR spectra were measured with a Bruker FTIR Vertex70 spectrometer equipped with an attenuated total reflection accessory. The measurements were carried out in the range of 200—4000  $\text{cm}^{-1}$ , with the ZnSe ATR crystal, 50 scans and resolution of 4  $\text{cm}^{-1}$ .

### 2.4. Differential Scanning Calorimetry (DSC)

Thermal transition of samples was measured by DSC Q100 (TA Instrument) Differential Scanning Calorimeter equipped with the cooling system that temperature can be decrease to -90°C. Samples were put in the aluminium capsule and empty capsule was used as inert reference. The sample and reference are enclosed in the same furnace. The sample and reference crucible are linked by good heat-flow path. The difference in energy required to maintain them at nearly identical temperature is provided by the heat change in the sample.

The calibration in temperature and energy was carried out with a standard Indium:

$$T_f = 156.6^\circ\text{C}$$

$$\Delta H_f = 28.45 \text{ J/g}$$

All experiments were carried out under nitrogen atmosphere at flow rate 50 mL/min with weight of sample 5 to 10 mg. Two scans from -85 to 150°C were performed with a heating and cooling rate of 10°C/min. The condition of the experiment is:

- Isothermal at -85°C during 1 min
- Heating from -85°C to 150°C with the heating rate 10°C/min



- Cooling from 150°C to -85°C with cooling rate 10°C/min
- Reheating from -85°C to 150°C with heating rate 10°C/min

## 2.5. Thermogravimetric analysis (TGA)

With thermogravimetric analysis (TGA) the mass of the sample is recorded continuously while the temperature is increased at the constant rate. Weight loss occurs when volatiles absorbed by the polymer are driven off and at higher temperature when degradation of the polymer occurs with the formation of volatile products [1].

Thermal degradation of polyurethane films was measured by TGA Q500 (TA Instrument). The instrument is composed of a high-precision balance with a platinum pan that is placed in a small furnace with a thermocouple to accurately give the temperature. All experiments were done under nitrogen atmosphere at the flow rate 90 mL/min with sample weight 15 to 20 mg. Samples were heated from room temperature to 600°C with rate 10°C/min. and the weight loss was recorded.

## 2.6 Wettability measurements

Surface energy of PU films is determined by wettability measurement. The contact angle of different liquids drops (water, polar liquid and diiodomethane or  $\alpha$ -bromonaphtalene, non polar liquids) is measured with an automated Kruss apparatus.

Standard liquids	Surface tension values [mJ/m <sup>2</sup> ]		
	$\gamma_L$	$\gamma_L^d$	$\gamma_L^p$
Distilled water	72.8	21.8	51
Diiodomethane	50.8	50.8	0
$\alpha$ -Bromonaphtalene	44.4	44.4	0

The contact angle results were obtained from the sessile drop measurements using the geometric mean method of Owens, Wendt, and Rabel.[1,2].They applied the young's Equation.[3]

$$\gamma_{sl} = \gamma_{sv} - \gamma_{lv} \cos \theta \quad 1.1$$

where  $\gamma$  refers to surface tension or surface energy, the subscripts  $sv$ ,  $sl$ , and  $lv$ , refer to the solid-vapor, solid-liquid, and liquid-vapor interfaces respectively, and  $\theta$  is the contact angle formed between a pure liquid and the surface of the solid as shown schematically in

Figure EP.1.

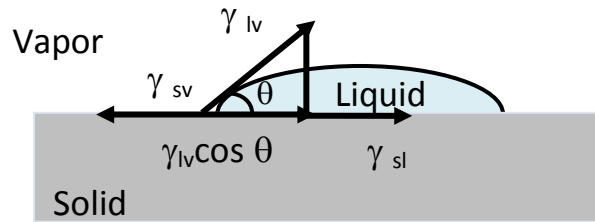


**Figure EP.1** Schematic illustration of the young's Equation (1.1) at the three phase boundary of a sessile drop on a solid surface.

Together with geometric mean method the  $\gamma_{sl}$  value defined by Good and Girifalco in Equation 1.2

$$\gamma_{sl} = \gamma_{lv} + \gamma_{sv} - 2\sqrt{\gamma_{lv}^d + \gamma_{sv}^d} - 2\sqrt{\gamma_{lv}^p + \gamma_{sv}^p} \quad 1.2$$

Where  $d$  and  $p$  refer to the disperse and polar parts of the surface tension, respectively.

By combining equation 1.1 and 1.2 leads to Equation 1.3:

$$\frac{(1 + \cos \theta)\gamma_{lv}}{2\sqrt{\gamma_{lv}^d}} = \sqrt{\gamma_{sv}^p} \cdot \sqrt{\frac{\gamma_{lv}^p}{\gamma_{lv}^d}} + \sqrt{\gamma_{sv}^d} \quad 1.3$$

Water is frequently used as polar liquid to determine the polar component of the surface energy. The polar ( $\gamma_{lv}^p$ ) and the disperse part ( $\gamma_{lv}^d$ ) of water surface tension are given in the previous table.

The square root of the ratio of the polar and disperse parts of the surface tension is used in the Owens, Wendt, and Rabel graphical data evaluation and this generates the intersection value of the  $x$ -axis. Whereas the intersection value of  $y$ -axis can be obtained by solving the left hand

side of Equation 1.3. After plotting and fitting the data by linear regression, the square of the slope  $((\gamma_{sv}^p)^{1/2})$  gives the polar part of the surface tension of the solid surface and the intercept with the y-axis  $((\gamma_{sv}^d)^{1/2})$  gives the disperse part of surface tension. The explanation of this calculation method is demonstrated in Figure EP.2.

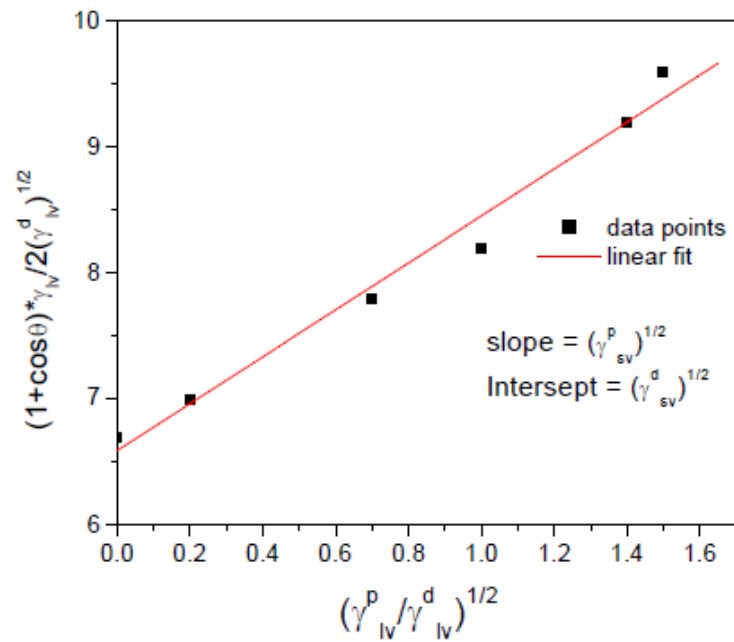


**Figure EP.2** A graphic representation of Owens, Wendt, and Rabel approach for calculation of surface tension [7]

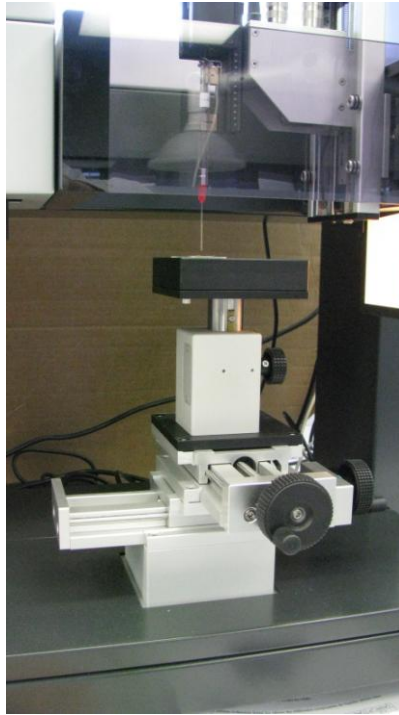


**Figure EP.3** Instruments for measuring contact angle and surface free energy.

## 2.7 Adherence measurements

Adherence of steel/PU/steel assemblies is quantified with a wedge test. The assemblies are submitted to a deformation in mode I by introducing a wedge (height = 0.4 mm) at 20°C, in ambient conditions. The wedge introduction induces a crack propagation until equilibrium. The final equilibrium is then measured.

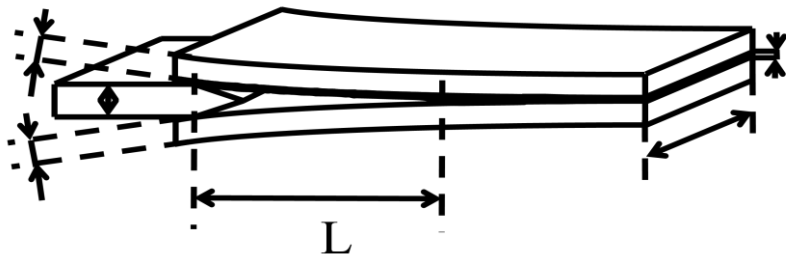


**Figure 1.4** Crack length  $L$  inside the assemblies at equilibrium

Upon introduction of the wedge, the crack propagates until a final length. This results in the creation of two new surfaces and release of elastic energy stored in the beams. If the deformation of the steel substrate is purely elastic, and if no energy is stored in the polymer layer, the equilibrium is reached when the rate of loss of elastic energy by the metal substrates is equal to the failure energy of the assembly (per unit area). The crack propagates on the adhesive/substrate interface or purely in the polymer itself (cohesive failure). Final crack lengths can therefore be directly compared to evaluate the adhesive performances of different assemblies: a high crack length corresponds to a low adherence and inversely.

### **3. Synthesis of precursors of polyurethane**

#### **3.1. Controlled degradation of cis-1,4-polyisoprene 1**

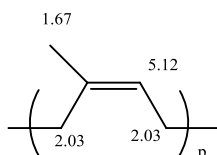
This reaction was done in 2 steps; the reaction of epoxidation of carbon-carbon double bond followed by a step of oxidative cleavage. The oxidation is promoted by periodic acid.

### 3.1.1. Synthesis of epoxidized cis-1,4-polyisoprene (EPI) 2

Cis-1,4-polyisoprene was purified by dissolving in dichloromethane (20 g PI in 500 mL CH<sub>2</sub>Cl<sub>2</sub>) and then precipitated in methanol 800 mL.

Characterization :

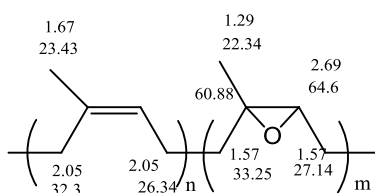
<sup>1</sup>H NMR



For the synthesis of epoxidized cis-1,4-polyisoprene (EPI10), m-CPBA 7.55 g(0.043 mole, 10% epoxidation) in CH<sub>2</sub>Cl<sub>2</sub> were dropwised into a solution of cis-1,4-polyisoprene 23.2 g(0.337 mole) in 400 mL CH<sub>2</sub>Cl<sub>2</sub> in a jacketed reactor cooled at 0°C. The reaction was performed for 6 h. Then the reaction solution was washed with saturated NaHCO<sub>3</sub> and NaCl aqueous solution, respectively. The epoxidized cis-1,4-polyisoprene was precipitated in 800 mL ethanol and dried under vacuum until constant weight. Yield = 93-97%

Characterization :

<sup>1</sup>H and <sup>13</sup>C NMR:



Attribution of IR peaks :

FTIR :  $\nu_{C=CH_2} = 3035 \text{ cm}^{-1}$ ,  $\nu_{CH_2}, \nu_{CH_3} = 2900-2730 \text{ cm}^{-1}$ ,  $\nu_{C=C} = 1664 \text{ cm}^{-1}$ ,  $\nu_{CH_2, CH_3, cis-1,4-isoprene} = 1440, 1375 \text{ cm}^{-1}$ ,  $\delta_{C-H} = 834 \text{ cm}^{-1}$ ,  $\delta_{C-O(epoxide)} = 870 \text{ cm}^{-1}$ .

**Table 1** Experimental conditions and characteristics of epoxidized polyisoprene **2**

Entry	Code	Eq.mol PI	Eq.mol m-CPBA	Weight of PI(g)	E (%)
1	EPI10	1	0.1	23.2	6.8
2	EPI11	1	0.1	24	6
3	EPI12	1	0.03	21.2	1.5
4	EPI13	1	0.1	17.8	8.7
5	EPI14	1	0.04	22.2	1.5

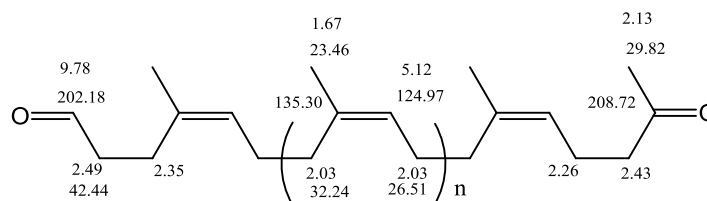
E(%) = percent of epoxidation, Eq.Mol PI = Equivalent mole of polyisoprene, Eq.mol mCPBA= Equivalent mole of meta-chloroperbenzoic acid

### 3.1.2. Synthesis of carbonyltelechelic cis-1,4-polyisoprene (CTPI) 3

Purified epoxidized cis-1,4-polyisoprene (EPI10) 22.1 g (0.321 mole) was dissolved in 400 mL of THF and periodic acid 5.47 g (0.024 mole) in THF was dropwised into a jacketed reactor at 30°C (reaction time : 6 h). The solution was filtered and solvent was then evaporated. After that, product was dissolved in CH<sub>2</sub>Cl<sub>2</sub> (200 mL) and washed with saturated NaHCO<sub>3</sub> and Na<sub>2</sub>S<sub>2</sub>O<sub>3</sub> aqueous solutions. The organic phase was collected and dried over MgSO<sub>4</sub>. The solution was filtered and solvent was evaporated to obtain the yellow viscous liquid. The product was dried under vacuum at 40°C until constant weight. Yield = 50-80%

Characterization :

<sup>1</sup>H and <sup>13</sup>C NMR:



Attribution of IR peaks :

FTIR :  $\nu_{C=CH_2} = 3035 \text{ cm}^{-1}$ ,  $\nu_{CH_2,CH_3} = 2900-2730 \text{ cm}^{-1}$ ,  $\nu_{C=O} = 1720 \text{ cm}^{-1}$ ,  $\nu_{C=C} = 1664 \text{ cm}^{-1}$ ,  $\nu_{CH_2,CH_3, \text{cis-1,4-isoprene}} = 1440, 1375 \text{ cm}^{-1}$ ,  $\delta_{C-H} = 834 \text{ cm}^{-1}$

**Table 2** Experimental conditions and characteristics of carbonyltelechelic cis-1,4-polyisoprene **3**

Entry	code	EPI	Eq.mol EPI	Eq.mol H <sub>5</sub> IO <sub>6</sub>	Mass of EPI (g)	Yield (%)	$\overline{M}_n$ (NMR)	$\overline{M}_n$ (SEC)
1	CTPI10	EPI10 (6.8%)	1	1.1	22.1	78	1340	-
2	CTPI11	EPI11 (6%)	1	1.1	20.5	52	1720	-
3	CTPI12	EPI12 (1.5%)	1	1.1	20.8	58	-	6600
4	CTPI13	EPI13	1	1.1	16.9	86	1108	940
5	CTPI14	EPI14	1	1.1	21.0	80	-	4500

Eq.Mol EPI = Equivalent mole of Epoxidized polyisoprene, Eq.mol H<sub>5</sub>IO<sub>6</sub>= Equivalent mole of periodic acid, Yield (%) = polymer recovery yields,  $\overline{M}_n$  (NMR) = determined with NMR,  $\overline{M}_n$  (SEC) = determined with SEC using polystyrene standards and correcting with Benoit factor (0.67 for polyisoprene)

### 3.2. Synthesis of hydroxytelechelic cis-1,4-polyisoprene (HTPI) 4

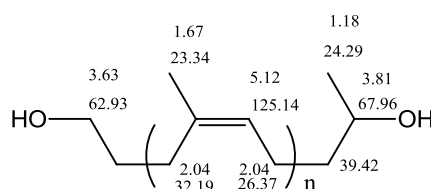
Sodium borohydride 4.85 g (128.3 mmol) in 20 mL THF was charged into a three-necked round bottom flask equipped with a condenser. Carbonyltelechelic cis-1, 4-



polyisoprene (CTPI10) 17.2 g (12.8 mmol) in 150 mL THF was dropwised into the round bottom flask. Then the reaction was performed at 60°C for 6 h. The reaction solution was cooled down to room temperature. 40g of ice in THF 60 mL was then dropwised into solution. After that, solution was washed with saturated NaCl aqueous solution. The organic phase was collected and dried over MgSO<sub>4</sub>. The solution was filtered and solvent was evaporated to obtain light yellow viscous liquid with yielding 80-91 %.

Characterization :

<sup>1</sup>H and <sup>13</sup>C NMR:



Attribution of IR peaks :

FTIR :  $\nu_{OH} = 3350 \text{ cm}^{-1}$ ,  $\nu_{C=CH_2} = 3035 \text{ cm}^{-1}$ ,  $\nu_{CH_2,CH_3} = 2900-2730 \text{ cm}^{-1}$ ,  $\nu_{C=C} = 1664 \text{ cm}^{-1}$ ,  $\nu_{CH_2,CH_3, \text{ cis-1,4-isoprene}} = 1440, 1375 \text{ cm}^{-1}$ ,  $\delta_{C-H} = 834 \text{ cm}^{-1}$ .

**Table 3** Experimental conditions and characteristics of hydroxytelechelic cis-1,4-polyisoprene **4**.

Entry	Code	CTPI	Eq. Mol CTPI	Eq.mol NaBH <sub>4</sub>	Mass of CTPI (g)	Yield (%)	M <sub>n</sub> (NMR)	M <sub>n</sub> (SEC)
1	HTPI10	CTPI10	1	10	17.2	90	1178	1000
2	HTPI11	CTPI11	1	10	10.2	80	1654	1000
3	HTPI12	CTPI12	1	10	12	83	-	8000
4	HTPI13	CTPI13	1	10	14.6	87	1040	900
5	HTPI14	CTPI14	1	10	17	91	-	4300

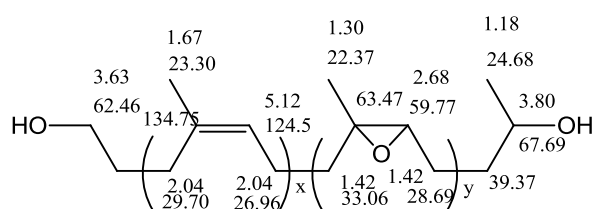
Eq.Mol CTPI = Equivalent mole of Carbonyl telechelic polyisoprene, Eq.mol NaBH<sub>4</sub>= Equivalent mole of sodiumborohydride, Yield (%) = polymer recovery yields, M<sub>n</sub> (NMR) = determined with NMR, M<sub>n</sub> (SEC) = determined with SEC using polystyrene standards and correcting with Benoit factor (0.67 for polyisoprene)

### 3.3. Synthesis of epoxidized hydroxytelechelic cis-1,4-polyisoprene (EHTPI)5

Hydroxytelechelic cis-1,4-polyisoprene (HTPI10) 3.53 g (2.99 mmol) was dissolved with 15 mL CH<sub>2</sub>Cl<sub>2</sub> in three-necked round bottom flask. Subsequently, m-CPBA ( 1.07g, 10% epoxidized, 3.06 g, 30%epoxidized and 5.35 g, 50%epoxidized) in CH<sub>2</sub>Cl<sub>2</sub> solution was added dropwise into the reaction solution at 0°C and solution was stirred at this temperature for 3 h. The solution was filtered and washed with saturated NaHCO<sub>3</sub> aqueous solution two times. Then, solution was dried with MgSO<sub>4</sub>. Finally, the solvent was evaporate under reduced pressure and dried under vacuum until weight constant. Yield was 82-90%.

Characterization :

<sup>1</sup>H and <sup>13</sup>C NMR:



Attribution of IR peaks :

FTIR :  $\nu_{OH} = 3350 \text{ cm}^{-1}$ ,  $\nu_{CH_2,CH_3} = 2900-2730 \text{ cm}^{-1}$ ,  $\nu_{CH_2,CH_3, \text{cis-1,4-isoprene}} = 1440, 1375 \text{ cm}^{-1}$ ,  $\nu_{C-O(\text{epoxide})} = 870 \text{ cm}^{-1}$ . Decreasing of peaks at  $3035 \text{ cm}^{-1}$  ( $\nu_{-CH_2}$ ),  $1664 \text{ cm}^{-1}$  ( $\nu_{C=C}$ ) and  $834 \text{ cm}^{-1}$  ( $\delta_{C-H}$ ) as percentage of epoxidation increases.

**Table 4** Experimental conditions and characteristics of epoxidized hydroxytelechelic polyisoprene 5.

Entry	Code	HTPI	Eq. Mol HTPI	Eq.mol m-CPBA	Mass of HTPI(g)	Yield (%)	$\overline{M}_n$ (NMR)	$\overline{M}_n$ (SEC)	E (%)
1	EH1	HTPI10	1	0.1	3.53	83	1194	1000	6.3
2	EH2	HTPI10	1	0.3	3.22	86	1306	1000	27.7
3	EH3	HTPI10	1	0.5	2.8	84	1474	1000	61.3
4	EH4	HTPI11	1	0.3	2.0	85	1708	1100	34.8
5	EH5	HTPI11	1	0.5	2.1	82	1936	1100	60.1
6	EH6	HTPI11	1	0.1	1.84	83	1718	1000	10.2
7	EH7	HTPI12	1	0.1	1.85	85	-	7200	9.2
8	EH8	HTPI12	1	0.3	2.17	84	-	6200	38
9	EH9	HTPI12	1	0.5	2.10	87	-	7600	62.5
10	EH10	HTPI13	1	0.1	3.1	90	1090	900	9.8
11	EH11	HTPI13	1	0.3	3.0	97	1150	1000	28.5
12	EH12	HTPI13	1	0.5	3.17	87	1220	1000	43.0
13	EH13	HTPI14	1	0.1	4.0	90	-	4100	8.2
14	EH14	HTPI14	1	0.3	4.0	89	-	4000	24.6
15	EH15	HTPI14	1	0.5	3.4	86	-	4000	47.6

Eq.Mol HTPI = Equivalent mole of Hydroxytelechelic polyisoprene, Eq.mol m-CPBA= Equivalent mole of meta-chloroperbenzoic acid, Yield (%) = polymer recovery yields,  $\overline{M}_n$  (NMR) = determined with NMR,  $\overline{M}_n$  (SEC) = determined with SEC using polystyrene standards and correcting with Benoit factor (0.67 for polyisoprene)

## 4. Preparation of polyurethane films

### 4.1. Synthesis of polyurethane films without chain extender

Polyurethane films were prepared according to the procedure previously described by Kebir *et al* [8, 9]. 0.5 g of hydroxytelechelic cis-1,4-polyisoprene or epoxidized hydroxytelechelic cis-1,4-polyisoprene ( $\overline{M}_n = 900, 1000, 4000$  and  $8000$  g/mol) was dissolved in dried THF (0.1 g/mL). DBTL and diisocyanate were then added into the solution with ratio of  $[\text{DBTL}]/[\text{OH}] = 0.045$  and  $[\text{NCO}]/[\text{OH}] = 1.2$ . After stirring for few minutes, the solution was poured into mould and put in desiccators under nitrogen atmosphere for 2 hours and in oven at  $60^\circ\text{C}$  for 12 hours.

### 4.2 Synthesis of polyurethane standing films with chain extender

Polyurethane films were synthesized according to method previously described. Different proportion of hydroxytelechelic cis-1,4-polyisoprene, glucose, 1,4 butanediol and glycerol (chain extender) were dissolved in dried THF with the concentration 0.1 g/mL. Then, DBTL was added with  $[\text{DBTL}]/[\text{OH}] = 0.045$ . After that, diisocyanates was added into the solution with  $[\text{NCO}]/[\text{OH}] = 1.2$ . After stirring for few minutes, the solution was pour into mould and put in desiccators under nitrogen atmosphere for 2-3 h and at  $60^\circ\text{C}$  overnight.

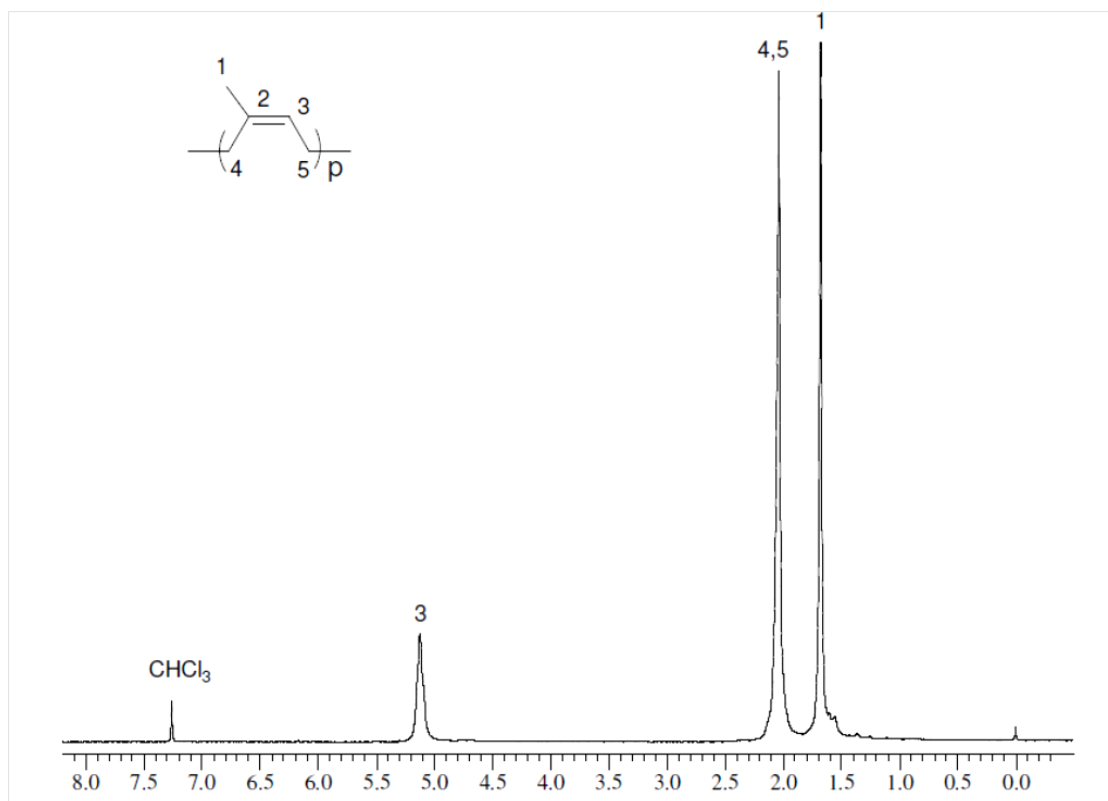
### 4.3. Preparation of polyurethane coated on steel

An hydroxytelechelic cis-1,4-polyisoprene (or epoxidized hydroxytelechelic cis-1,4-polyisoprene), DBTL and diisocyanate solution prepared according to previous procedure was dropped onto a steel and put in desiccator under  $\text{N}_2$  atmosphere for 2 hours and in oven at  $60^\circ\text{C}$  for 12 hours. Finally, films were completely dried in vacuum oven at  $50^\circ\text{C}$  overnight. Steel/PU/steel assemblies are also prepared. Steel plates were previously cleaned with acetone and dried.

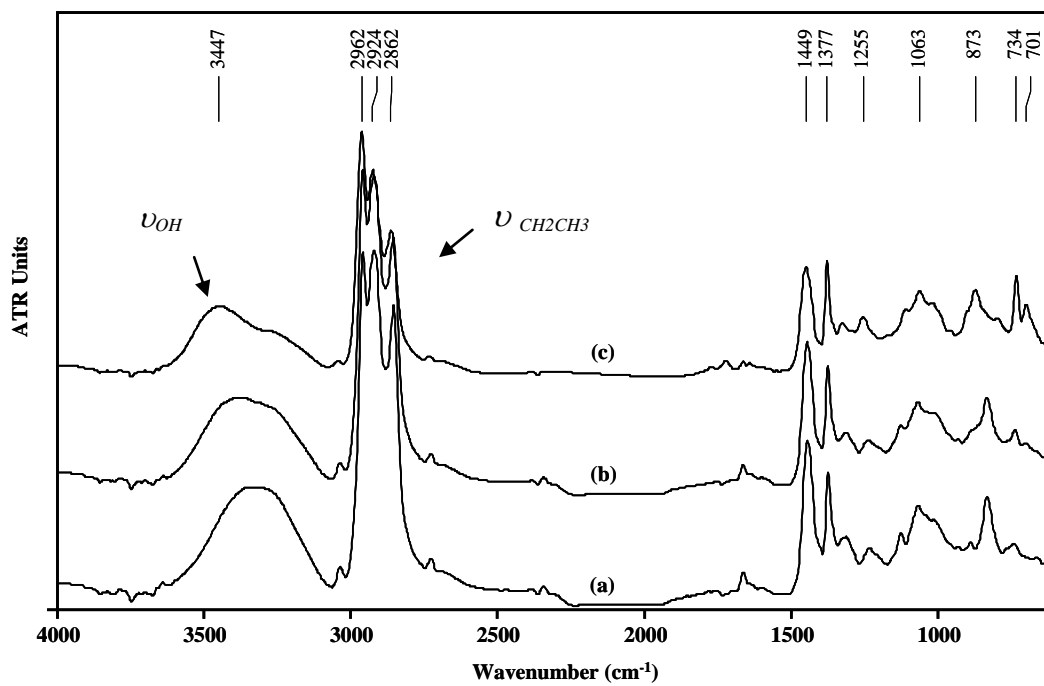
## References

- [1] F. M. Fowkes., *Ind Eng. Chem.*, **1964**, 56, 40.
- [2] L.M. Lander, L. M. Siewierski, W. J. Brittain, E. A .Volger., *Langmuir.*, **1993**, 9, 2237
- [3] T. Young., *Trans. R. Soc. London* **1805**, 95, 65.
- [4] R. J. Good., *S. C. T. Monogr.* **1967**, 25, 328
- [5] L. A. Girifalco., R. J Good., *J. Phys. Chem.* **1957**, 61, 904.
- [6] R. J. Good., *J. Adhes. Sci. Technol.* **1992**, 6, 1269.
- [7] N. Marhmood. *Investigations on the Adhesion of Polyurethane Foams on Thermoplastic Material Systems.* **2005**.
- [8]N. Kebir, G. Morandi, I. Campistron, A. Laguerre, J.-F. Pilard, *Polymer*, **2005**, 46 6844.
- [9]. N. Kebir, I. Campistron, A. Laguerre, J.-F. Pilard, C. Bunel, J.-P. Couvercelle, C. Gondard, *Polymer* , **2005**, 46, 6869.

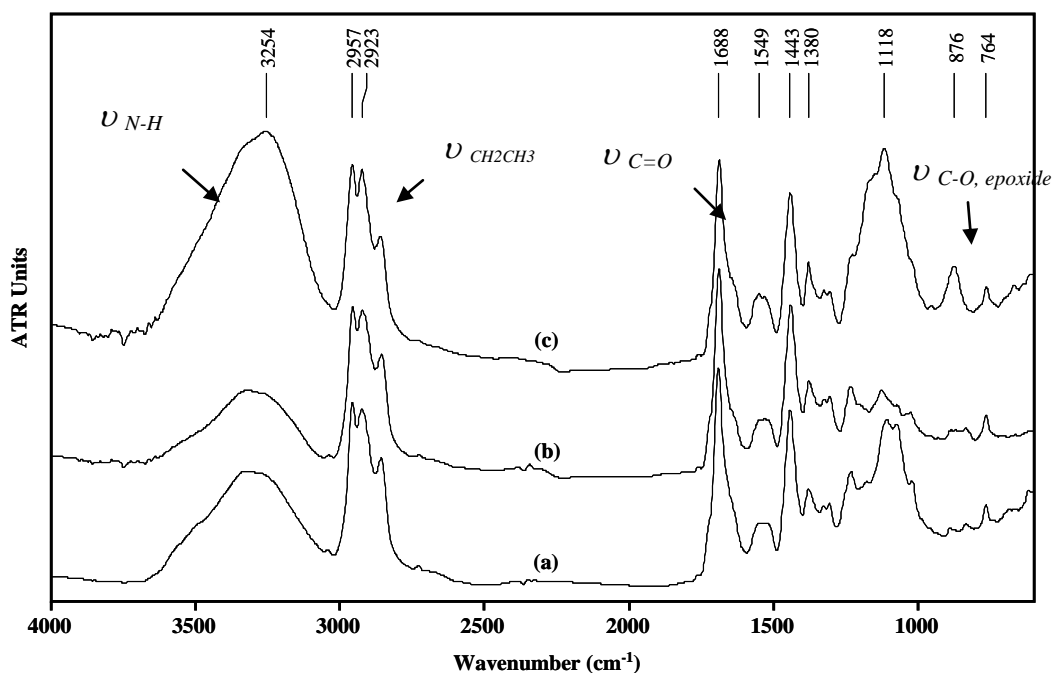
## *Appendix*

Appendix 1.1  $^1\text{H}$  NMR of cis-1, 4-polyisoprene

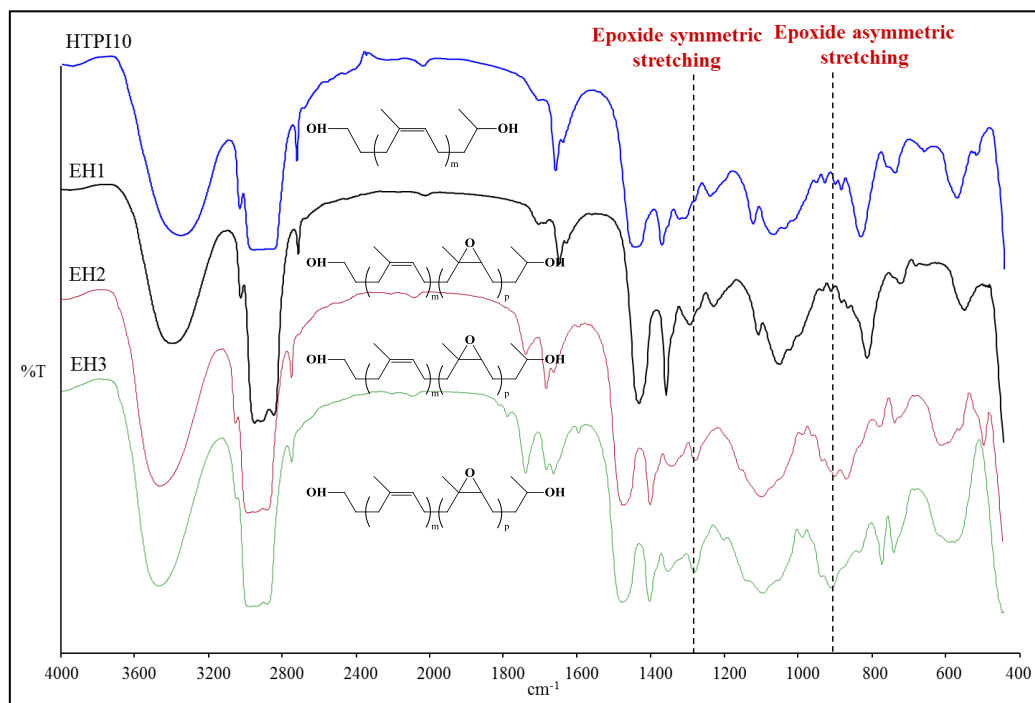
## Appendix 1.2 IR- spectrum (ATR) of comparison in (a)HTPI, (b)EHTPI 10 and (c)EHTPI 50



**Appendix 1.3** ATR-FTIR spectra of (a) PU(HTPI)film (b)PU(EHTPI10)film and (c) PU(EHTPI50) film.

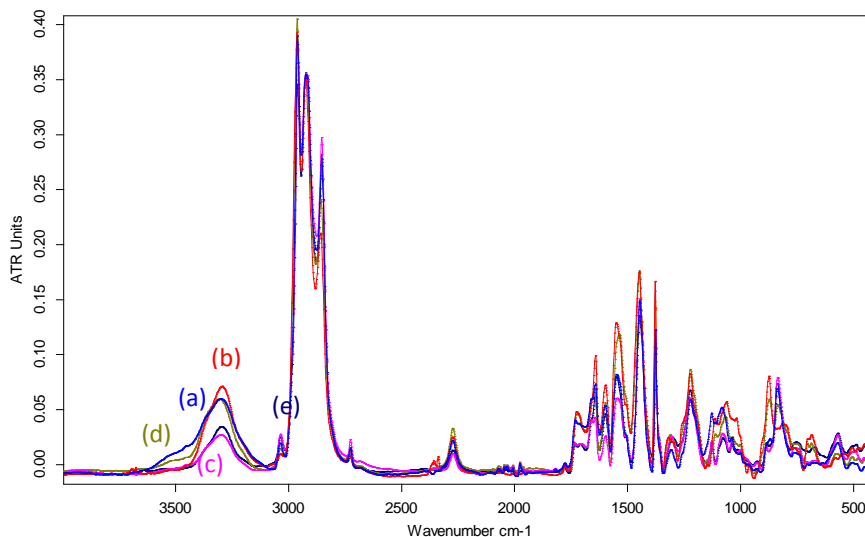


**Appendix 1.4** IR- spectrum of comparison in HTPI10( $\overline{M}_n$ 1000), EH1(%epoxidation =6.3) , EH2(%epoxidation =27.7), EH3(%epoxidation =61.3)





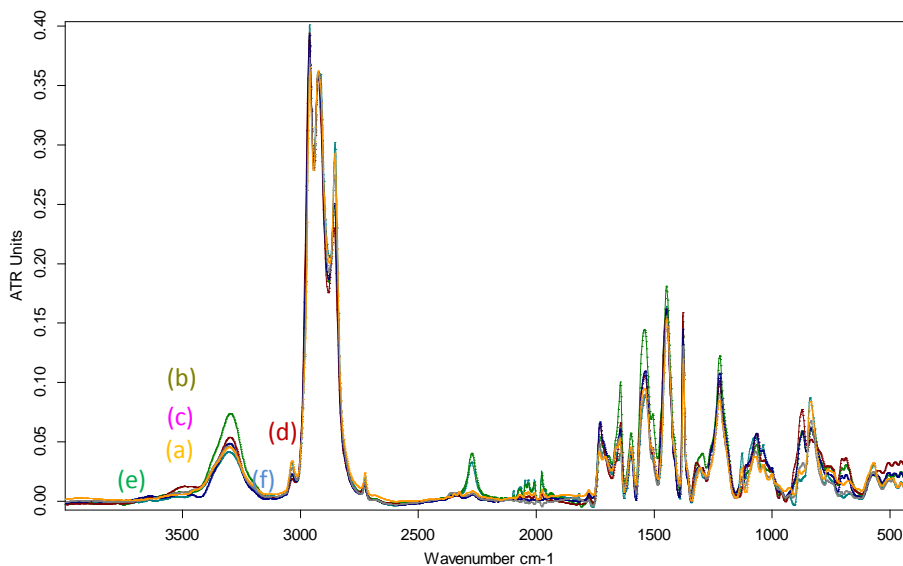
**Appendix 1.5** Comparison between ATR FT-IR spectra of PU(HTPI12  $M_n$  8000, varied %E) (a) PU25(EH7, %E = 9.2), (b) PU26(EH9, %E = 62.9), (c) PU27 (HTPI12, %E = 0), (d) PU28(EH8, %E = 38) and (e) PU 42(HTPI12, %E = 0)



C:\DATA\ekasit\PU25 d.0	PU25 t	ATR DTGS	14/01/2010
C:\DATA\ekasit\PU26.0	PU26	ATR DTGS	13/01/2010
C:\DATA\ekasit\PU27.0	PU27	ATR DTGS	14/01/2010
C:\DATA\ekasit\PU28.0	PU28	ATR DTGS	14/01/2010
C:\DATA\ekasit\PU42d.0	PU42d	ATR DTGS	01/02/2010

Seite 1 von 1

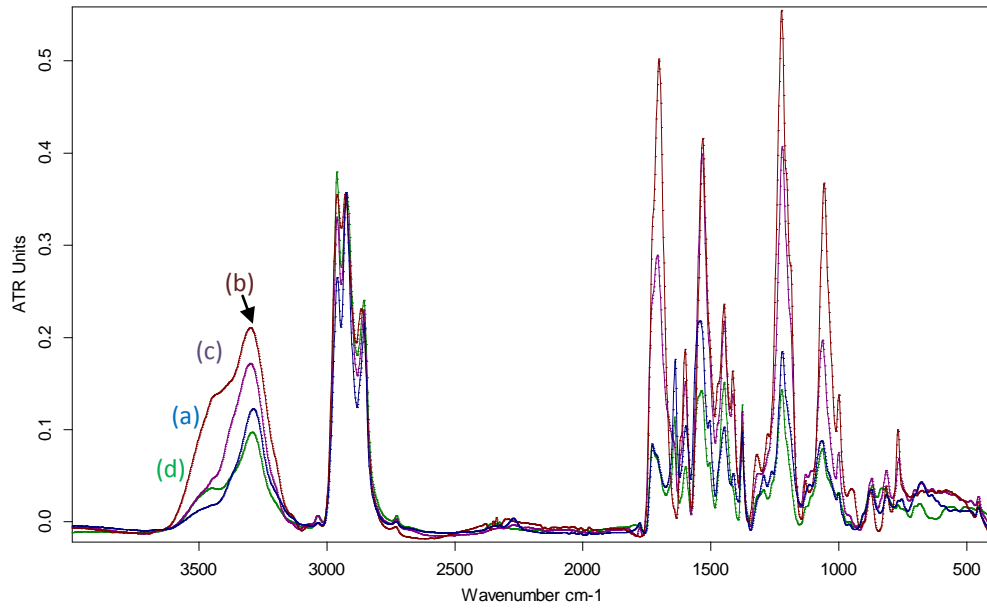
**Appendix 1.6** Comparison between ATR FT-IR spectra of PU(HTPI14  $M_n$  4300, varied %E) (a) PU29(HTPI14, %E = 0), (b) PU30(EH13, %E = 8.2), (c) PU31 (EH14, %E = 24.6), (d) PU32(EH15, %E = 47.6), (e) PU41(EH14, %E = 24.6) and (f) PU 43(HTPI14, %E = 0)



C:\DATA\ekasit\PU29.0	PU29	ATR DTGS	14/01/2010
C:\DATA\ekasit\PU30.0	PU30	ATR DTGS	14/01/2010
C:\DATA\ekasit\PU31.0	PU31	ATR DTGS	14/01/2010
C:\DATA\ekasit\PU32.0	PU32	ATR DTGS	14/01/2010
C:\DATA\ekasit\PU41d.0	PU41d	ATR DTGS	01/02/2010
C:\DATA\ekasit\PU43.0	PU43	ATR DTGS	17/02/2010

Seite 1 von 1

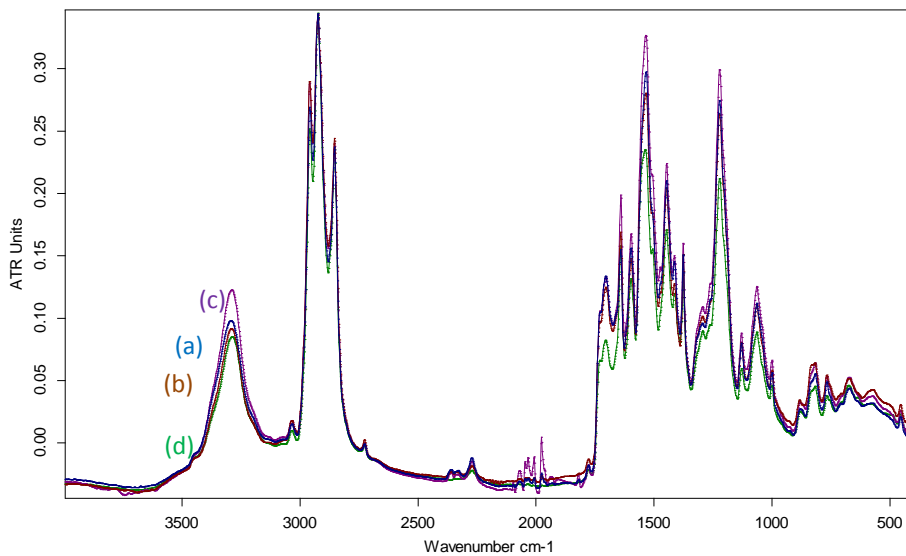
**Appendix 1.7** Comparison between ATR FT-IR spectra of PU (EH / chain extender) (a) PU5(EH3), (b) PU13(EH3/1,4 butanediol), (c) PU14( EH3/ glycerol) and (d) PU20 (EH4)



C:\DATA\ekasit\PU5 d.0	PU5 d	ATR DTGS	13/01/2010
C:\DATA\ekasit\PU13.0	PU13	ATR DTGS	13/01/2010
C:\DATA\ekasit\PU14 d.0	PU14 d	ATR DTGS	13/01/2010
C:\DATA\ekasit\PU20.0	PU20	ATR DTGS	13/01/2010

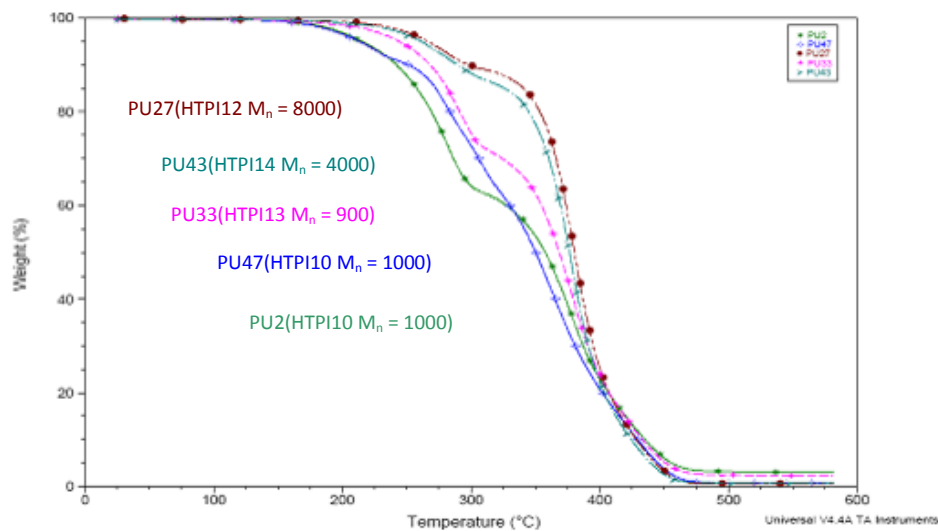
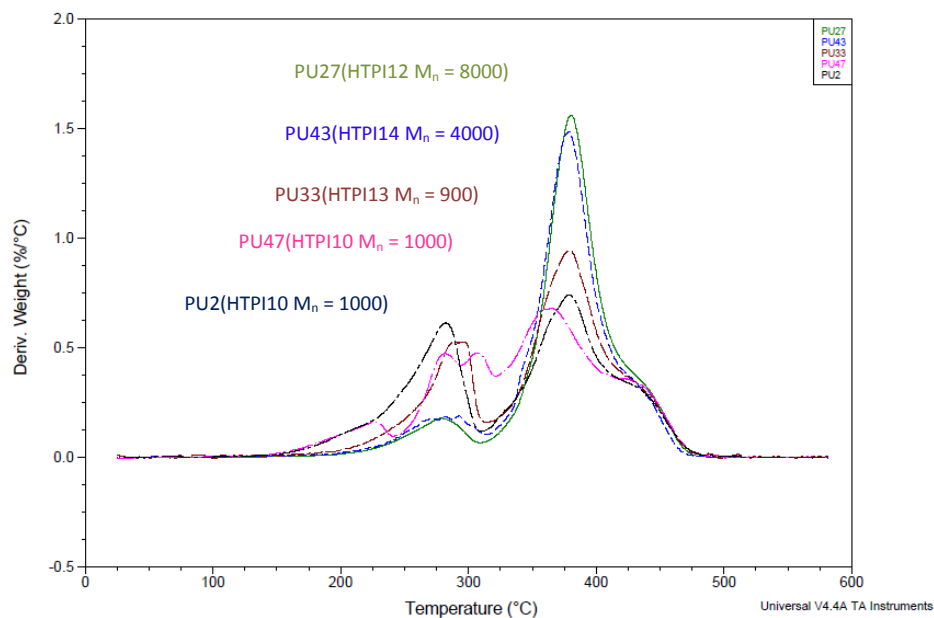
Seite 1 von 1

**Appendix 1.8** Comparison between ATR FT-IR spectra of PU(HTPI10 M<sub>n</sub> 1000 + EH) (a) PU2(HTPI10), (b) PU6(HTPI10+EH1), (c) PU7(HTPI10+EH2) and (d) PU8(HTPI10+EH3)

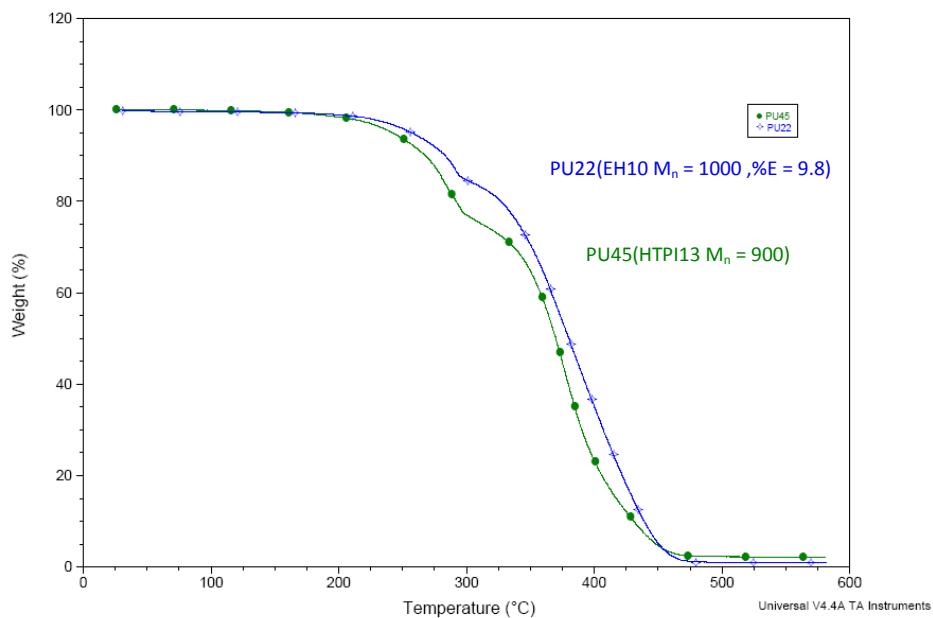


C:\DATA\ekasit\PU2 d.0	PU2 d	ATR DTGS	13/01/2010
C:\DATA\ekasit\PU6 d2.0	PU6 d2	ATR DTGS	13/01/2010
C:\DATA\ekasit\PU7 d.1	PU7 d	ATR DTGS	13/01/2010
C:\DATA\ekasit\PU8 d.0	PU8 d	ATR DTGS	13/01/2010

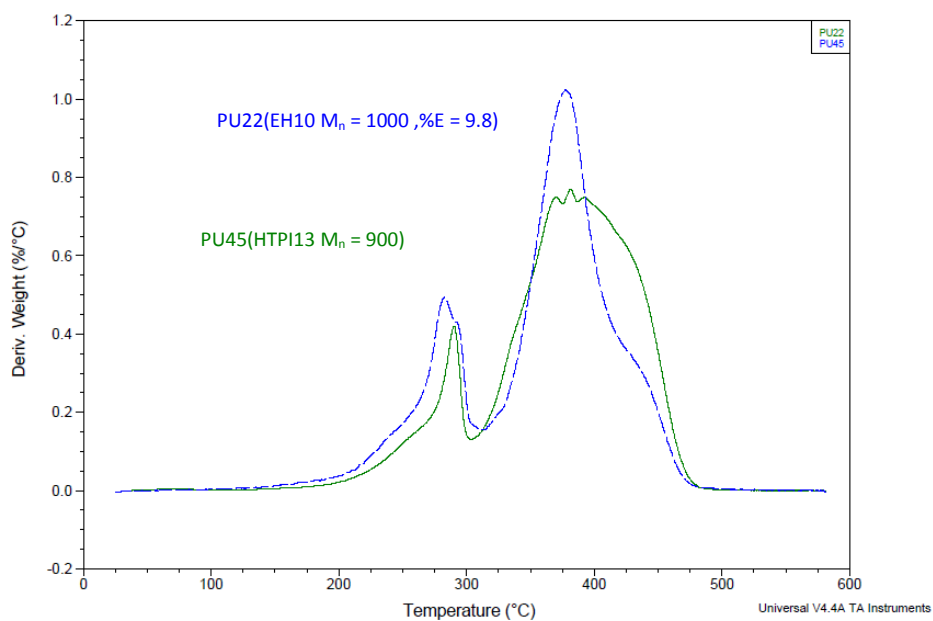
Seite 1 von 1

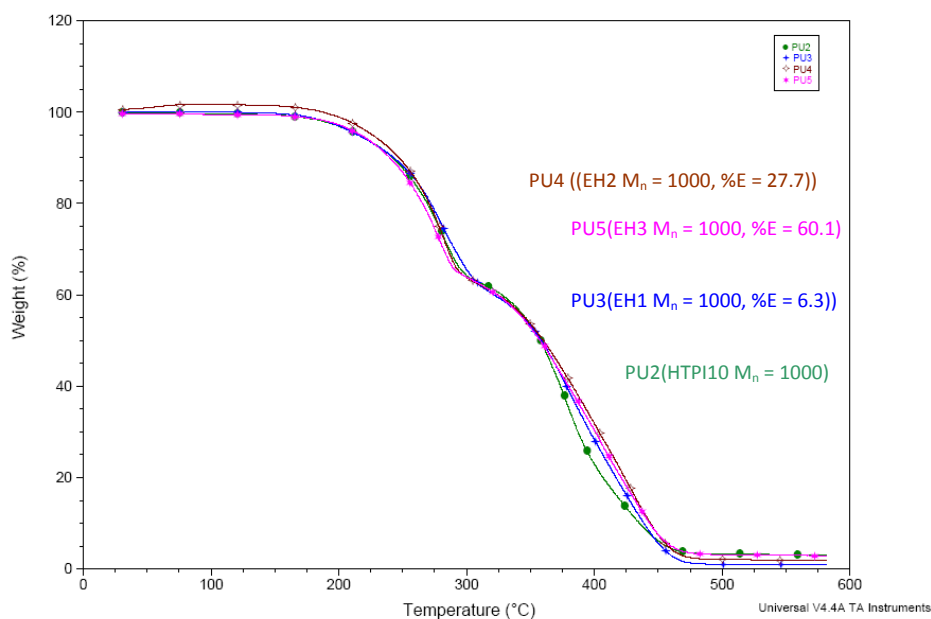
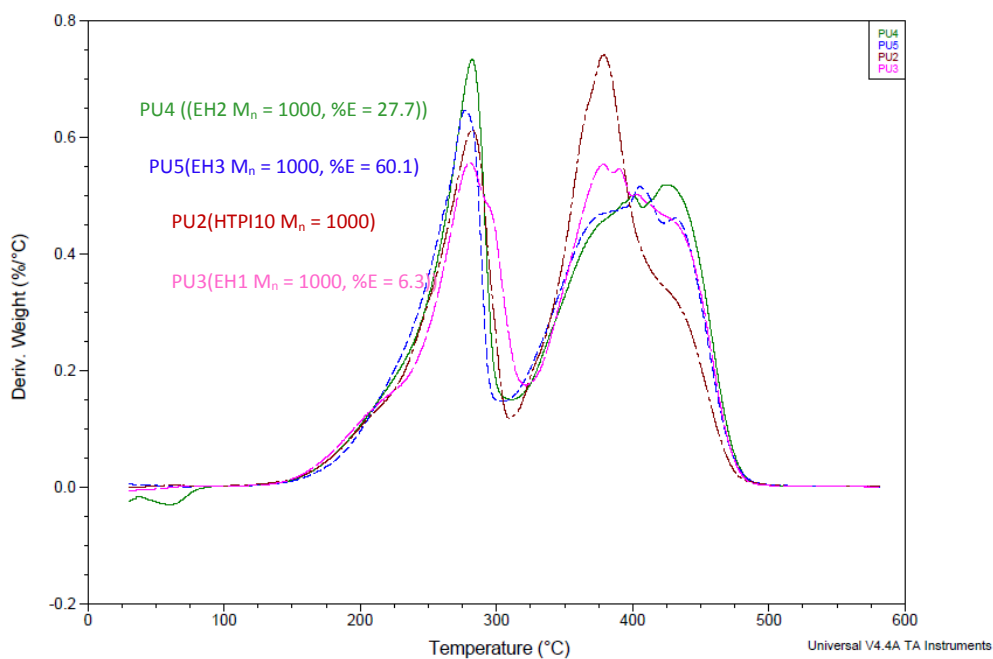
**Appendix 2.1** TGA thermograms of polyurethanes with different  $\overline{M}_n$  of HTPI**Appendix 2.2** DTG curves of polyurethanes with different  $\overline{M}_n$  of HTPI

**Appendix 2.3** TGA thermograms of polyurethanes ( $\overline{M}_n$  of PI about  $900\text{g}\cdot\text{mol}^{-1}$ ) with different percentages of epoxidation

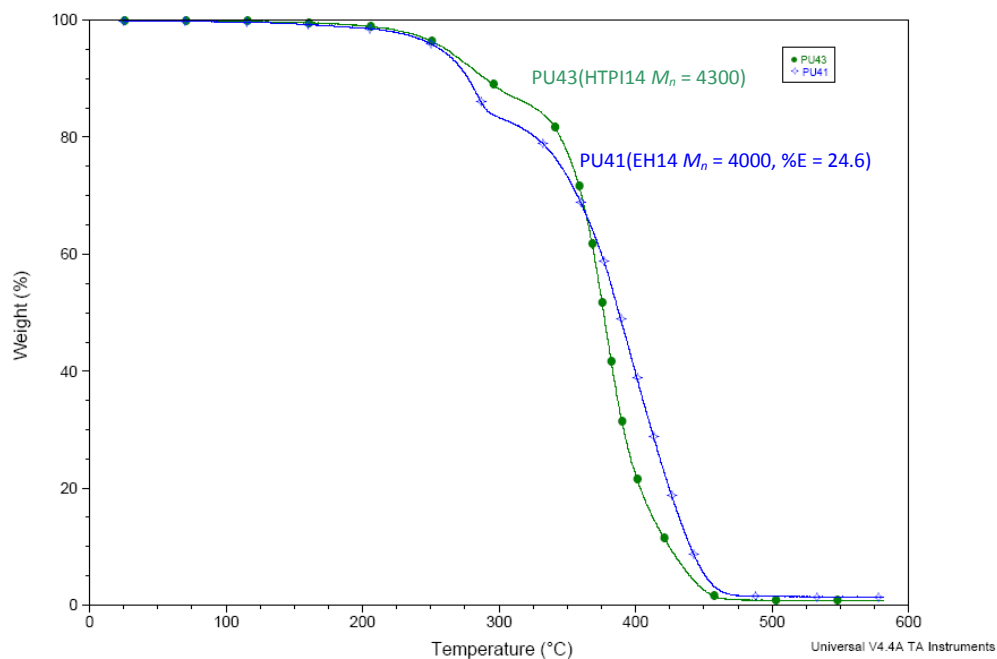


**Appendix 2.4** DTG curves of polyurethanes ( $\overline{M}_n$  of PI about  $900\text{g}\cdot\text{mol}^{-1}$ ) with different percentages of epoxidation

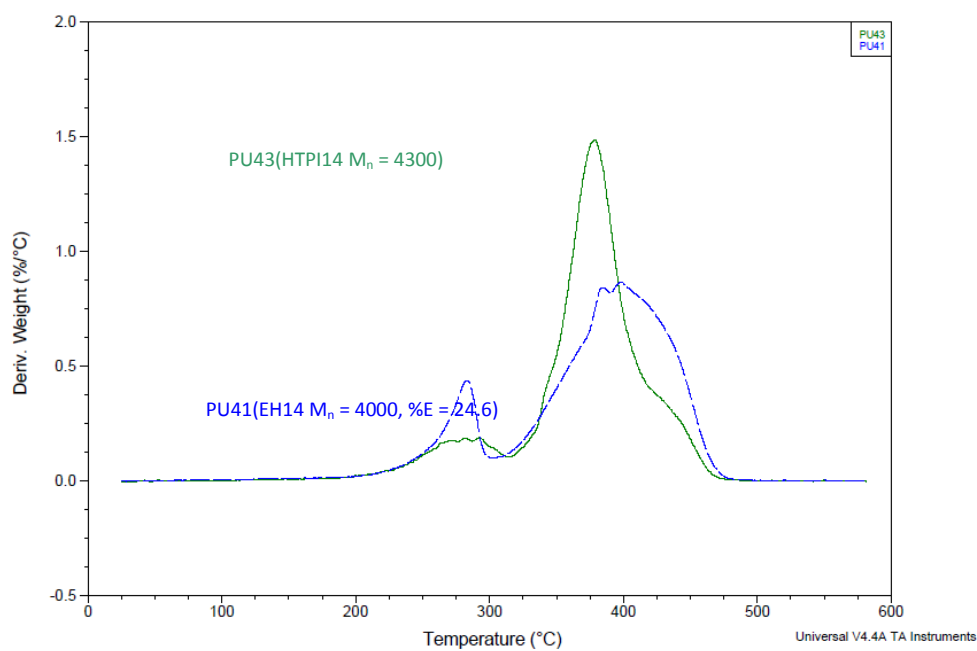


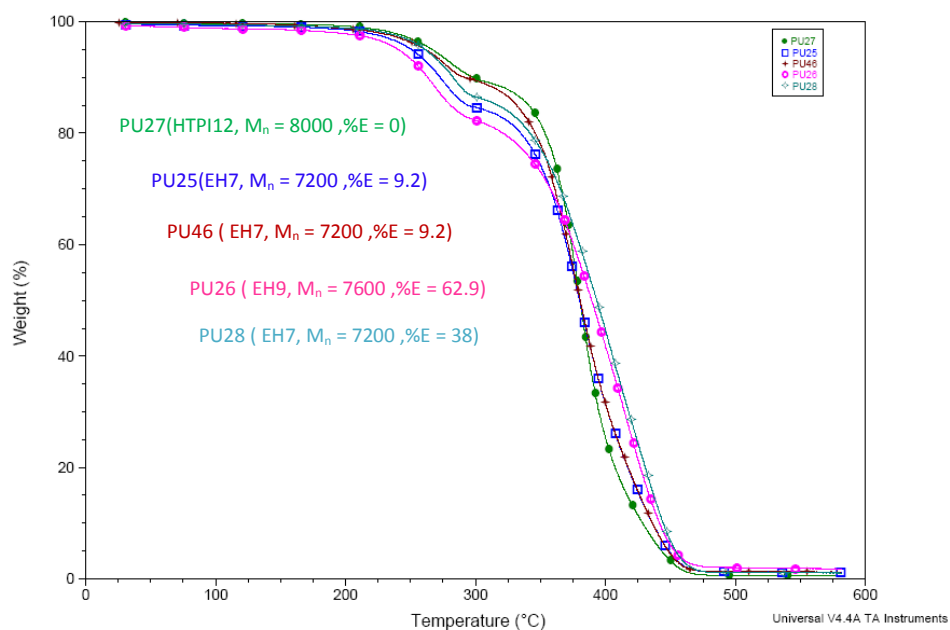
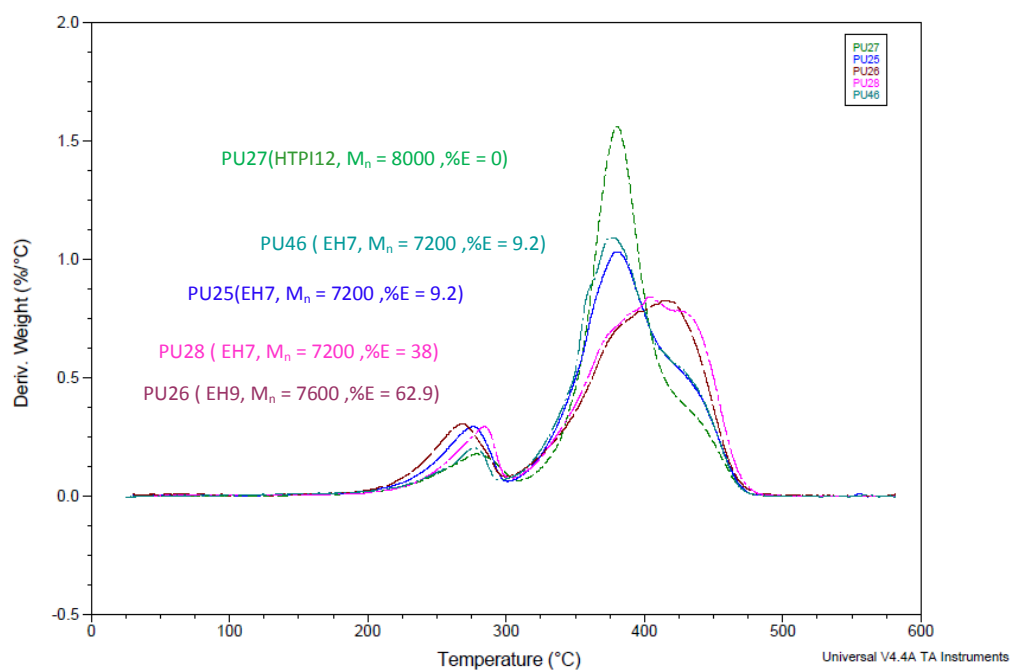
**Appendix 2.5** TGA thermograms of polyurethanes ( $\overline{M}_n$  of PI about  $1000 \text{ g}\cdot\text{mol}^{-1}$ ) with different percentages of epoxidation**Appendix 2.6** DTG curves of polyurethanes ( $\overline{M}_n$  of PI about  $1000 \text{ g}\cdot\text{mol}^{-1}$ ) with different percentages of epoxidation

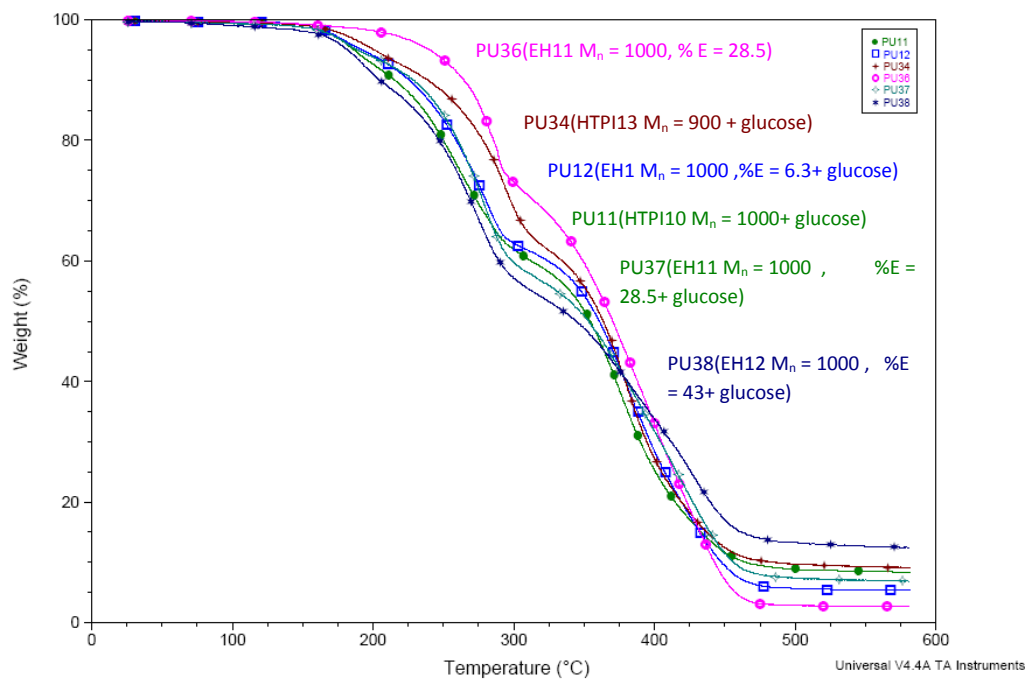
**Appendix 2.7** TGA thermograms of polyurethanes ( $\overline{M}_n$  of PI about  $4000 \text{ g}\cdot\text{mol}^{-1}$ ) with different percentages of epoxidation



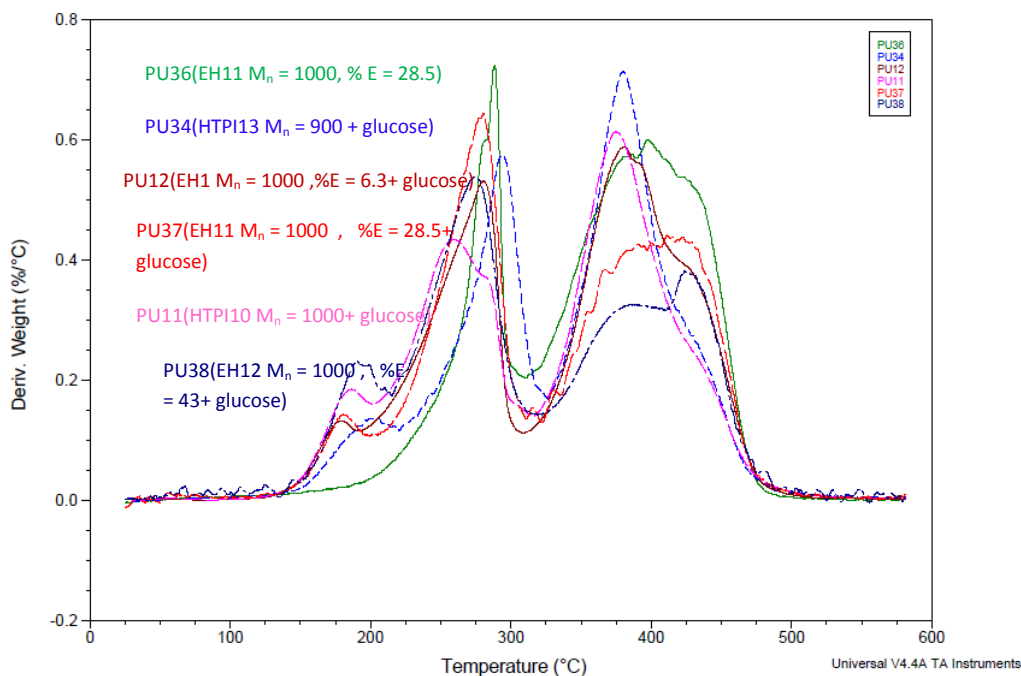
**Appendix 2.8** DTG curves of polyurethanes ( $\overline{M}_n$  of PI about  $4000 \text{ g}\cdot\text{mol}^{-1}$ ) with different percentages of epoxidation



**Appendix 2.9** TGA thermograms of polyurethanes ( $\overline{M}_n$  of PI about 8000 g.mol<sup>-1</sup>) with different percentages of epoxidation**Appendix 2.10** DTG curves of polyurethanes ( $\overline{M}_n$  of PI about 8000 g.mol<sup>-1</sup>) with different percentages of epoxidation**Appendix 2.11** TGA thermograms of polyurethanes (HTPI/EH / D-glucose)

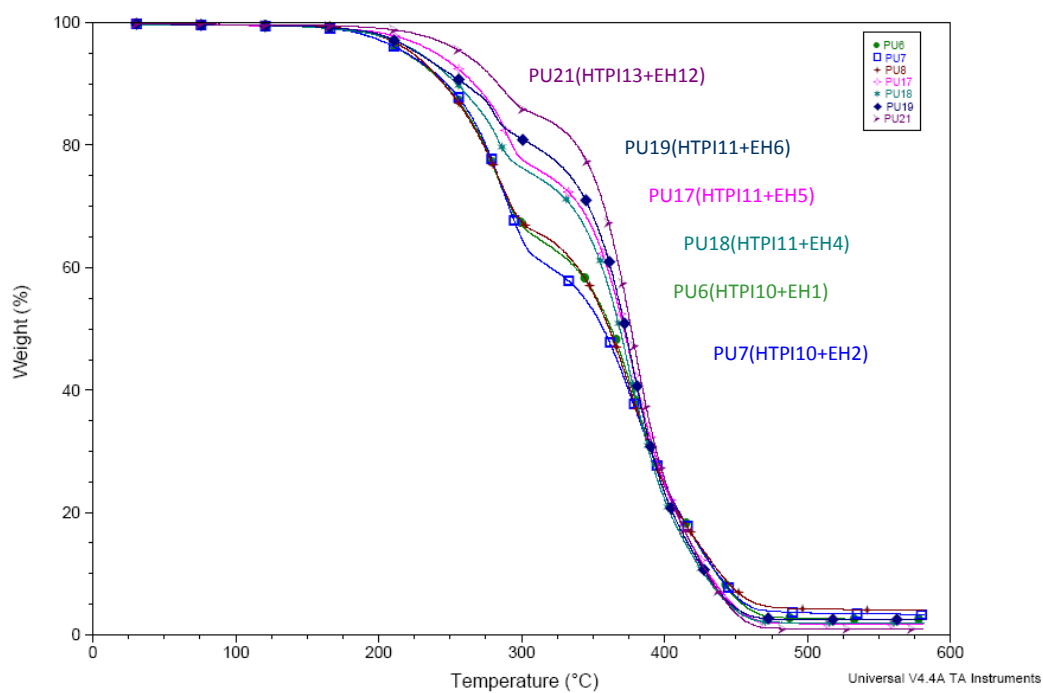


Appendix 2.12 DTG curves of polyurethanes (HTPI/EH / D-glucose)

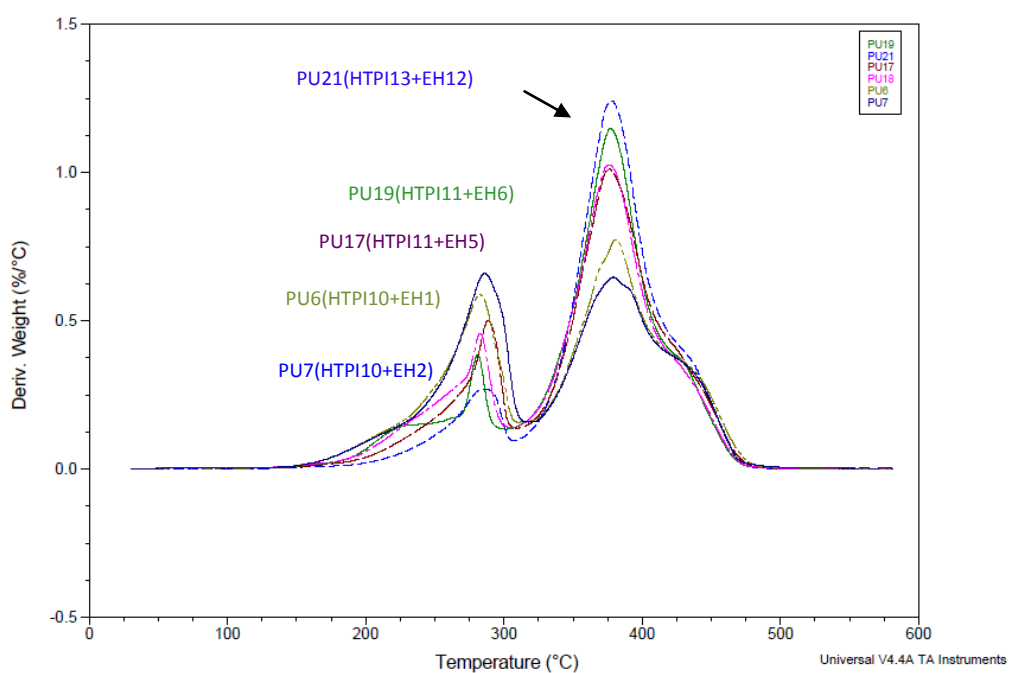


Appendix 2.13 TGA thermograms of polyurethanes ( $M_n$  of HTPI about  $1000 \text{ g}\cdot\text{mol}^{-1}$ +EH)

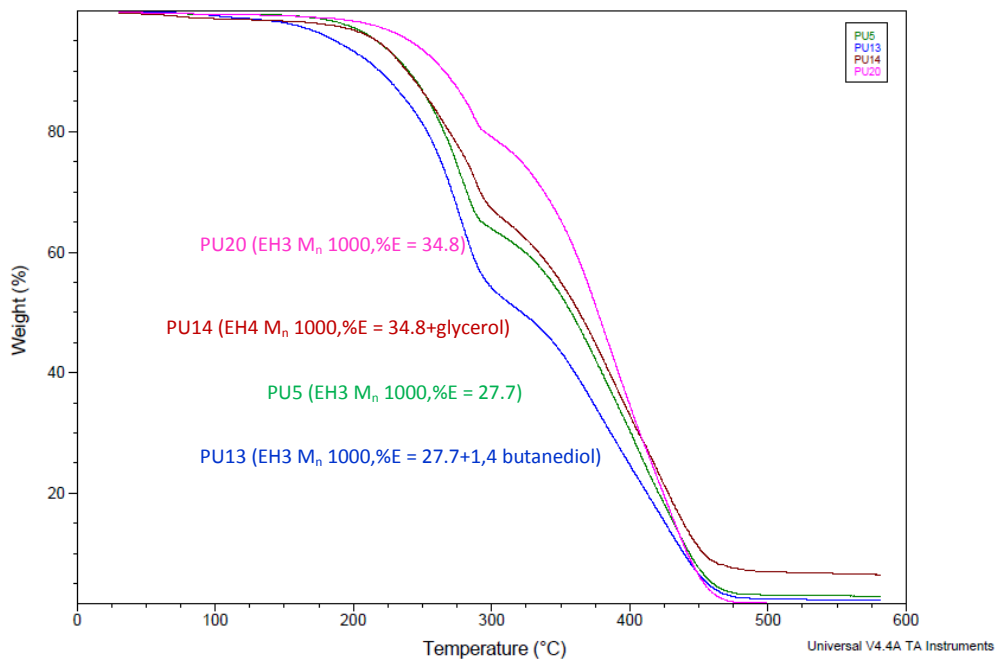




Appendix 2.14 DTG curves of polyurethanes ( $M_n$  of HTPI about  $1000 \text{ g}\cdot\text{mol}^{-1}$ +EH)



Appendix 2.15 TGA thermograms of polyurethanes (Varied chain extender)



**Appendix 2.16 DTG curves of polyurethanes (Varied chain extender)**

